Establishment of an Experimental Method for a Grooved Composite Subjected to Out-of-Plane Contact Loading

by

Yusuke Kobayashi

B.Eng. Aeronautics and Astronautics
University of Tokyo, 2007

Submitted to the Department of Aeronautics and Astronautics
in partial fulfillment of the requirements for the degree of

Master of Science in Aeronautics and Astronautics

at the

MASSACHUSETTS INSTITUTE OF TECHNOLOGY

September 2009

Author .....
Department of Aeronautics and Astronautics
July 6, 2009

Certified by ....
Paul A. Lagace
Professor, Department of Aeronautics and Astronautics
and of Engineering Systems
Thesis Supervisor

Accepted by .....
Prof. David L. Darmofal
Associate Department Head
Chair, Committee on Graduate Students

Establishment of an Experimental Method for a Grooved Composite Subjected to Out-of-Plane Contact Loading

by

Yusuke Kobayashi

Submitted to the Department of Aeronautics and Astronautics on July 6, 2009, in partial fulfillment of the requirements for the degree of Master of Science in Aeronautics and Astronautics

Abstract

A specimen and an experimental method to observe the behavior of a grooved composite subjected to out-of-plane contact loading is established and verified, and its response is examined. The specimen is designed so that the variability of stress-strain state is negligible across the width of the specimen. The dominant concept of the design is to isolate the response of the specimen around the groove from any other effects. Geometric parameters, stacking sequence (layup), and boundary conditions are determined for the specimen. With simply-supported boundary conditions, specimens fail in a simple beam shear mode as determined from the overall structural response of the specimen, thereby indicating that this configuration is not appropriate for the primary design goal. Thus, the rigid backface boundary condition is chosen and verified as the appropriate configuration. Contact, load transfer, and alignment issues arose in the first set of rigid backface tests and were solved by introducing finer machining, harder material for the indenter, and overall alignment with better accuracy. This resulted in the final test specimen configuration and associated test method, consisting of a specimen with a length of 56.00 mm, a width of 25.00 mm, an approximate thickness of 12.5 mm, and a maximum groove depth of 3.48 mm. The standard layup used for the tests is $[\mp 45/0/90]_{10S}$, while an alternate layup of $[\mp 30/0]_{13S}$ was also used. In these tests, a number of key behaviors were observed: mode of failure, load-per-stroke slope, and "knee load". Specimens failed in two different modes: a delamination near the bottom of the groove (Mode A), and a crack under the groove propagating to a delamination near the midplane (Mode B). From observations, it is concluded that damage is generated at the bottom of the groove and then propagates in the longitudinal and the thickness direction, resulting in Mode A or B respectively. A "knee load" is defined as a point where the load-per-stroke slope deviates from linear behavior. Failure Mode B and the presence of the "knee load" are observed in the standard layup, but are not applicable to the alternate layup. The presence of 90° plies is indicated as the main cause of the observed differences. The test results clearly show that a specimen and a test method is established and verified for the objectives of the current work, and furthermore is valid for tests with different test parameters. Recommendations are made with regard to extension of the basic testing established herein.

Thesis Supervisor: Paul A. Lagace

Title: Professor of Aeronautics and Astronautics and of Engineering Systems, Massachusetts Institute of Technology

Acknowledgments

The completion of this work was not possible without the help of many people around me; from lab mates sitting right next to me, to friends encouraging me from the other side of the globe.

First of all, I express all my thanks to my advisor, Paul. His keen suggestions and guidance were irreplaceable through this work, and through my academic life at MIT. Without Paul, this thesis could not have become what it is, and therefore he has my greatest gratitude. I just can't wait to celebrate the Red Sox win again!

I was so lucky to be surrounded by the wonderful people of TELAMS. Thank you all for your friendship and support throughout my days at MIT. Brian and John, thank you for the accurate suggestions and help in the lab. Chris, Alberto, and Holly, thank you for giving me thoughts for my research and helping things out, and also talking with me about random topics. I hope our works support each other, and good luck with the future work! Jeff, Fabio, Hulya, Namiko, Kyoko, Roberto, Sunny, Stevie, Woo Sik, Miso, Hai, and Jonathan, it was always fun to work with you. I will miss you all.

My life here couldn't have been as fantastic as how it actually was without my great Japanese friends, my awesome AeroAstro friends, and my talented friends in the chamber groups. It's just so exciting to imagine the glorious future of you guys! I specially would like to thank the entertaining members of Wasabis and Shitennou for the days full of laughter, and Aya for encouraging me through the tough days.

Last, but definitely not least, I give all my thanks to my family who have always supported me, encouraged me to fulfill my dream, and loved me. I cannot put my gratitude into words.

Foreword

This investigation was conducted in the Technology Laboratory for Advanced Materials and Structures (TELAMS) of the Department of Aeronautics and Astronautics at the Massachusetts Institute of Technology. This work was sponsored by The Boeing Company under the General Terms Agreement between M.I.T. and Boeing as Boeing Award Number MIT-BA-GTA-1.

Table of Contents

List of Figures

List of Tables

Nomenclature

d_{cyl}	diameter of cylindrical indenter
E_i	Young's modulus in the i-direction ($i = 1, 2, 3$)
F_i	failure normal stress in the i-direction ($i = 1, 2, 3$)
F_{ij}	failure shear stress in the i-j plane ($i, j = 1, 2, 3$)
F^{sbs}	short-beam strength
G_{ij}	shear modulus in the i-j plane ($i, j = 1, 2, 3$)
h_{grv}	groove depth
L	specimen length
L_{span}	test span length for simply-supported tests
P_f	failure load
R_{cyl}	radius of cylindrical indenter
R_{grv}	groove radius
t	specimen thickness
t_{ply}	ply thickness
t_{sb}	thickness of specimen below the groove
v_{f}	fiber volume fraction
w	specimen width
w_{f}	width of flattened section of deformed indenter
w_{ind}	width of deformed indenter
x_1	direction equivalent to the 1-direction
x_2	direction equivalent to the 2-direction

Nomenclature (continued)

x_3	direction equivalent to the 3-direction
α	groove angle
ϵ_{ij}	strain tensor component $(i, j = 1, 2, 3)$
ν_{ij}	Poisson's ratio relating stress in the i-direction to strain in the j-direction $(i, j = 1, 2, 3)$
σ_{ij}	stress tensor component $(i, j = 1, 2, 3)$

Chapter 1

INTRODUCTION

The use of composites and their laminates as structural materials has been significantly increasing in the recent few years. This can be attributed to properties such as their high specific stiffness and specific strength, corrosion- and fatigue resistance, and the ability to customize their properties for individual applications. However, the adoption of composites has been relatively slow in general structural applications, primarily due to the complexity of their behavior. The heterogeneity of composites results in complex responses to loadings, and their failure is not yet explained or correlated well by theory [1]. Lack of reinforcement in the out-of-plane (laminate stacking) direction also restricts its use. As a result, composite laminate structures implemented in general structural applications have been limited to relatively simple geometries such as plates and shells, where the loading primarily occurs in-plane.

The fact that composites are utilized in the most recent commercial aircraft of Boeing, the 787, at over 50% by weight [2] shows that the use of the material is rapidly expanding within the aerospace field. This weight percentage exceeded that of the recent jumbo aircraft of Airbus, A380, in which composites make up 25% of the total airframe [2]. Composites make up much of the wings and fuselage, whereas previous versions had these materials generally restricted to less critical sections. To continue expanding the role of composite laminates, their response to both in-plane and out-of-plane loads, and usage in complex geometry needs to be examined to a

greater extent.

The response of composite laminates to out-of-plane loadings has been an issue of particular concern, especially that due to impact and quasi-static indentation. The response to impact is crucial in identifying the properties of composites after debris strikes and other accidental impacts during operation and maintenance of aircraft and in other applications. Quasi-static indentation tests has been shown to be a good alternative to impact tests when particular conditions are satisfied [3, 4, 5]. The objective of both areas of research is to understand the response of composite laminates to short-duration contact loading that is undesirable for the structure, but that the structure must be able to bear. While there has been substantial work addressing this issue, there has been very little work examining composite laminates specifically designed to carry sustained out-of-plane loads. This type of structure, and the understanding of its behavior, may be required in further expanding the use of composites.

Out-of-plane loadings on a composite laminate are generated via contact between the laminate surface and another object. Large contact stresses may be generated depending on the geometries and properties of the two contacting bodies. This is because contact theoretically begins at a single point, gradually forming a small contact area as the contacting bodies deform. As a result, the bodies are subject to large contact stresses even when the applied load can be relatively low. Working to minimize these contact stresses should increase the load-carrying capability of a composite laminate. A particular means for such is to maximize the contact area, which can be realized by designing the two bodies geometrically complementary. For composite laminates, this requires a geometry more complex than a flat plate, shell, or a beam.

One example of such a design is a grooved laminate and a spherical object. An application of this type of structure is presented in the telescopic wing design by Czajkowski, Clausen, and Sarh [6]. This morphing structure is a major component of the wing in the design of an Advanced Flying Automobile (AFA) [7]. Roadable aircraft designs have existed since 1918 [8], but have remained impractical due to poor

performance and difficulty in satisfying both road and air configurations. Attempts to overcome these challenges are presented in this specific design [6] by using a telescopic wing that can be stored inside the vehicle's roof during road operation. The spars of the wing in the design are segmented, utilizing overlapping tubes with helical grooves on their inner and outer surfaces. Adjacent segments are connected via ball bearings embedded between the outer grooves of one tube and the inner grooves of the other. During flight, aerodynamic loads on the wing are transferred from the outer (tip) segments to the inner (root) segments, and finally to the fuselage. The ball bearings are the only connection between spar segments in such a design, and all loads are thus transferred from one spar segment to the next via contact with the ball bearings. Analysis showed that replacing 4 of the 7 steel segments with carbon composite segments results in reducing overall spar weight by approximately 50% [6]. In this case, the grooved composite tubes would primarily be loaded out-of-plane, via contact with the ball bearings. With the spars being the most critical load-carrying structures within a wing, the behavior of grooved composites under out-of-plane contact must be well understood and tested before such a design can be realized. This design is one representative of potential applications that require out-of-plane contact loading with a composite structure. Such load transfer ability addresses an important item in advancing composite structural applications.

The primary objective of the present work is to design and verify an experimental specimen and method to determine the behavior of a grooved composite under a sustained out-of-plane contact loading, particularly its failure. A review of previous research applicable to the current work is presented in Chapter 2. This includes grooved composite structures, contact behavior, and specimen establishment. In Chapter 3, objectives of this work and the basis of the specimen establishment are presented and explained. The manufacturing procedures taken for the composite specimens are explained in Chapter 4. The general testing procedures employed throughout the entire work are explained in Chapter 5. Descriptions of tests, their results, and discussion thereof are explained in Chapters 6, 7, and 8 for each of the specimens in the design evaluation. Finally, conclusions from this work and recommendations for

future research are presented in Chapter 9.

Chapter 2

PREVIOUS WORK

The present work focuses on the development of a specimen for experiments on contact between a grooved composite and an indenter. It is therefore beneficial to review previous work dealing with grooved composite structures, and contact loading (including impact and quasi-static loading) on composites. Since the specimen establishment refers to the short-beam shear test method as a guide, research related to this is presented, as well as discussion concerning the geometric parameters of a specimen.

2.1 Grooved Composite Structures

The behavior of grooved composite structures has received very little attention. The few works available have focused mainly on specific designs for particular applications. Montay et al. [9] studied flat grooves incrementally drilled into a composite laminate as part of applying the compliance method to composite laminates. This is a means to determine the residual stresses generated during its manufacture process. As a groove is drilled into the laminate, it deforms to achieve a new state of equilibrium. This deformation, measured by strain gages and optical devices, provides information about the residual stress previously carried by the removed volume of the material. Composites with buttress grooves, a structure which looks like the blade of a handsaw and is typically used to transmit shear loads, were examined by Hoppel

et al. [10]. They studied the strength of a single groove by transferring a shear load from a test fixture with a projection, and suggested a laminate configuration that maximizes the ability of the structure to carry shear loads. Liu et al. [11] worked with grooved (mentioned as "notched" in the article) cross-ply laminates with the objective to observe their failure. The grooves were completely through thickness, and the laminates were subjected to in-plane loads. These grooves were not designed for a load-carrying purpose, but intended to observe how grooves influence the initiation of the growth of damage in a laminated plate. Taking into consideration multiple failure modes (transverse cracks, longitudinal racks, and notch-induced splits and delamination), a model was developed and failure simulations were run. Compared with experimental results, it was shown that interaction of splits, transverse cracks, and delamination took place and all of these must be taken into account to achieve a correct prediction of failure.

The first two works address specific applications of grooved composites, either to predict the residual stress within composite laminates or to characterize the strength of particular structures. Liu worked with the general response of a grooved composite, however the groove of the structure is not utilized as a means to transfer load. The lack of available literature with grooved composite structures, beyond these cited, demonstrates that basic research is necessary to build knowledge on the general response of such structures.

Finally, the analytical investigation most related to this current work was done by Bastien [12]. For both isotropic and laminated configurations, finite element analyses were run to observe the stress-strain behavior of a grooved plate subjected to static out-of-plane contact loading. From the results, it was concluded that the overall structural response of such a structure is composed of three key items: (1) a global response due to the overall structural configuration and global aspect of the loading; (2) a local response due to the removal of material to create the groove; and (3) a local response due to the specifics of the introduction of the loading. The results demonstrated that the boundary conditions of the structure are a major contributor to the global response. The local response around the groove is not affected by the

groove depth. However, the groove-to-thickness ratio has significant influence on this response. It was also observed that large stress gradients local to the groove influence stress fields around the groove via the requirements of differential equilibrium. However, simple beam bending or classical laminated plate theory behavior is recovered away from the groove with a distance which is dependent upon the particular conditions.

The work of Bastien does not deal with experimental work. Thus, comparison of analytical and experimental work is left for future work. However, the basic knowledge of the response of a grooved laminate to static contact loading that is presented in that work forms an important background for the discussion made in Chapter 3 of the current work.

2.2 Contact Behavior

The response of a simple composite laminate under general contact loading, both static and impact loading, has received considerable interest from researchers because of its significance in the aerospace industry. The sensitivity of composite laminates to out-of-plane impacts has motivated a large amount of research in this area, since impacts do occur during manufacture, operations, and maintenance. An excellent review of foundational work in this area has been provided by Abrate [13, 14]. The experimental studies that are referenced in this review have led to the establishment of the standard test method for impact testing, ASTM D7136 [15]. However, impact testing is relatively complicated and requires control of numerous factors.

Quasi-static indentation testing became an interest in relation to impact work as it provides an alternative for evaluating the impact response of composite laminates, with a simpler experimental method. Various researchers have attempted to establish the conditions under which quasi-static indentation tests can precisely simulate impact response of composite laminates (e.g. [3, 4, 5]). These works demonstrate that maximum contact force can be utilized as a key value for correlating quasi-static indentation with impact testing. Work on this topic has lead to the establishment of

an ASTM standard to measure the damage resistance of laminated composite plates via concentrated quasi-static indentation [16].

For the analytical aspect in this field, stress and deformation occurring in two elastic, isotropic bodies under contact was initially addressed by Hertz [17]. This 'Hertzian' contact solution can be used for the prediction of contact area, contact stress distribution, and relative approach of two bodies. Much of the analytical work on this topic refers to this classical solution. A number of researchers applied this solution to quasi-static indentation cases for composite laminates, and have obtained results that compare favorably with experimental data (e.g. [18, 19, 20]). Recently, commercial software for finite element modeling has become accessible to researchers, and analyses with the use of such software has also become extensive in research in this area for composites (e.g. [12, 21, 22, 23]).

The two test standards presented have the objective of observing the response of a composite structure to an out-of-plane load that the structure is not designed to undertake. Very few experimental works have been performed for composite structures that are designed to undertake such loads. Therefore, work needs to be done in regard to the establishment of specimens and testing procedures for such observation.

2.3 Specimen Establishment

A specimen and a test method that is standardized for a similar objective can be utilized as a guide for the goal of this work. The short-beam test method is an experimental method that can be used for this purpose because that configuration is subjected to a continuous contact loading in its test method. Before a test standard was established for such a configuration, experimental and analytical work was performed. Work of Kedward [24] is one of the earliest works in that regard. He focused on the short beam test method as a valid method to examine the interlaminar shear strength of a composite laminate. He noted that the beam geometry and laminate construction have significant influence on the distribution of stresses. With works succeeding Kedward (e.g. [25, 26]), an ASTM standard [16] for testing short-beam

strength of composites was established. Both the finalized test standard and the process of establishing this short-beam test method serve as guides for the establishment of the specimen and the test method presented in the current work.

In the design of a specimen, the determination of the geometries of the specimen is of primary importance. This is demonstrated by the previous works showing the effects of parameters on test results, both for short beam tests and quasi-static indentation tests. For the short beam test, Sankar [27] concluded that the small width-to-thickness ratio and large length-to-thickness ratio are required in order that contact stress distribution is close to that of theoretical half-plane contact, as determined from both analytical methods and numerical simulation. Mahajan [21] argued that material and geometric properties have effects on the indentation depth, maximum contact pressure, and contact length.

In literature regarding the quasi-static indentation and impact tests, it is presented that the thickness and the deformation in the thickness direction have a large effect on the response. Comparing the experimental results of Tan and Sun [19] and Wu and Shyu [28] with the contact laws proposed by Yang and Sun [18], it can be seen that the results and predictions agree well for small indentations, but considerable deviation is seen for larger indentations. Analytically, Chen et al. [29] discussed the importance of the thickness effect on the contact behavior of a laminate under indentation. Introducing a modified Hertzian contact law, which takes into consideration the thickness of the composite laminate, he concluded that the thickness of the laminate has considerable effect, particularly on the force-indentation response. In particular, he showed that the indentation depth is less for thinner laminates, under simply-supported boundary conditions.

These previous works suggest clearly that geometric parameters need to be considered carefully in establishing a specimen. Because of the existence of the groove, it is expected that the specimen that is to be designed in this work will be subjected to a somewhat different stress-strain state around the contact area than in the case without a groove. However, the knowledge from the previous works can be applied to the global response of the specimen, and thus referenced as the background for

determining the overall geometry of the specimen.

The few available experimental works considering grooved composite laminates do not provide much knowledge regarding their general response to out-of-plane contact loads. They either characterize specific applications or consider grooves as defects in a composite. Impact tests and quasi-isotropic tests have been an interest in the composites field and such tests have considered composite structures subjected to out-of-plane loads. However, very few experimental works have been performed on composite structures that are designed to carry out-of-plane loads. These facts demonstrate the necessity of basic research in understanding the response of a grooved composite loaded by out-of-plane static loading. The current work assists in this process by establishing a specimen and a test method for this objective, and observing the response of such a configuration. Results of analytical work on grooved composites and the effects of specimen geometries on the structural response that are presented in previous works are taken into consideration throughout this work.

Chapter 3

OBJECTIVES AND BASIS OF SPECIMEN ESTABLISHMENT

The primary objective of the present work is to design and verify an experimental specimen and method to determine the behavior of a grooved composite under a sustained out-of-plane contact loading. In particular, the desire is to determine the load-carrying capability of such a configuration. With this primary focus as background, the goal of the specimen and experimental design is to be able to observe the effects of the groove separated from any other effects.

The important factors that were taken into consideration in designing the initial specimen are explained in this chapter. These are particularly applicable in the design of the initial specimen, but remain pertinent as the specimen design evolved. The key concepts for the design are first discussed. The background on the choice of parameters are then explained. It should be noted that in this chapter, the specific values of each of the parameters are left to be determined.

3.1 Key Concepts

The important aim of the specimen and the test procedure is to observe the general response of a composite laminate with a groove under load. To address this, a block with a rectangular cross-section was chosen as the overall shape of the specimen. The

longitudinal direction is defined as the 1-direction, and the out-of-plane direction of the laminate coordinates is defined as the 3-directon. The groove was set to be along the 2-direction and through the centerline of the specimen. The origin of the axis system is placed at the center of the top face of the specimen.

The experimental method and the specimen is designed to result in a stress-strain state in the specimen that does not vary in the 2-direction and can thus be thought of as "two-dimentional". This is to allow acquisition of the response to a two-dimensional state before including the increased complexity of three-dimensional variability. The specimen geometry is therefore constant in the 2-direction. It is recalled here that one possible application of this work is a grooved composite with a ball-bearing. In order to simulate a load transferred from a ball into the groove without variability along the 2-direction, the loading medium is chosen as a cylindrical indenter. This has a circular cross-section, and the geometry is constant along the 2-direction. An isometric view of the specimen, cylindrical indenter, and the coordinate system are illustrated in Figure 3.1.

The specimen is to be designed such that the overall specimen size has no effect on the local stress-strain state resulting from the contact loading at the groove. This leaves the relative thickness of plies, the laminate configuration, and the groove geometry as the key parameters affecting the local stress-strain state.

In terms of overall size, a larger specimen enables acquisition of strain measurements at more points since a strain gage occupies a finite area. A specimen with a larger geometry at the groove, however, requires larger load to reach failure, knowing that failure load is proportional to the contact area. Larger specimens require more material, thereby requiring more time and resources to manufacture a single specimen. For these reasons, a balance must be achieved in the design, with the specimen to be sufficiently small to keep time and resources for a specimen low; but to be sufficiently large enough such that experimental ease is obtained and the primary purpose of isolating the local stress-strain state is achieved.

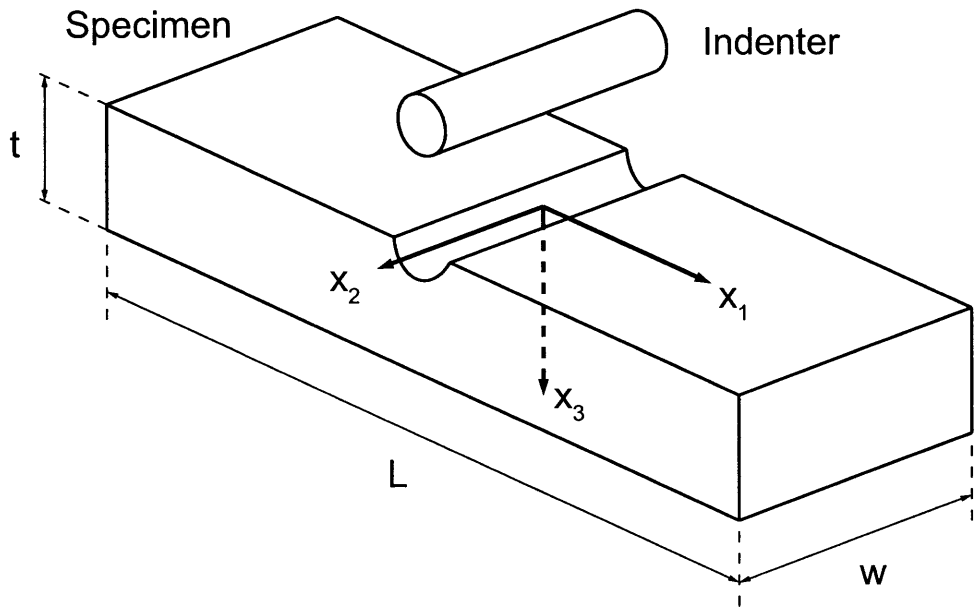

Figure 3.1 Isometric view of the specimen and the coordinate system.

3.2 Parameters of the Specimen

In the previous section, it was indicated that the basic configuration of the specimen is a grooved block. The three overall dimensions of the specimen, length (L), width (w), and thickness (t) are expected to not have primary effect on the local stress-strain state around the groove. It is the geometric parameters of the groove that are expected to have critical effects on the local stress-strain state around the groove. These key parameters discussed are the radius of the groove R_{grv}, the radius of the indenter R_{cyl}, the depth of the groove h_{grv}, and the groove angle α. These parameters are illustrated in Figure 3.2 along with the overall specimen dimensions. In addition to these geometric parameters, the stacking sequence (layup) of the laminate is a key design parameter.

Recalling the primary objective to isolate the local stress-strain state at the groove from effects of the boundary conditions and the global response of the structure, the radius of the groove, R_{grv}, governs the scale of the specimen. Thus, choosing R_{grv} large will make the specimen large and vice versa. All geometric parameters can be ratioed directly to R_{grv} except for ply thickness, t_{ply}, which is determined by the material. It is noted that the ply thickness can be used as the basis for all geometric parameters including R_{grv}. However, in this work it was decided to choose the value of R_{grv} and work from there.

The value of the radius of the cylindrical indenter, R_{cyl}, is determined relative to R_{grv}. Recalling that ball-bearings are one of the possible applications of grooved composites, theories of metallic ball-bearings are taken into account. For metallic ball-bearings, Harris et al. [30] suggest that the ratio of radii of the groove to the ball radius should be in the range of 1.02 to 1.08. Since the cylinder is chosen to give a circular cross-section for loading like a ball-bearing, the cylinder radius is chosen based on this ratio for ball-bearings. This gives an expression for the cylinder radius:

$$1.02 \leq \frac{R_{\text{grv}}}{R_{\text{cyl}}} \leq 1.08 \tag{3.1}$$

It is noted from the work of Harris [30] that higher ratios are for high-speed ball

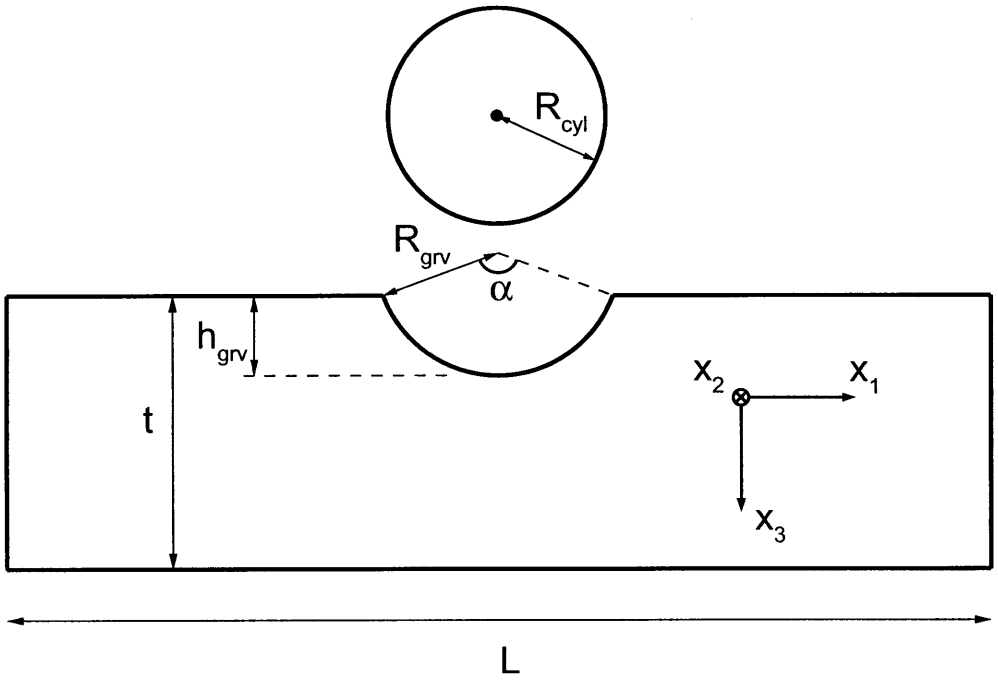

Figure 3.2 Illustration of specimen geometry parameters.

bearings in order to decrease friction. Such a usage is not assumed in the application of ball bearings in the current considered applications in composite structures. As the current work is concerned with static loading and seeks to minimize contact stress by maximizing contact area, a low ratio of R_{grv} to R_{cyl} of approximately 1.02 is chosen.

The groove depth, h_{grv}, and the groove angle, α, are test parameters and their relationship is simply determined by the following equation from simple geometry:

$$h_{\text{grv}} = R_{\text{grv}} \left(1 - \cos \frac{\alpha}{2}\right) \tag{3.2}$$

Because h_{grv} and α are directly related, only the parameter of groove depth is subsequently discussed with the value of groove angle directly tied to this value. It should be noted that the ply that is segmented by the bottom of the groove is dependent on the laminate chosen and the ply thickness of the material for a chosen value of groove depth. In addition to this, the ply thickness may differ slightly after each curing process. This, therefore, must be taken into consideration in final specimen manufacture. This is addressed in Chapter 8.

In determining the thickness of the specimen in order to isolate the local stress field from the effect of the backface, the key parameter to consider is the ratio between the groove depth and thickness of specimen, h_{grv}/t. From the work of Bastien [12], where a two-dimensional finite element analysis of a grooved plate subjected to out-of-plane contact loading was performed, it was shown that values of h_{grv}/t larger than 0.25 result in interference of the local stress field around the groove by a rigid backface boundary conditions. Since the object of the test is to determine the local response of the composite specimen due to the contact from the indenter at the groove, the effect of boundary conditions should be small enough to be able to be ignored. On the other hand, smaller h_{grv}/t values result in thicker specimens, when the value of groove depth is constant. This runs counter to one of the key concepts. In working the balance to a smaller specimen, the base minimum value of h_{grv}/t of 0.25, where there is virtually no influence of the backface on the local stress field due to the groove, is chosen.

The stacking sequence of the laminate is a test parameter, but also interacts with overall thickness and thus the parameter of h_{grv}/t. Another requirement is that the laminate should be symmetric in order to prevent bending after curing.

In setting the width of the specimen, w, the primary objective is to maintain a uniform state of loading across the specimen. In the ASTM test standard for the short-beam test method on composites [31], it is recommended that the width of a specimen should not exceed twice the value of the thickness, t. A width-to-thickness ratio, w/t, greater than 2.0 can result in a significant widthwise shear stress variation [26]. Thus, a ratio of width to thickness is chosen to be approximately 2.0.

In setting the length of the specimen, L, once again a key objective is that the length does not affect the local stress state due to the loading at the groove. In the ASTM test standard for the short-beam test method on composites [31], it is recommended that the span length (distance between the two supporting points) should be equal to six thicknesses and leave one thickness hanging over the supporting points. In the work of Bastien [12], the analysis of grooved plates subjected to out-of-plane contact loading with simply-supported boundary conditions indicates that the stress state around the supporting points interferes with the stress state around the groove for specimens with spans shorter than about five thicknesses. Thus, for such a simply-supported configuration, the test span length, L_{span}, i.e. the length between two supporting points, is chosen to be greater or equal to six thicknesses ($6t$). Adding the length overhanging the supporting points, the length of the specimen, L, was thereby chosen to be greater or equal to eight thicknesses ($8t$).

For rigid backface tests, the stress around the groove is less affected by the length of the specimen. The analysis by Bastien [12] indicates that the local stress field due to the groove dissipated within a distance from the groove in the direction of length equal to one thickness. Thus, for the configuration of a rigid backface, the length is set to greater or equal to two thicknesses ($2t$).

A summary of the relationship of parameters as determined herein is given in Table 3.1. It is again noted that the actual values of these parameters are not discussed in this chapter. The choices are described in the ensuing chapters where the details for

each particular test configuration are presented.

Table 3.1 Relationship of geometric parameters

$R_{\text{grv}}/R_{\text{cyl}} \approx 1.02$
$h_{\text{grv}} = R_{\text{grv}}\left(1 - \cos\frac{\alpha}{2}\right)$
$h_{\text{grv}}/t = 0.25$
$w/t = 2.0$
$L \geq 8t$ (simply supported) ; $L \geq 2t$ (rigid backface)

Chapter 4

MANUFACTURING PROCEDURES

Manufacturing procedures are very important in achieving specimens of the same properties, especially when dealing with composite materials. In this chapter, the manufacturing procedures for the specimens are described in three sections; procedures for layup, for curing, and for machining. TELAC/TELAMS standard procedures [32] are used as the main reference in the manufacturing. The preinpregnated (prepreg) material used for the current work is Toray Composites P707AG-15. The prepreg is supplied in 610 mm wide rolls and is in a unidirectional configuration. The material consists of Toray T700GC-12K-31E carbon fibers impregnated with Toray Composites #2510 matrix system. The carbon fiber has a volume fraction of approximately 65%. The nominal properties for this material, as provided by the supplier, are provided in Table 4.1.

4.1 Layup Procedures

The prepreg tape is stored in a sealed bag inside a freezer at a temperature below -18°C. Before cutting, the prepreg is removed from the freezer and allowed to warm for approximately 1 hour while sealed inside its bag. This is done to prevent moisture condensation. The prepreg is unrolled for the length needed and then necessary plies

Table 4.1 Nominal properties*† of P707AG-15 material after cure (provided by manufacturer)

Moduli [GPa]		Failure Stress [MPa]	
E_1^t	127.0	F_1^t	1661
E_1^c	114.6	F_1^c	1397
E_2^t	9.05	F_2^t	53.0
E_2^c	14.09	F_2^c	282.5
ν_{12}	0.35	F_{12}	159.5
G_{12}	5.22	F_{13}	86.1

Thickness per ply, $t_{\text{ply}} = 0.15 \pm 0.01$ mm

Volume Fraction, $v_f = 65$ %

Curing Temperature = 132°C

*t: Tensile, †c: Compressive.

are cut with a sharp utility knife, using non-porous teflon (GNPT) coated aluminum pattern templates as a guide. The size of the laminate to be achieved in this work is 152 mm by 178 mm.

The cutting procedure differs for each ply angle, as illustrated in Figure 4.1. Plies of 0° direction are easily made by cutting the sheet to its desired geometry using the template. The 90° plies can also be cut using the 0° template by rotating it by 90°. However, in order to save material, one should cut from the roll with two templates, parts 2 and 3, as shown in Figure 4.1. Angle plies (the +45° ply is shown as an example) are cut with two templates: one is in the shape of a parallelogram to make an initial cut from the roll, and the other is in a quadrilateral shape to cut the parallelogram piece into two parts, 4 and 5, as in Figure 4.1. For both 90° plies and angle plies, the resulting two pieces are then assembled into a rectangular shape, with the seam running parallel to the fiber direction. With this seam direction, high quality of the laminate is ensured by having only matrix joints. Once all the plies are cut, the roll of prepreg is returned to its bag and the freezer.

The next step is to stack the plies to form the laminate. Two aluminum bars that provide an established 90° corner are fixed on a aluminum plate, with double-sided tape where the plies should rest. This aluminum jig is used to provide alignment of the angles in the laminate. One bar is referred to as the 1-direction, and the other is referred to as the 2-direction. This reference is maintained throughout the layup procedure. The cut plies are placed so that their appropriate right-angled corner rests squarely in the corner of the jig. The first ply is placed with the backing paper face down and pressed firmly so that the backing paper adheres to the double-sided tape. For subsequent plies, the backing paper is faced up, and the ply face is pressed firmly and equally onto the ply face of the stacked ply face. The backing paper is then peeled off and this process is repeated for the remaining plies. However, the backing paper is kept on the final ply. The corner of the laminate that is placed in the right corner of the aluminum jig is assumed to have the most accurate ply stacking, and therefore is referred to as the "good corner". An "X" is marked on the backing paper to identify this "good corner".

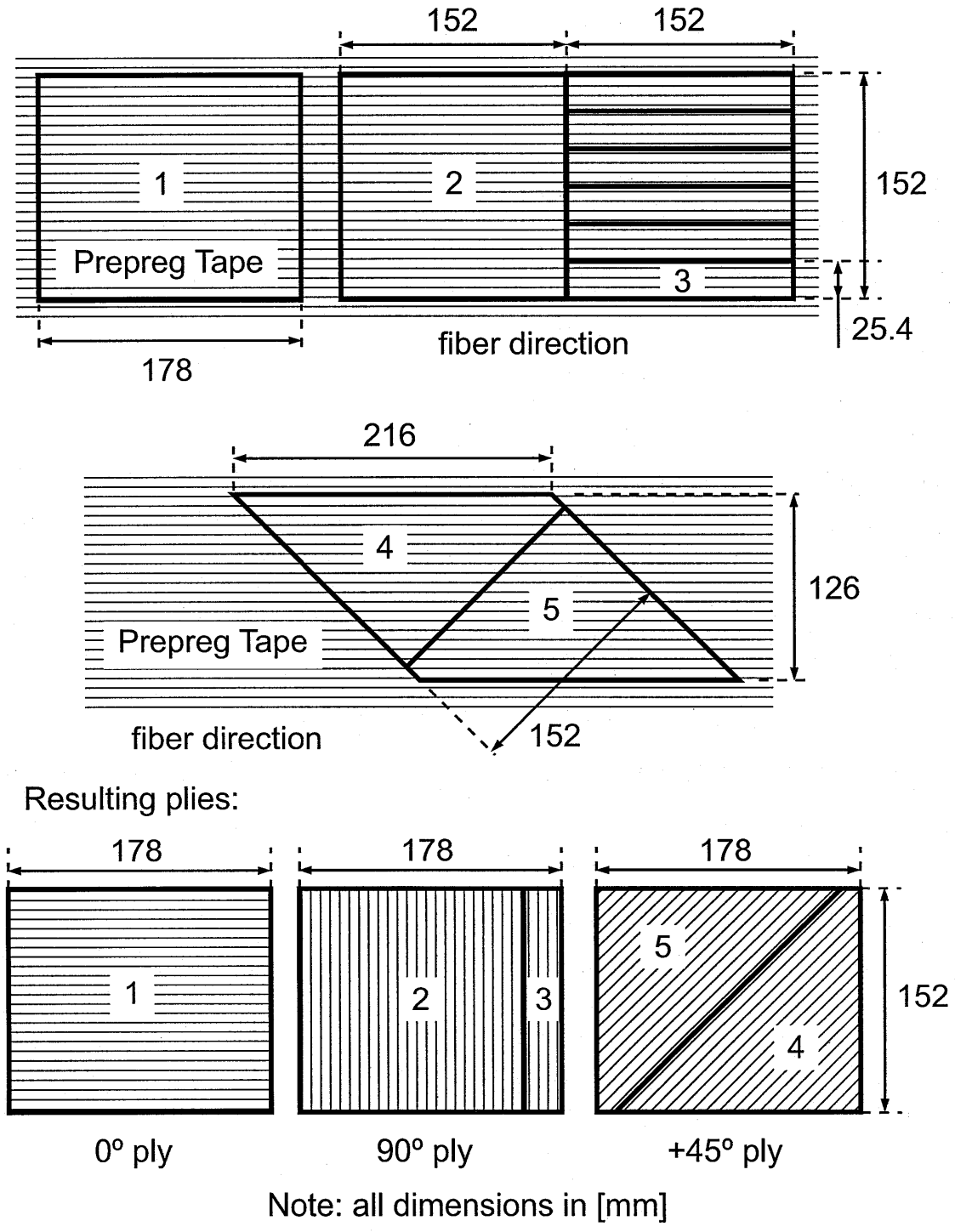

Figure 4.1 Illustration of ply cutting and assembly.

For all laminates in this work, the laminate is relatively thick. Thick laminates can contain more voids than thin laminates, and thus there is a need to eliminate the voids before the curing process by applying a uniform pressure and vacuum on subgroups of plies. This was set at 20 plies for this material. Thus, one first stacks up to only about twenty plies. The arrangement for the application of vacuum on such a sub-laminate is illustrated in Figure 4.2. First, a sheet of nonporous teflon that covers the whole cure plate is taped onto the cure plate with the use of flash tape. Cork dam is then placed and built up on the nonporous teflon sheet. A cork dam is built up by stacking cork tapes to an appropriate height. Cork tape is a strip of cork material with a width of 25 mm and a thickness of 2 mm, with adhesive on one side. The frame made by the dams is of the size as the sub-laminate, and its height is adjusted to be as high as the height of the sub-laminate and top plate added together so that uniform pressure is applied during vacuum. The sub-laminate is placed in the frame made by the dams, and the top plate subsequently is placed on top. A layer of fiberglass is laid on this configuration to provide an airway from the vacuum duct to the plate. Finally, a vacuum bag is placed over the entire assembly and attached to the cure plate by vacuum tape to create a tight seal between the bag and the plate. Each sub-laminate is vacuumed under approximately 710 mm Hg for 10 minutes.

The final step is to stack the sub-laminates into a complete laminate. This is done by using the aluminum jig and removing backing papers on outer layers of each sub-laminate, leaving the backing paper on the two outer ply surfaces. This is similar to the process of stacking a single ply to a sub-laminate as the sub-laminates are stacked in the appropriate sequence.

4.2 Curing Procedures

The preparation for curing begins with the laminate as stacked per the procedures of Section 4.1. The backing paper of the stacked laminate are first removed and peel ply (about 10 mm larger than the plate on three edges and 40 mm larger on the short edge adjacent to the good corner) is placed on both the top and bottom surfaces

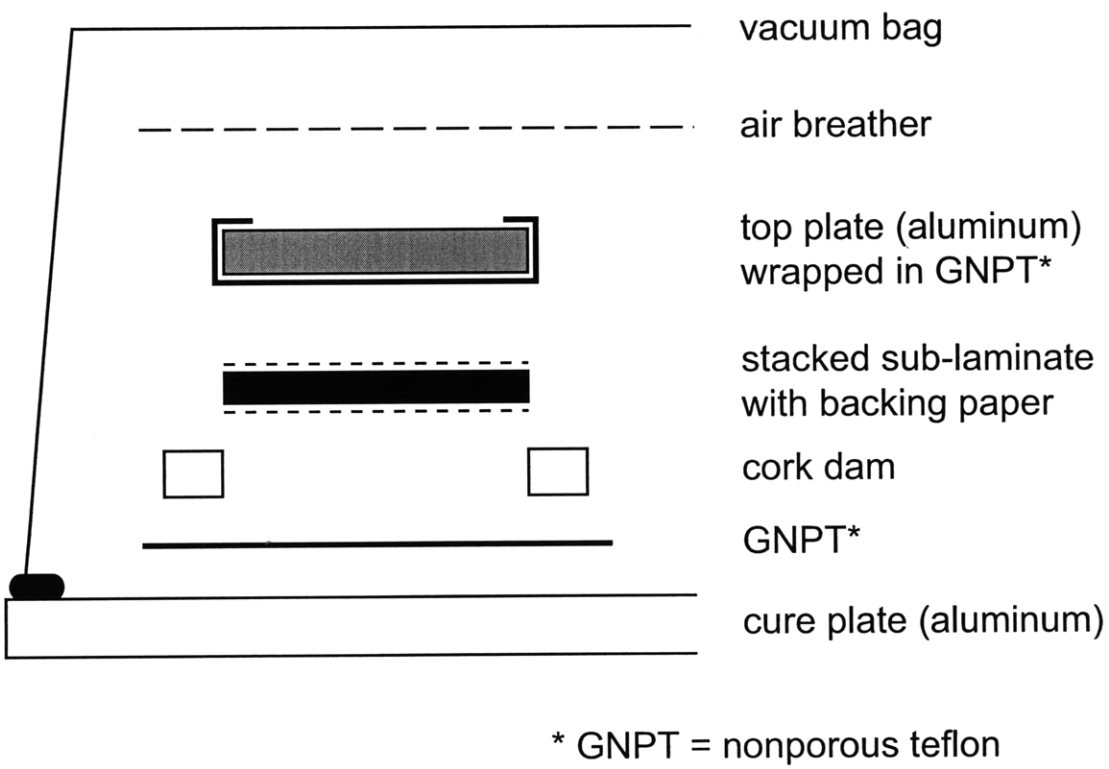

Figure 4.2 Schematic of materials used in sub-laminate vacuuming.

and pressed firmly and smoothly on the laminate. This provides a subtly textured surface when removed after cure. The "good corner" is marked on the peel ply for identification. The laminates are sealed in a vacuum bag and left out for no longer than twenty-four hours before undergoing cure.

The arrangement of the laminate in various curing materials on an aluminum cure plate is illustrated in Figure 4.3. Nonporous teflon (GNPT) lies between the laminate and the cure plate, the dam, and the top plate to prevent resin from adhering to them. A sheet of nonporous teflon that covers the whole cure plate is first taped onto the cure plate with the use of flash tape. Then the aluminum and cork dams are placed and built up on the nonporous teflon sheet. The aluminum dam establishes the 90° corner where the "good corner" of the laminate rests, and the cork dams establish the corner diagonally from this. The frame made by these dams is of the size of the laminate to be cured, and its height is adjusted to be as high as the height of the laminate and top plate added together so that uniform pressure is applied during vacuum. The height of the aluminum dam is adjusted by adding cork tape on the aluminum dam, as necessary. A sheet of porous teflon is placed on top of the laminate, followed by an aluminum top plate covered by nonporous teflon. The porous teflon and the top plate are the same planar size as the laminate. A sheet of nonporous teflon that is large enough to cover the laminate, porous teflon, and the top plate stacked together is prepared. The stack is placed in the center of this and the edges of the nonporous teflon are wrapped onto the top of the aluminum plate and attached tightly with flash tape. The "good corner" is marked on the nonporous teflon for identification. This group is subsequently put inside the frame of the dams, placing the "good corner" against the corner made by the aluminum dam. The entire cure plate is covered by a sheet of porous teflon of a size that covers the plate and the dams. Subsequently, a layer of fiberglass is placed on this configuration to provide an airway from the vacuum duct to the plate. Finally, a vacuum bag is placed over the entire assembly and attached to the cure plate by vacuum tape to create a tight seal between the bag and the plate.

A vacuum check is performed before proceeding to the curing process. This is done

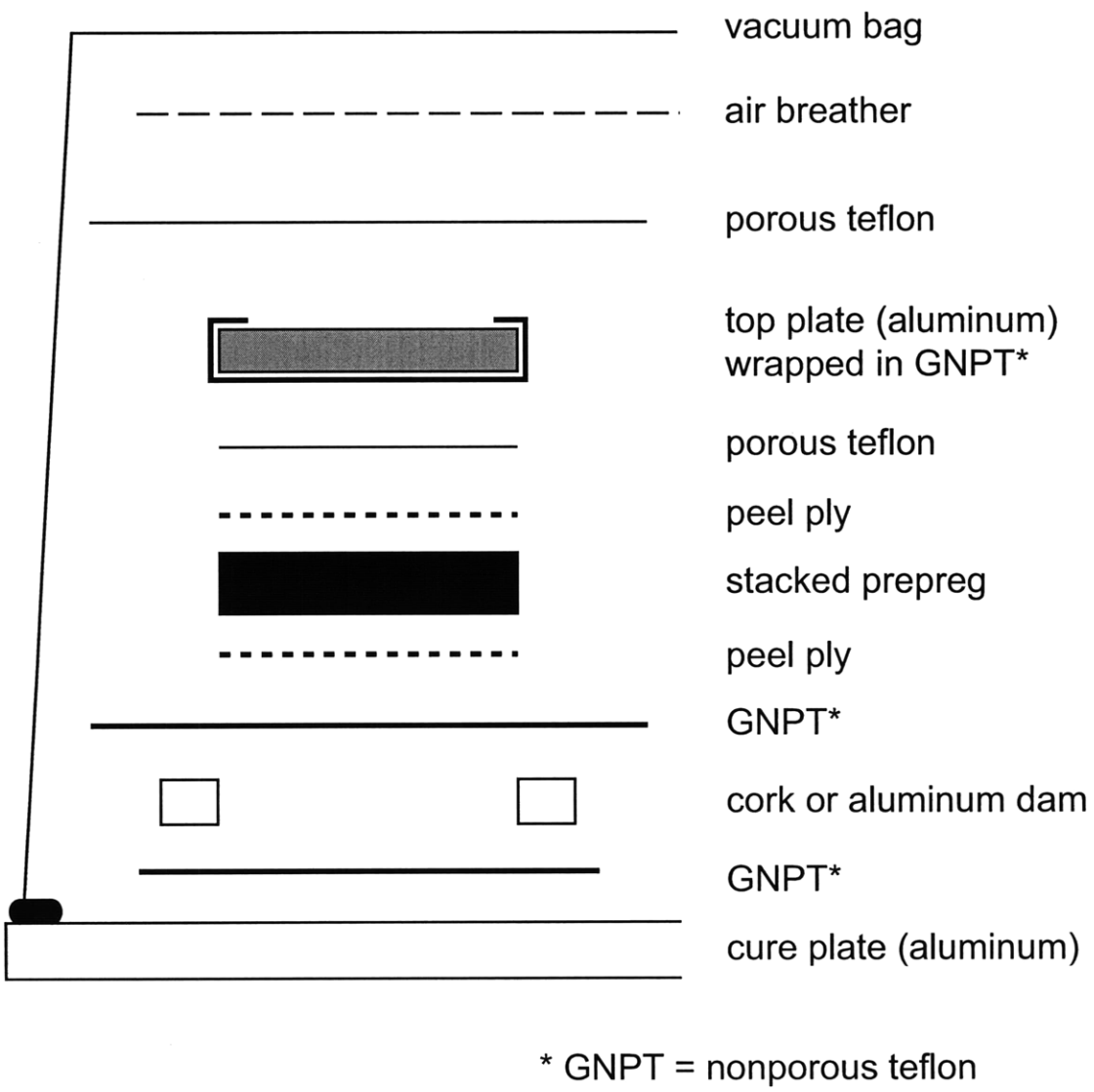

Figure 4.3 Schematic of materials used in cure.

by applying a vacuum of approximately 710 mm Hg to the plate and then shutting off the vacuum pump. The seal is considered sufficient if less than 130 mm Hg is lost after five minutes has passed. If the seal is unsatisfactory, any leaks in the vacuum bag and/or tape are found and repaired. When a sufficient seal is achieved, the cure plate is placed inside the autoclave.

Once the autoclave is closed tightly with the cure plate inside, a vacuum of 710 mm Hg or higher is applied. The curing is performed as per the cycle recommended by the manufacturer for P707AG-15. Revision was made for autoclave curing time as it was found that a longer time was necessary for the center of thick laminates to reach the desired temperature and maintain the required duration at cure temperature. Measurement of temperature at the center of the laminate using thermocouples showed that approximately 30 minutes was necessary for the entire laminate to reach the required temperature as set for the autoclave.

The overall curing cycle resulted as follows. The temperature of the autoclave is first raised to 82°C. After dwelling at this temperature for 30 minutes, the autoclave is raised to the curing temperature of 132°C. After 150 minutes at this temperature (inclusive of the 30 minutes noted previously), the cure cycle is completed by decreasing the autoclave temperature at the rate of 2-3°C per minute to about 65°C by the use of a water cooling system. The autoclave atmosphere is then cooled to the room temperature by opening the door of the autoclave. Such a cycle is illustrated in Figure 4.4. A vacuum of 710 mm Hg is maintained throughout the cure cycle. After cooling, the laminate is removed from the vacuum bag and peel ply layers are peeled off the cured laminate. The thickness of the laminate is measured with a micrometer at the corners and at the center of each side to confirm that the thickness is uniform and that the value lies in the range calculated from the nominal single-ply thickness of the manufacturer (t_{ply}) of 0.15 ± 0.01 mm.

In this work, three plates (noted as Plates B, C, and D) with the "standard" layup, $[\mp 45/0/90]_{10S}$ (80 plies), and one plate (noted as Plate 30-A) with the "alternate" layup, $[\mp 30/0]_{13S}$ (78 plies), were manufactured and the specimens were cut from these. The measured values and the average value of the thickness for each laminated

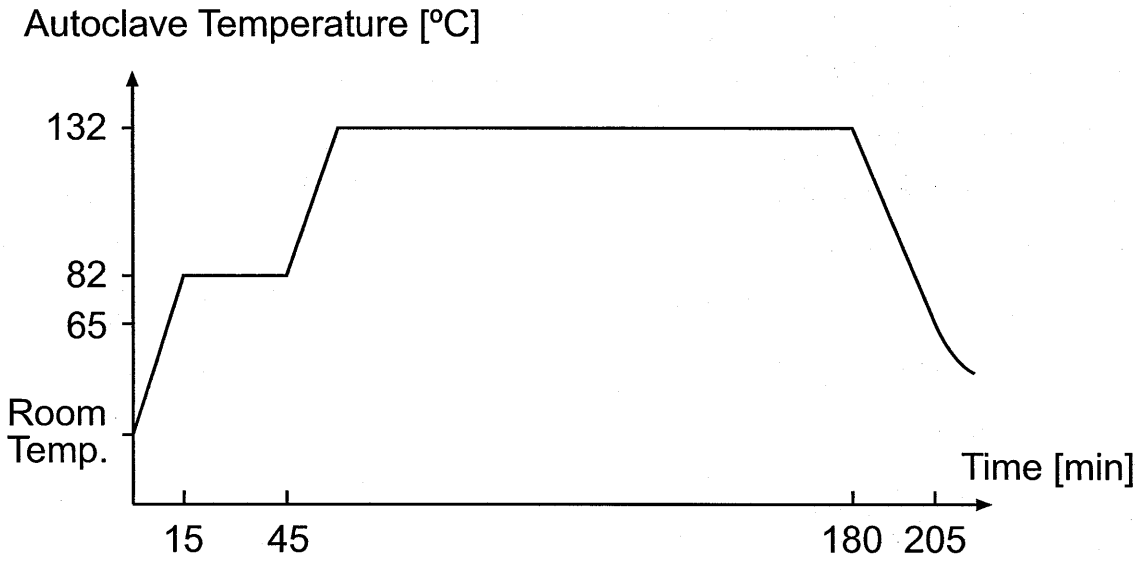

Figure 4.4 Illustration of temperature cure cycle for P707AG-15 prepreg material.

plate are presented in Table 4.2. The nominal thickness for an 80-ply and 78-ply laminate are 12.16 mm and 11.89 mm, respectively. The average thickness per ply for Plates B, C, D, and 30-A calculated from the measurements made are 0.16 mm $\pm 0.4\%$, 0.15 mm $\pm 0.6\%$, 0.16 mm $+0.5, -0.2\%$, and 0.15 mm $\pm 2\%$.

4.3 Machining Procedures

Machining of the specimens is a two-step process. The first step is to cut the cured plate into blocks of the approximate specimen size. This step is done with a 254 mm diameter, water-cooled, 220-grit diamond cutting wheel rotating at 1100 rpm. The laminate is fed on a table at a controlled rate of 279 mm per minute. The specimens are aligned for cutting by placing an edge with known alignment against a reference bar that is fixed on the milling table. This bar is set to be parallel to the cutting blade. To provide extra spacing for cuts of different widths, a spacer (an aluminum plate or a glass-fiber plate) of appropriate geometry and alignment are placed between the reference bar and the laminate plate to be cut. For the first two cuts, sides adjacent to the "good corner" of the cured laminate are set against the reference bar with an appropriate spacer. With this setup, 5 mm of those edges are trimmed off. The remaining two edges of the plate are subsequently trimmed off 5 mm, using the resulting edges from the previous cut. Next, the desired width dimensions are cut by aligning the good corner of the laminate to the reference bar, and cutting off a part with the desired width. Note that this piece has the "good corner" of the laminated plate. Here, the "good corner" is effectively transmitted to the corner of the remaining laminated plate, since the new edge of the laminate is parallel to the edge that was adjacent to the original "good corner". This new "good corner" can be used as a reference, and this continues throughout the cutting process. Finally, the desired length is cut by measuring the length from the good corner and cutting across the width direction at that point, again aligning the good corner with the reference bar.

After this basic cutting step, a second step of machining is performed to bring the

Table 4.2 Layup and thickness of laminated plates

Plate	Layup	Measured Thickness [mm]				Average and variation [mm]
B	$[\mp 45/0/90]_{10S}$	12.84	12.87	12.94	12.91	12.89 ± 0.05
		12.87	12.90	12.84	12.94	
C	$[\mp 45/0/90]_{10S}$	11.86	11.94	11.96	11.80	11.88 ± 0.08
		11.82	11.92	11.82	11.94	
D	$[\mp 45/0/90]_{10S}$	12.63	12.62	12.62	12.63	$12.65 + 0.07, -0.02$
		12.72	12.62	12.70	12.63	
30-A	$[\mp 30/0]_{13S}$	11.52	11.90	11.52	11.82	$11.71 + 0.20, -0.19$
		11.56	11.91	11.54	11.90	

specimen to final dimensions and needed alignment. This finer milling was performed on a 3-axis milling machine with a Crystallume 4-flute, 2200-grit diamond-coated, square-end mill of 0.375 in (9.53 mm) diameter with a tolerance of +0.0005 in and -0.0010 in. Nomenclature used in reference to specimen faces and axes is shown in Figure 4.5. During the curing process, $\pm x_3$-faces are pressed against flat surfaces of aluminum plates. The $+x_3$- and $-x_3$-faces are checked for being parallel by measuring laminate thickness at the center of each edges of the specimen using a micrometer. The faces were considered parallel if thicknesses varied by less than 0.2 mm. Any productions exceeding this were not used. In addition to the two x_3-faces, one of the x_2-faces is chosen by placing each of the x_2-faces on a known flat surface and determining which is more flat by checking the gap between the flat surface and the x_2-face by eye and by rocking the specimen. In the description that follows, it is assumed that the $+x_2$-face is initially chosen. If the $-x_2$-face is initially chosen, the faces in the following description need to be changed appropriately.

Two spacers of the same height are placed on the working table of the milling machine (referred to as horizontal). The $+x_2$-face is placed on the spacers, and this makes the $+x_2$-face parallel to the working table. The x_3-faces are then gripped tightly with grips that are set to be perpendicular to the working table. With this setup, the $-x_2$-face is milled by the square-end of the tool with a rotation rate of 1000 rpm, feeding in the x_1-direction with a speed of 5 mm/sec or less so that it is parallel to the working table. Following this, the grip is released and the specimen is flipped over, and the now-machined $-x_2$-face is placed on the spacers. The specimen is gripped again and the $+x_2$-face is milled similarly. A caliper is used to measure the width of the specimen, and milling is repeated until the width is adjusted as designed. With this process, two parallel x_2-faces are produced perpendicular to the x_3-faces. The process then proceeds to the x_1-faces. The $-x_3$-face is aligned with the table and the x_2-faces are gripped. The x_1-faces are then milled in a similar sequence by the side of the tool feeding in the x_2-direction. A caliper is used to measure the length of the specimen, and milling is repeated until the length is adjusted as designed.

Grooving is performed on a 3-axis milling machine with a Crystallume 4-flute,

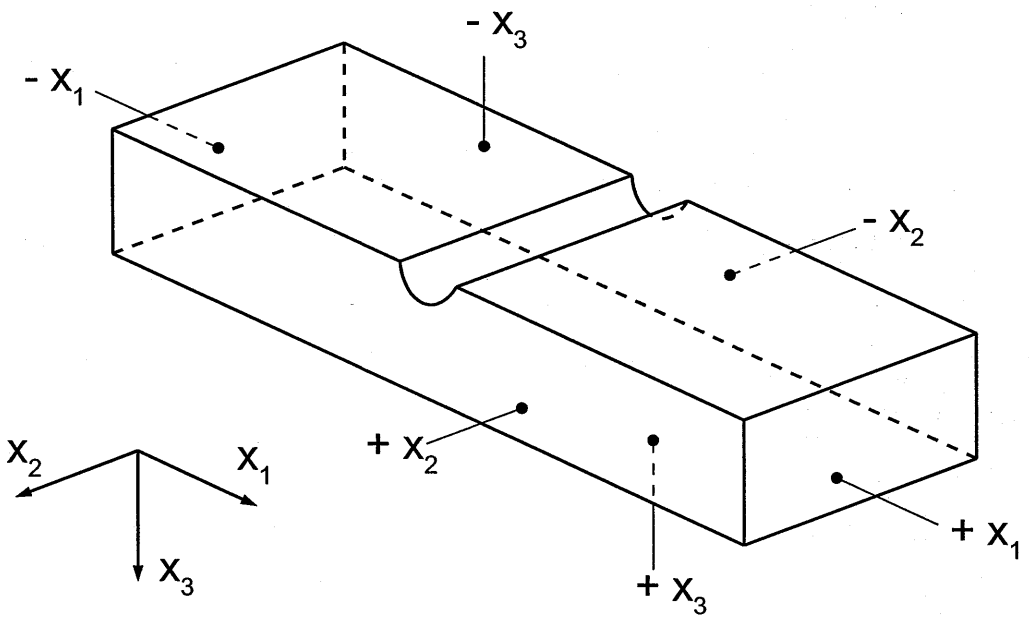

Figure 4.5 Illustration of specimen axis and surface nomenclature.

2200-grit diamond-coated, ball-end mill of 0.250 in (6.35 mm) diameter with a tolerance of +0.0005 in and -0.0010 in. This is equal to the designed groove diameter of 6.35 mm. The centerline of the specimen, where the groove is to be made, is marked beforehand using a caliper and a marker. The $+x_3$-face is placed on the spacers to the working table. The groove is machined along the marked line to the desired depth, h_{grv}, by raising the table to the same value as h_{grv}. The groove is milled by feeding the tool in the x_2-direction with a rotation rate of 1000 rpm, and a speed of feed 5 mm/sec or less.

Chapter 5

GENERAL TESTING PROCEDURES

Throughout this work, test configurations were changed several times and details of the test procedures differ for each configuration. However the strain gage placement procedure, the data acquisition system, general control of the testing machine, and the damage evaluation procedure are basically the same for all cases. These items are described in this chapter, with details that differ for each test configuration described in the following chapters dealing with the specific configurations.

Strain gages were used to measure strain on the specimens. The strain gages used were Vishay Micro-Measurements & SR-4 General Purpose Strain Gages EA-06-031DE-120. A sample gage is shown in Figure 5.1. The gages have a gage area of 0.79 mm by 0.79 mm. This type of gage outputs reliable strain values up to a magnitude of 30,000 μstrain (3 % strain). However, strain data was recorded beyond this point of reliability up to values of 40,000 μstrain (4 % strain). The strain gages were bonded on the specimens using a cyanoacrylate adhesive, Vishay Micro-Measurements M-Bond 200, with 200 Catalyst-C. The gages were applied at the locations designated for each specimen. For gages that require greater accuracy in position, a microscope was used to check that the location of the gage to was within 0.5 mm of the designated location. Once attached, copper lead wires were soldered to the terminals of the gage and a terminal strip. Testing with an ohmmeter, it was considered acceptable when

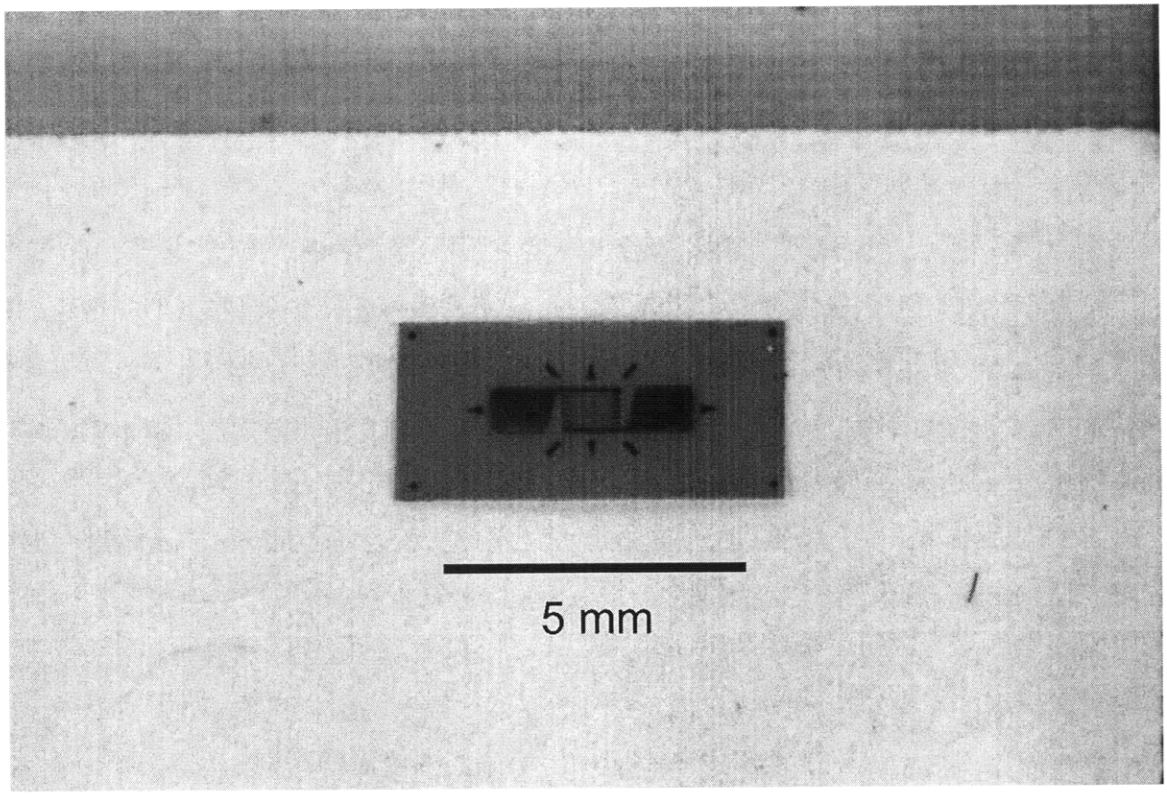

Figure 5.1 Photograph of Strain Gage EA-06-031DE-120.

the resistance of the gage read 120 ± 1 ohm. When unacceptable, gages and wires were checked and repaired or replaced as necessary.

All tests were conducted using a hydraulic uniaxial testing machine. The test fixture used to support the specimen during a test (referred to as the lower fixture) is mounted on the lower head of the machine. A load cell of an appropriate capacity and a fixture for the indenter (referred to as the upper fixture) is mounted on the upper head of the machine. The initial position and placement of the indenter differs for each test configuration and details are provided in the following chapters. By raising the lower head, the fixture moves up, thereby also raising the specimen. A simple illustration of this overall arrangement is given in Figure 5.2.

A computer data acquisition system is used to record load and stroke from the testing machine, and strain from the strain gages. This system consists of a 16-bit National Instruments A/D data acquisition board model PCI-6031E connected to a Power Macintosh G3 computer. Outputs of the strain gages are amplified by Measurements Group 2310 Signal Conditioning Amplifiers before transferring data to the data acquisition board. LabView 5.0 is used to record the load and stroke of the testing machine, as well as the amplified strain gage outputs. Data is recorded during the test by the acquisition system at a minimum rate of 1 Hz. Specific rates are noted in further detailed descriptions.

The tests are carried out as follows. Fixtures are placed on both the lower and upper heads and their locations are first adjusted by eye. This is followed by a more accurate placement to the closest 1 mm for the final instrumental setup for the rigid backface test configuration. The specimen subsequently is placed on the lower fixture and the strain gages are balanced and zeroed. The load reading of the testing machine is set to 0 kN at this point in order to neglect the weight of the fixtures. After positioning the specimen on the fixture (details provided in following chapters), the lower head is moved up using the "actuator moving" button on the control panel (speed rate of approximately 4 mm/sec) until the upper and lower parts are relatively close. Then the "actuator jogging" button, also on the control panel, (speed rate of approximately 0.8 mm/sec, pushed on and off when precise adjustment is needed)

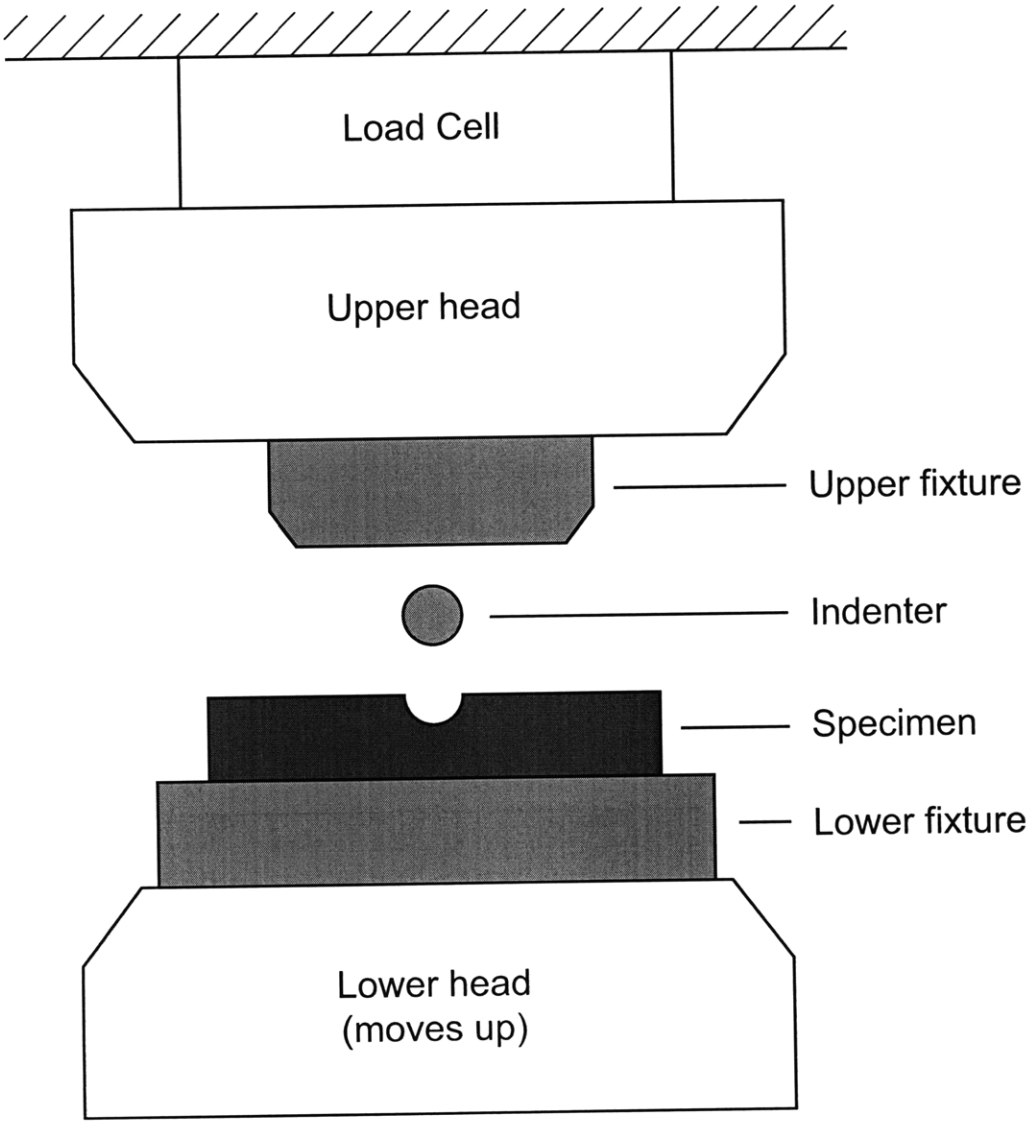

Figure 5.2 Illustration of general test setup.

is used to jog up the lower head until all the parts have contact. This contact is detected by a load change of 0.05 kN (compressive) on the monitor. The testing machine is run in stroke control, with the head speed rate set to an appropriate value for each boundary condition (simply-supported and rigid backface, as described in the chapters for these specific cases). The test is run until the maximum load is reached. This is determined by a sudden load decrease of 2.0 kN or larger, or an obvious failure observed by sound or eye. The "finish" button is pressed on the control monitor to stop the lower head stroke motion. Data acquisition is also stopped at this point. The test is completed by lowering the lower head to its original position.

Damage evaluation is done by visual inspection. The overall appearance of the specimen is recorded by a Nikon D60 digital camera. A Zeiss Axiotech optical microscope with Axiovision is used to examine specimen cross-sections closely. The damaged region was magnified 2X to 20X to identify delaminations, matrix cracks, and fiber damage, and their location.

Chapter 6

INITIAL SPECIMEN

In Chapter 3, the base criteria of the geometric parameters were discussed, with the values of parameters left to be determined. In this chapter, the choice of test parameters and the test configuration for the initial specimens is explained in detail based on these base criteria. This is followed by a presentation of the results for the testing of these specimens, and a discussion of the results.

6.1 Choice of Test Parameters

For the initial specimens, the boundary condition was selected as simply-supported. This is based on the ASTM standard for the short-beam shear test method [31] which was referred to as a guide to initially set the backgrounds for geometric parameters and to establish the test method.

The first geometric parameter to be chosen is the radius of the groove, R_{grv}, the governing geometric parameter. Recalling that one possible application of this structure is a grooved telescopic spar with ball bearings, a practical diameter of 3.18 mm (0.125 in) was chosen. This size is characteristic of the groove radii proposed in the telescopic wing design of Czajkowski, Clausen, and Sarh [6], and also the value chosen in the work of Bastien [12]. With this value, the ball-end mill for grooving is available without custom ordering. Other values of groove radius could be used, but changes in subsequent dimensions, based on the discussion in Chapter 3, would be

necessary.

In Chapter 3, the ratio of the radius of the groove to the indenter was determined to be 1.02. This results in a radius of the cylinder, R_{cyl}, of 3.12 mm (0.123 in). A standard rod in such a dimension is available. This is known as a "letter-size D" rod and was used for all indenter rods.

The groove depth, h_{grv}, was chosen as a test parameter in this work. The basic value for h_{grv} was chosen to be equal to the groove radius, 3.18 mm, so that the cross-section of the groove is a semicircle. For the initial specimens, this value applies to Specimen 5. In order to observe the effect of this parameter, the depth was decreased to one half of this size, 1.59 mm, for Specimen 6.

In Chapter 3, the relationship between the groove depth and the thickness, t, of a specimen was determined to be a ratio of 0.25. From the basic value of 3.18 mm for h_{grv}, this gives a value of aproximately 12.7 mm for the thickness, t. Referring to the data of Table 4.1, the range of thickness per ply for the material, t_{ply}, is 0.15 ± 0.01 mm. Thus, an 80-ply laminate should result in a thickness range of 12.16 ± 1.03 mm. This includes the targeted value of 12.7 mm from the operative criterion. Thus, 80-ply laminates were chosen for Specimens 5 and 6. The laminate is a test parameter, with a symmetric configuration desired. Combined with the target of 80 plies, this results in a laminate configuration of $[\mp 45/0/90]_{10S}$.

The width should be under twice the value of the thickness. With the thickness around 12.7 mm, this results in a desirable value of width, w, of 25.00 mm. For simply-supported boundary conditions, the criterion for the test-span length of the specimen, L_{span}, was presented in Chapter 3 as this being greater than or equal to eight thicknesses ($8t$). An extra margin of one thickness was added to each side to ensure that the interference of stress around the support points with the stress around the groove is negligible. Thus, the test-span length and the specimen length were chosen as L_{span} of 130.0 mm, and L of 165.0 mm. These are approximately 10 and 13 times the thickness. This leaves a distance of $1.5t$ hanging from the center of the support on each side. An illustration of the specimen for the simply-supported test configuration is shown in Figure 6.1.

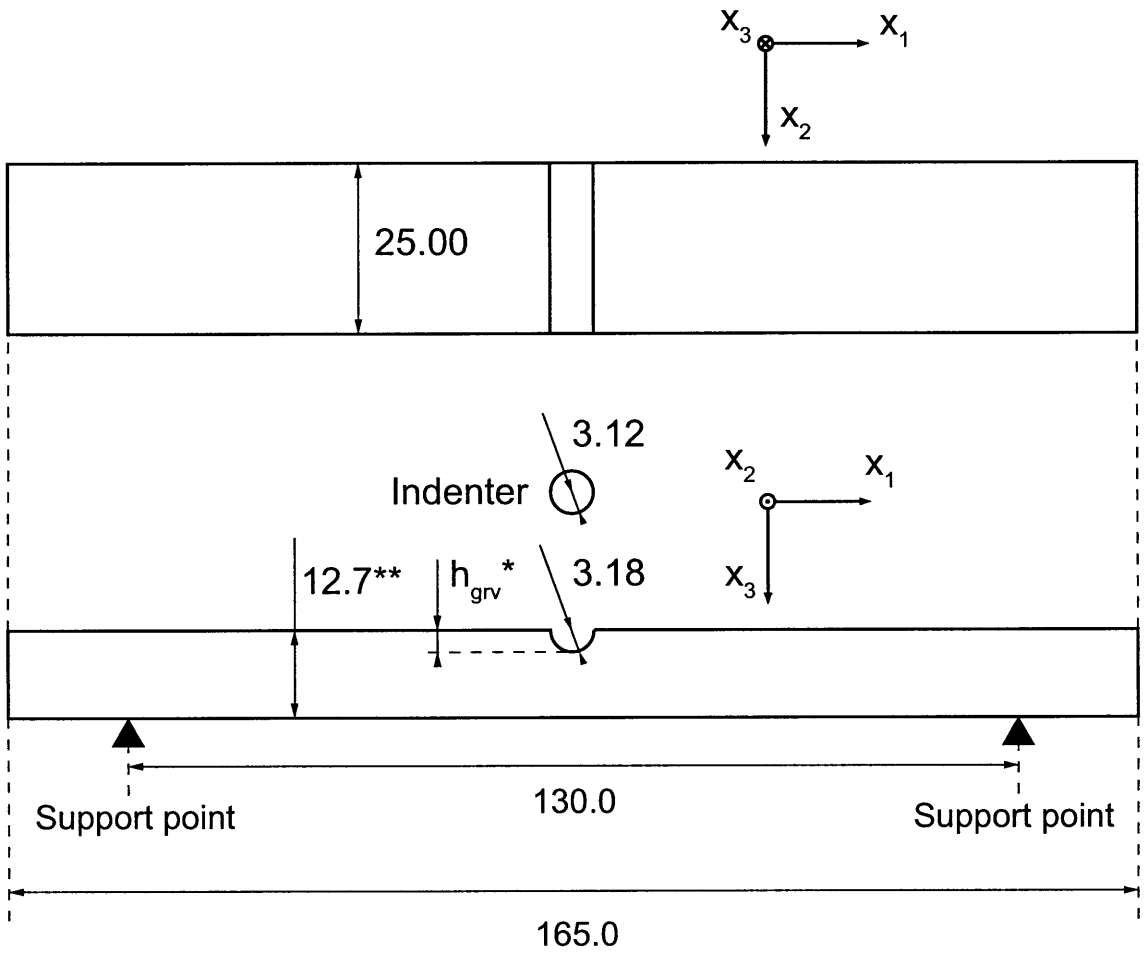

Notes: All dimensions in [mm]
Figure to scale except for the following:
*h_{grv} : test parameter
**thickness : designated value -- differs by laminate

Figure 6.1 Illustration of a specimen for simply-supported test configuration.

6.2 Test Configuration

The manufacturing procedures are explained in Chapter 4. For the initial specimens, refinement machining of the faces of the specimens, which is included in order to obtain the appropriate parallel/perpendicular alignment of the faces, was not performed. Specimens 5 and 6 were cut out from laminate Plate B using the cutting wheel, and further processing proceeded directly to the grooving with a ball-end mill. In this initial work, it had not been expected that the tolerance of the faces would have a large effect on the response of the specimen as demonstrated by the initial results and shown in the subsequent sections.

Before the test, the geometric parameters t, w, and L were measured. The thickness was measured using a micrometer, with an accuracy of 0.01 mm, near the groove at 4 different points. The average value was recorded. The width was measured using a caliper, with an accuracy of 0.01 mm, near the groove at 2 different points. The average value was recorded. The length was measured using a ruler with an accuracy of 0.5 mm.

Strain gages were placed on the $-x_3$ face of the specimen near the groove in locations illustrated in Figure 6.2. The numbers in the figure indicate the number used for identification of the gages. These gages were placed in these locations with a purpose of measuring the strain around the groove in order to determine if the specimen is deforming uniformly along the x_2-axis. This is done by comparing the strain from gages that have the same x_1-coordinate (i.e. gages 1, 2, and 3; and gages 4, 5, and 6).

All the general test procedures explained in Chapter 5 are performed unless noted. A hydraulic servo-controlled testing machine, Instron model 1332, was used for the initial set of specimens. A small aluminum plate was gripped in both the upper and lower grips prior to the test, with a pressure of 3000 psi or more, to prevent the relative movement of the heads. The lower test fixture consisted of a steel I-beam with two rods each on a block. These rods serve as the support points. The I-beam has a thickness of 7.8 mm throughout, a width of 75 mm, and a height of 130 mm.

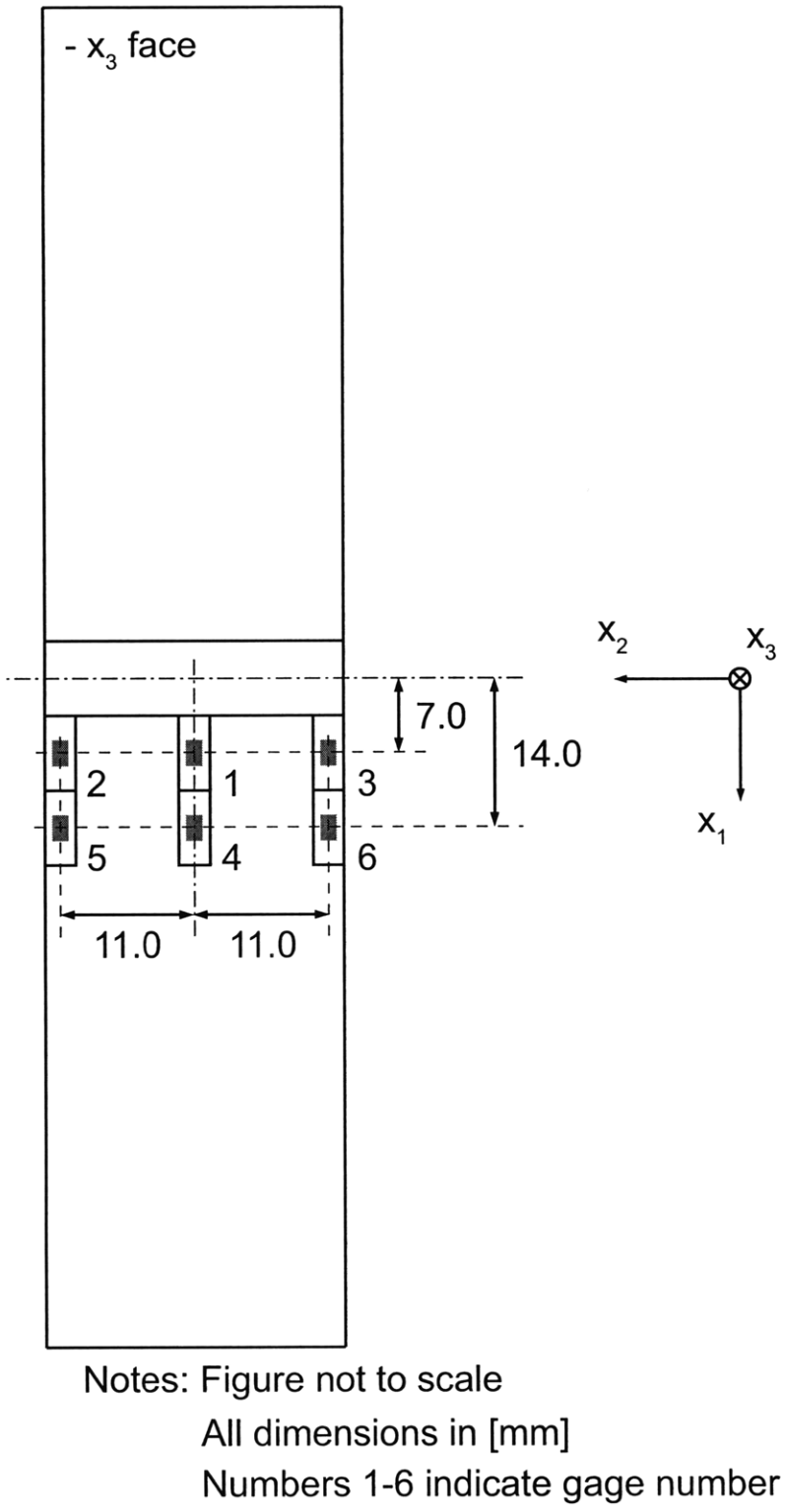

Figure 6.2 Strain gage positions for simply-supported test specimens (Specimens 5 and 6).

The rods have a length of 90 mm and a diameter of 10.0 mm. The distance between the support points can be adjusted and then fixed by tightening bolts that are part of the blocks. For the current work, the distance was adjusted to 130.0 mm using a ruler with an accuracy of 0.5 mm, and then fixed. A line that is parallel to the two rods is marked on the centerline of the fixture for a reference of the x_2-axis. The lower fixture is then placed on the lower head and centered by aligning the centers of the fixture and the head by eye with the aid of a ruler with an accuracy on the order of 1 mm.

The indenter has a length of 27.0 mm. W-1 alloy steel was initially chosen as the material for the indenter. Double-sided tape is put on both the top and bottom surfaces of the steel-plate upper support. The indenter is attached to the center of the bottom surface of the upper support via this tape with their 1-directions aligned. This is done by holding the upper support by hand, and the alignment is done by eye. This group is placed on the lower fixture with the longitudinal direction of the indenter aligned by eye with the centerline marked on the lower fixture. The lower head of the test machine is brought up using the "actuator moving" button on the control panel until the top surface of the upper support and the upper head have a firm contact of a load of 1.0 kN. The two heads are subsequently set apart using the "actuator moving" button, with the upper support with the indenter having been attached onto the top head with the aid of double-sided tape.

The specimen is aligned by eye on the lower support by referring to the supporting points that were marked previously on the specimen with an accuracy of 0.5 mm. The resulting overall configuration is illustrated in Figure 6.3. Finally, the lower head is moved upward until the specimen has contact with the indenter, following the procedures described in Chapter 5. The stroke speed-rate was set to 1.00 mm/min (compressive), because the short-beam shear test standard ASTM D2344/D2344M [31] was referred to as a model and a guide for establishing this test procedure. This stroke speed-rate was chosen as the standard value in that test standard.

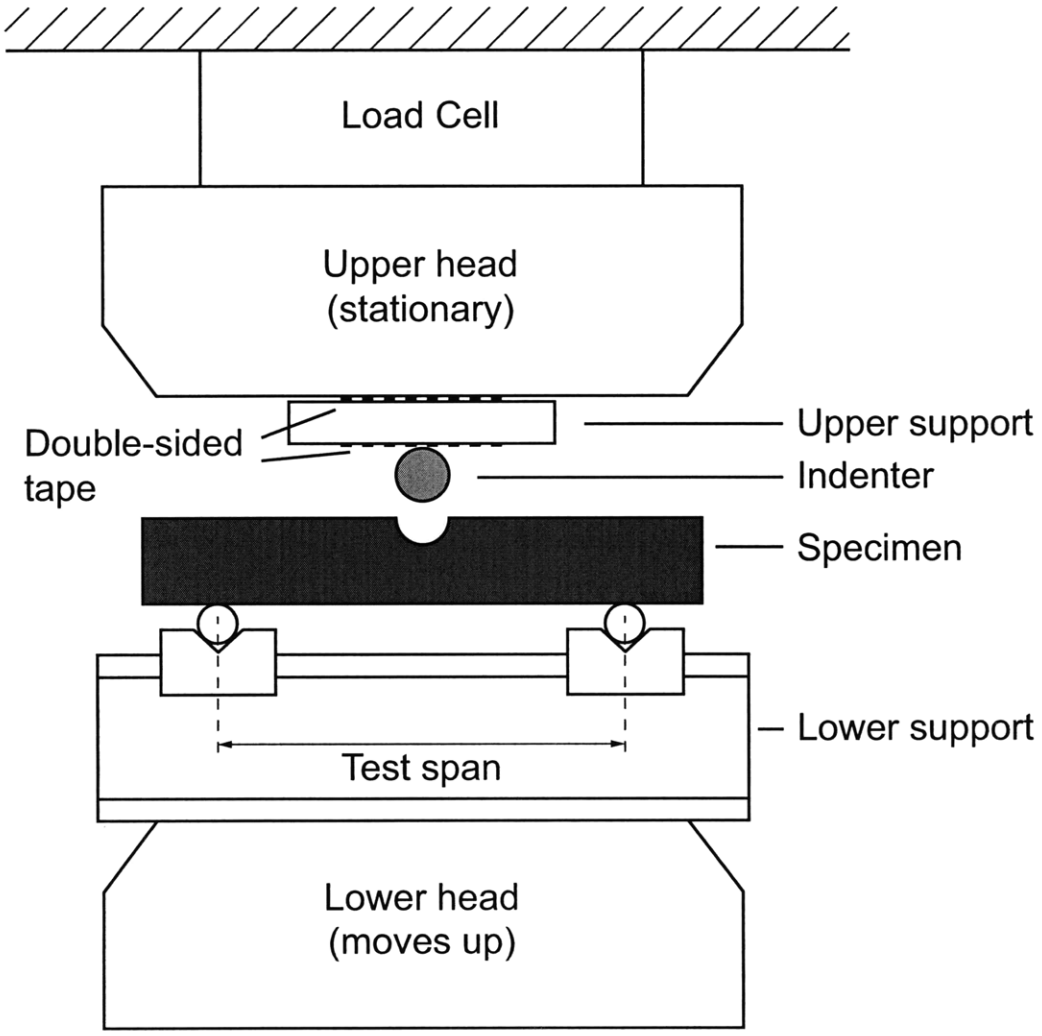

Figure 6.3 Illustration of simply-supported test setup.

6.3 Results

The load-versus-stroke plots, load-versus-strain plots, and photographs of the specimens after failure are shown in Figures 6.4 through 6.11 for the two initial specimens, Specimens 5 and 6. Values of the load, stroke and strain in thee figures are all in compression, and presented as positive. The photographs capture the region around the groove for both the side view and the failure surface view. For the failure surface view photos, the top piece (the piece with the $-x_3$ face) is flipped over. Axis directions are shown for reference. Gage 5 for Specimen 5 and Gage 2 for Specimen 6 output tensile values with random jumps in values that were not proportional to the load. This indicates a problem with the gage connection and the data are therefore considered invalid, and are omitted from the plots.

The measured geometric values of the specimens, failure load P_{f}, and the location of delaminations are given in Table 6.1. The failure load, P_{f}, is defined as the maximum load measured during the test. The location of delamination is notated by the two plies that determine the interface, separated by a slash. A ply is notated with the ply orientation followed by the ply set number counted from the top of the plate ($-x_3$ face) in parentheses (e.g., $-45°$ (6) indicates the $-45°$ ply in the 6th ply set from the top of the plate).

Both specimens had a delamination failure between plies 0°(10) and 90°(10). This is an interface that is a distance of 0.15 mm away from the midplane, which is the thickness of one ply. This indicates that the failure in both cases is likely due to transverse shear at that interface as is designed for the configuration of a short beam shear specimen [31]. Further evidence pertinent to this hypothesis using the simple-beam theory analysis as per ASTM D2344 [31] follows.

The thickness under the groove is used as the important thickness for short beam shear calculation:

$$t_{\mathrm{sb}} = t - h_{\mathrm{grv}} \tag{6.1}$$

Using this thickness, Equation 1 as presented in the ASTM D2344 standard [31] is

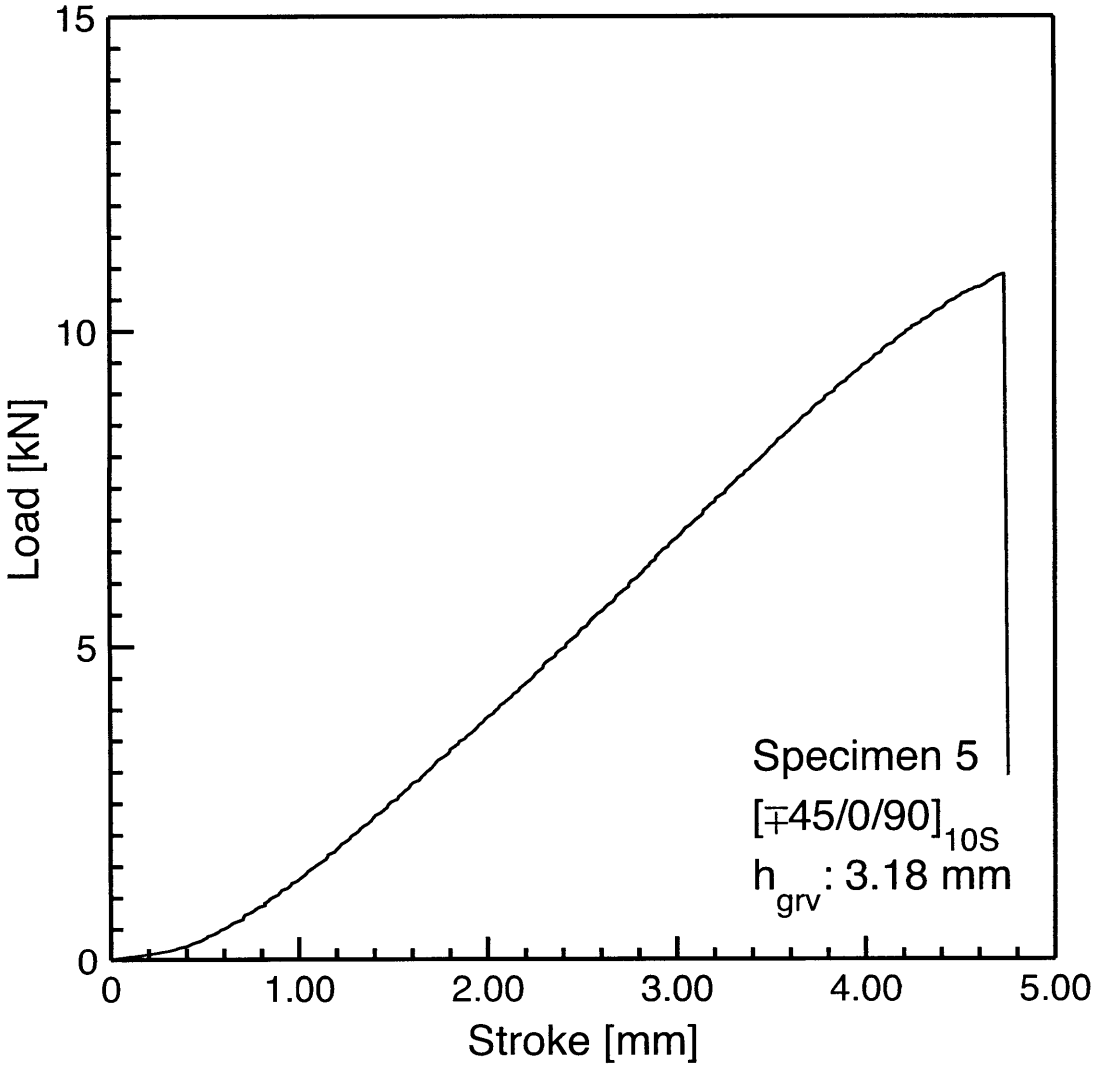

Figure 6.4 Load vs. stroke plot for Specimen 5: layup $[\mp 45/0/90]_{10S}$ with $h_{\text{grv}} = 3.18$ mm.

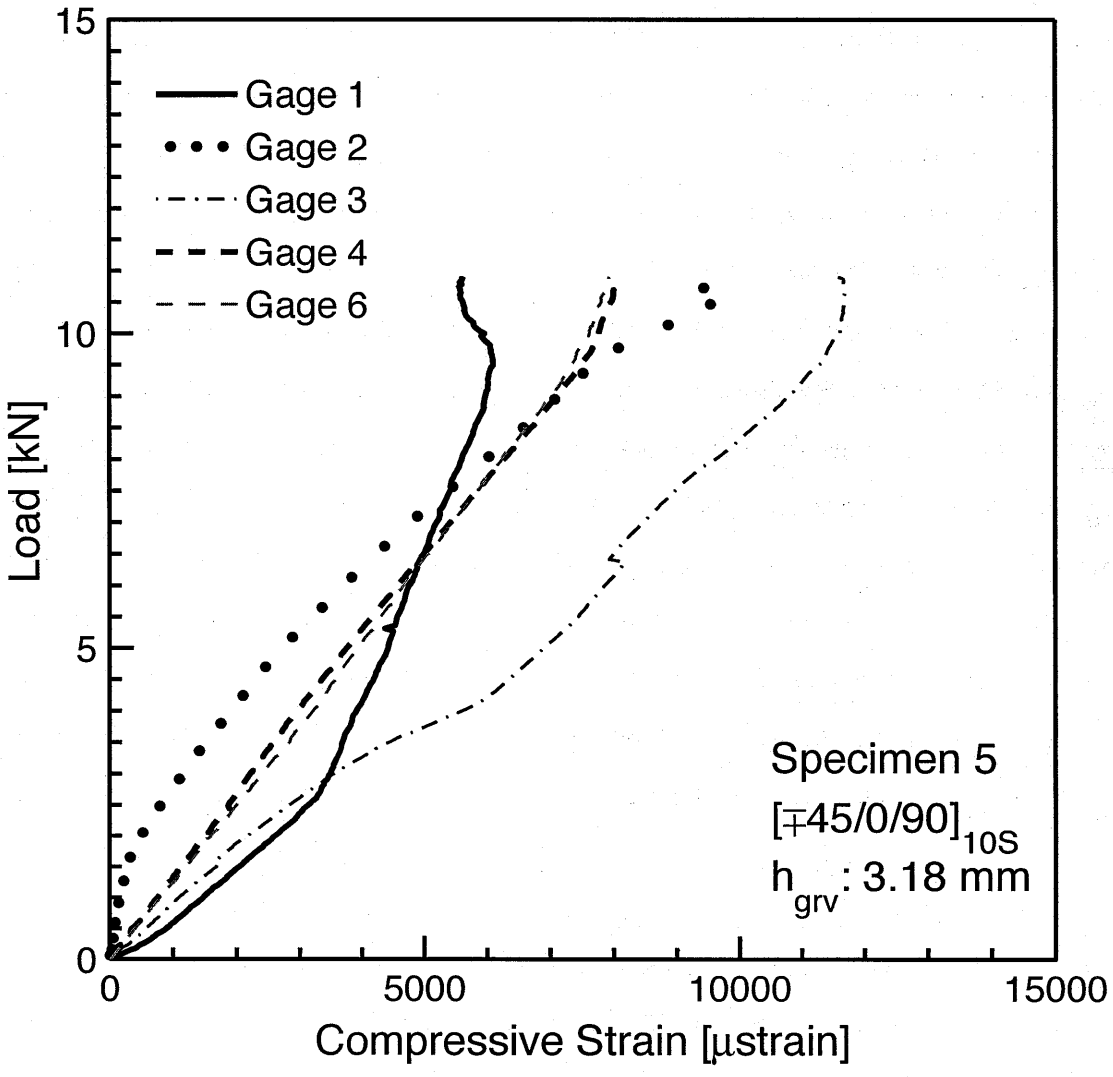

Figure 6.5 Load vs. compressive strain plot for Specimen 5: layup $[\mp 45/0/90]_{10S}$ with $h_{\text{grv}} = 3.18$ mm.

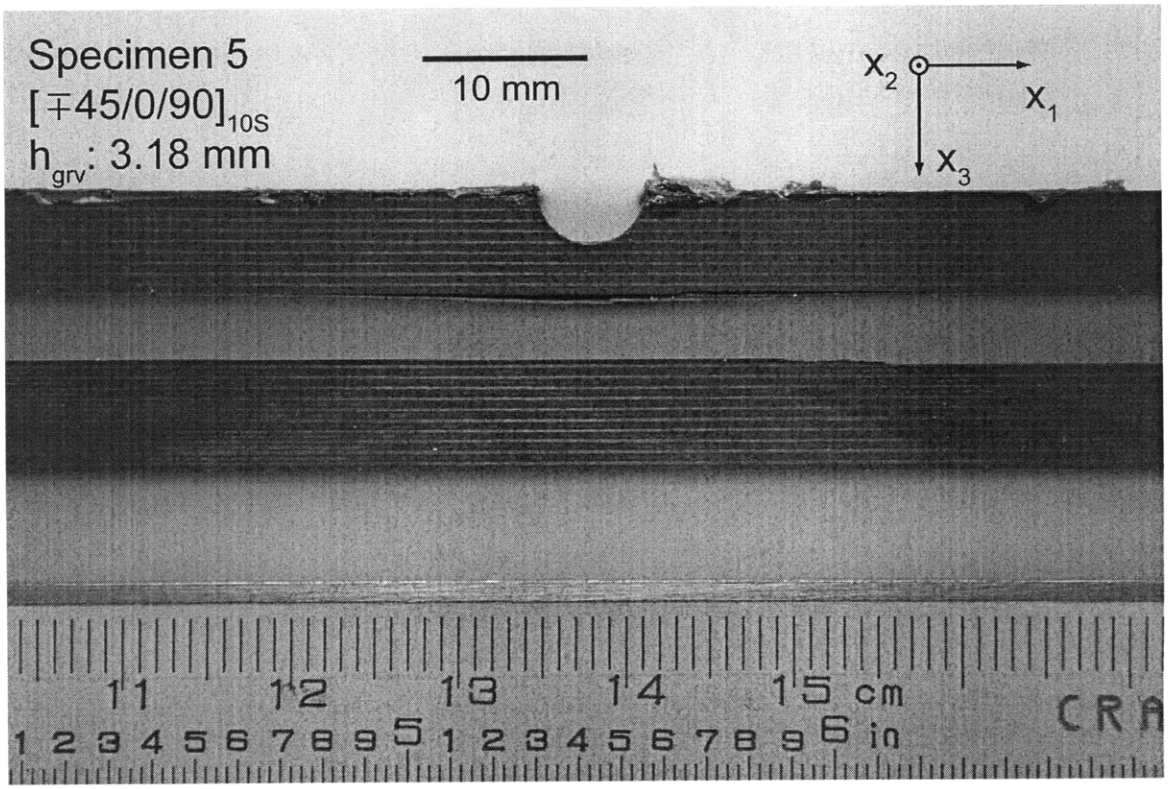

Figure 6.6 Sideview photograph after failure of Specimen 5: layup $[\mp 45/0/90]_{10S}$ with $h_{\text{grv}} = 3.18$ mm.

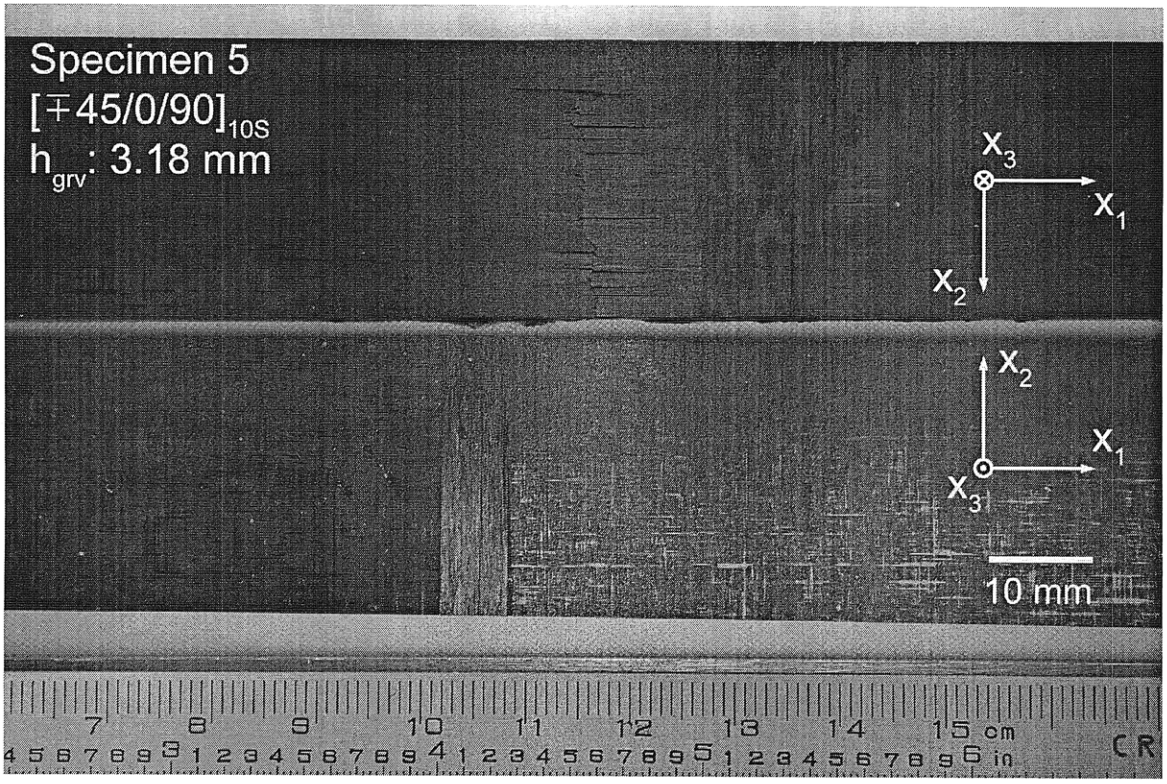

Figure 6.7 Failure surface view photograph, with top piece flipped, after failure of Specimen 5: layup $[\mp 45/0/90]_{10S}$ with $h_{\text{grv}} = 3.18$ mm.

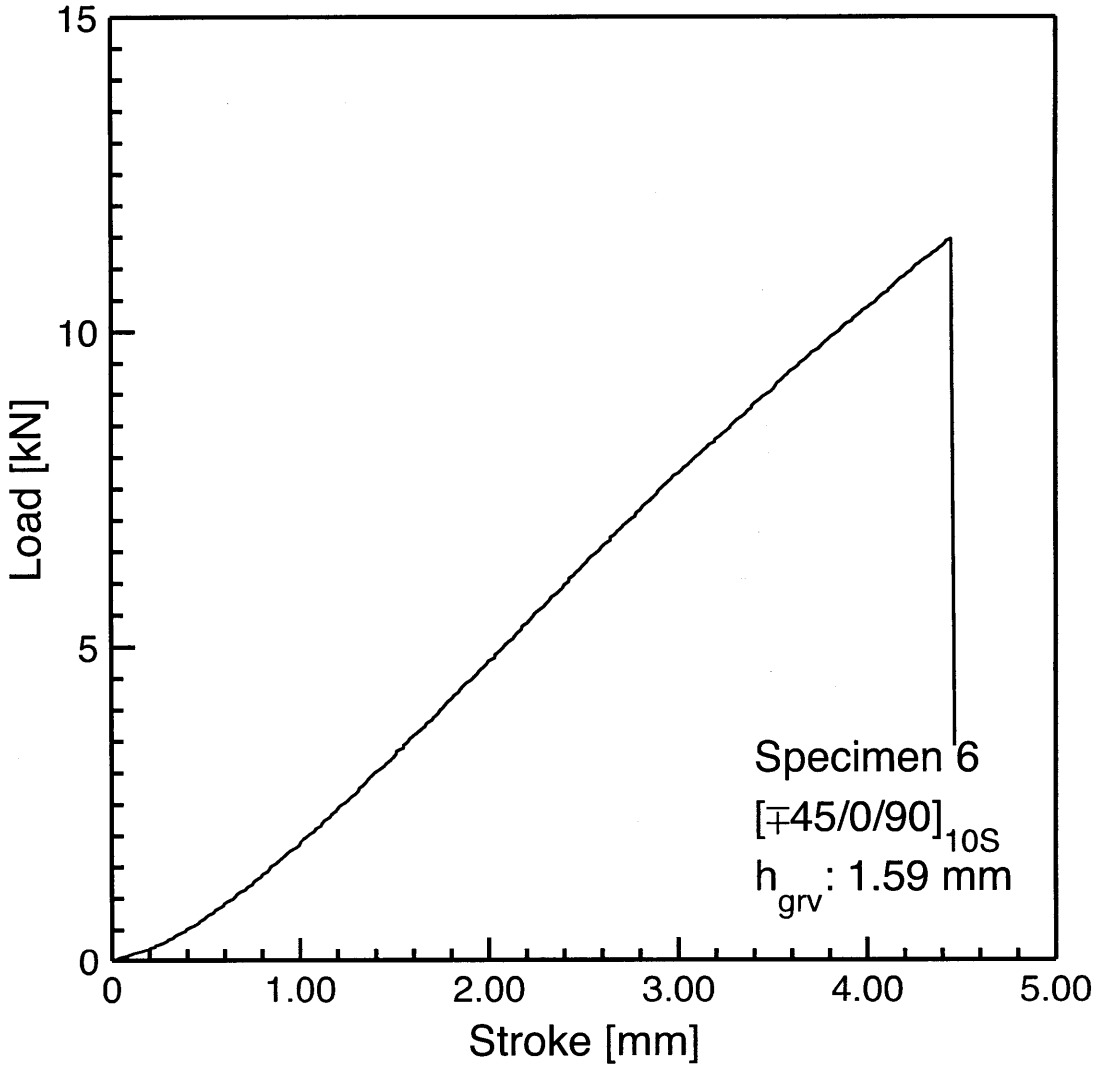

Figure 6.8 Load vs. stroke plot for Specimen 6: layup $[\mp 45/0/90]_{10S}$ with $h_{\text{grv}} = 1.59$ mm.

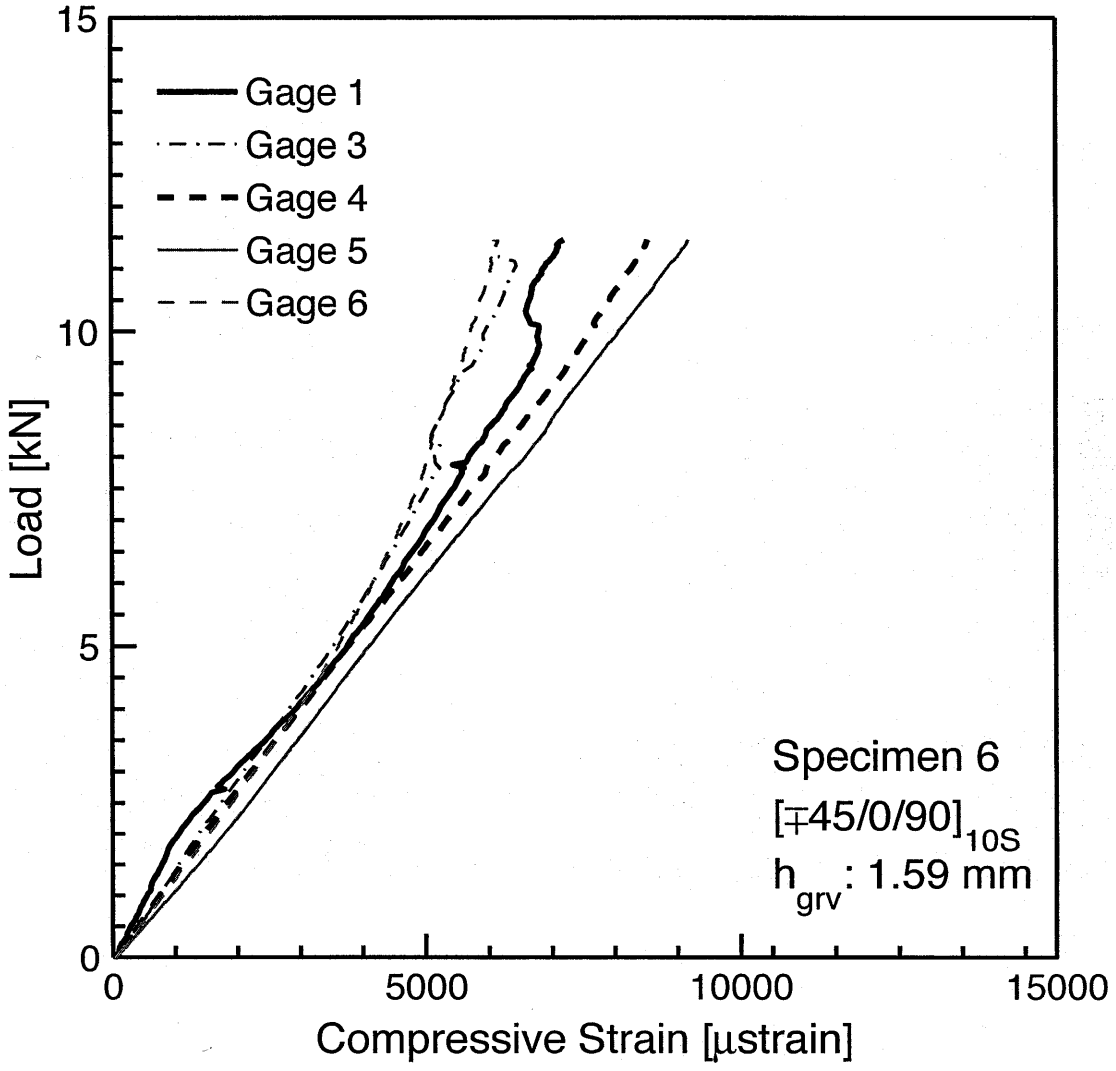

Figure 6.9 Load vs. compressive strain plot for Specimen 6: layup $[\mp 45/0/90]_{10S}$ with $h_{\text{grv}} = 1.59$ mm.

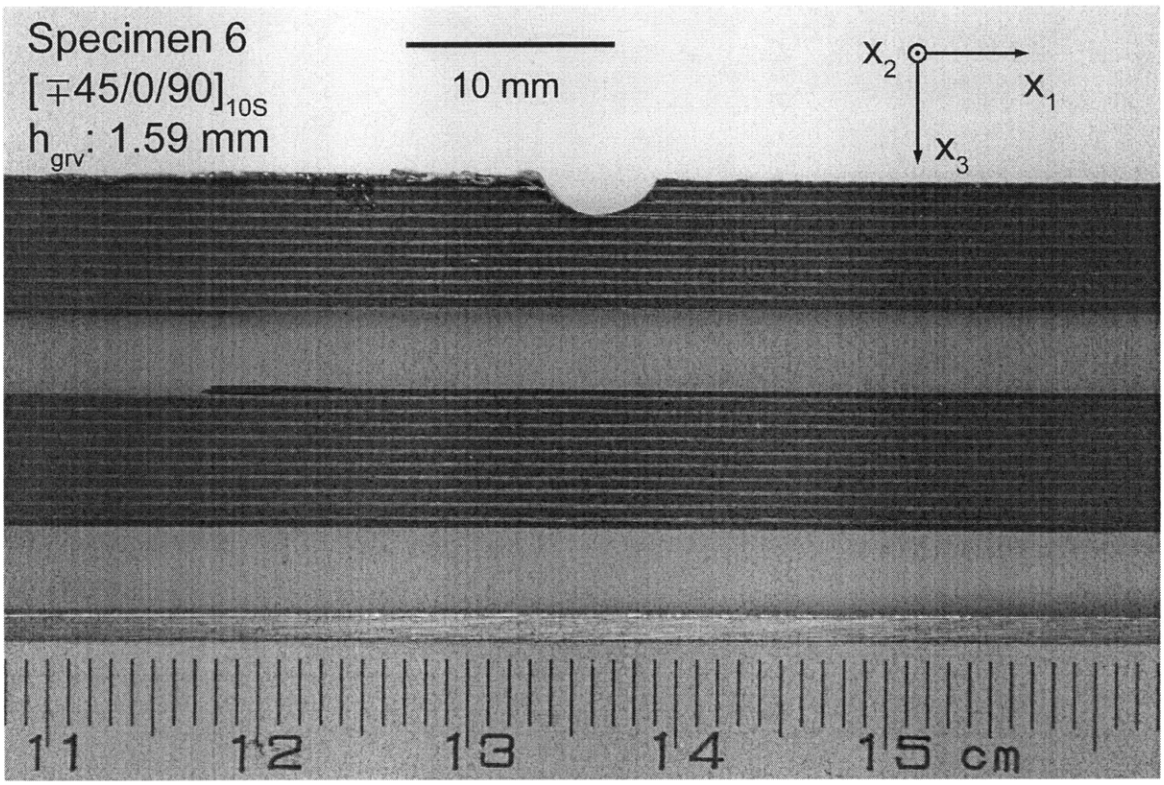

Figure 6.10 Sideview photograph after failure of Specimen 6: layup $[\mp 45/0/90]_{10S}$ with $h_{\text{grv}} = 1.59$ mm.

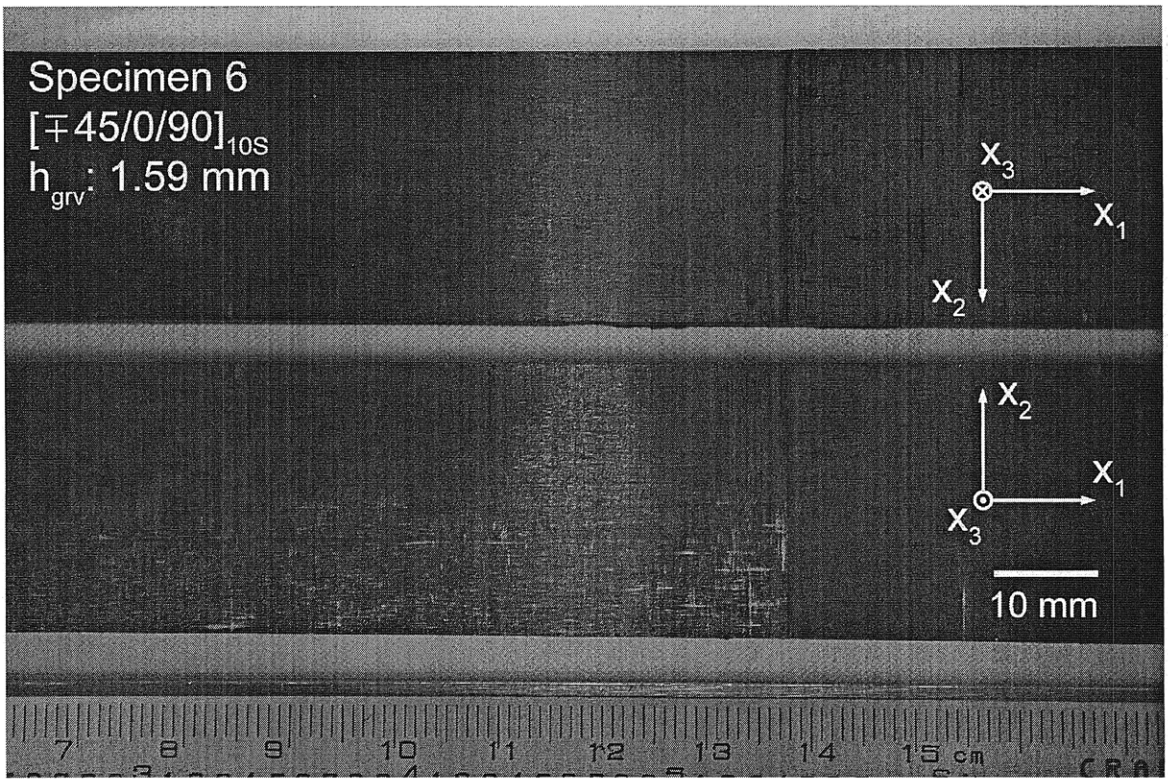

Figure 6.11 Failure surface view photograph, with top piece flipped, after failure of Specimen 6: layup $[\mp 45/0/90]_{10S}$ with $h_{\text{grv}} = 3.18$ mm.

Table 6.1 Measured parameters and test results of Specimens 5 and 6

Specimen	Geometric Parameters [mm]				Failure Load [kN]	Delamination location
	h^*_{grv}	t	w	L		
5	3.18	12.97	26.80	166.0	10.90	0°(10)/90°(10)
6	1.59	12.92	26.40	166.0	11.47	0°(10)/90°(10)

*h_{grv}: Designed value.

used in order to calculate the short-beam strength:

$$F^{\text{sbs}} = 0.75 \times \frac{P_{\text{f}}}{w \times t_{\text{sb}}} \tag{6.2}$$

From the test results, maximum shear stress for Specimens 5 and 6 are thus calculated as 31.16 MPa and 28.76 MPa, respectively. These values differ from the interlaminar shear strength, F_{13}, as provided by the manufacturer. However, taking into account that the two values are close and the fact that the delamination occurred at the midplane of the structure, it is quite apparent that the specimens failed in a short-beam shear mode.

6.4 Discussion

The failure mode of both Specimens 5 and 6 is considered to be a result of short-beam shear. Transverse shear failure mode is a result of the global response of the specimen. Thus, these specimens and the test procedure are not appropriate for the goal of this work of observing the local response due to the groove. In order to have the failure due to the local response around the groove and not due to the global response of the structure, it is necessary that the transverse shear stress resulting from the bending is relatively small and thus can be ignored compared to the stress around the groove. To have this realized, the thickness of the specimen needs to be considerably larger. However, a thick specimen (or laminate) works against the desire to keep the specimen relatively small.

Another issue in determining the necessary thickness is that it is not possible to determine a single value that would be applicable to all specimens with different test parameters. It is expected that a thicker specimen is required for a specimen with a larger groove depth. This is because the thickness under the groove is assumed to be the critical value for the global response of the specimen. It is therefore concluded that the boundary condition should be altered to rigid backface, in which condition the global structural response due to bending does not existent. As discussed in Chapter

3, the stress resulting from the rigid backface support is existent. However, it can be sufficiently avoided by designing the thickness of the specimen large relative to the groove depth. This necessary thickness is assumed to be effectively smaller than that of the simply-supported boundary condition. This makes it possible to determine a thickness value that would be sufficient for various specimens with various groove depths.

Chapter 7

STEPS TO FINAL SPECIMEN

It was discussed in Chapter 6 that a configuration with a rigid backface boundary condition is more appropriate to achieve the goals of this work. In this chapter, the choice of test parameters for this configuration is first described. In the second section, the critical issues that arose as the early tests were performed are described in their order of occurrence. These involve the machining, the indenter, and the instrument alignment. Finally, the overall issues of these steps are discussed in the third section of this chapter.

7.1 Choice of Test Parameters and Configurations

As indicated, the boundary condition selected is rigid backface. The only criterion that changes between the configurations with simply-supported boundary conditions and rigid backface boundary conditions is the relation between the length and the thickness. This becomes $L \geq 2t$, as given in Chapter 3 for the rigid backface configuration. Thus, the values of all the other geometrical parameters ($R_{\text{grv}}, R_{\text{cyl}}, h_{\text{grv}}, t$, and w) are not altered. The layup of the laminate is also maintained.

The criterion for the length, $L \geq 2t$, indicates that a length larger than 25 mm is required for a specimen with a thickness of approximately 12 mm. For ease of manufacturing, the specimens were cut from a laminated plate by setting the specimen length to approximately one-third of the length of the plate as measured by a ruler.

This results in manufacturing specimens with a length of approximately 56 mm (4.5 thicknesses), which satisfies the criterion. However, it must be noted that the length was not considered as an important geometric parameter at this point in establishing the test capability of the specimen. Therefore, the length of the specimens that are manufactured and tested in this chapter varied by up to 10 mm.

7.2 Issues that Arose with Rigid Backface Specimens

The procedures described in Chapter 4 were used to produce the specimens described in this chapter. The specimens are labeled as 7L, 7R, and 9, and were tested in that order. These specimens were all cut from laminated Plate B. Refinements and changes were made to the specimens and the testing procedure in moving through the sequence of specimens and learning from each. These specifics are subsequently described.

For Specimen 7L, the refined machining of the faces had not yet been determined and thus was not performed. Before this test, the geometric parameters t, w, and L were measured. The thickness, t, was measured with a micrometer to the closest 0.01 mm at 4 different locations at the edges adjacent to the groove, and the average value was 12.87 mm. The width, w, was measured with a caliper to the closest 0.01 mm near the $+x_1$-face and the $-x_1$-face, and the average value was 26.53 mm. The length, L, was measured with a caliper to the closest 0.01 mm near the $+x_2$-face and the $-x_2$-face, and the average value was 55.95 mm.

Strain gages were placed on the $-x_2$- and $+x_2$-faces near the groove as illustrated in Figure 7.1, with their labeled numbers as noted. These gages were placed in order to measure the compressive strain in the x_3-direction, ϵ_{33}. All gages are located at the same location along the x_3-direction. With this configuration, one can verify if the specimen is deforming similarly along the x_2-axis by comparing the strain from gages that have the same x_1-coordinate (and x_3-coordinate) on the two different x_2-faces

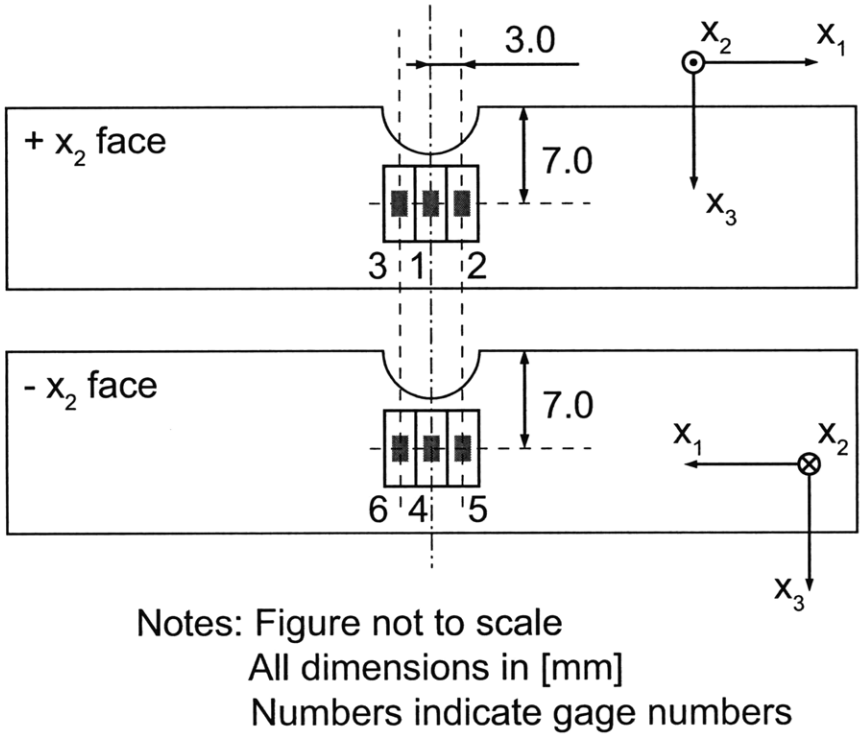

Figure 7.1 Strain gage positions for rigid backface test specimens.

(i.e. gages 1 and 4, 2 and 5, and 3 and 6), and if the deformation is symmetric about the centerline by comparing gages 2 and 3, and 5 and 6.

All the general test procedures explained in Chapter 5 were performed unless as noted. A hydraulic servo-controlled MTS testing machine was used for testing the rigid backface specimens. The top crosshead has a self-leveling flat platen. The details of the test configuration differ for each specimen, resulting from knowledge from the previous specimen and its test. These are subsequently described.

The overall setup for Specimen 7L is shown in Figure 7.2. A steel plate was used as the lower fixture, and was placed on the lower head and centered by eye. A steel plate was used as the upper fixture as well, and was centered by eye and attached to the top head with double-sided tape. The two plates are referred to as the upper support plate and the lower support plate, respectively. The specimen was placed on the lower fixture and centered by eye. The material of the indenter was chosen first as W-1 alloy steel, and the indenter had a longitudinal length of 27 mm. This indenter was placed on the groove of the specimen and centered in the x_2-direction by eye, letting 1.0 mm of the rod hanging over each side of the specimen. The lower head was brought up until the indenter had contact with the upper support plate, as described in Chapter 5. The stroke rate had to be decreased significantly because the load-per-stroke rate was expected to by much larger than that of a test with simply-supported boundary conditions. Thus, the stroke rate was initially chosen to be one-tenth of the value used for simply-supported tests, which results in 0.10 mm/min (compressive). This value was kept for all the rigid backface specimens described in this chapter. The test was stopped at the load of 45 kN, before failure was observed, because a gap was observed between the indenter and the top plate on the $-x_2$ side. The strain data were monitored up to 20,000 μstrain due to observations from previous tests. The resulting load vs. stroke plot and load vs. strain plots are given in Figures 7.3 and 7.4.

As described, a gap was observed between the indenter and the upper support plate at the $-x_2$-side during the test. This indicates that the contact between the indenter and the top plate was not uniform along the x_2-direction. It is expected

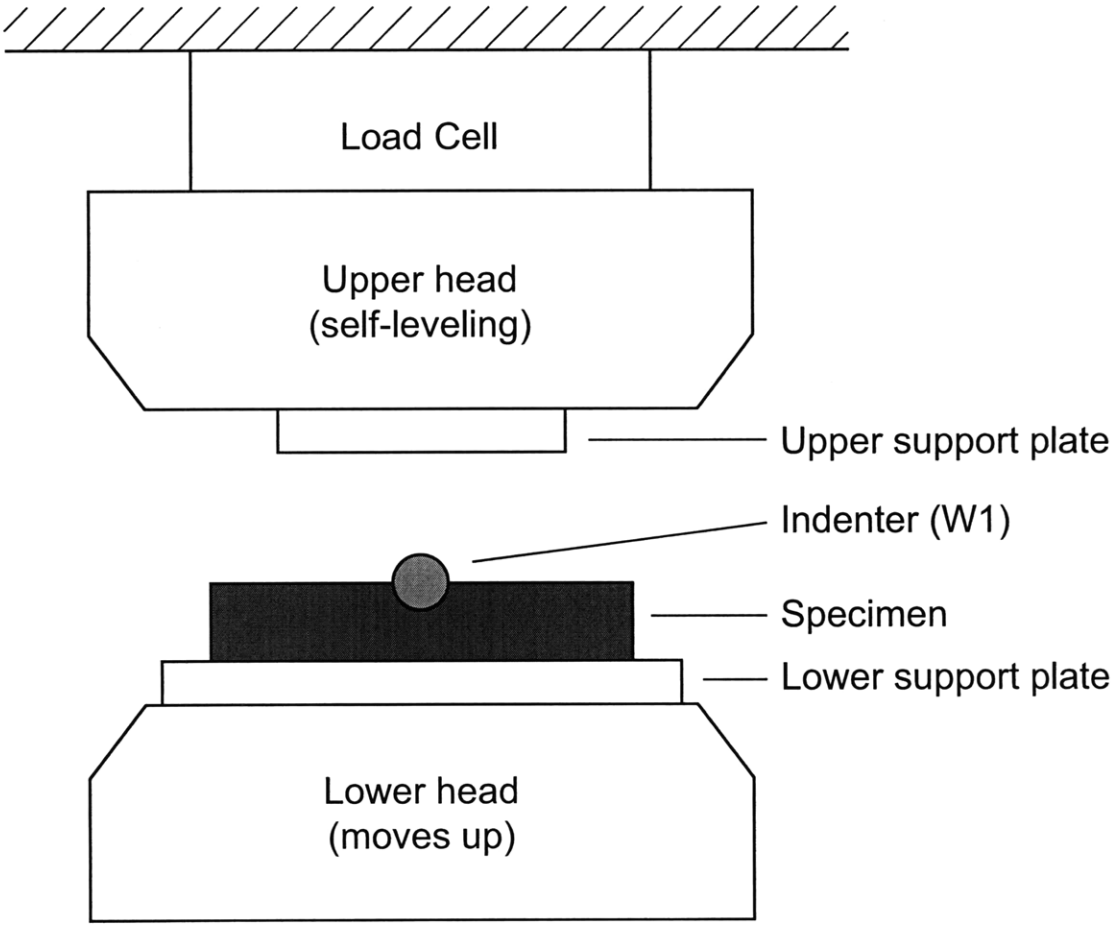

Figure 7.2 Illustration of initial rigid backface test setup.

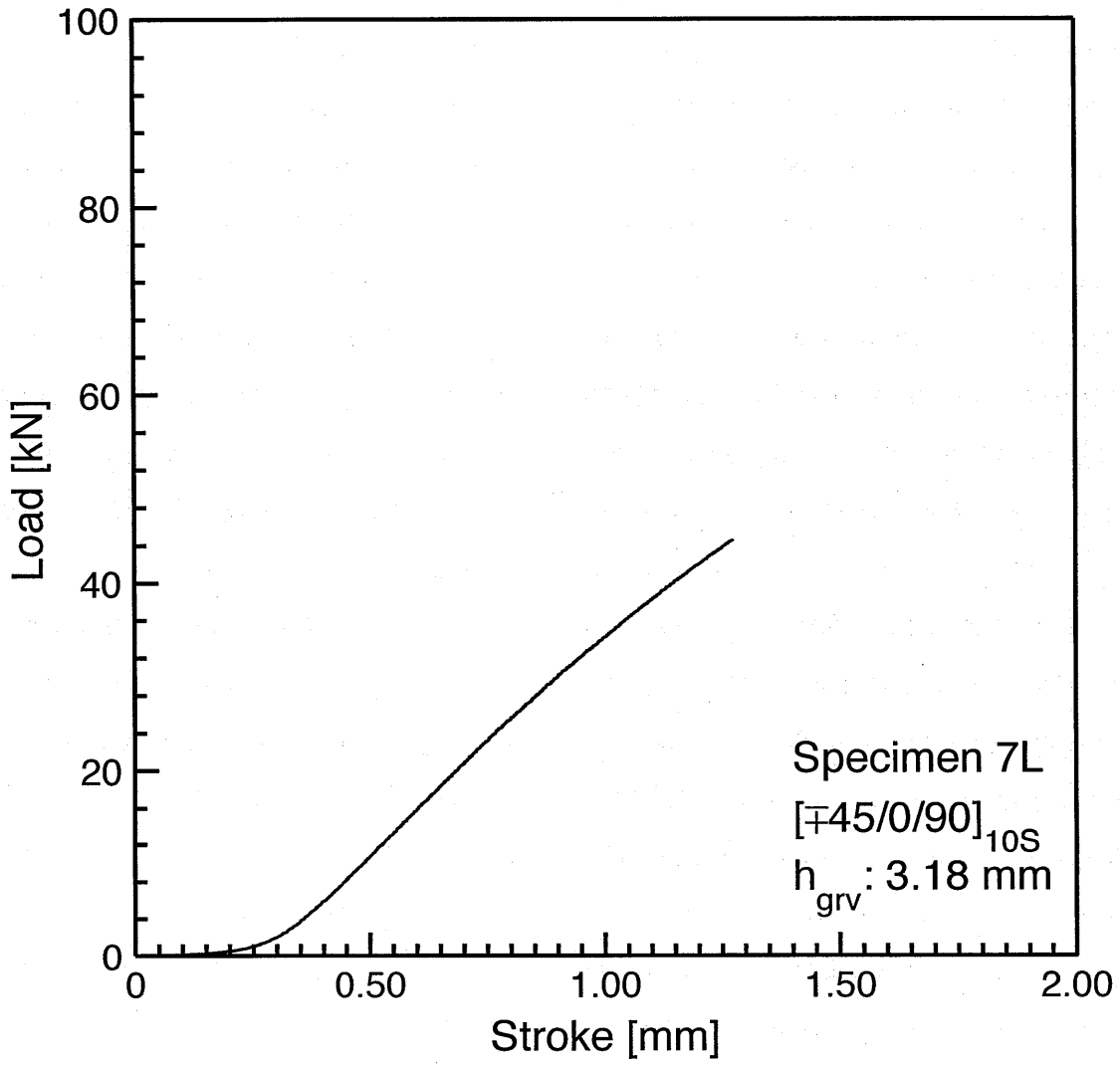

Figure 7.3 Load vs. stroke plot for Specimen 7L: layup $[\mp 45/0/90]_{10S}$ with $h_{\text{grv}} = 3.18$ mm.

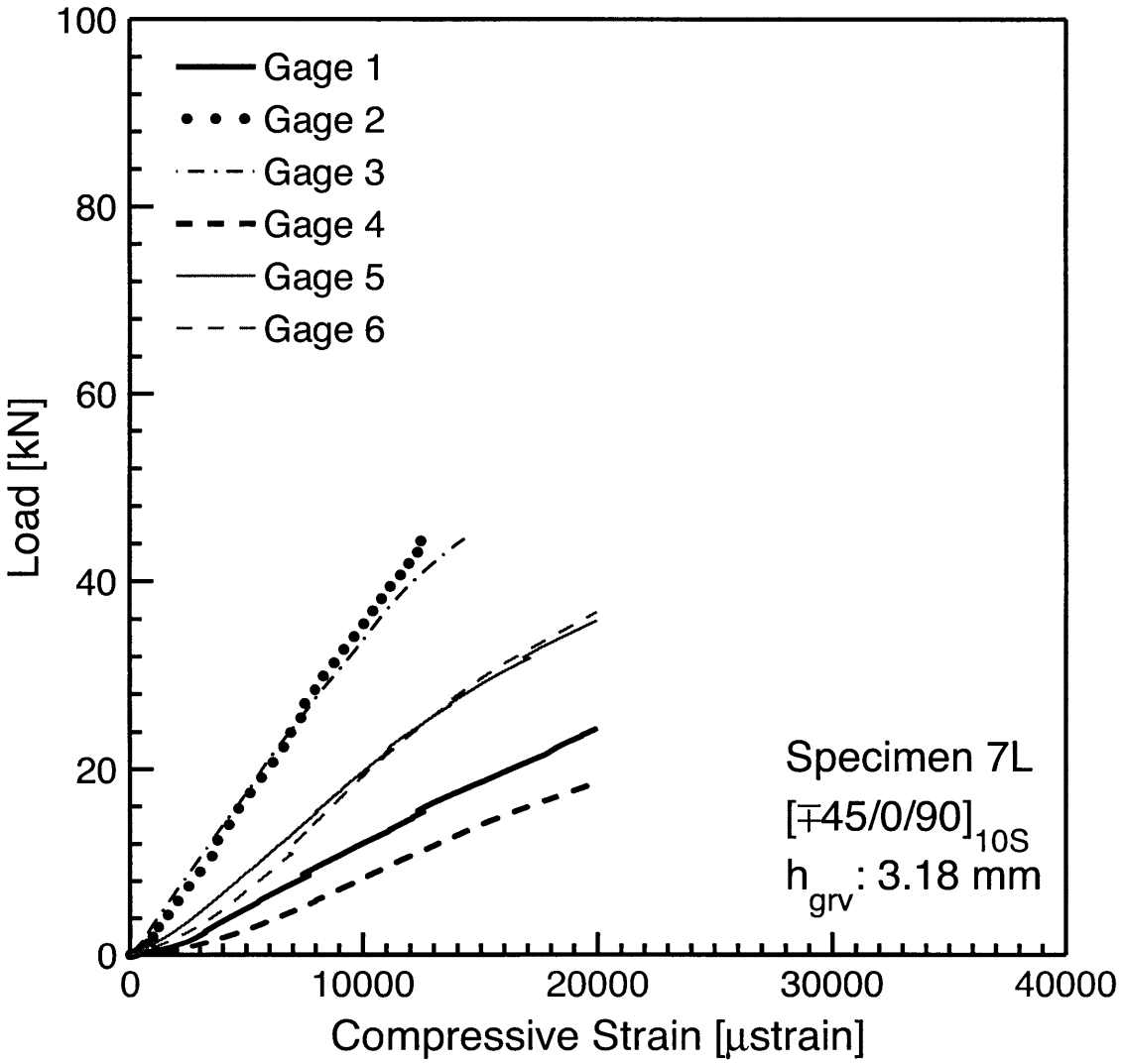

Figure 7.4 Load vs. compressive strain plot for Specimen 7L: layup $[\mp 45/0/90]_{10S}$ with $h_{\text{grv}} = 3.18$ mm.

that this results in a varying stress state and, thus, a varying strain state along the x_2-direction. Provided that a stress distribution independent of the x_2-direction is realized in the specimen, gage sets 1 and 4, 2 and 5, and 3 and 6 should result in plots with the same slopes. From the strain plots in Figure 7.4, however, it is obvious that the slope differs between the $+x_2$- and $-x_2$-faces. This contact issue also resulted in a very shallow slope near the origin on the load vs. stroke plot in Figure 7.3. A sudden slope change occurred when complete contact between the specimen, indenter, and the upper support plate was established. On the other hand, it is observed that the slopes of load vs. strain is equal for gage sets 2 and 3, and 5 and 6. This indication of symmetry about the x_2-axis indicates that the loading was symmetric about the x_2-axis. It was also observed upon post-test observation that the groove had been cut through different plies at its bottom, judged from the pattern of the plies in the groove seen by eye. It was therefore concluded that this contact issue is a result of not having the bottom surface of the groove properly aligned with the $+x_3$-face of the specimen.

This leads to a need for improvement in the machining procedure. For Specimen 7L and the previous specimens described in Chapter 6, the groove was milled by grabbing the x_2-faces without any check of these two faces being parallel. The improved machining procedure for refining the faces of the specimens was established as described in Section 4.3 in order to assure that the faces are parallel or perpendicular to each other. Specimens discussed hereon have undergone this procedure.

The test for Specimen 7R, with the faces refined and the groove surface aligned parallel to the $+x_3$-face, was performed under the same configurations as for Specimen 7L. The measured geometric parameters of Specimen 7L were 12.86 mm for the thickness, 25.14 mm for the width, and 71.69 mm for the length. For this specimen, it was observed by eye that the bottom of the groove segmented only one ply, indicating that the bottom of the groove was close to being parallel to the $+x_3$-face. This ply that is segmented at the bottom of the groove is used as a test parameter in the tests in Chapter 8, and is described in detail there. The test was run until the failure of the specimen. This occurred at a load of 70.48 kN. A delamination was observed on

the $+x_1$ half of the specimen, between the $-45°$ ply and the $+45°$ ply in the 5th set. The load vs. stroke plot and the load vs. strain plots are shown in Figures 7.5 and 7.6. A photograph of the specimen after failure is given as Figure 7.7.

Valid strain data was only acquired from Gages 1 and 2. Other strain data were not proportional to the load with random jumps in values, and therefore considered invalid. Thus, it is not possible to verify if the contact issue was resolved. However, the shallow-slope section on the load vs. stroke plot did decrease. This behavior indicates an improvement in the contact issue. There was another critical issue that did occur. This is the deformation of the indenter, as it was observed that the cross-section of the cylindrical indenter changed as the load applied increased significantly from previous tests. This change in cross-section is illustrated in Figure 7.8. The original diameter of the cylindrical indenter, d_{cyl}, is 6.35 mm. The width of the flattened region, w_{f}, was measured by a caliper to be 2.34 mm. The width of the indenter after test, w_{ind}, was measured by a micrometer to be 6.40 mm.

The deformation of the indenter must be avoided, particularly its expansion in width as this results in the load being transferred to the specimen in a different manner from what is desired and one that could not be easily and clearly determined. The fact that the failure mode was a delamination around the groove indicates that the interlaminar shear stresses, particularly σ_{13}, are key. Contact stresses at the groove surface with values in the x_3-direction have a large effect on such stresses in the specimen. This gives a good reason to improve the indenter so that it will not deform during the test, and the contact stress state can be directly determined based on the knowledge of the indenter geometry.

The alternate material chosen for the indenter is M2/M7 steel alloy. This material was chosen because of its high hardness, Rockwell hardness C62-C64, which was one of the hardest steel alloy available without custom ordering. This is in contrast to the W1 alloy that had an approximate hardness of Rockwell C23. The diameter of the rod of the M2/M7 steel alloy is 0.246 in (6.35 mm) with a tolerance of +0.0000, -0.0002 in (+0.000, -0.005 mm). The straightness tolerance is 0.001 in (0.025 mm) over a length of 4.00 in (101.6 mm). This was cut and adjusted to the length of 27.0

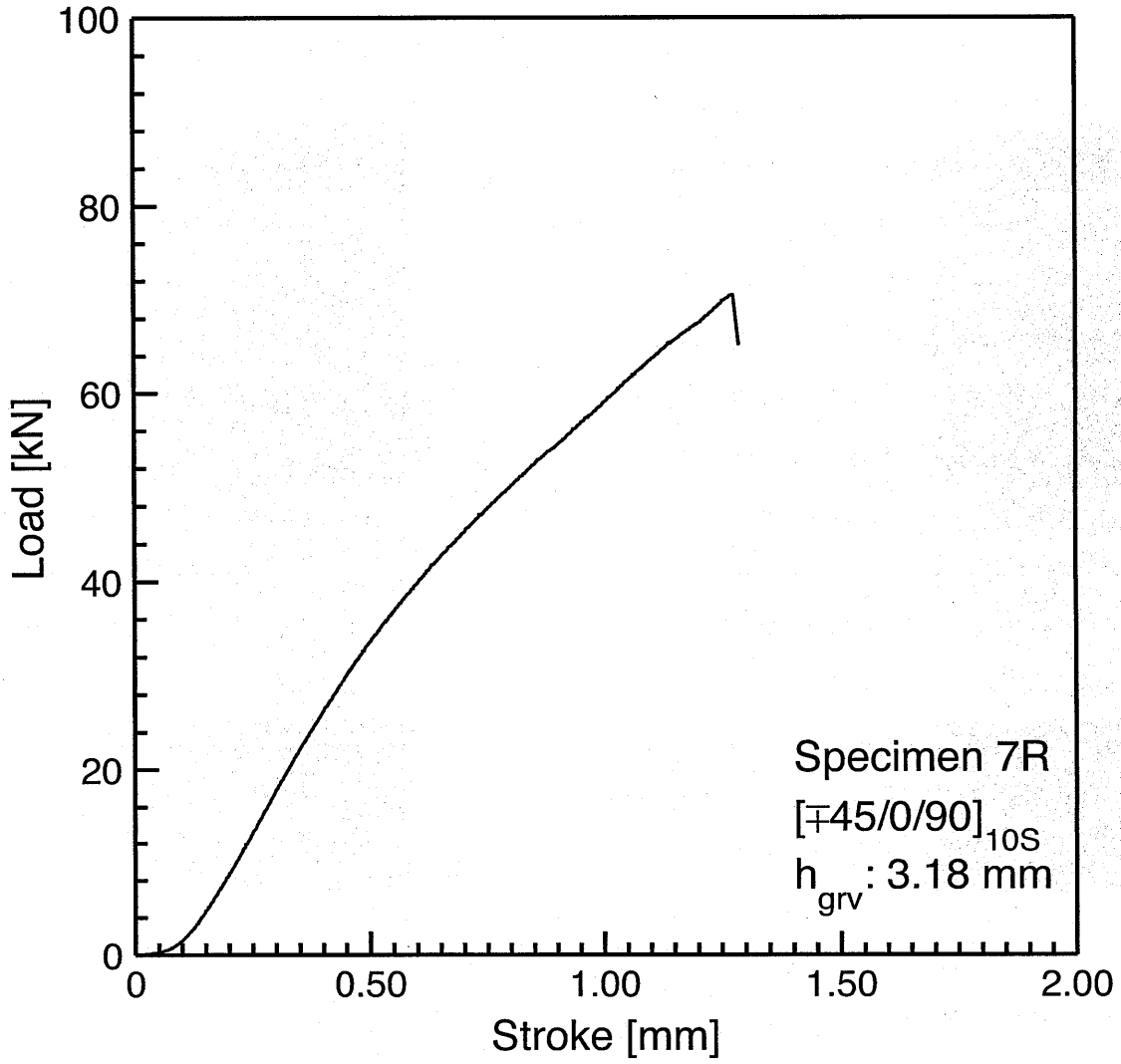

Figure 7.5 Load vs. stroke plot for Specimen 7R: layup $[\mp 45/0/90]_{10S}$ with $h_{\text{grv}} = 3.18$ mm.

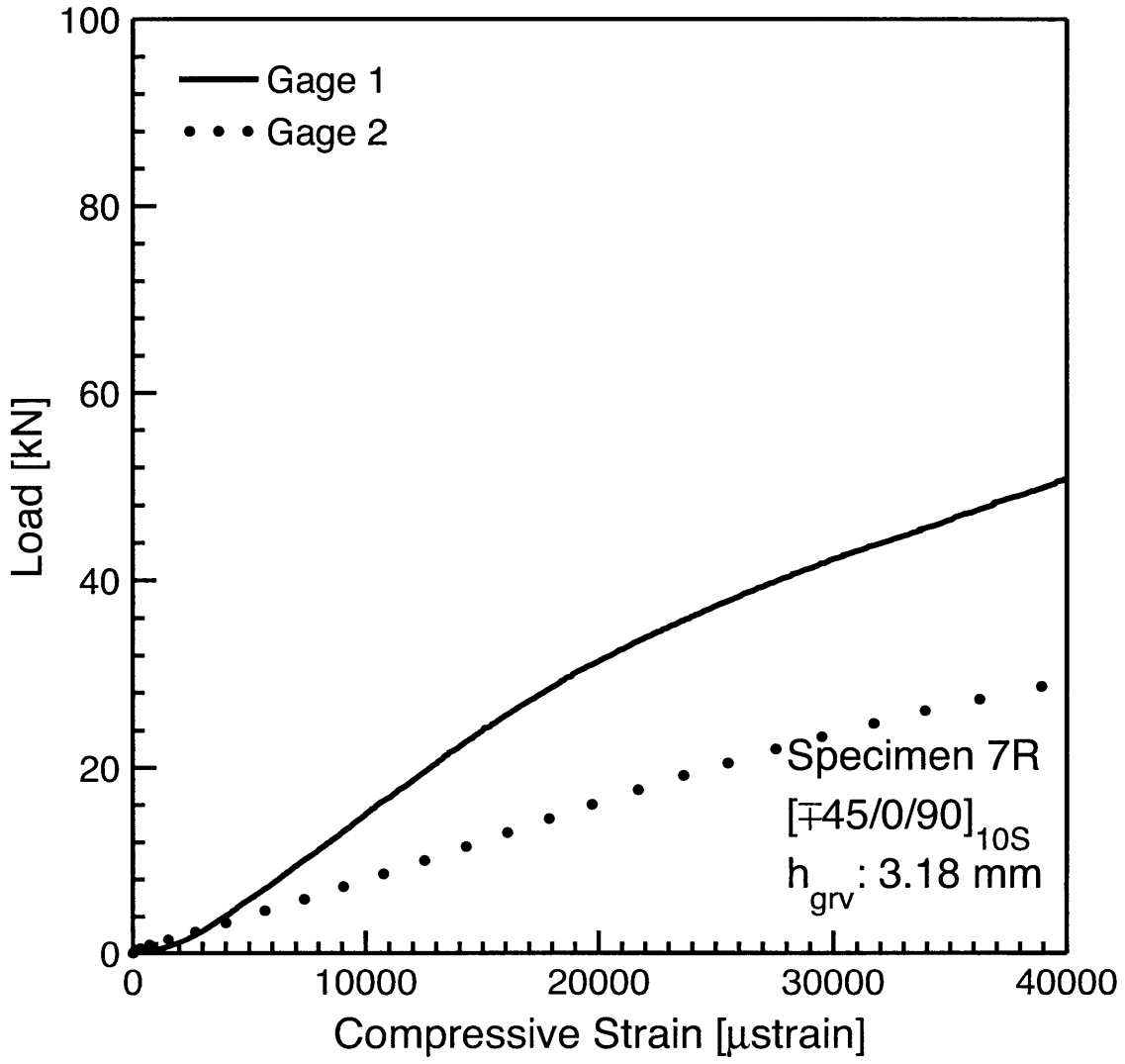

Figure 7.6 Load vs. compressive strain plot for Specimen 7R: layup $[\mp 45/0/90]_{10S}$ with $h_{\text{grv}} = 3.18$ mm.

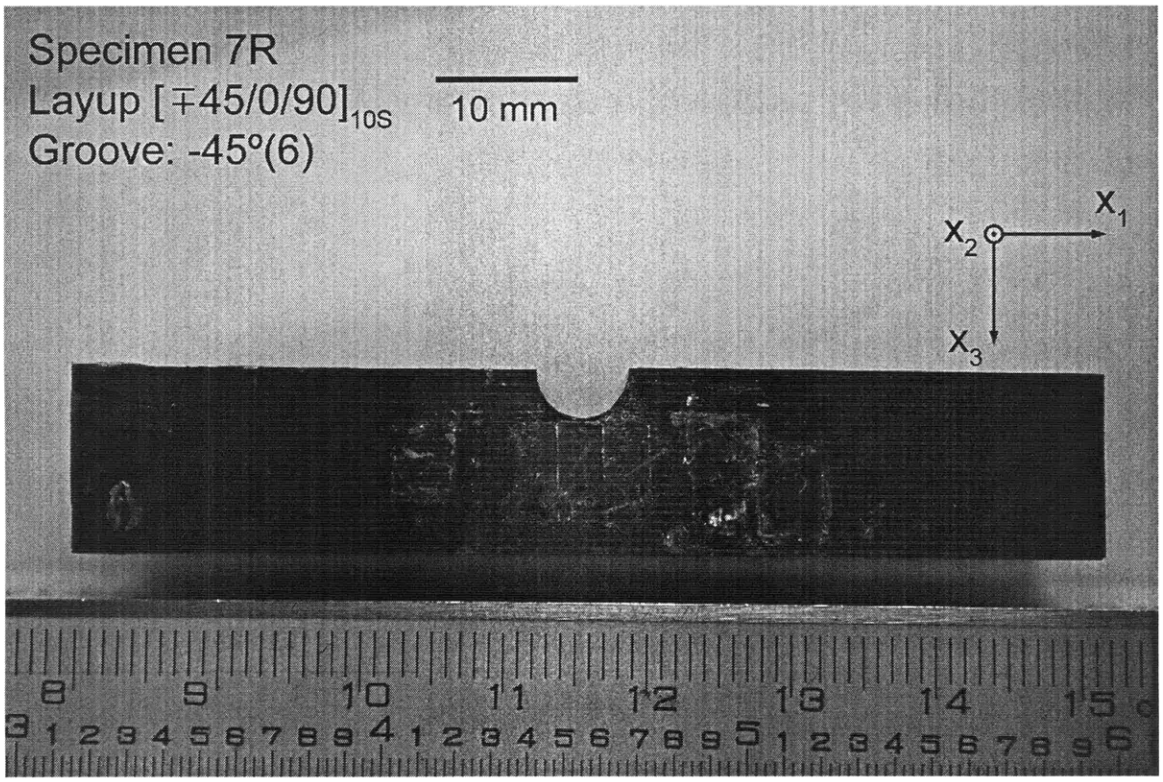

Figure 7.7 Sideview photograph after failure of Specimen 7R: layup $[\mp 45/0/90]_{10S}$ with $h_{\text{grv}} = 3.18$ mm.

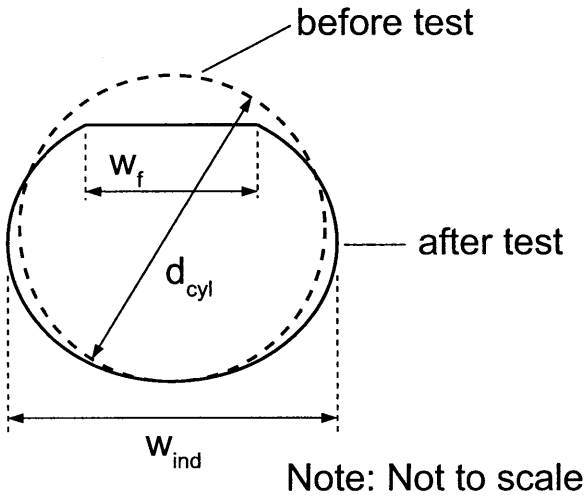

Figure 7.8 Illustration of the cross-section of the cylindrical indenter before and after the test.

mm with a grinder. Because of the hardness of the indenter, improvement of the upper support plate became necessary so that the indenter did not indent the plate. The solution to this was to introduce a test block with increased Rockwell hardness of C61 (referred to as the "hard block") between the indenter and the upper support plate. This hard block is attached to the upper support plate with double-sided tape. A simple illustration of the improved overall test setup is given in Figure 7.9. This configuration was used to test Specimen 9.

The geometric parameters of Specimen 9 were measured to be 12.91 mm for the thickness, 24.91 mm for the width, and 52.67 mm for the length. The faces of this specimen were refined with the improved machining procedures. It was observed by eye that the bottom of the groove segmented only the $-45°$ ply in the 6th set. In this test, the upper head with the upper support plate and the hard block (referred to, hereon, as the "upper parts") suddenly rotated around the indenter at a load of approximately 85 kN before failure was reached. The plots from this test are given in Figures 7.10 and 7.11. The diameter of the indenter was measured after the test with a micrometer at two ends and at the center of the rod. The values were all 6.35 mm, indicating that the indenter did not deform during the test.

This rotation of the upper parts is a result of the misalignment of the indenter. When the indenter is not aligned at the centerline of the upper head, moment is generated around the centerline of the upper head. This moment increases as the load increases, resulting in the rotation of the upper parts. In order to prevent this, it is necessary that the indenter is aligned at the centerline of the upper head. This can be done by aligning the lower support plate at the center of the lower head, and subsequently aligning the specimen at the center of the lower support with accuracies of 1 mm or more. This procedure is described in detail in the next chapter, Section 8.1.

At the load of 40 kN, the difference of strain values between gages 1 and 4, 3 and 6, 2 and 5 was approximately 10%. From the load-versus-strain plots in Figure 7.11, it is observed that the plots of these sets of gages are relatively close to each other. These facts indicate that the contact and the load transfer between the indenter and the

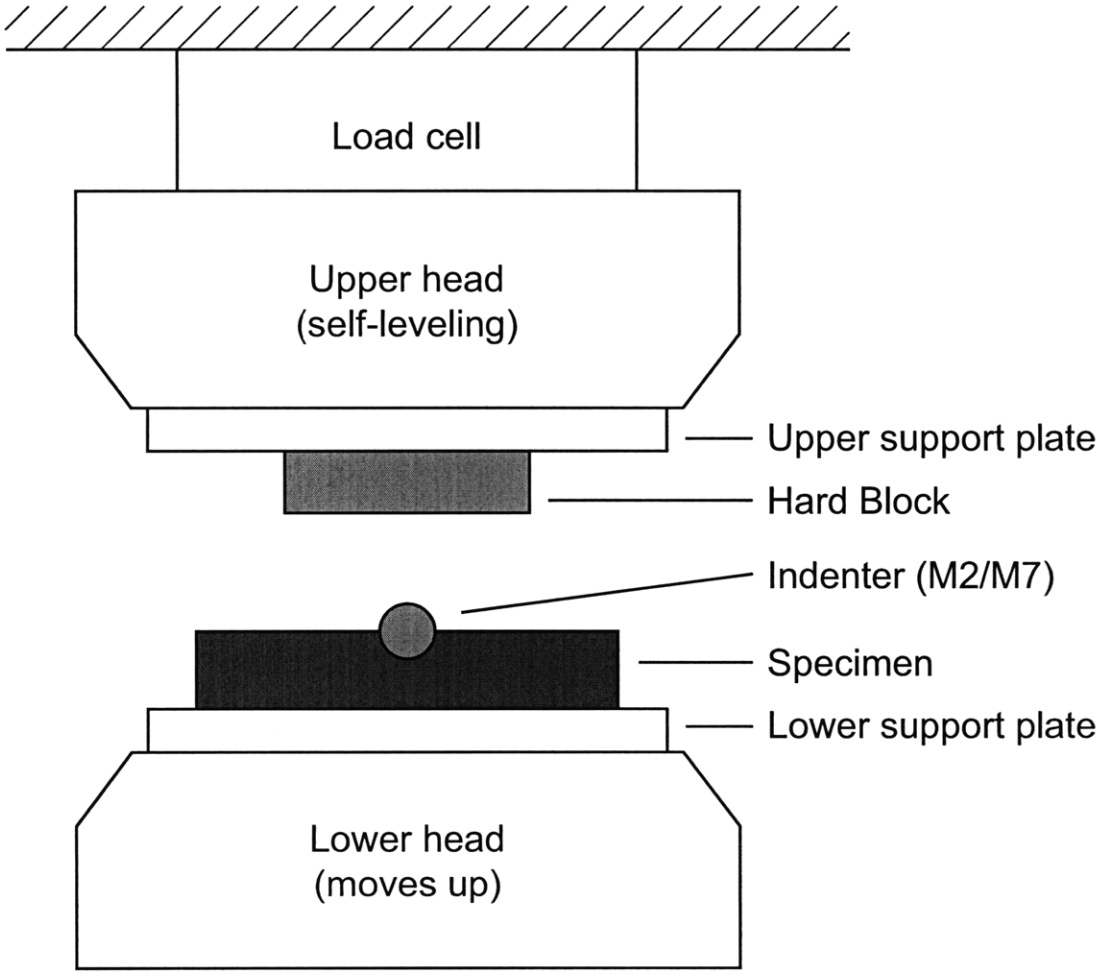

Figure 7.9 Illustration of improved rigid backface test setup.

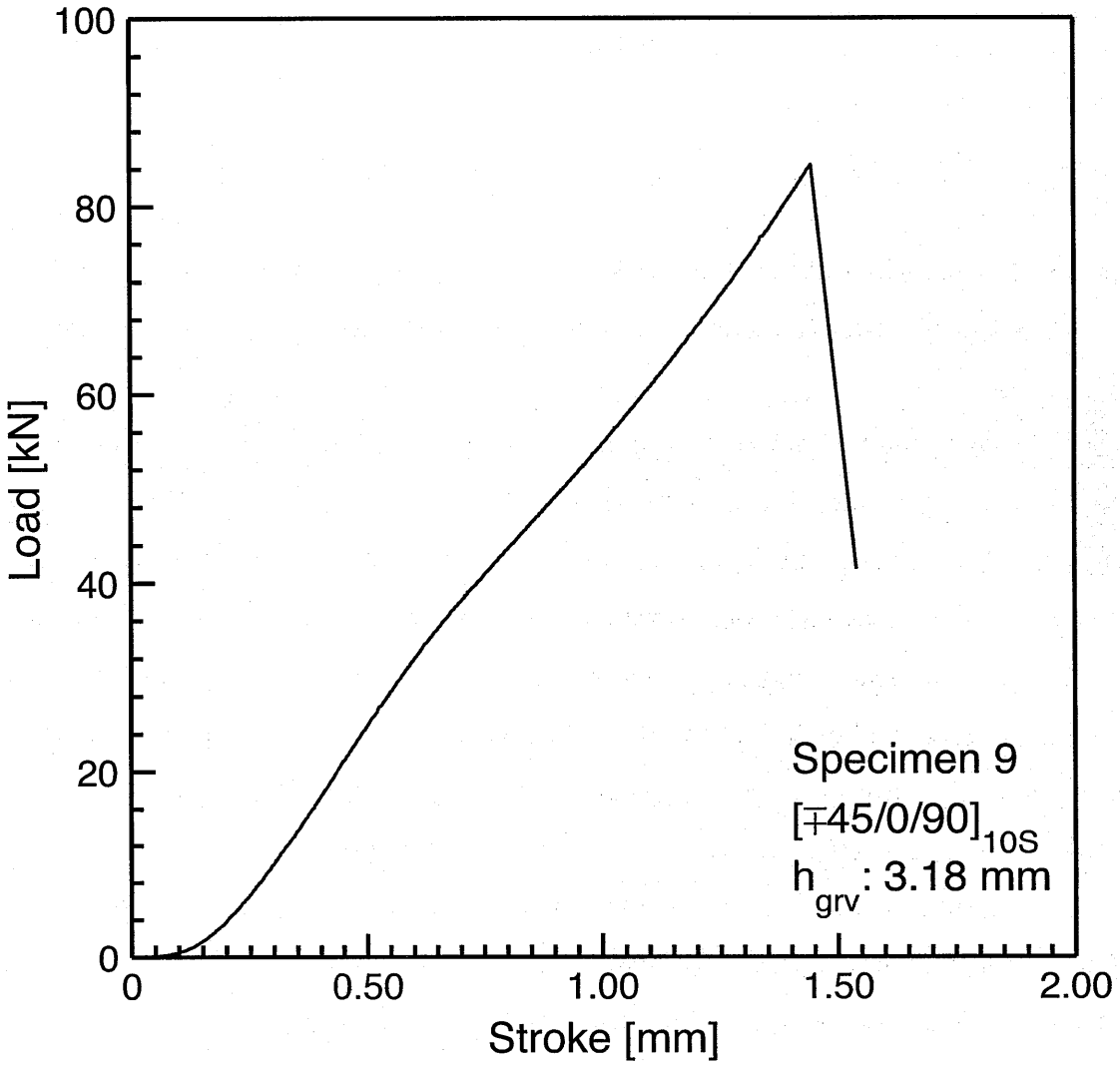

Figure 7.10 Load vs. stroke plot for Specimen 9: layup $[\mp 45/0/90]_{10S}$ with $h_{\text{grv}} = 3.18$ mm.

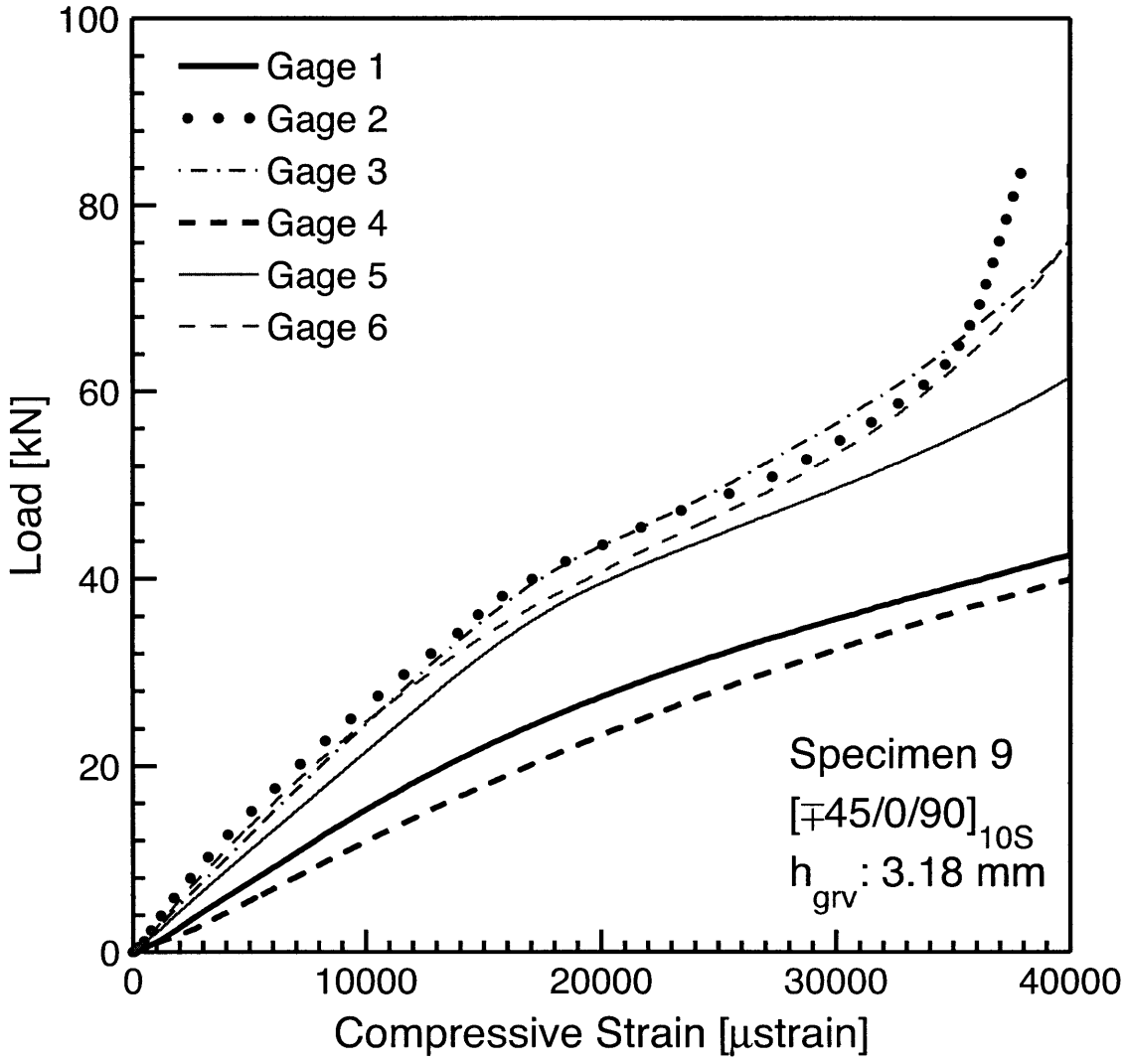

Figure 7.11 Load vs. compressive strain plot for Specimen 9: layup $[\mp 45/0/90]_{10S}$ with $h_{\text{grv}} = 3.18$ mm.

groove were improved. Further discussion of the strain values is left to be presented in the following chapter.

As previously noted, the diameter of the indenter after the test was 6.35 mm. This is identical to the original diameter of the rod. This indicates that no obvious deformation occurred during the test and that the M2/M7 steel alloy is appropriate for the indenter material.

7.3 Discussion

In this chapter, three improvements were performed with the rigid backface specimens and test configurations: improving the machining procedure, the indenter, and the alignment setup.

The machining procedure was improved in order to have the bottom of the groove parallel to the $+x_3$-face of the specimen. This was done by refining the faces of the specimen to be parallel/perpendicular to each other. The load-versus-strain plot of Specimen 9 indicated that this improvement solved the contact issue between the indenter and the specimen had a uniform load transfer along the x_2-axis.

The material of the indenter was altered to a very hard steel alloy M2/M7 in order to prevent the deformation of the indenter during the test. This was certified by the fact that the diameter of the indenter did not change after the test of Specimen 9.

These two improvements were applied to the final specimens, as presented in the next chapter. The importance of the alignment of the indenter and the specimen in order to avoid the rotation of the self-leveling upper head was also noted herein. However, the improved method of alignment and a test with such a configuration is not presented in this chapter. This is because the test with the improved configuration is maintained throughout the remaining tests, and determined as the final configuration for the current work. The description and the results of the tests are thus presented in the next chapter.

Chapter 8

FINAL SPECIMEN

Through the work presented in Chapter 7, the critical issues of machining, indenting, and alignment arose and were addressed. In this chapter, the tests using the final specimen configuration are presented. The parameters and the test configuration are described in detail in the first section. The determination of the test sequence for the final specimens are then described. The results for the standard specimens are presented in the third section. In the fourth section, specimens with an alternate layup are established and their test results are presented. Finally, the overall test results are discussed. Load-stroke response data and failure data for all specimens are given in Appendices A and B. In this chapter, results of several specimens, representatives of categories observed in the results, are shown and described in detail.

8.1 Final Test Configuration

The arguments of Section 7.1 apply to the final specimens for the selection of geometric parameters, except for the depth of the groove, h_{grv}. This parameter was chosen as a test parameter, where 3.18 mm was selected as the base value. This parameter is discussed in detail later in this section.

The selection of the base layup was kept to be $[\mp 45/0/90]_{10S}$ with a total of 80 plies. This quasi-isotropic layup is considered as a standard choice. Results from this configuration are compared with those from a $[\mp 30/0]_{13S}$ layup. These latter results

are presented in Section 8.4. For this latter case, all the geometric parameters remain the same except the thickness.

The following description of the test configurations are for the standard layup, where most of the procedure is also applicable to the alternate layup. The geometric parameters for the standard specimens were determined to be 25.00 mm for the width, 56.00 mm for the length, 3.18 mm for the groove radius, 3.12 mm for the indenter radius, and a nominal value of 12.20 mm for the thickness. The specimens with the standard layup were cut from Plates C and D, with thicknesses presented in Table 4.2. The laminated plate from which a specimen was cut is identified for each of the specimens because this difference had an effect on the results due to different thicknesses resulting from the manufacturing. This is further described in Section 8.3 and discussed in Section 8.5.

The depth of the groove and the ply that it intersects are related by the ply thickness of the material and the laminate used. The ply intersected by the bottom of the groove is a key consideration since the occurrence of delaminations and other failures can depend upon the ply intersected. Thus, the bottom ply that is segmented by the groove is regarded as the test parameter replacing the value of h_{grv}. For example, when the thickness of a single ply is assumed to be the nominal value of 0.15 mm, a groove with the depth of the base value (3.18 mm) should segment the 21st ply at its bottom. For the standard layup, this is the $-45°(6)$ ply. Thus, the nominal value for this adapted "groove ply parameter" is $-45°(6)$. For this configuration, it is noted as "Groove: $-45°(6)$" on the results. This groove parameter was changed among $90°(5)$, $-45°(6)$, $+45°(6)$, and $0°(6)$ in the tests, and this parameter is explicitly noted on the results in order to determine the effect this has on the behavior. It is noted that the thickness of the laminate differed for Plates C and D, and thus the thickness of a single ply also differed. Thus, to achieve a specific ply intersected by the groove, the value of h_{grv} needs to vary somewhat depending upon from which plate the specimen is cut.

The manufacturing procedure is described in Chapter 4. All the procedures described were performed. However, additional description is needed for the groove

machining due to this variation in ply thickness. The first specimen from a particular plate is grooved to the nominal depth of 3.18 mm. The surface of the groove is observed by eye, and by microscope if necessary, in order to identify the ply that is segmented by the bottom of the groove. Using the number of plies from the $-x_3$-face to the bottom of the groove, the approximate value for the thickness of a single ply is calculated for all specimens from that plate by dividing the nominal depth, 3.18 mm, by that number of plies. Using this value, the necessary depth for each value of the groove ply parameter was calculated based on the ply that the bottom of the groove is to segment. This was subsequently used for the machining procedure. It was confirmed by the use of a microscope that the groove was cut halfway through the chosen ply of the groove ply parameter for all the specimens presented.

Strain gages were placed on the $-x_2$- and $+x_2$-faces near the groove, as illustrated in Figure 7.1, for a number of specimens. The locations of the strain gages were kept the same as the specimens presented in Chapter 7. These gages are used to measure the compressive strain in the x_3-direction, ϵ_{33}. The strain values are compared to verify that the strain state of the specimen is the same along the x_2-direction and symmetric about the centerline. Once it was determined that this strain state was being achieved and thus verified that the load was transferred from the indenter to the specimen uniformly along the x_2-direction, the use of this strain gage configuration was considered to be no longer necessary. Thus, strain gages were not placed on the latter specimens (Specimens 20 through 30).

All of the general test procedures explained in Chapter 5 were performed. A hydraulic servo-controlled MTS testing machine with a 50 metric ton capacity load cell was used. The upper crosshead consists of a self-leveling flat platen. A steel rectangular plate was used as the lower support. A 56.0 mm by 25.0 mm rectangle was centered and marked on the steel plate with a permanent marker, showing the exact position where the specimen should be placed. The centering of the marking was done by measuring with a caliper to the closest 0.5 mm. Next, this plate was placed on the lower head and centered in both the x_1- and x_2-directions to the closest 0.5 mm by measuring with a caliper. The position of this lower steel plate was fixed

by taping the plate to the testing machine lower head. A steel plate of the same size and the hardness test block, both described in Chapter 7, were used as the upper fixture. The test block was centered on the upper steel plate to the closest 0.5 mm with a caliper and was attached by double-sided tape. This upper fixture was centered on the upper head in the same manner as for the lower plate, and was attached by double-sided tape.

With these fixtures set, the lower head was moved up using the "actuator moving" button of the testing machine until the lower plate had firm contact with the test block. This was done by setting the maximum load as 1.0 kN. This procedure has the aim of attaching the upper fixture to the upper head firmly, and of making the faces of the two heads parallel. Then the two heads were set apart, leaving space to place the specimen. The specimen subsequently is placed on the lower plate at the marked location. For the indenter, an M2/M7 steel alloy rod of 27 mm length was used. It was placed on the groove of the specimen, with 1 mm hanging over both sides. A simple illustration of the overall setup is given in Figure 7.9. The lower head was then brought up until all the parts had contact with each other, as described in Chapter 5. The stroke speed-rate was chosen to be 0.10 mm/min (compressive), keeping the value used in Chapter 7.

All but one specimen was tested until failure, as described in Chapter 5. For Specimen 30, the test was completed before large damage was observed. This test was performed to observe the crushing under the groove before major delamination occurred in the specimen. The test was completed by stopping the lower head when there was a decrease in the rate of the load increase. This was observed on both the load value and the load-versus-stroke plot that is drawn on the computer monitor while the test is conducted.

8.2 Determination of Test Sequence

All of the specimens described in this chapter were tested with the same configuration. However, the purpose(s) of the tests differ. These purposes are described in

this section. The specimens used for each test sequence are labeled with numbers in chronological order. They are described in this section in chronological order and the determination of the following test sequence is described. A brief explanation of the results of the specimens are presented for this purpose. Details of the results for each specimen are left to be presented in Section 8.3. The plate from which each specimen was cut, the measured geometric parameters, and the groove ply parameter for the specimens are presented in Table 8.1.

Specimens 13 and 14 with the nominal groove ply parameter, $-45°(6)$, were first tested with the test configuration described in the previous section. The failure mode of both specimens was a delamination near the bottom of the groove, and the failure load differed by less than 1 kN. The failure mode and the delamination location were therefore expected to be basically the same for the same groove parameter, and the interest became the effect of the groove parameter. Thus, the next set of specimens (Specimens 15, 16, and 17) were tested with different groove ply parameter values of $+45°(6)$, $0°(6)$, and $90°(5)$. The failure mode for each of these three specimens was also a delamination near the bottom of the groove, although not consistent as to the interfaces at which these occurred. The failure loads also differed by over 20 kN. Thus, it was determined that more test data was necessary associated with the nominal groove parameter in order to determine the failure mode and failure load, and possible variability associated with these. Specimens 18 and 19 were tested for this purpose. Since Specimen 18 failed very differently from the previous specimens, it was concluded that even more results were necessary to study repeatability and to reach a conclusion with regard to the failure mode and load. Thus, a new laminated plate (Plate D) was manufactured and ten specimens (20 through 29) were machined from this plate with the same value of the groove ply parameter, $-45°(6)$.

From the strain data acquired from Specimens 13 through 19, it was verified that the test configuration used for the specimens was sufficient for the load to be transferred from the indenter to the specimen uniformly along the x_2-direction. Therefore, it was concluded that it was no longer necessary to use the strain gage configuration.

From the failure of Specimens 18 through 29, it was observed that the specimens

Table 8.1 Properties of Specimens 13 through 30

			Geometry [mm]		
Specimen	Plate	Groove	t	w	L
13	C	$-45°(6)$	11.99	24.99	56.12
14	C	$-45°(6)$	11.96	24.84	56.06
15	C	$+45°(6)$	11.93	25.04	55.95
16	C	$0°(6)$	11.81	25.04	55.92
17	C	$90°(5)$	11.90	24.88	56.05
18	C	$-45°(6)$	11.94	25.05	55.85
19	C	$-45°(6)$	11.96	25.03	55.85
20	D	$-45°(6)$	12.62	25.03	55.85
21	D	$-45°(6)$	12.74	25.04	56.24
22	D	$-45°(6)$	12.65	24.93	56.08
23	D	$-45°(6)$	12.71	24.93	56.00
24	D	$-45°(6)$	12.69	25.04	55.80
25	D	$-45°(6)$	12.68	24.91	55.91
26	D	$-45°(6)$	12.68	24.89	56.00
27	D	$-45°(6)$	12.61	24.94	56.01
28	D	$-45°(6)$	12.71	25.02	55.85
29	D	$-45°(6)$	12.68	25.01	55.89
30	D	$-45°(6)$	12.72	24.99	55.94

with a groove parameter of $-45°(6)$ have a possibility to fail in two different modes. One mode (noted as Mode A in the following section) is characterized as a major delamination near the groove. This was observed in the earlier set of specimens. The other mode (Mode B) is characterized by a major delamination near the midplane of the specimen, with also a crack in the transverse direction at the bottom of the groove that propagates to that delamination. In order to try to observe the mechanism of this failure, Specimen 30 was tested and stopped during the propagation of the damage prior to failure.

8.3 Results

In this section, results of the specimens with the standard layup, $[\mp 45/0/90]_{10S}$, are presented. First, the strain data that were acquired from Specimens 13 through 19 are presented. These data are used to verify that the specimen and the test configurations are properly established for the objectives of the current work. The load-versus-stroke response, the failure load, and the failure locations are then presented.

8.3.1 Strain Response

Specimens 13 through 19 were tested with the strain gage configuration shown in Figure 7.1. These specimens were all cut from laminated Plate C. The load-versus-strain plots are given in Figures 8.1 through 8.7. The strain data from gage 6 of Specimen 17 were invalid, and are thus omitted from that plot.

As described in Section 7.2, the strain measurements are taken to verify that a "two-dimensional" state is realized in the specimen, i.e. no variation in the x_2-direction. In addressing this verification, there are several factors that must be taken into account. The contact issue between the specimen, indenter, and the upper parts, as described in Chapter 7, was to be solved by the refined machining procedure. However, it is still considered to be very difficult to have a contact and a load transfer that is uniformly distributed along the x_2-direction between the indenter and the

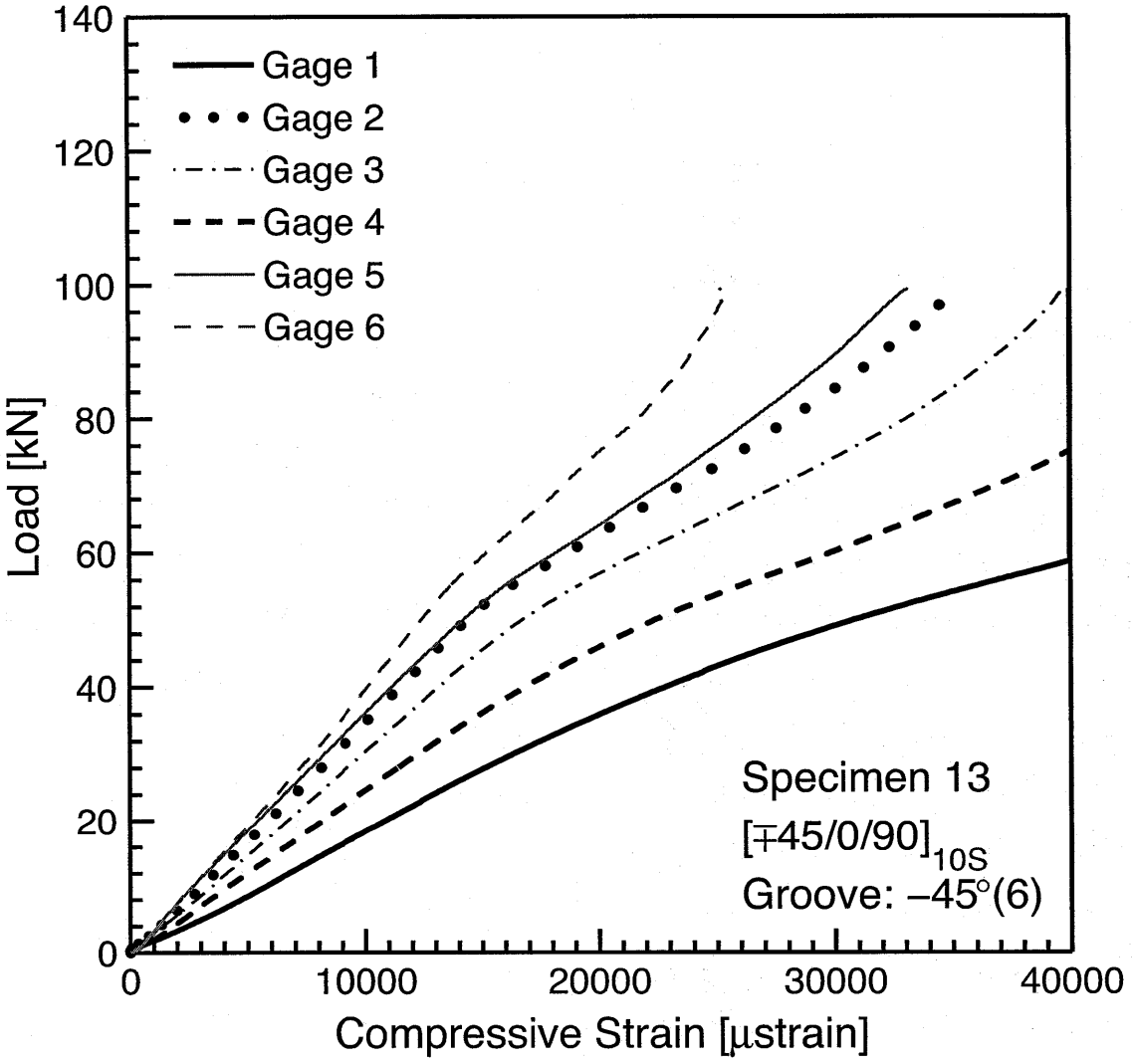

Figure 8.1 Load vs. compressive strain plot for Specimen 13: layup $[\mp 45/0/90]_{10S}$ with groove at $-45°$ ply in 6th set.

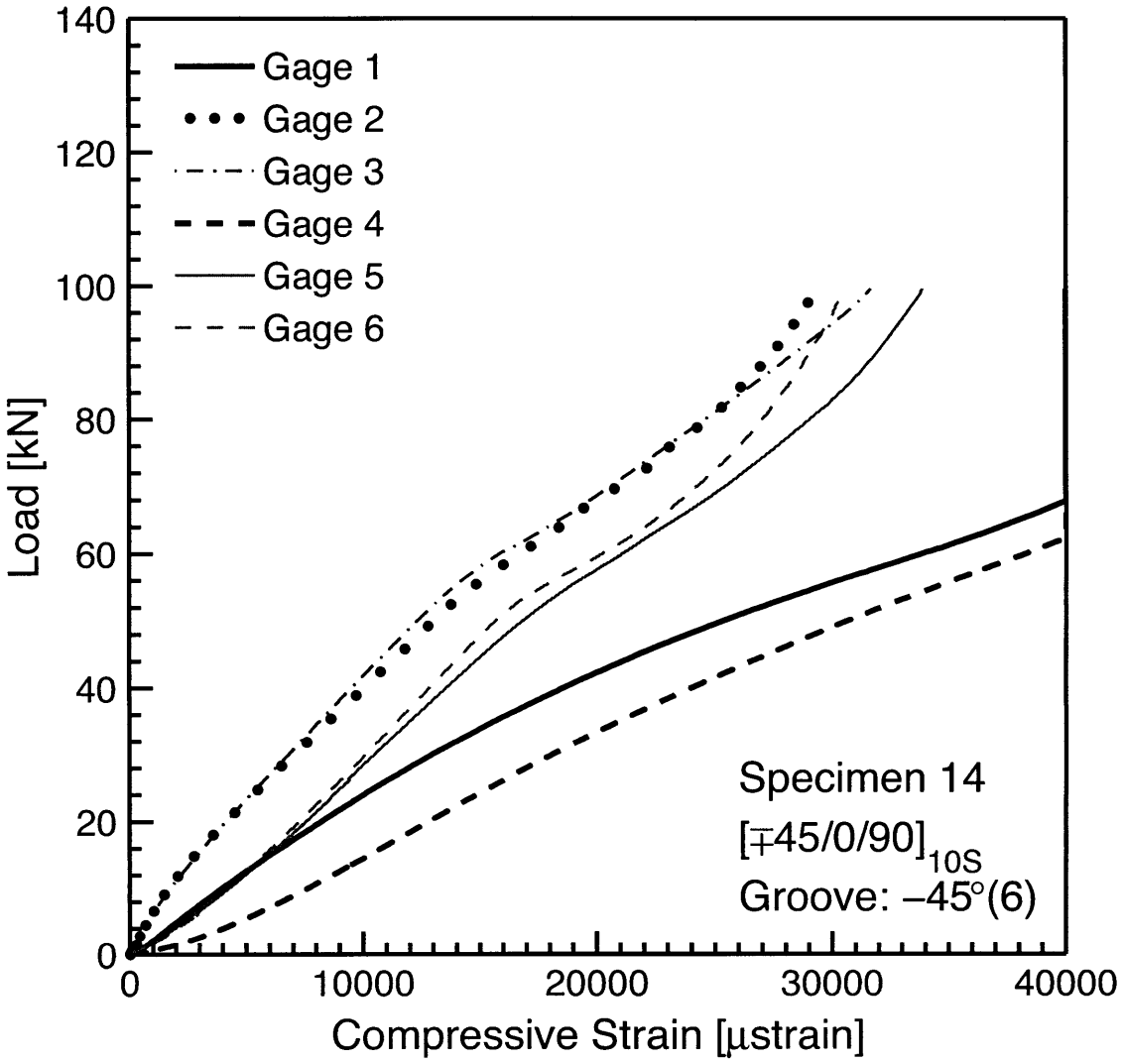

Figure 8.2 Load vs. compressive strain plot for Specimen 14: layup $[\mp 45/0/90]_{10S}$ with groove at $-45°$ ply in 6th set.

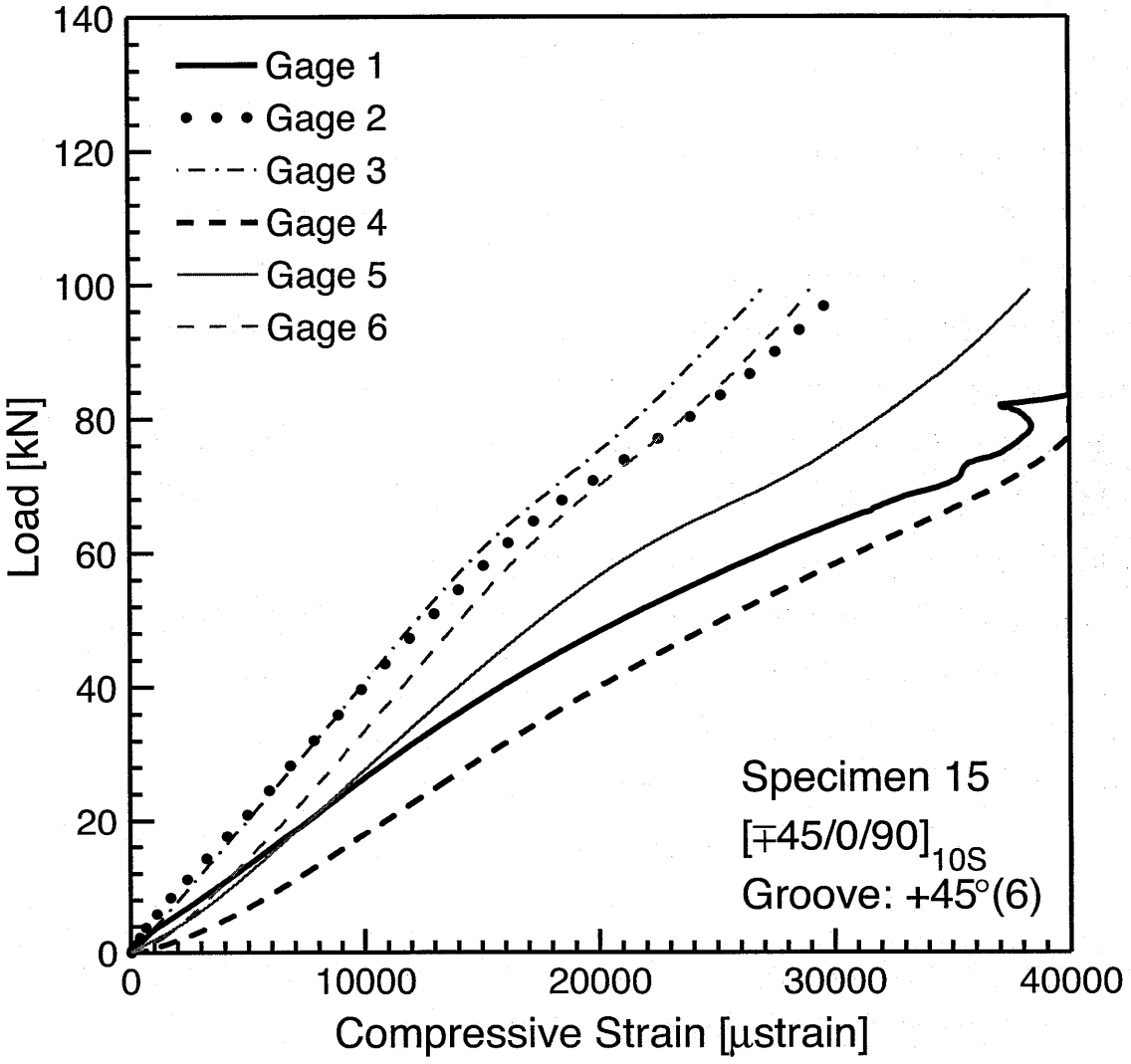

Figure 8.3 Load vs. compressive strain plot for Specimen 15: layup $[\mp 45/0/90]_{10S}$ with groove at +45° ply in 6th set.

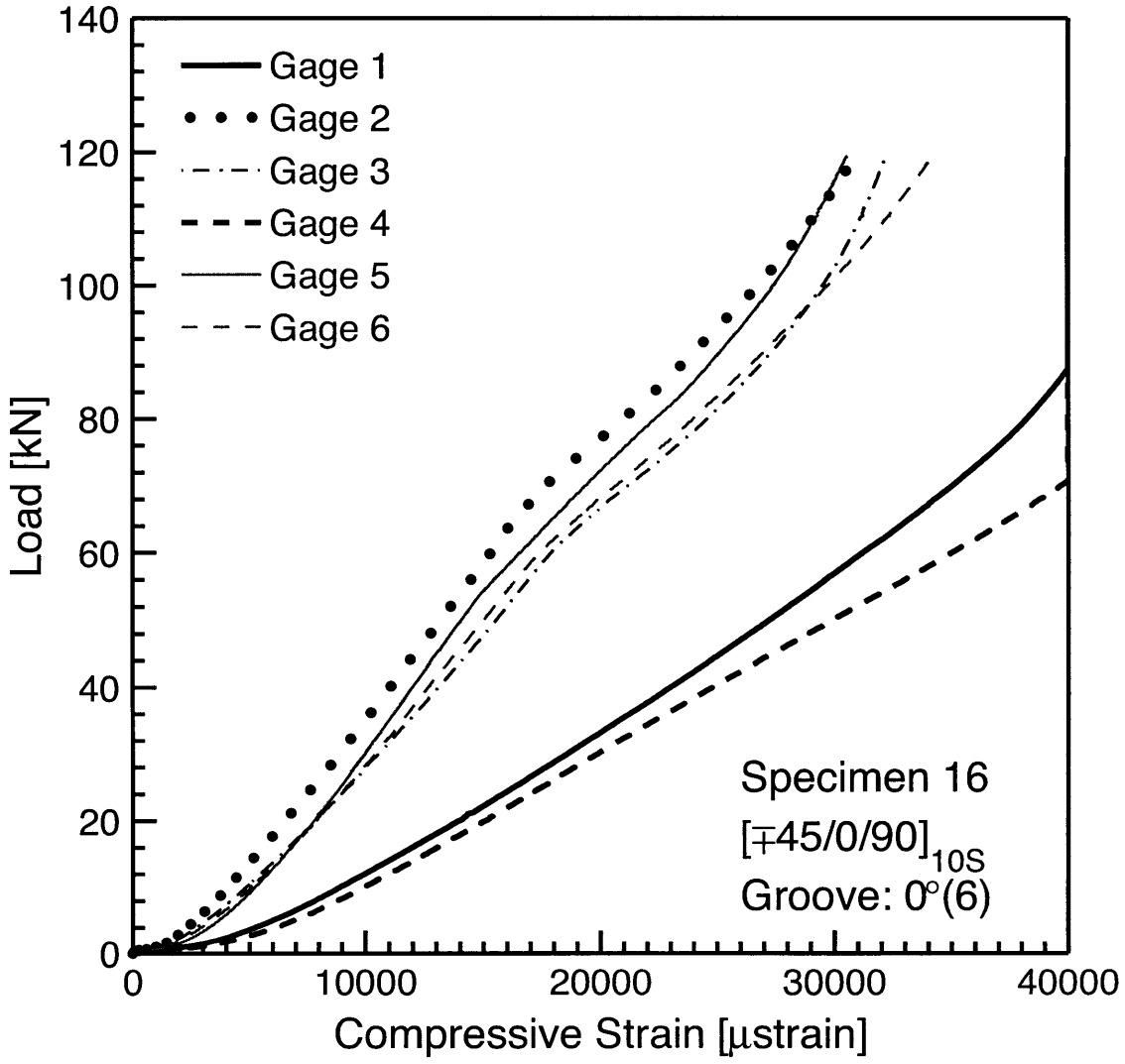

Figure 8.4 Load vs. compressive strain plot for Specimen 16: layup $[\mp 45/0/90]_{10S}$ with groove at 0° ply in 6th set.

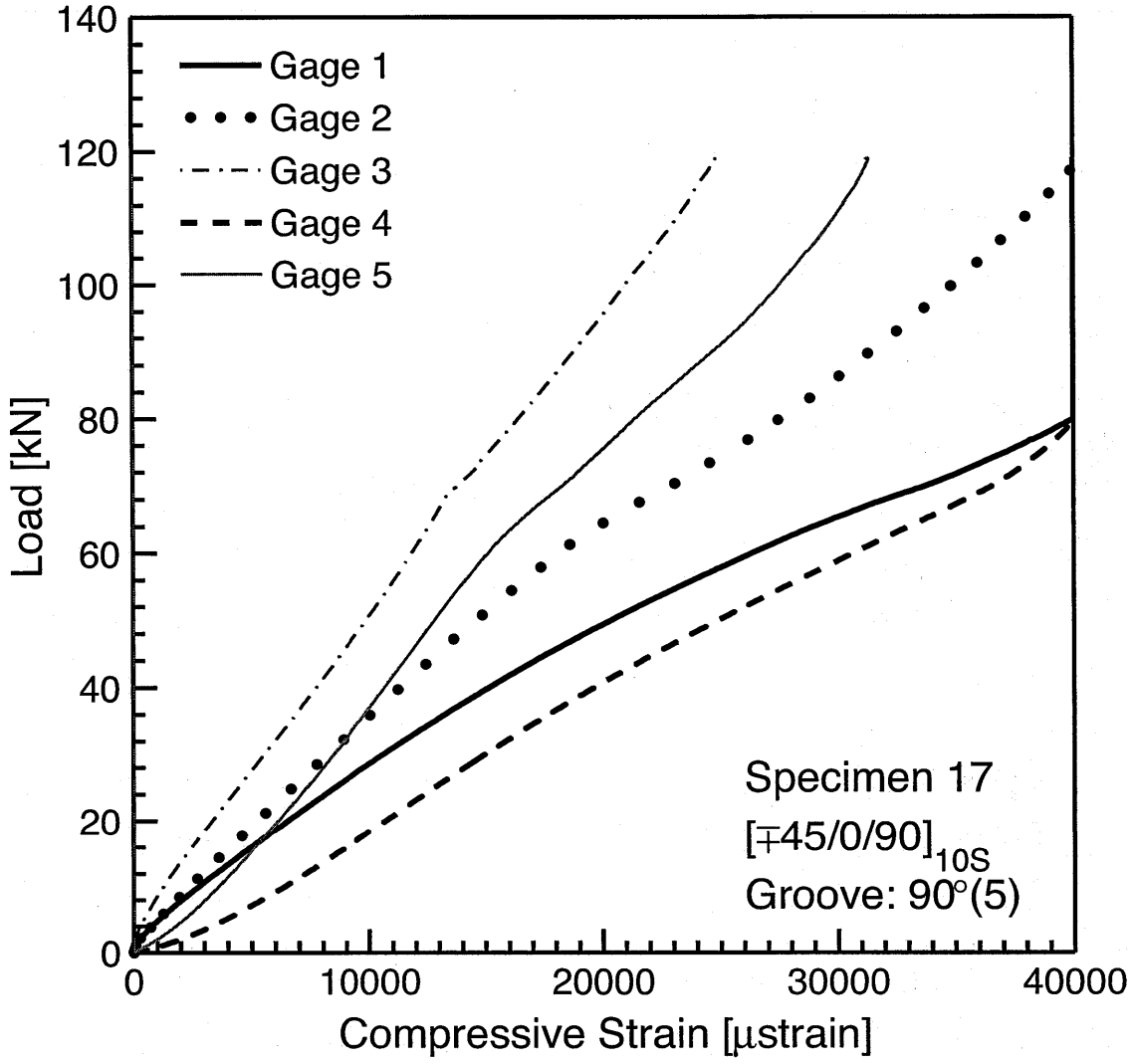

Figure 8.5 Load vs. compressive strain plot for Specimen 17: layup $[\mp 45/0/90]_{10S}$ with groove at 90° ply in 5th set.

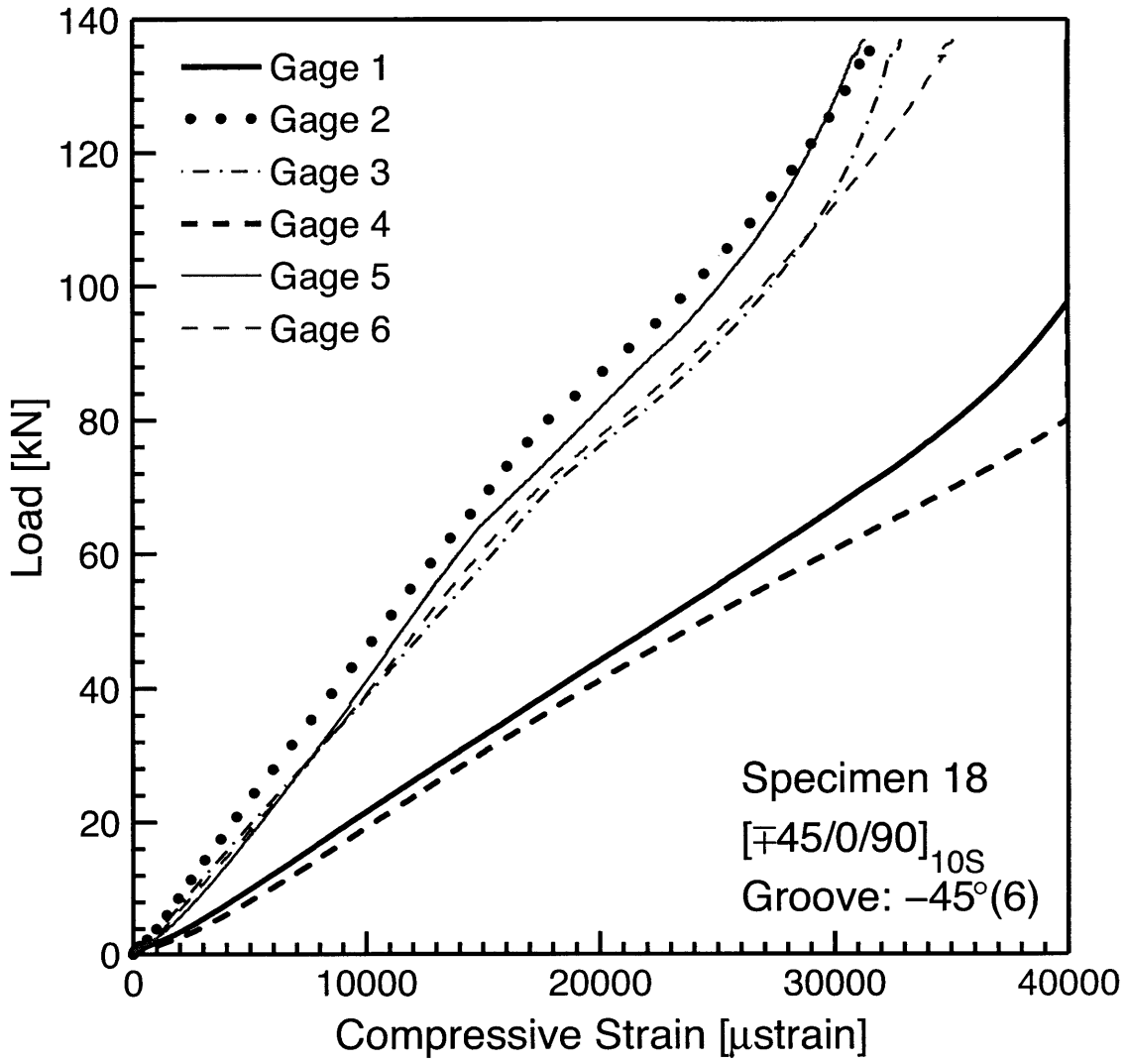

Figure 8.6 Load vs. compressive strain plot for Specimen 18: layup $[\mp 45/0/90]_{10S}$ with groove at $-45°$ ply in 6th set.

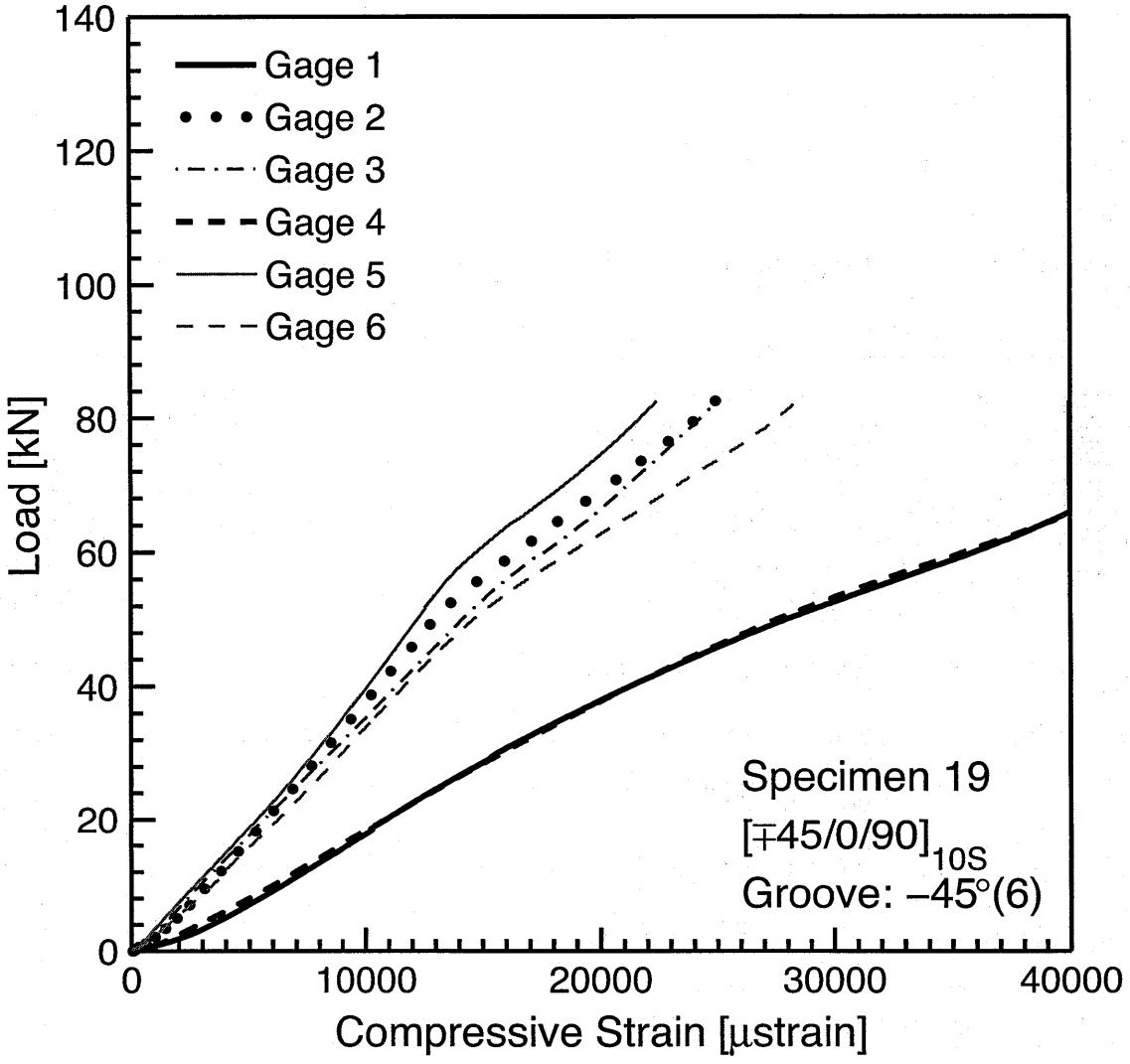

Figure 8.7 Load vs. compressive strain plot for Specimen 19: layup $[\mp 45/0/90]_{10S}$ with groove at $-45°$ ply in 6th set.

groove. This is due to the surfaces of the indenter and the groove having a finite roughness, and not being perfectly circular. The straightness of the indenter has a finite tolerance, as presented in Section 7.2. The groove also has a straightness tolerance due to the machining accuracy, and it cannot be made perfectly parallel to the $+x_3$-face of the specimen. Thus, the contact and the load transfer between the indenter and the groove is considered to have a variability along the x_2-axis, and thus the strain values measured on the two x_2-faces can differ somewhat. However, this variability is assumed to be not proportional to the load but only to the initial overall configuration. The verification of the "two-dimensional" state therefore should be performed by comparing the strains that are proportional to the load. Thus, the comparison should be done at relatively high loads, where the non-proportional component of the strain is considerably smaller than the proportional component.

On the other hand, when the load becomes close to the maximum load, it is expected that damage occurs within the specimen. Such damage can have variability along the x_2-axis, and therefore, can result in differences in the measured strain values on the $+x_2$- and $-x_2$-faces. Thus, the comparison of strain values should not be performed at loads close to the maximum load, where damage may have occurred. It was therefore concluded that a load of 40 kN be chosen at which the strain values are compared. The average strain of the two compared gages and the variation, in percentage, for these gages are given for each specimen in Table 8.2. Since the strain data of gage 6 of Specimen 17 were not valid, comparison regarding gage 6 for this specimen was not possible.

The accuracy of the placement of the gages is considered to have an effect on the variation of the compared strain values. This is attributed to the expected gradient around the groove of the compressive normal strain in the x_3-direction, ϵ_{33}, which is somewhat proportional to the normal stress in the x_3-direction, σ_{33}. From the stress contour plots of σ_{33} presented by Bastien [12], it is observed that the magnitude of σ_{33} changes by 10% when the coordinate value of x_3 changes by 1.0 mm around the location of strain gages 1 and 4. Because ϵ_{33} is directly related to σ_{33}, it is expected that ϵ_{33} would also change by approximately 10% when the coordinate value of x_3

Table 8.2 Comparison of strain data of Specimens 13-19 at load of 40 kN (Average value in [μstrain] and variation in %)

	Gages				
Specimen	1 & 4	2 & 5	3 & 6	2 & 3	5 & 6
13	19900 ± 15%	11300 ± 2%	11600 ± 13%	12400 ± 7%	10600 ± 5%
14	21400 ± 13%	11800 ± 15%	11200 ± 15%	9800 ± 3%	13300 ± 3%
15	17900 ± 12%	12000 ± 17%	10800 ± 8%	9900 ± 1%	12800 ± 9%
16	24000 ± 4%	11300 ± 2%	11600 ± 13%	12400 ± 7%	10600 ± 5%
17	17500 ± 13%	11000 ± 3%	–	9600 ± 19%	–
18	18800 ± 3%	9300 ± 6%	10300 ± 0%	9500 ± 8%	10000 ± 2%
19	21300 ± 0%	10400 ± 2%	11600 ± 1%	11000 ± 4%	10900 ± 7%

changes by 1.0 mm. With the method used in this work for placing the strain gages, as described in Chapter 5, a strain gage can be placed in its designated position with the accuracy of ± 0.5 mm. With this accuracy, the x_3-coordinate of gages 1 and 4 could be up to 1.0 mm apart. In addition to this, the gages may not be aligned exactly parallel to the x_3-axis nor be aligned on the x_3-axis to have the x_1-coordinate zeroed. These two misalignments make the output of the strain gage different from the true ϵ_{33} value at the designated location. With all these factors, the strain gage outputs can differ more than approximately 15% even if the desired two-dimensional state is realized in the specimen, and true ϵ_{33} values are equal on the $+x_2$-face and the $-x_2$-face. A similar discussion can be applied to gage sets 2 and 5, 3 and 6, 2 and 3, and 5 and 6.

With all these factors taken into consideration a 15% variation of the measured strains on the $+x_2$- and the $-x_2$-face is considered sufficient to verify that a specimen has a stress-strain state that does not vary along the x_2-direction. Therefore, from Table 8.2, Specimens 18 and 19 verify this situation, noting that 15% is equivalent to $\pm 7.5\%$ for the experiment. For the other specimens, not all the compared values satisfy this criterion, but several sets are satisfactory, particularly for Specimen 16. It is recalled here that Specimens 13 through 19 were cut from the same laminated plate, machined with the same procedure, and tested with the same configuration. Thus, the manufacturing and testing procedures were consistent for these specimens. This implies that any differences in result are attributable to other factor than such procedures. Therefore, it is concluded from this data that the testing procedure is established and verified. Thus, the strain gage configuration was no longer necessary for the following specimens.

8.3.2 Load-Stroke Response and Failure

A number of key items are determined from the data and reported here. These are the maximum load, the load-per-stroke slope, the "knee load", and the locations of delamination. These are subsequently described.

In the results for the specimens in this chapter, the maximum load observed

during the test is reported instead of the load at final failure. This is done because, for some specimens, the load decreased slightly before a large drop in the load was observed and a breakage sound was heard. It is difficult to define the final failure load in these cases. The load-per-stroke slope is calculated by performing a linear fit to the data in the load range from 20 to 40 kN. This was done by the use of Microsoft Excel. A "knee load" is defined in this work as the point of load where the load-per-stroke rate decreases. This is determined roughly by eye, placing a ruler against the linear section (load range of 20 to 40 kN) on the load-versus-stroke plot. For the delamination location, the most obvious "major" delamination location is reported for both the left and right side (observed on the $+x_2$-face) of the groove. "N/A" is reported when no major delamination was observed. The plies indicated are separated with a double slash (//) when three or more plies are observed in the delamination, i.e. two or more ply interfaces are involved. Here, a delamination is considered as "major" when it completely divides the specimen into two parts, or has a length of more than 15 mm. "Minor" delaminations are those that do not qualify to be major, but are seen by eye or microscope. Minor delamination locations are illustrated in figures presented later in this section. With these definitions, the maximum load, the load-per-stroke slope, and the knee load are presented in Table 8.3. The major delamination locations are presented in Table 8.4.

From the test results, it is observed that the failure mode can be separated into two cases. One mode is the case in which the failure load is below 120 kN, and the delamination occurs near the bottom of the groove. This is defined as Mode A. The other mode is the case in which the failure load is above 120 kN, and the delamination occurs both near the bottom of the groove and near the midplane of the specimen, along with a crack at the bottom of the groove that runs in the x_3-direction to the delamination at the midplane. This is defined as Mode B. A summary of the specimens with the base groove ply parameter of $-45°(6)$ is given in Table 8.5 as categorized by their failure mode and with the average maximum load for each category. The responses were very similar among the specimens that were cut from the same laminated plate and failed with the same failure mode. Specimen behavior

Table 8.3 Results of the standard layup specimens

Specimen	Plate	Max. Load [kN]	Load/Stroke [kN/mm]	Knee Load [kN]
13	C	99.5	107.1	54
14	C	99.7	106.3	55
15	C	99.3	112.7	62
16	C	119.4	114.7	64
17	C	119.0	111.5	60
18	C	137.0	111.0	68
19	C	82.5	105.1	55
20	D	126.1	88.8	49
21	D	95.5	81.6	44
22	D	126.2	81.5	44
23	D	125.7	77.9	48
24	D	104.9	82.9	45
25	D	127.1	79.0	41
26	D	104.9	82.3	44
27	D	105.3	86.5	44
28	D	125.1	80.3	41
29	D	130.3	79.5	45
30	D	N/A	82.0	44

Table 8.4 Delamination locations of the standard layup specimens

	Delamination Location	
Specimen	Left	Right
13	N/A*	+45°(6)/0°(6)
14	+45°(7)/0°(7)	−45°(6)//0°(6)
15	N/A	+45°(5)//0°(5)
16	+45°(7)/0°(7)	−45°(6)//0°(6)
17	−45°(7)//0°(7)	−45°(6)//0°(6)
18	90°(11)/0°(11)	−45°(6)//0°(6)
19	N/A	+45°(5)/0°(5)
20	90°(5)// + 45°(6)	−45°(8)//0°(8)
21	N/A	90°(5)// + 45°(6)
22	−45°(9)//0°(9)	−45°(8)//0°(8)
23	−45°(9)//0°(9)	+45°(6)//0°(6)
24	90°(5)// + 45°(6)	N/A
25	N/A	90°(11)/0°(11)
26	90°(5)// + 45°(6)	−45°(7)//0°(7)
27	N/A	90°(5)// + 45°(6)
28	−45°(8)/ + 45°(8)	−45°(10)/ + 45°(10)
29	90°(11)/0°(11)	−45°(7)//0°(7)
30	N/A	N/A

*N/A = none observed

can be put into four categories based on the plate from which the specimen is made and the failure mode observed. Therefore Specimens 14 (Plate C, Mode A), 18 (Plate C, Mode B), 21 (Plate D, Mode A), and 28 (Plate D, Mode B) are presented in this section as representatives of each category. Specimens 15, 16, and 17 are all cut from laminated Plate C and failed with Mode A. However, since these specimens have different groove ply parameters, results are presented in detail for each of these cases in order to describe the effect of the groove ply parameter. The load-versus-stroke plots are given in Figures 8.8 through 8.14. The photographs of the specimens after failure, and illustrations of the damage locations are given in Figures 8.15 through 8.28.

Large differences in the load-per-stroke rate and the value of knee load are observed between the specimens cut from Plates C and D, while an obvious difference in the maximum load is not seen. For the load-per-stroke rate, the specimens cut from Plate C have an average of 109.8 kN/mm with a variation of +4.9, -4.7 kN/mm (±4%). The specimens cut from Plate D have an average of 82.0 kN/mm, with a variation of +6.8, -4.1 kN/mm (+8, -5%). For the knee load, the specimens from Plate C have an average of 60 kN with a variation of +8, -6 kN (+13, -10%). The specimens from Plate D have an average of 44 kN with a variation of +5, -4 kN (+11, -10%). These differences between specimens from the two plates can be attributed to the difference of the thicknesses of the specimens. Specimens cut from Plate C have an average thickness of 11.93 mm and specimens from Plate D have an average thickness of 12.68 mm. This difference in thickness is considered to be the result of the difference in the volume of resin that flowed out of the laminate during the curing procedure. Thus, when the layup is maintained the same, a thinner laminate indicates a higher fiber volume fraction. From the simple rule of mixture, the compressive modulus in the transverse direction enlarges as the fiber volume fraction increases. The load-per-stroke rate is expected to be proportional to the compressive modulus in the x_3-direction, resulting in the difference between specimens cut from Plates C and D.

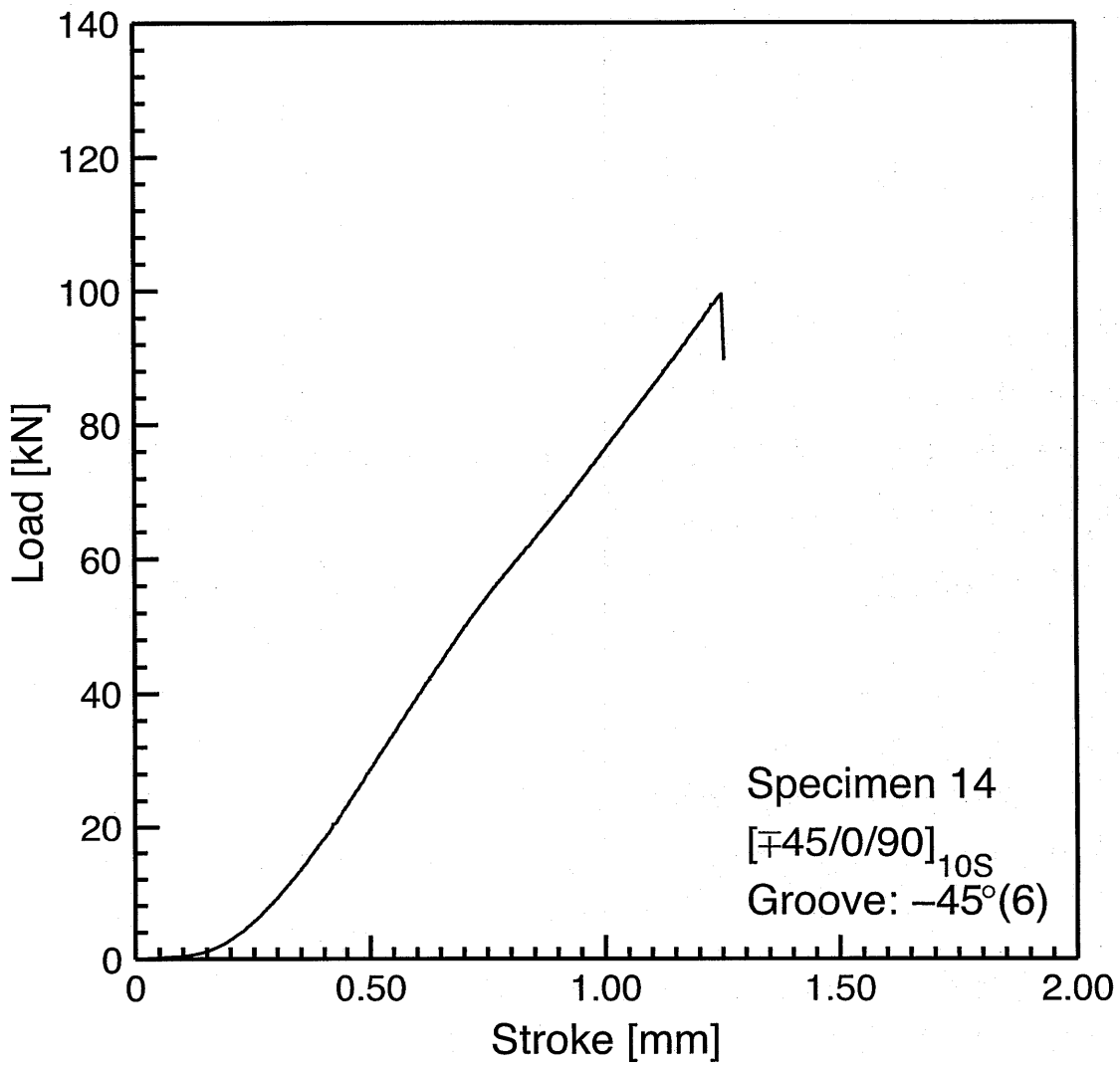

Figure 8.8 Load vs. stroke plot for Specimen 14: layup $[\mp 45/0/90]_{10S}$ with groove at $-45°$ ply in 6th set.

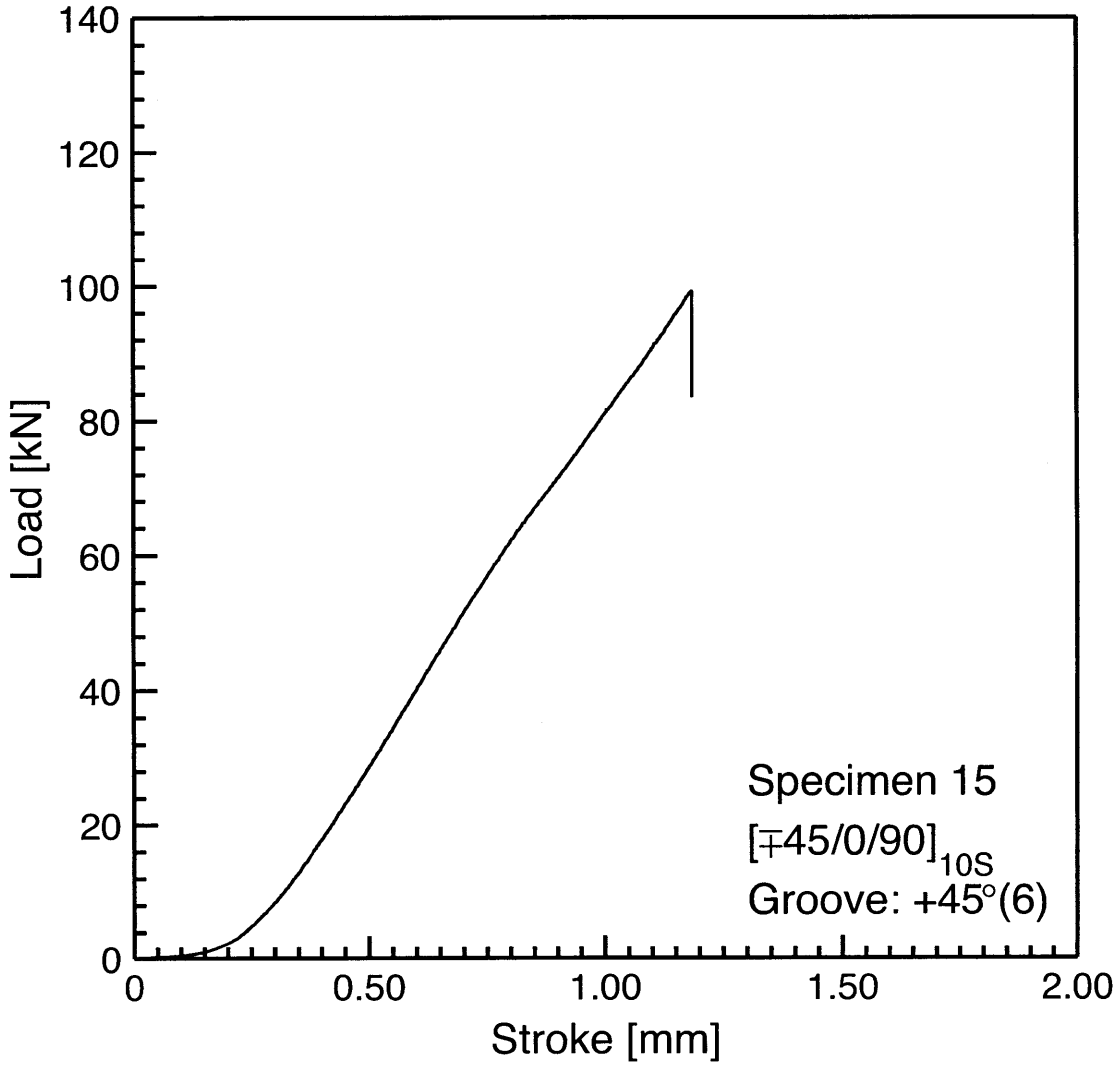

Figure 8.9 Load vs. stroke plot for Specimen 15: layup $[\mp 45/0/90]_{10S}$ with groove at $+45°$ ply in 6th set.

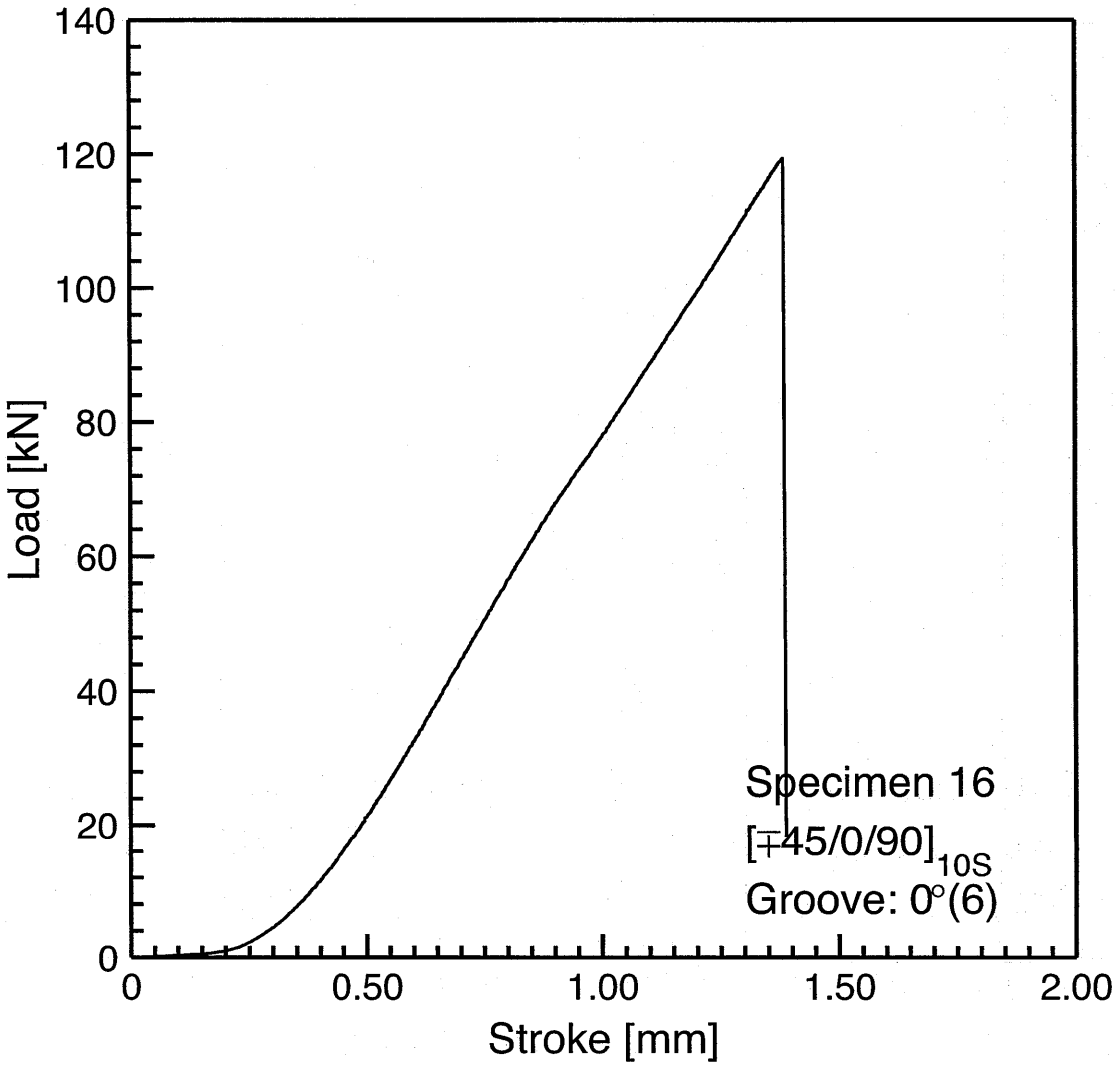

Figure 8.10 Load vs. stroke plot for Specimen 16: layup $[\mp 45/0/90]_{10S}$ with groove at 0° ply in 6th set.

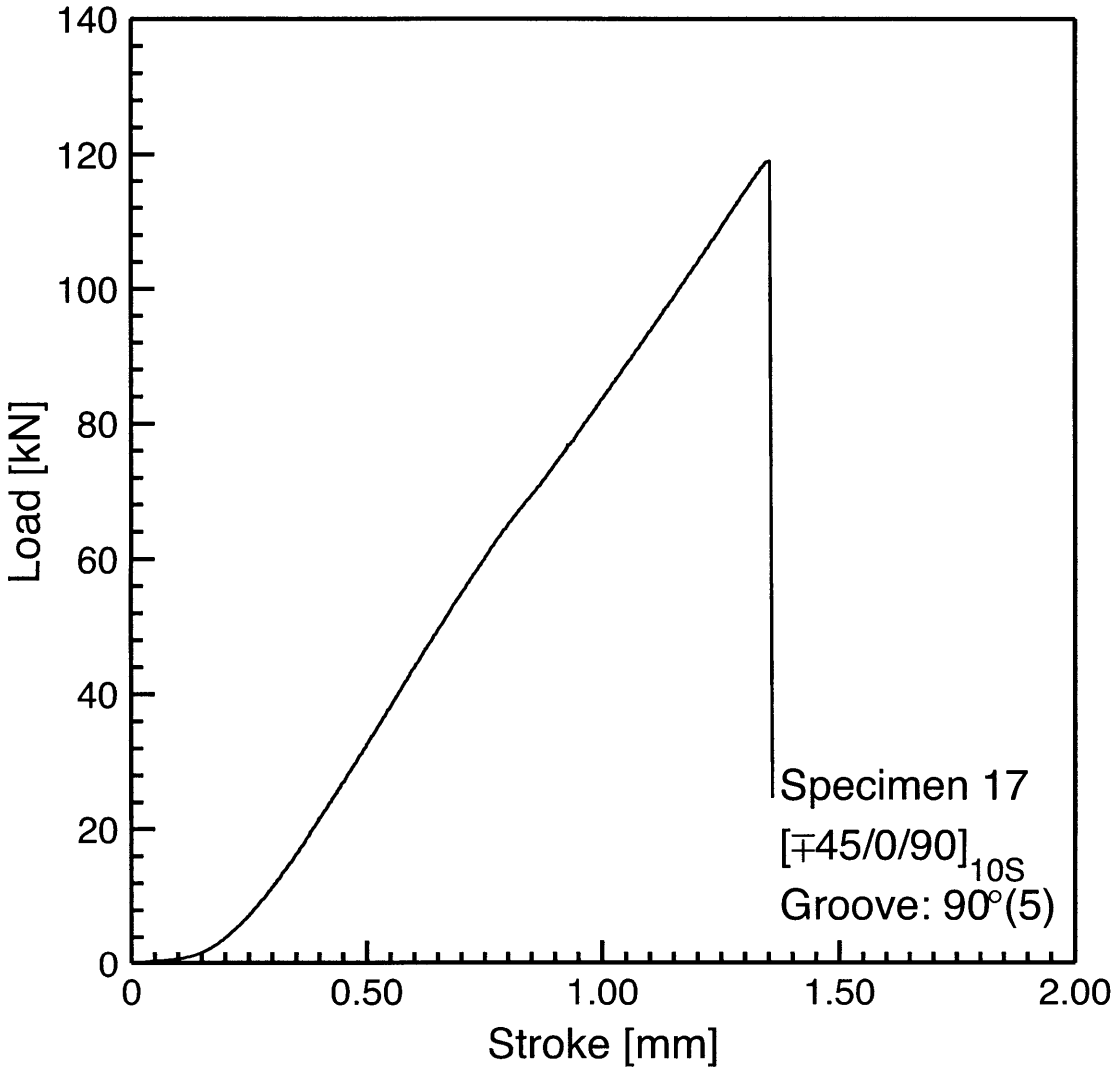

Figure 8.11 Load vs. stroke plot for Specimen 17: layup $[\mp 45/0/90]_{10S}$ with groove at 90° ply in 5th set.

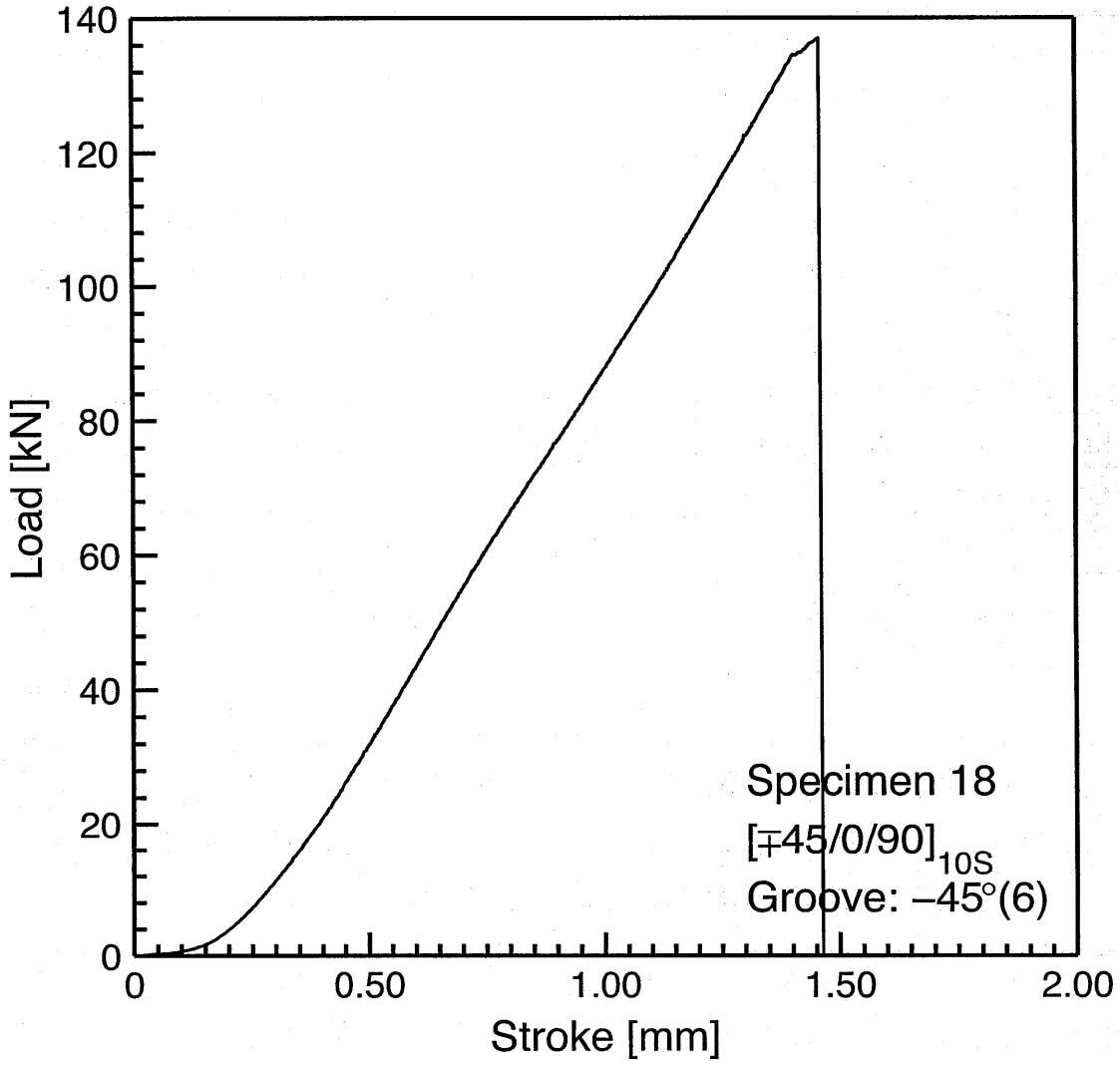

Figure 8.12 Load vs. stroke plot for Specimen 18: layup $[\mp 45/0/90]_{10S}$ with groove at $-45°$ ply in 6th set.

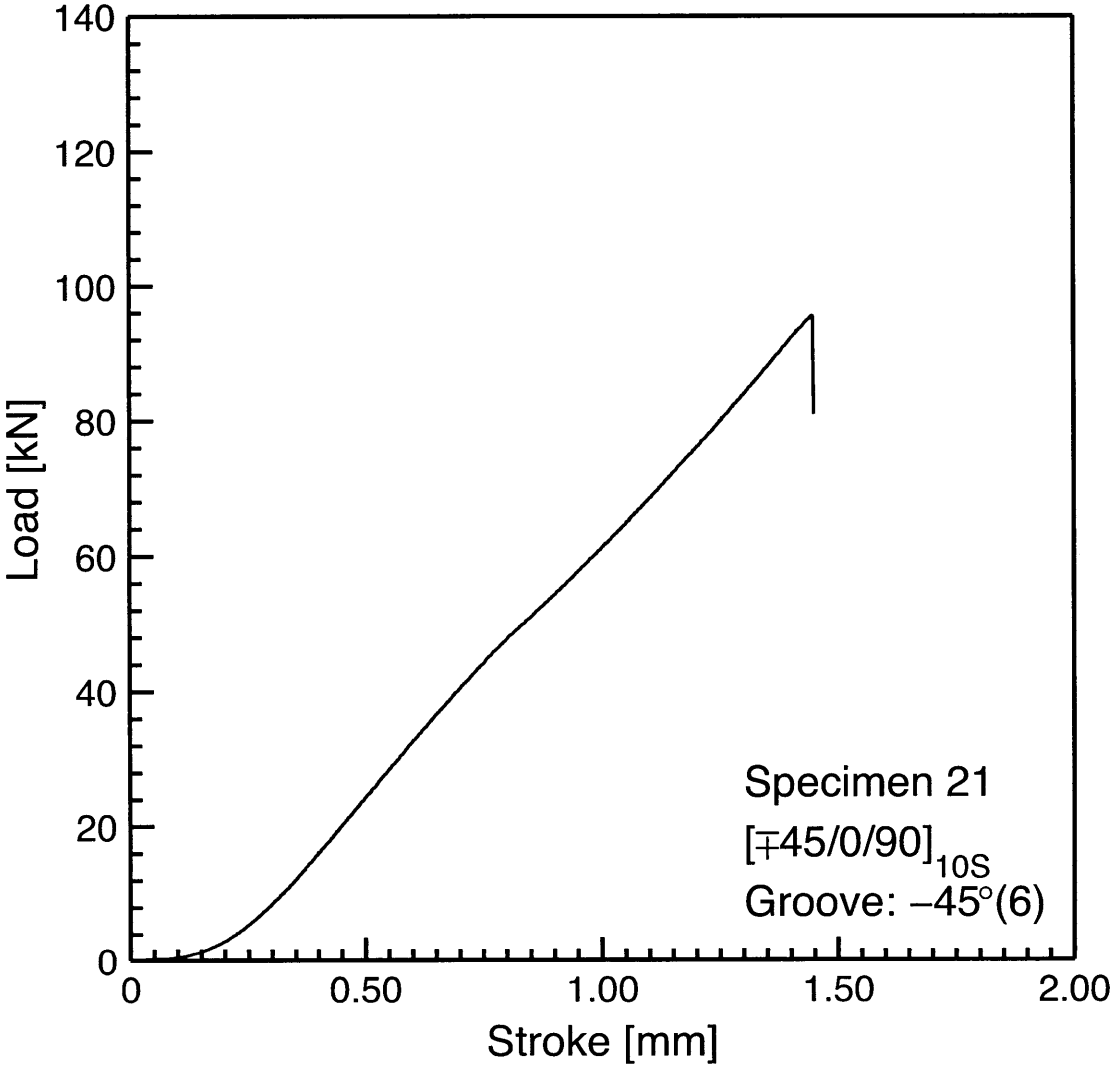

Figure 8.13 Load vs. stroke plot for Specimen 21: layup $[\mp 45/0/90]_{10S}$ with groove at $-45°$ ply in 6th set.

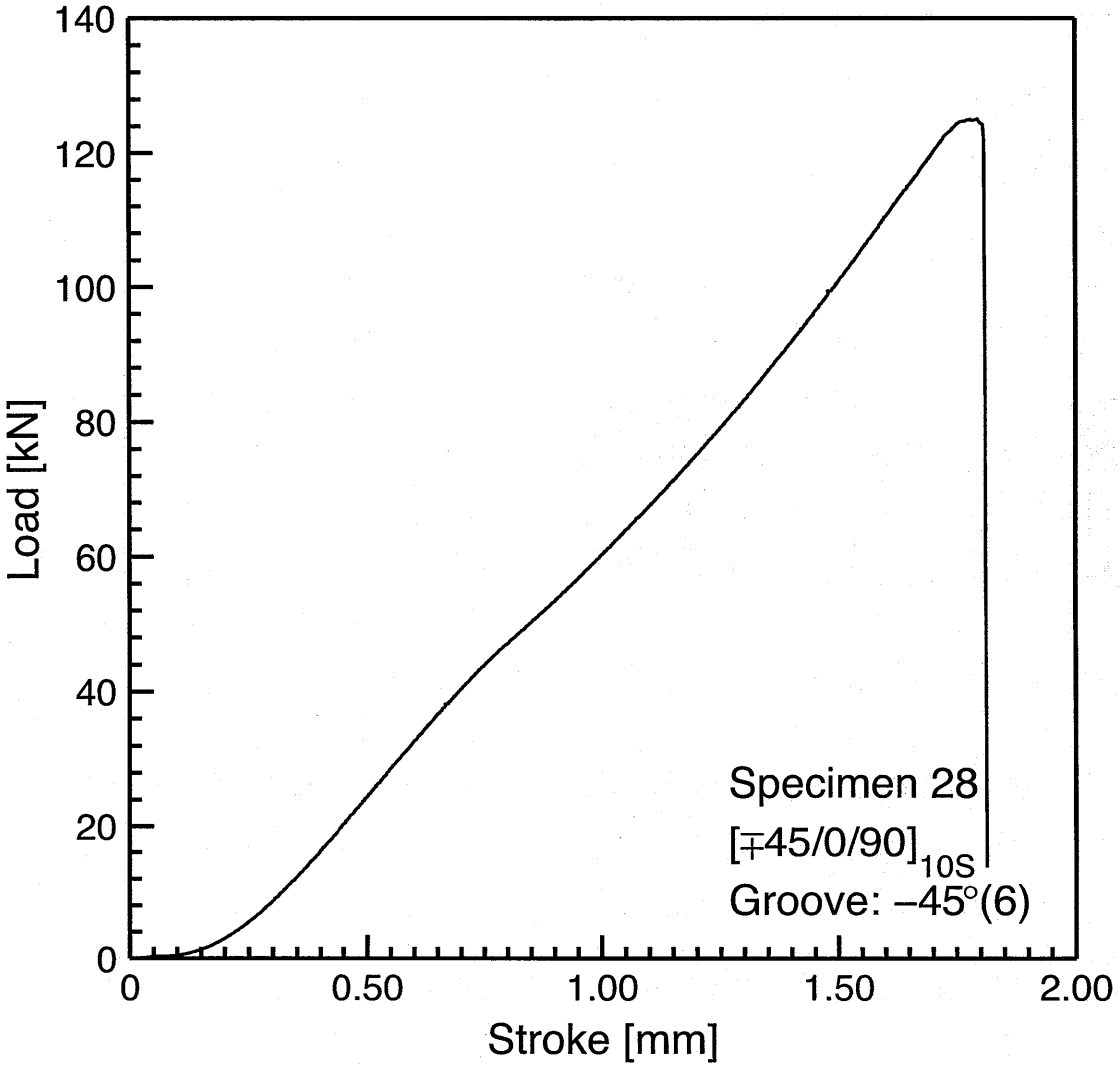

Figure 8.14 Load vs. stroke plot for Specimen 28: layup $[\mp 45/0/90]_{10S}$ with groove at $-45°$ ply in 6th set.

Table 8.5 Failure modes and average failure loads of the standard layup specimens with groove at $-45°$ ply in 6th set

Mode	Plate	Specimens	Ave. maximum load [kN]
A	C	13, 14, 19	93.93
	D	21, 24, 26, 27	104.2
B	C	18	137.0
	D	20, 22, 23, 25, 28, 29	126.8

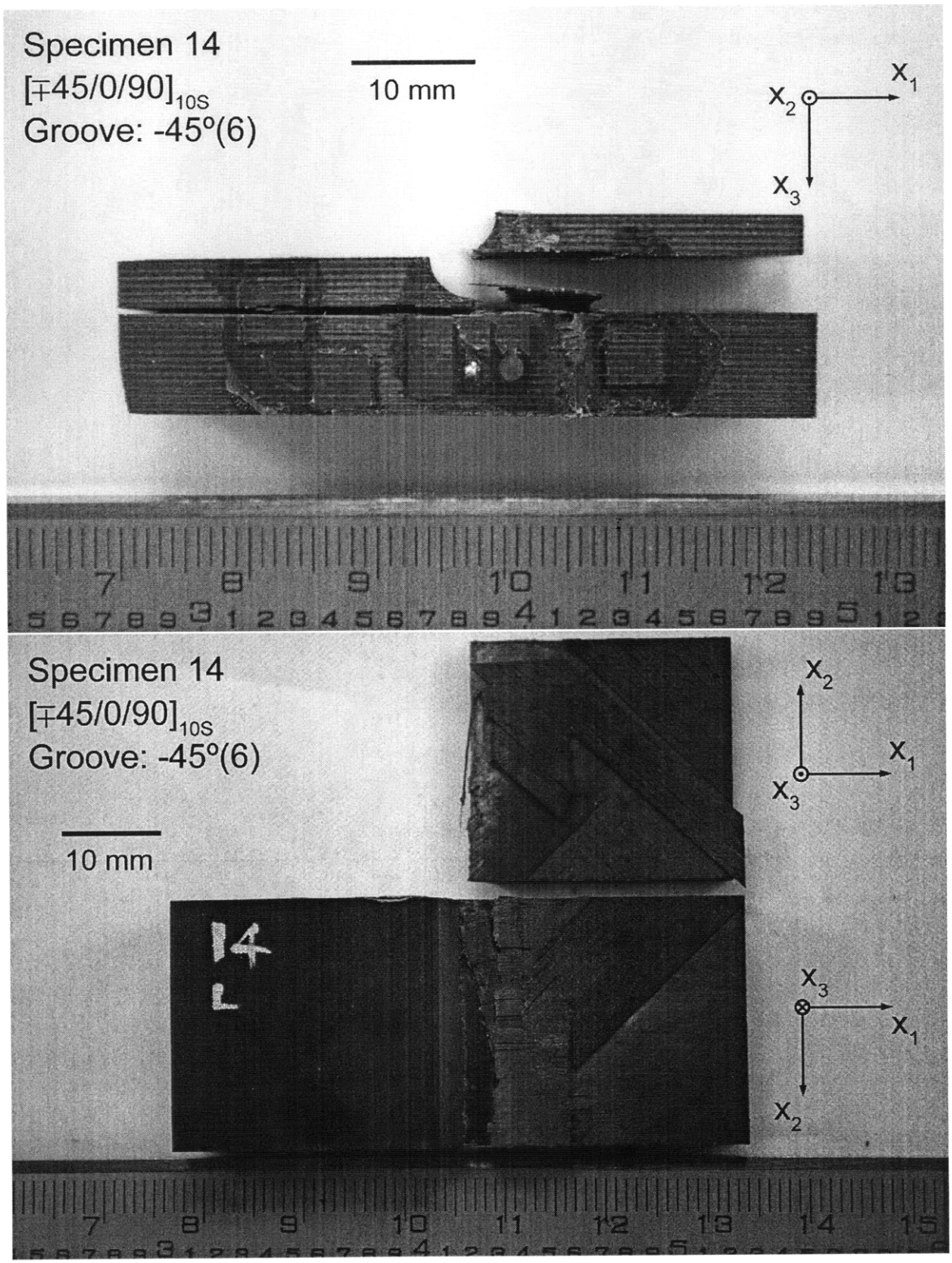

Figure 8.15 Photographs after failure of Specimen 14 (layup $[\mp 45/0/90]_{10S}$ with groove at $-45°$ ply in 6th set) with *(upper)* side view, and *(lower)* failure surface view.

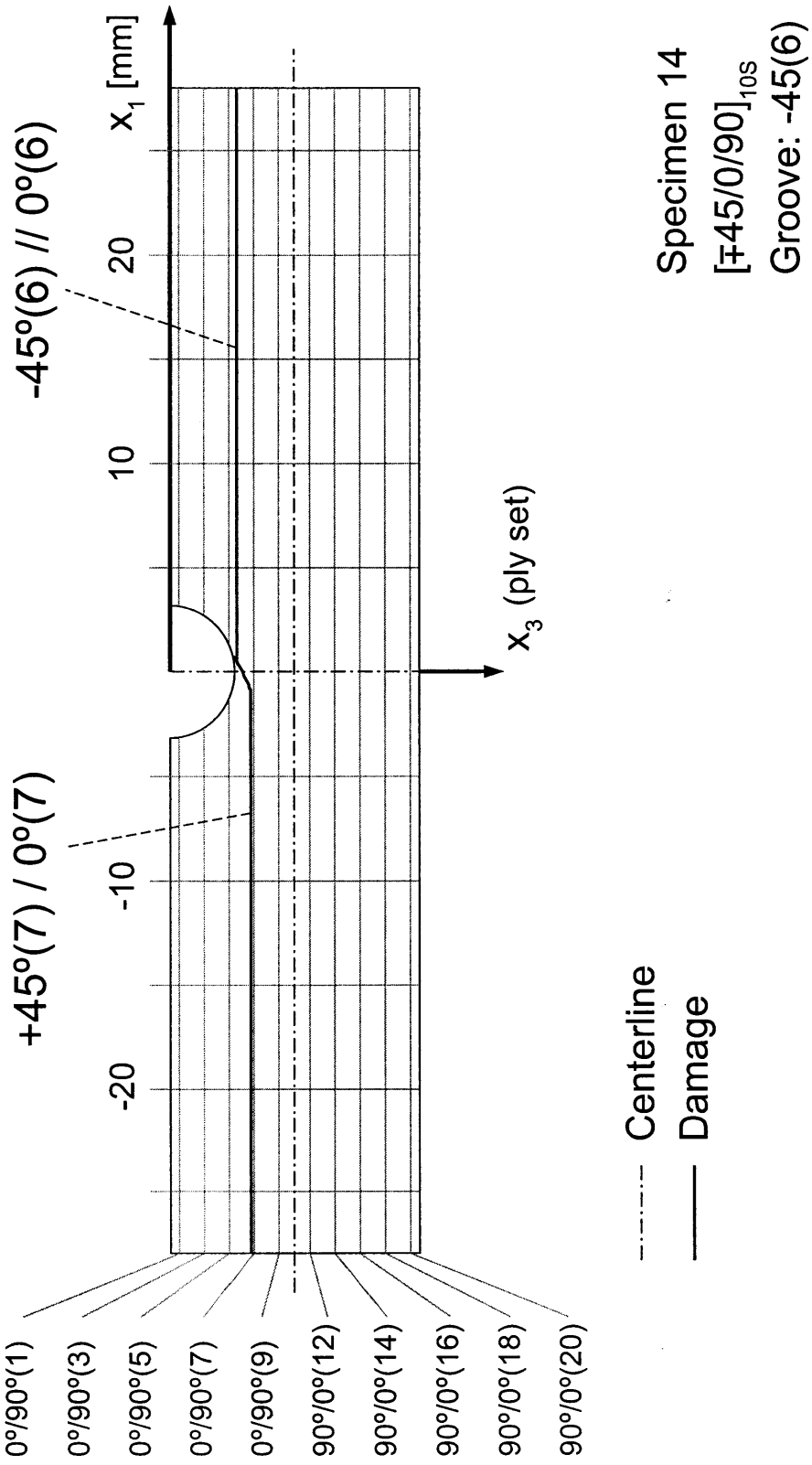

Figure 8.16 Illustration of failure for Specimen 14: layup $[\mp 45/0/90]_{10S}$ with groove at $-45°$ ply in 6th set.

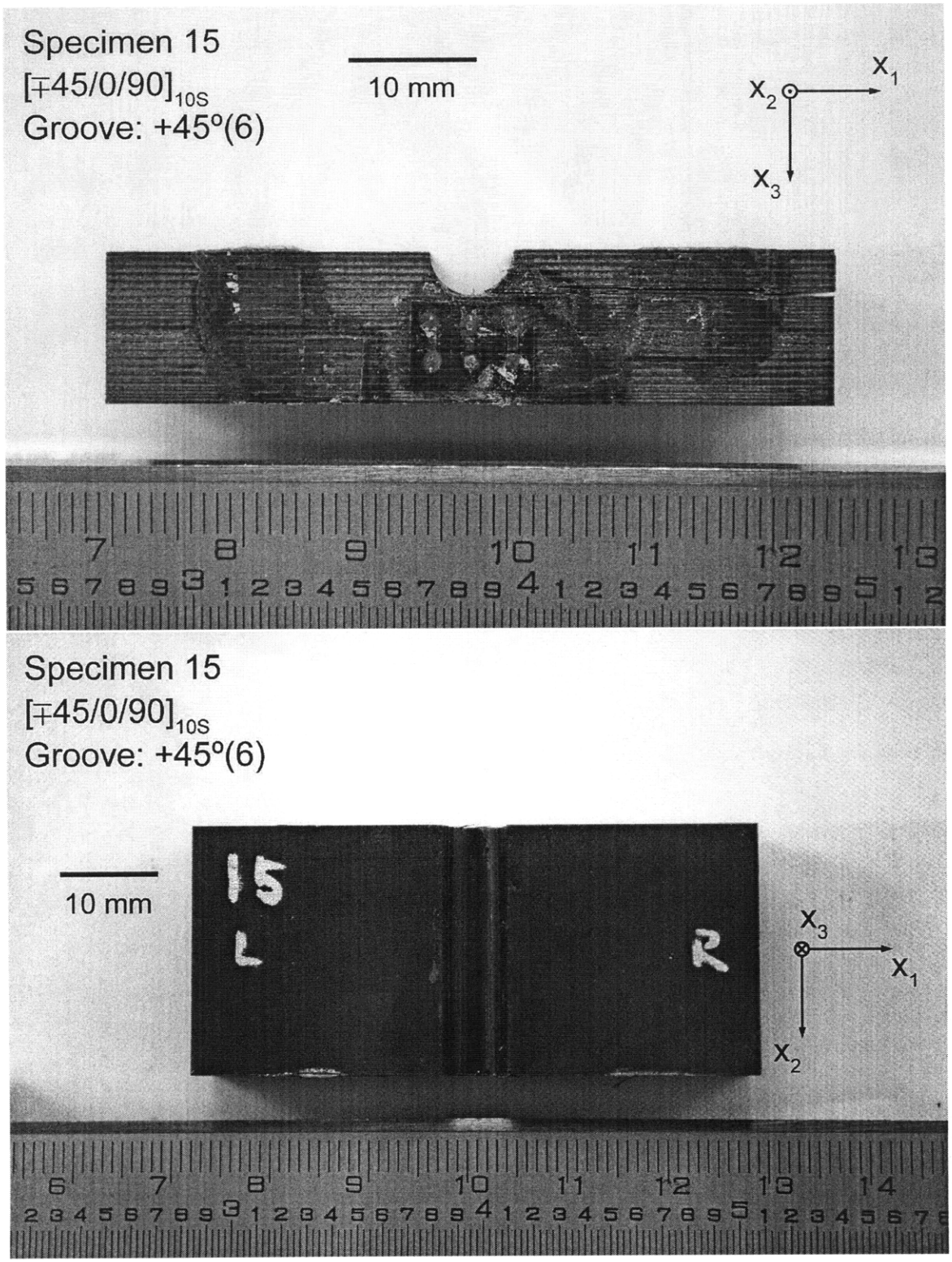

Figure 8.17 Photographs after failure of Specimen 15 (layup $[\mp 45/0/90]_{10S}$ with groove at +45° ply in 6th set) with *(upper)* side view, and *(lower)* failure surface view.

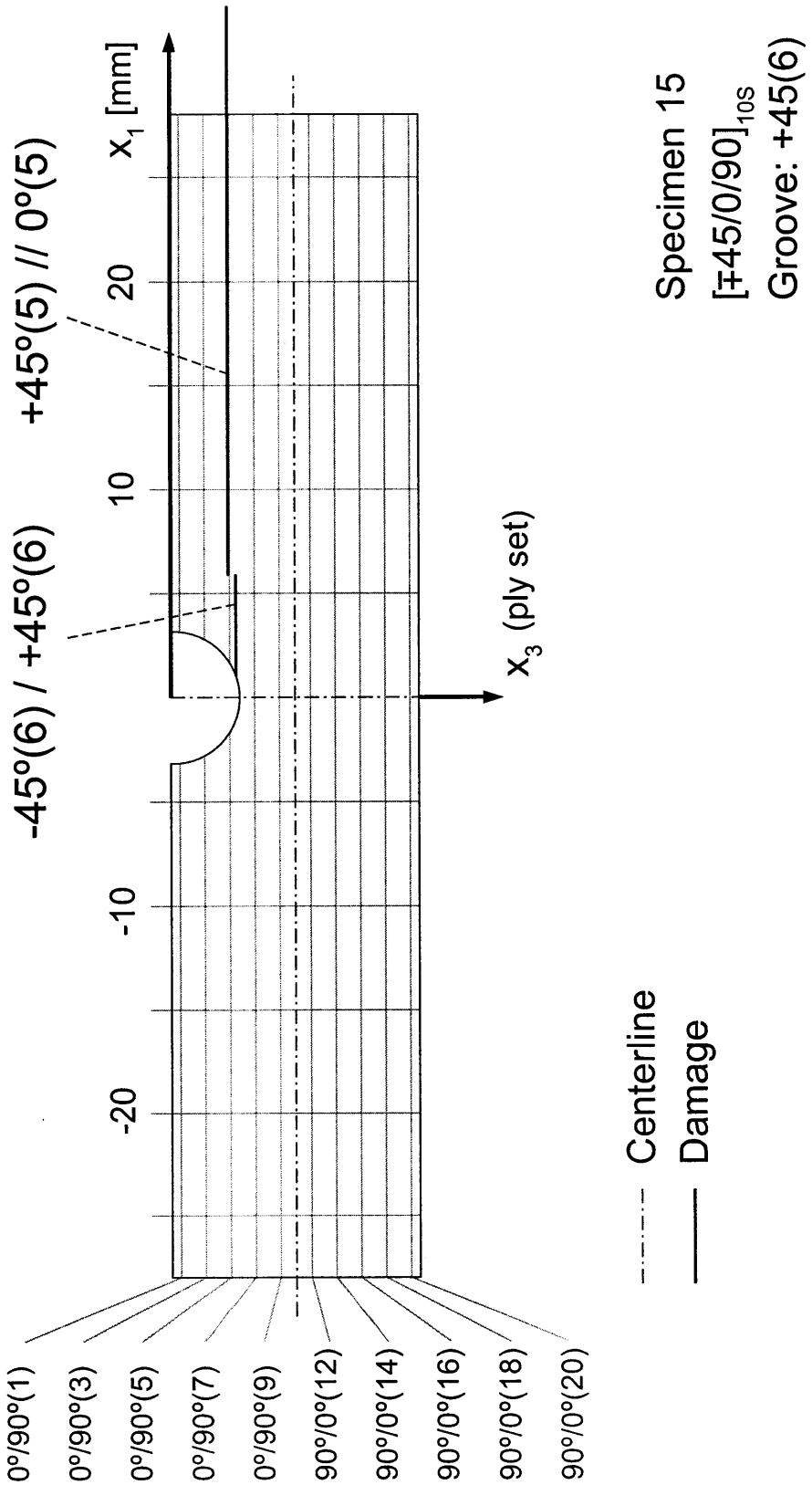

Figure 8.18 Illustration of failure for Specimen 15: layup $[\mp 45/0/90]_{10S}$ with groove at +45° ply in 6th set.

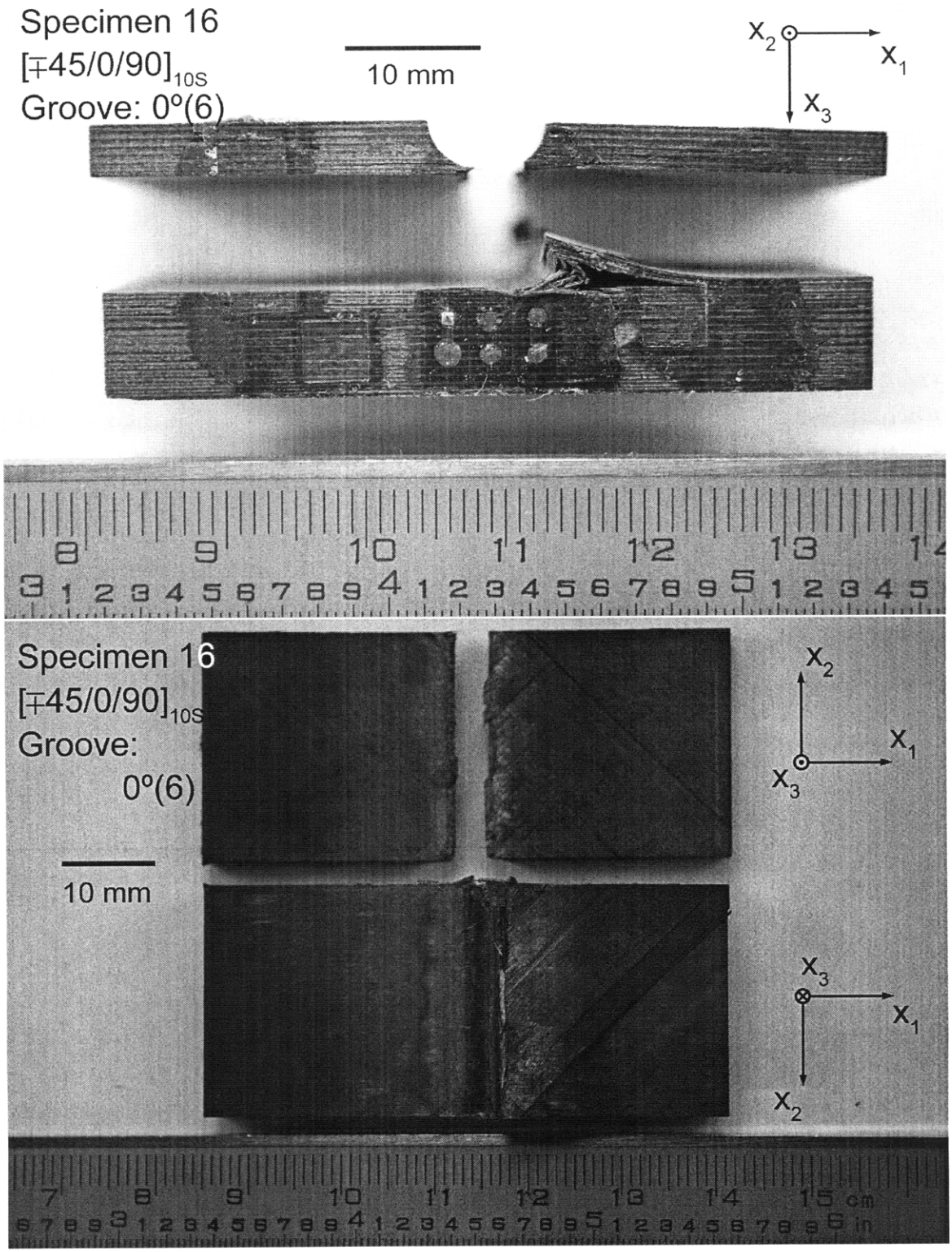

Figure 8.19 Photographs after failure of Specimen 16 (layup $[\mp 45/0/90]_{10S}$ with groove at 0° ply in 6th set) with *(upper)* side view, and *(lower)* failure surface view.

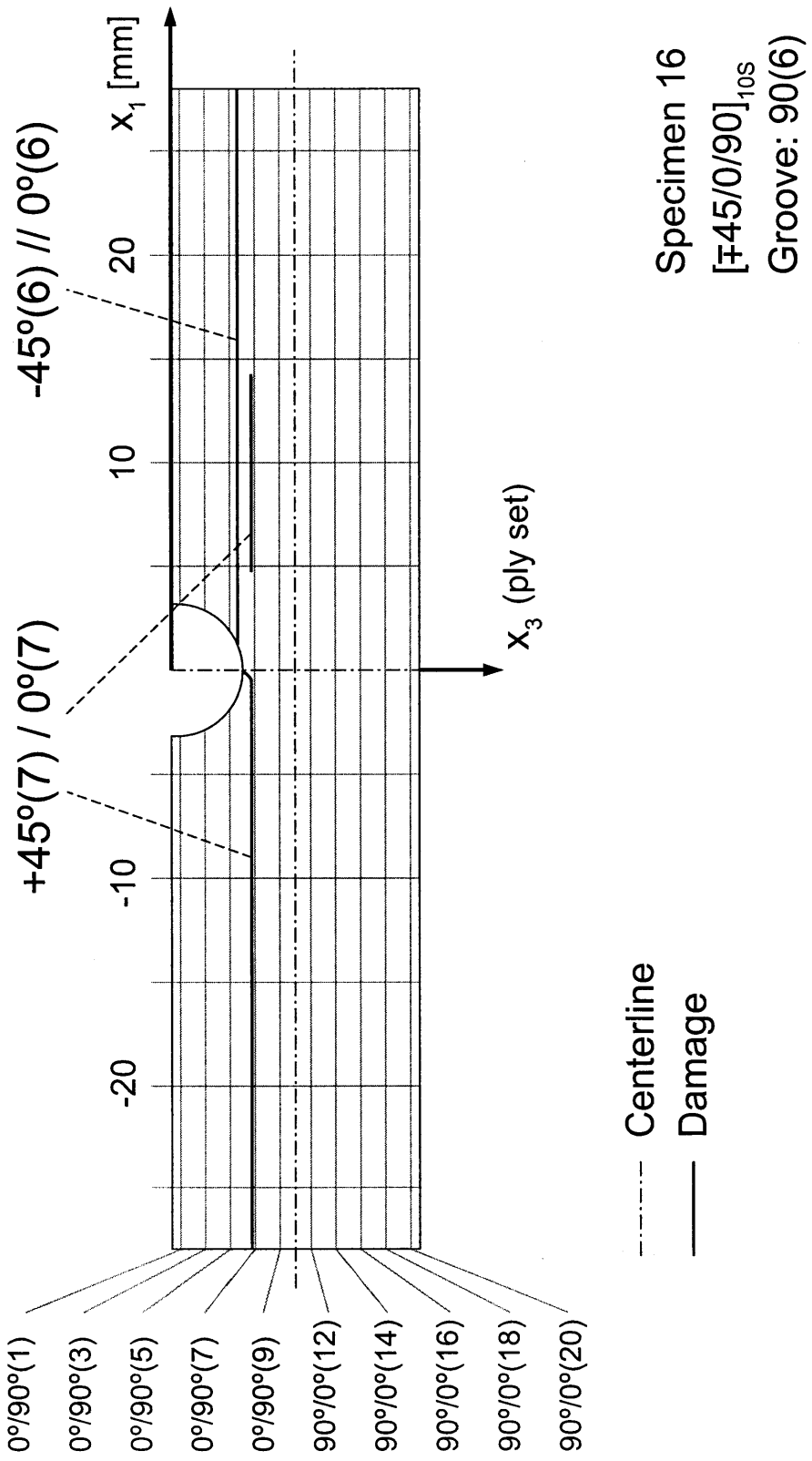

Figure 8.20 Illustration of failure for Specimen 16: layup $[\mp 45/0/90]_{10S}$ with groove at 0° ply in 6th set.

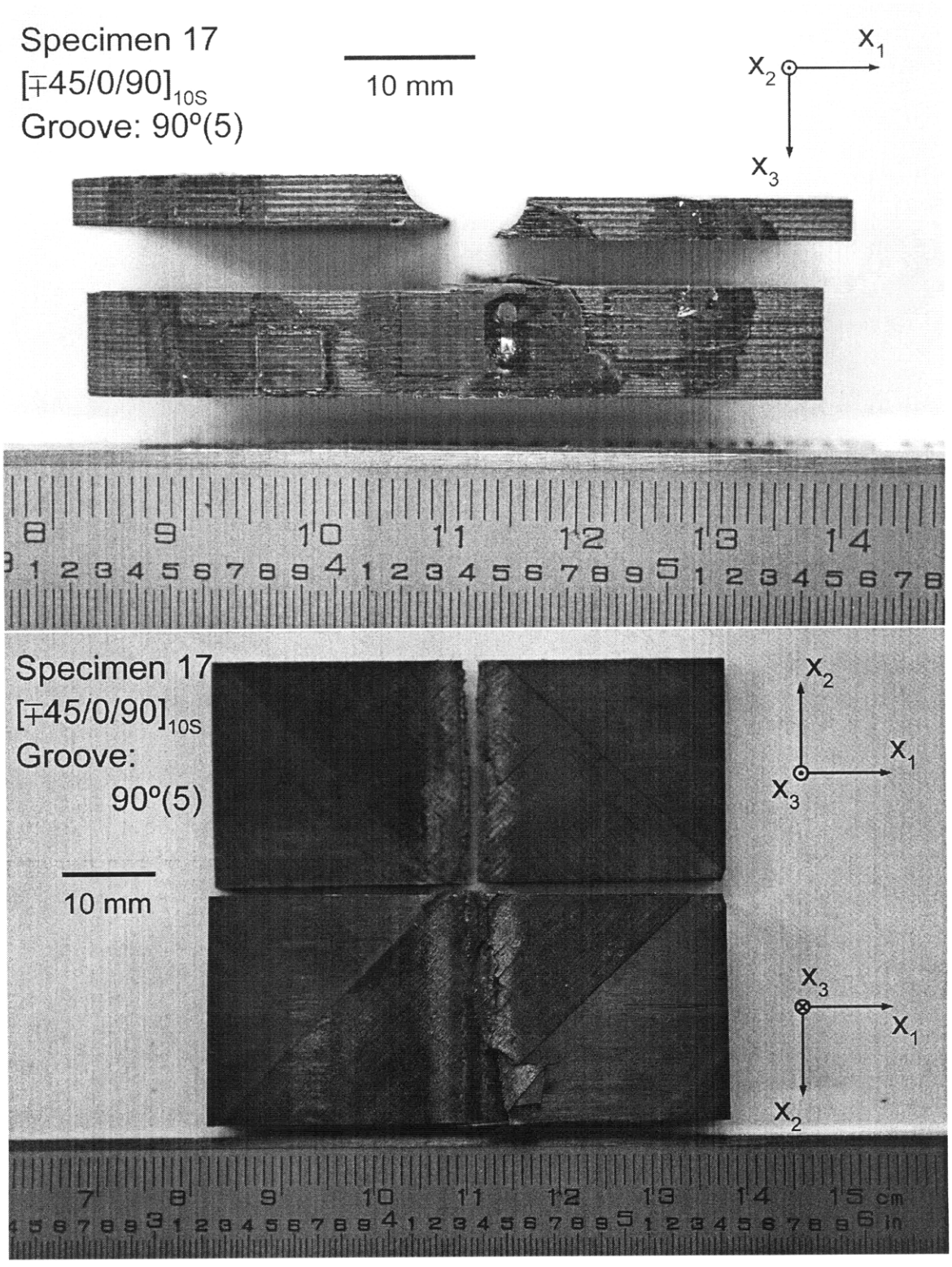

Figure 8.21 Photographs after failure of Specimen 17 (layup $[\mp 45/0/90]_{10S}$ with groove at 0° ply in 5th set) with *(upper)* side view, and *(lower)* failure surface view.

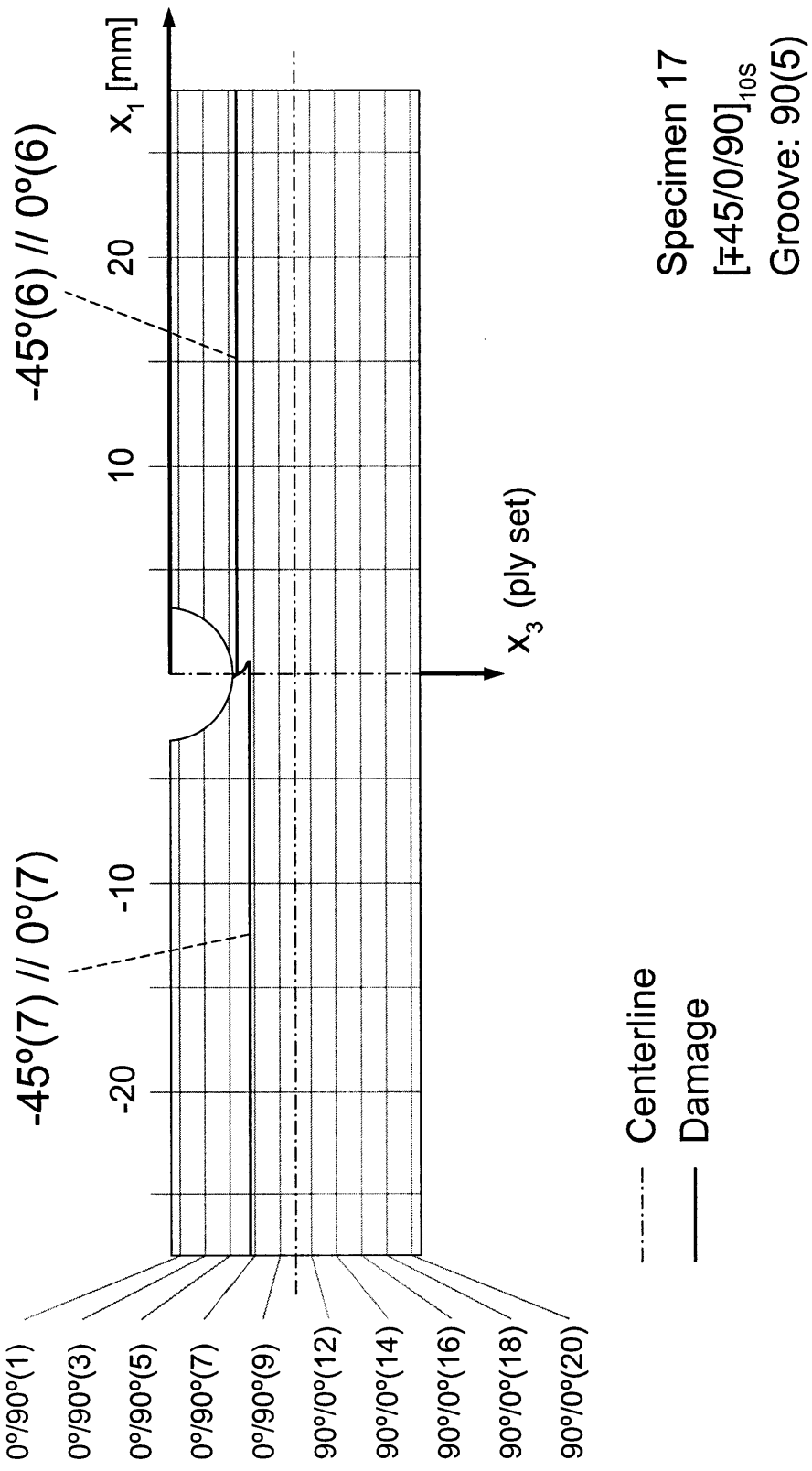

Figure 8.22 Illustration of failure for Specimen 17: layup $[\mp 45/0/90]_{10S}$ with groove at 90° ply in 5th set.

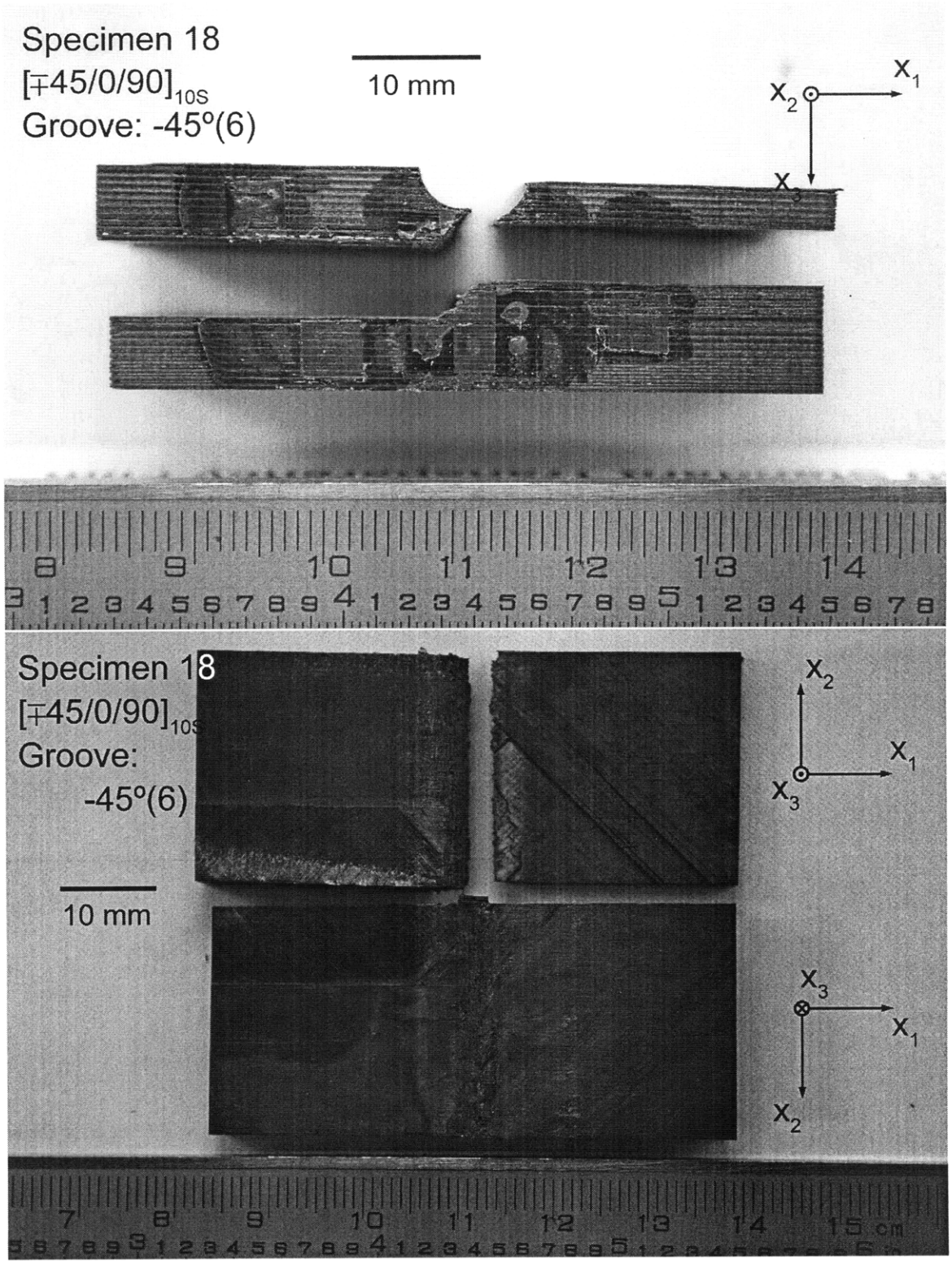

Figure 8.23 Photographs after failure of Specimen 18 (layup $[\mp 45/0/90]_{10S}$ with groove at $-45°$ ply in 6th set) with *(upper)* side view, and *(lower)* failure surface view.

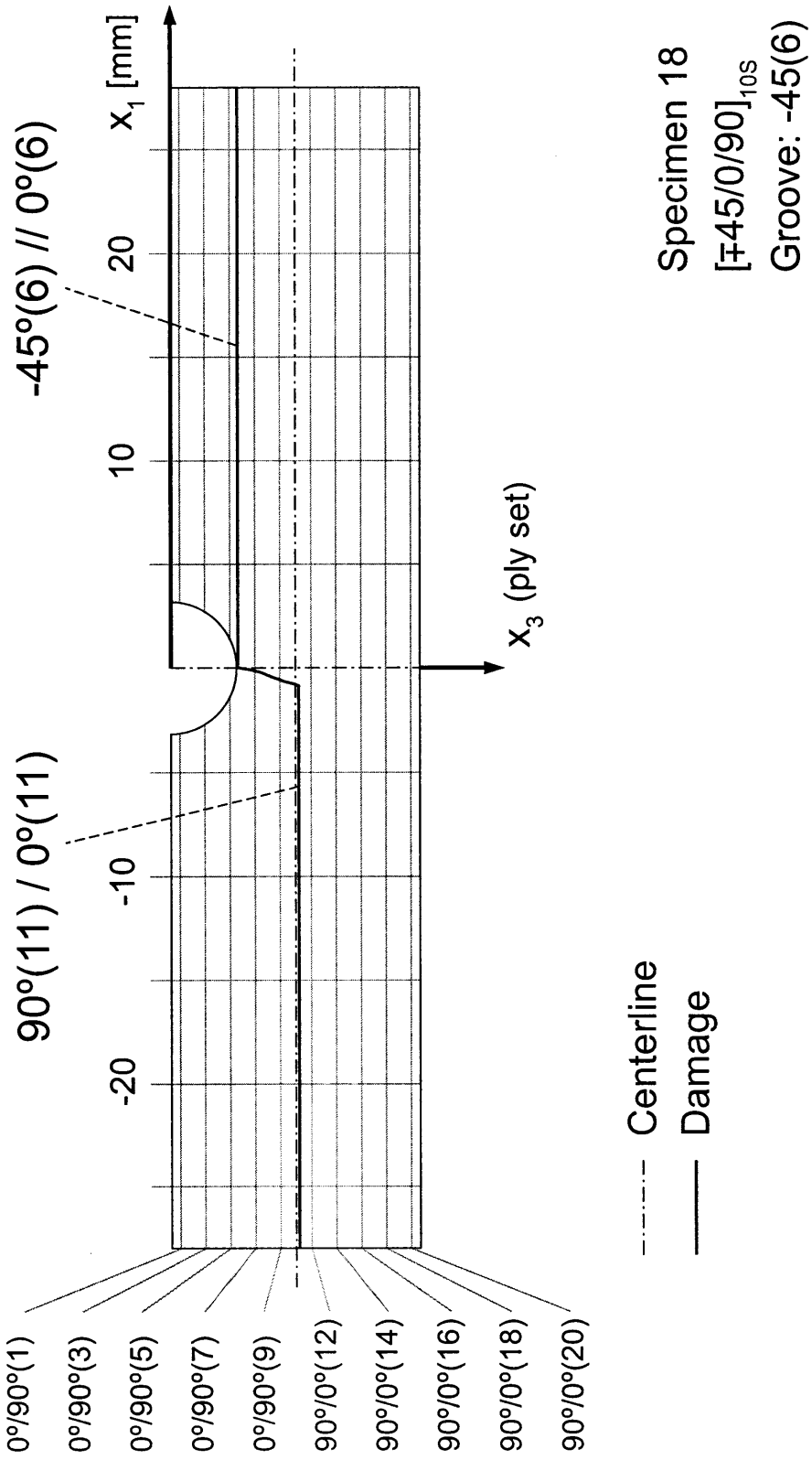

Figure 8.24 Illustration of failure for Specimen 18: layup $[\mp 45/0/90]_{10S}$ with groove at $-45°$ ply in 6th set.

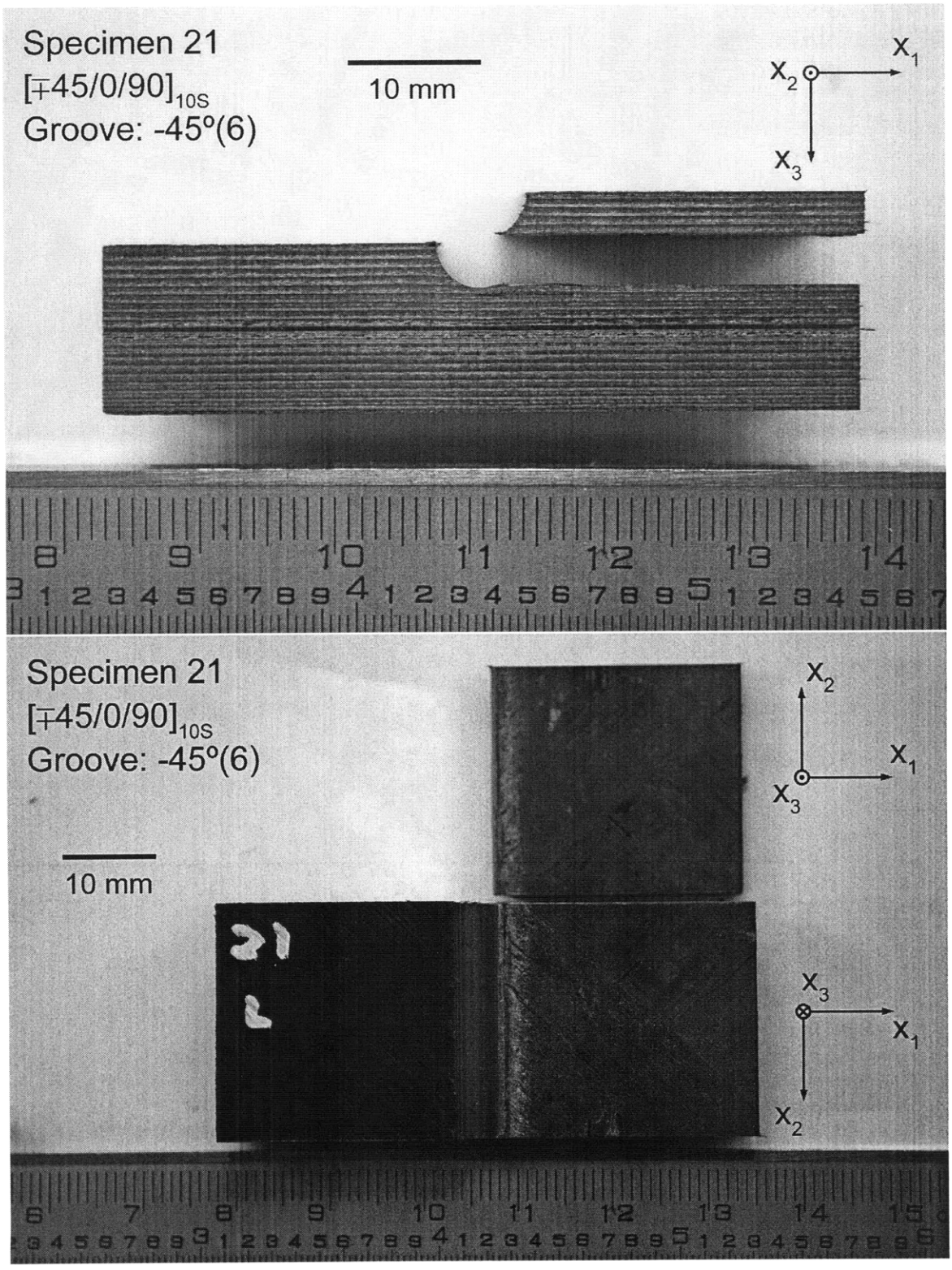

Figure 8.25 Photographs after failure of Specimen 21 (layup $[\mp 45/0/90]_{10S}$ with groove at $-45°$ ply in 6th set) with *(upper)* side view, and *(lower)* failure surface view.

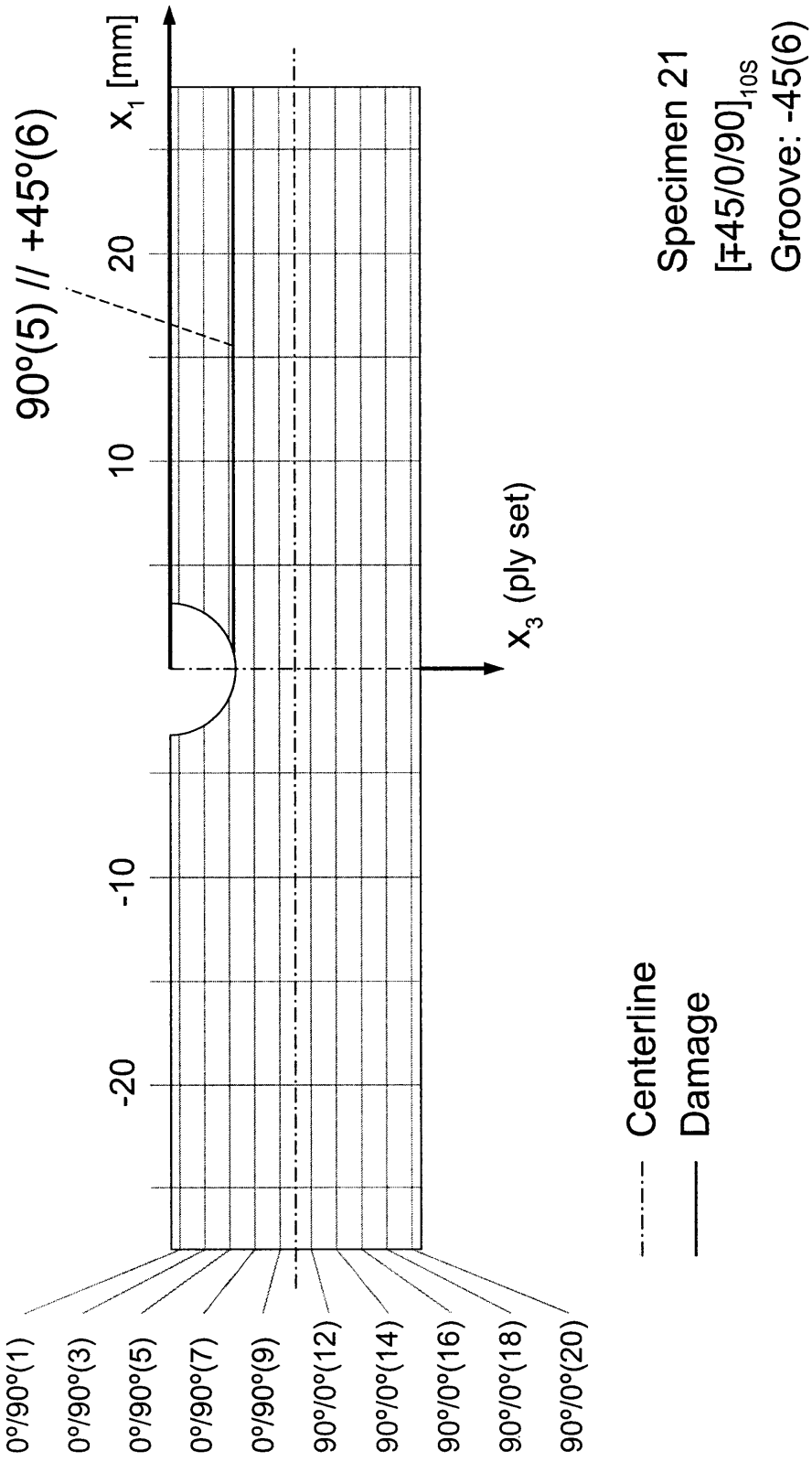

Figure 8.26 Illustration of failure for Specimen 21: layup $[\mp 45/0/90]_{10S}$ with groove at $-45°$ ply in 6th set.

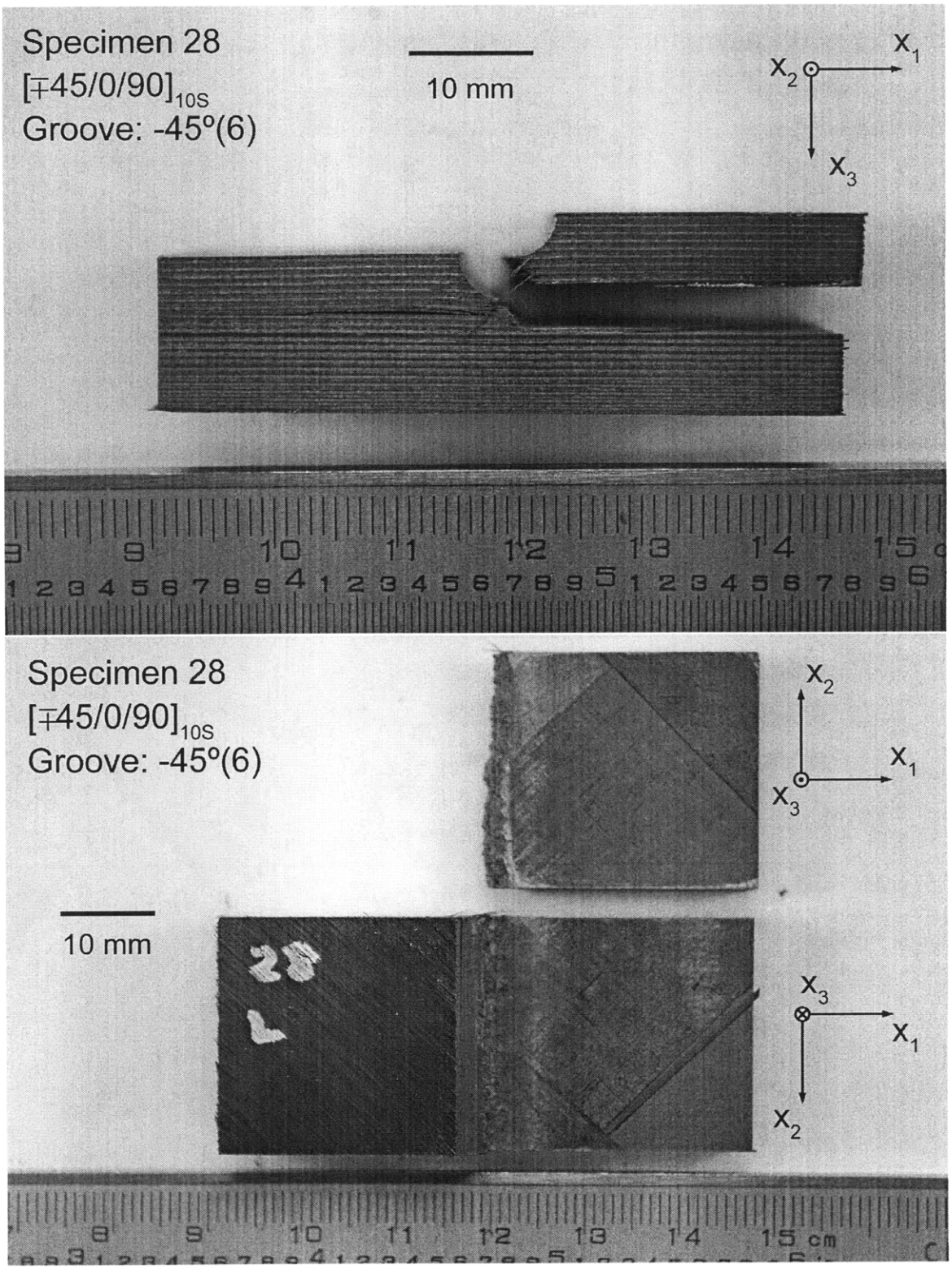

Figure 8.27 Photographs after failure of Specimen 28 (layup $[\mp 45/0/90]_{10S}$ with groove at $-45°$ ply in 6th set) with *(upper)* side view, and *(lower)* failure surface view.

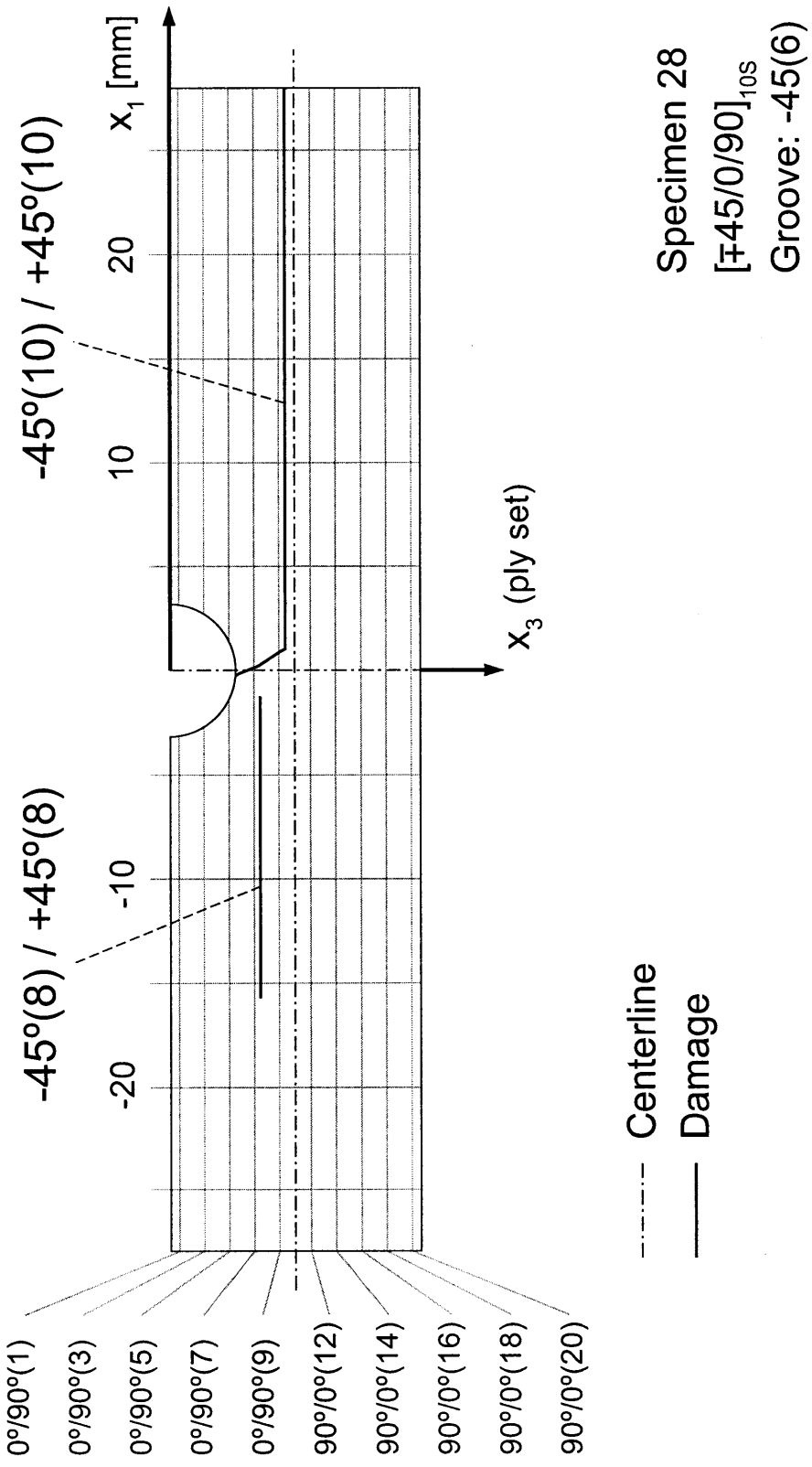

Figure 8.28 Illustration of failure for Specimen 28: layup $[\mp 45/0/90]_{10S}$ with groove at $-45°$ ply in 6th set.

It is also observed from the plots that the "knee load" occurred at the same stroke value of approximately 0.80 mm for both specimens cut from Plates C and D. The ratio of the average load-per-stroke slopes and the average knee load values between the specimens cut from Plates C and D are 0.75 and 0.73, respectively. These two values are very close, supporting the observation that the knee load occurred at the same stroke value, and indicating that the value of knee load is proportional to the modulus of the specimen in the x_3-direction.

As described earlier in this chapter, two different modes of failure were observed (referred to as Mode A and Mode B). For the specimens presented in this section, Specimens 18 and 28 fall under Mode B. From the load-versus-stroke plots of these specimens, presented in Figures 8.12 and 8.14, the load-per-stroke rate decreases before a major load drop is observed. It appears that damage occurred and propagated in this load region that finally triggered the final failure, as seen in Figures 8.23 and 8.27. Taking notice of this behavior, it was attempted on Specimen 30 to stop the loading within this load region in order to observe the propagation of the initial damage. The procedure is described in Section 8.1. The load-versus-stroke plot for this specimen is given in Figure 8.29. The side view photograph (close-up near the groove) and the 5X microscope photograph around the groove after the test is given in Figure 8.30. The centerline is drawn for a reference of $x_1 = 0$.

Under the groove of Specimen 30, small damage is observed. Fibers of the 0° plies are seen to come out of the x_2-face, indicating damage inside the ply and delamination. The locations of these damaged regions are from $x_1 = -1.0$ mm to $x_1 = 2.3$ mm for 0°(6), from $x_1 = -1.0$ mm to $x_1 = 1.4$ mm for 0°(7), and $x_1 = -0.8$ mm to $x_1 = 0.5$ mm for 0°(8) on the $+x_2$-face. Matrix cracks are observed in the magnified photograph of Figure 8.30 (lower). The ellipses drawn on the photograph indicate the area where these cracks are located. The upper ellipse indicates the location of a "through-ply matrix crack" in the +45°(6) ply. This crack is inclined to the x_1 and x_3 directions with a length of 0.67 mm in the x_1-direction, while the ply thickness is 0.15 mm. The lower ellipse indicates a through-ply crack in the −45°(7) ply. This crack has a length of 0.15 mm in the x_1-direction. From these observations, the damage

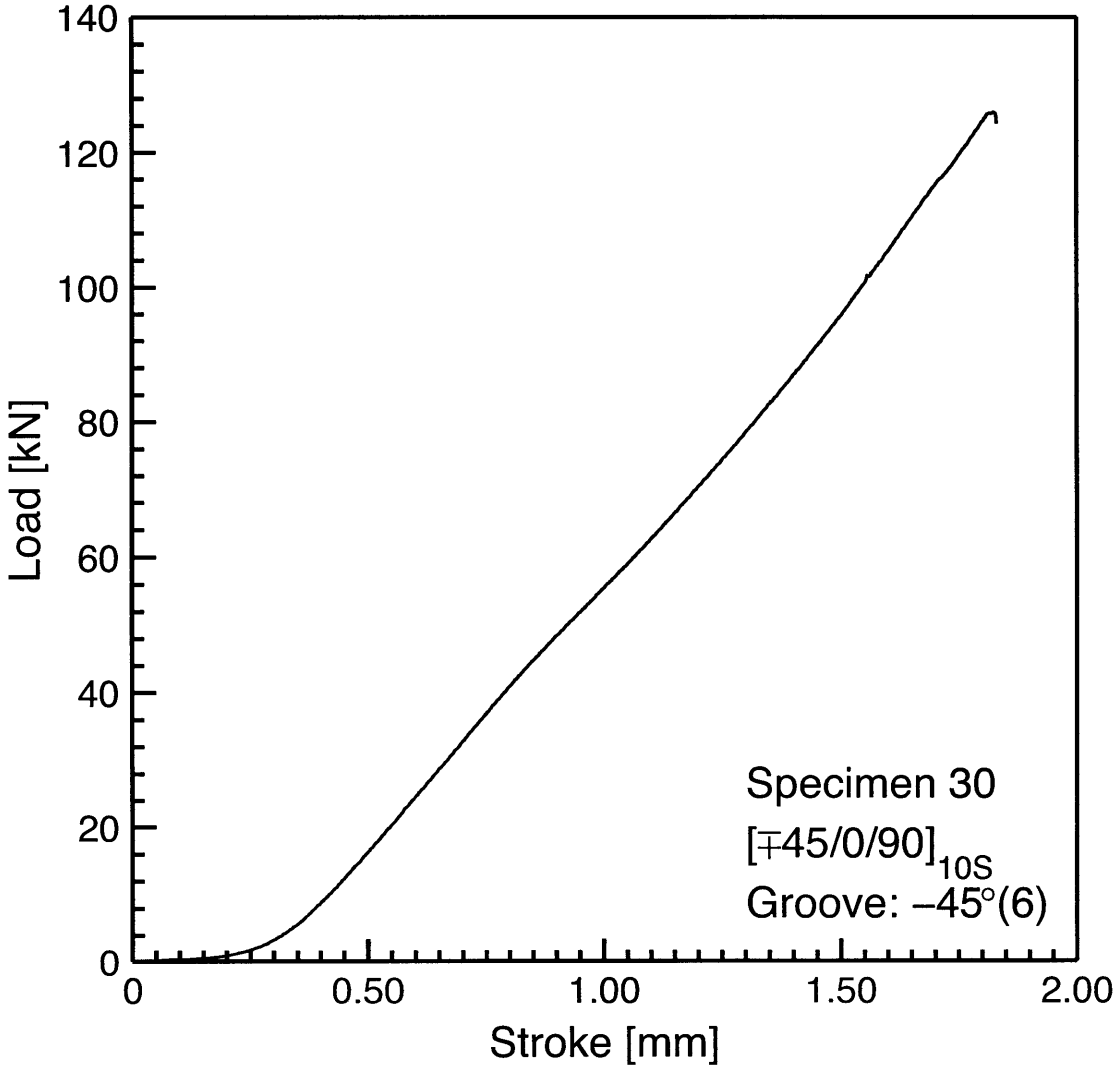

Figure 8.29 Load vs. stroke plot for Specimen 30: layup $[\mp 45/0/90]_{10S}$ with groove at $-45°$ ply in 6th set.

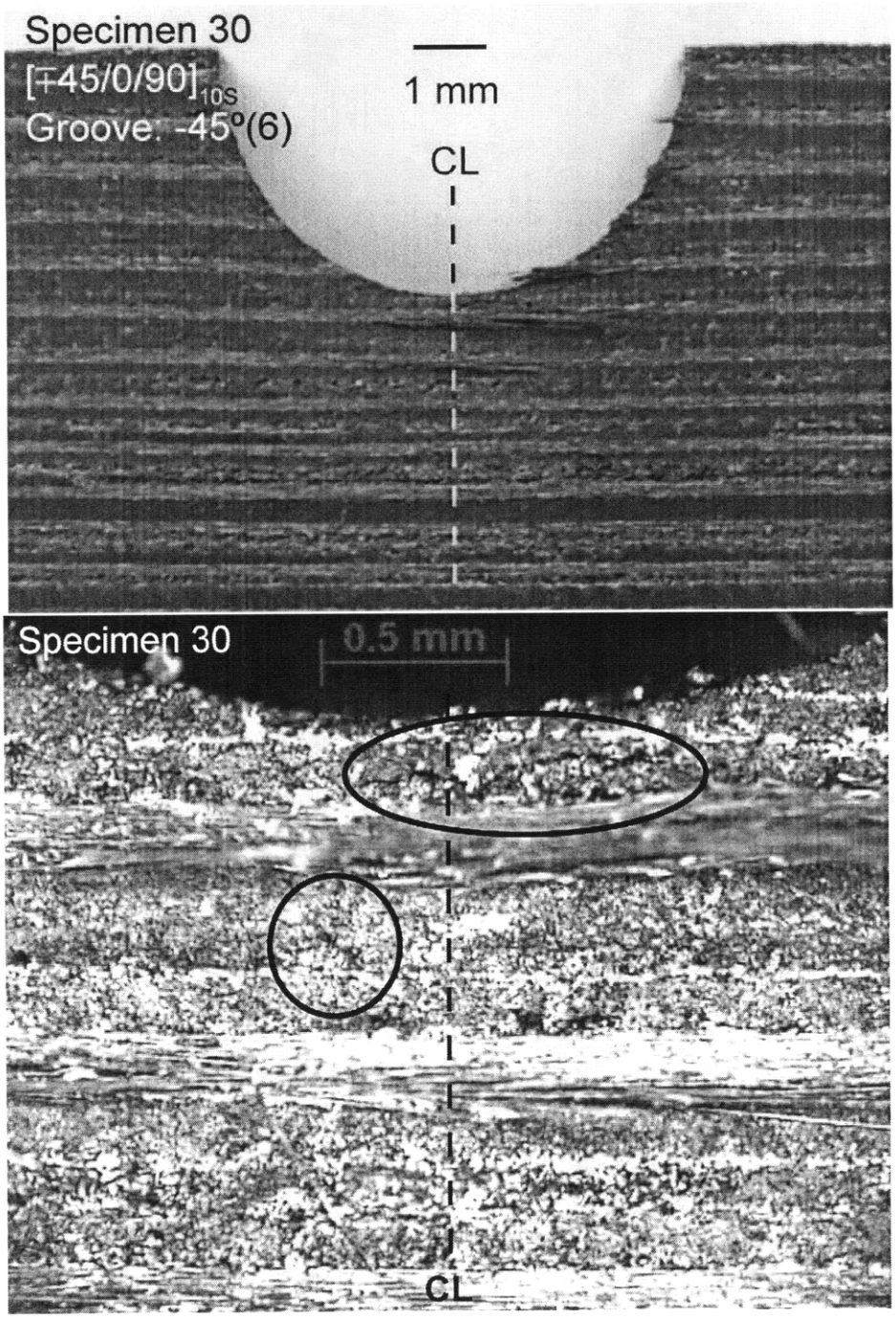

Figure 8.30 Photographs after testing of Specimen 30 (layup $[\mp 45/0/90]_{10S}$ with groove at $-45°$ ply in 6th set) with *(upper)* side view, and *(lower)* side view under microscope with 5X magnification.

at failure is likely to be larger near the groove, and decrease in size as the distance from the groove in the x_3-direction increases. The aspect ratio of through-ply cracks also differ, with the angle of inclination decreasing with increase in distance from the groove in the x_3-direction. Overall, the damage observed in the result of Specimen 30 is considered to be a combination of through-ply matrix cracks and delamination.

8.4 Tests with Alternate Layup

As noted previously in Section 8.1, a set of tests was performed with specimens with a different layup. The alternate layup chosen is $[\mp 30/0]_{13S}$. A sequence of $[\mp 30/0]$ was chosen in order to observe the effects of the 90° plies (not included in this case) and of the different angle in the angled plies. In order to target the total number of plies close to that of the standard layup (80 plies), the set number was chosen to be 13 and symmetric, resulting in 78 plies in total. This gives a nominal thickness of 11.86 mm. All of the other geometric parameters are kept the same as for the standard layup.

All of the manufacturing procedures described in Section 8.1 were performed, except for the grooving procedure. For the specimens of this alternate layup, the depth of the groove was chosen to be 3.18 mm. This was done because 3.18 mm has been the base value for the test parameter, h_{grv}, in this work. The primary objective of testing specimens with a different layup is to observe the effect of the stacking sequence, and not the effect of the ply that is segmented at the bottom of the groove. It was observed that the ply at the bottom of the groove was $+30°(8)$ for all of the specimens tested. Specimens 30-1 through 30-6 were tested for this alternate layup. These specimens were cut from laminated Plate 30-A. The measured geometric parameters are given in Table 8.6.

All of the testing procedures described in Section 8.1 were performed. Strain gages were placed on Specimens 30-1 and 30-2 in order to verify that the "two-dimensional" strain state is realized in the specimens with the alternate layup. The load-versus-strain plots are given in Figures 8.31 and 8.32. Gage 4 of Specimen 30-2 shows a

Table 8.6 Measured geometries of the specimens with alternate layup, $[\mp 30/0]_{13S}$

	Geometry [mm]		
Specimen	t	w	L
30-1	11.45	24.80	56.10
30-2	11.71	24.91	56.01
30-3	11.26	24.94	56.15
30-4	11.25	25.04	56.12
30-5	11.30	25.09	56.06
30-6	11.40	24.82	56.10

jump on the plot, which is considered to be caused due to loose connections of cords. Although its validity is questioned, it is presented to show the trend of the strain. The discussion in Subection 8.3.1 with regard to strain applies to the results of Specimens 30-1 and 30-2. Thus, the load value of 40 kN is chosen to compare the strain values. The average strain of the two compared gages and the variation in percentage is given for the specimens in Table 8.7. Comparison of gages 1 and 4 of Specimen 30-2 is put in parentheses because the validity of strain data from gage 4 is questioned, as mentioned earlier. Applying the same discussion presented in Subsection 8.3.1, the strain distribution is verified to be uniform along the x_2-direction, and therefore strain gages are not used for the specimens that followed these two.

The definitions of the maximum load, the load-per-stroke rate, and delamination locations are the same as those presented in Section 8.3. The "knee load" is not reported for these specimens, as an obvious change in the slope was not observed in the load-versus-stroke plots. The maximum load and the load-per-stroke rate are presented in Table 8.8. The locations of the largest major delamination are given in Table 8.9.

The results of Specimens 30-1, 30-2, 30-3, 30-4, and 30-6 are very similar. The locations of delamination were virtually the same, and the maximum loads have an average of 99.5 kN with a variation of +5.3, -6.9 kN (+5, -7%). The result of Specimen 30-1 is presented in detail as a representative of these specimens. Specimen 30-5 had a result different from the other specimens as the location of the delamination was different and the failure load was more than 10 kN higher than the other five. Results for this specimen are thus also presented in detail.

The load-versus-stroke plots are given in Figures 8.33 and 8.34. From these plots, it is observed that the deviation of the load-stroke plots from being linear is small and gradual, whereas the point of deviation was relatively well-definable in the standard $[\mp 45/0/90]_{10S}$ layup. Deviations of linearity over the entire load-stroke plot were less than 5% for these specimens, whereas they approached 10% in the $[\mp 45/0/90]_{10S}$ layup. The definition of a "knee load" as described in the results of the standard layup specimens are thus not applicable here.

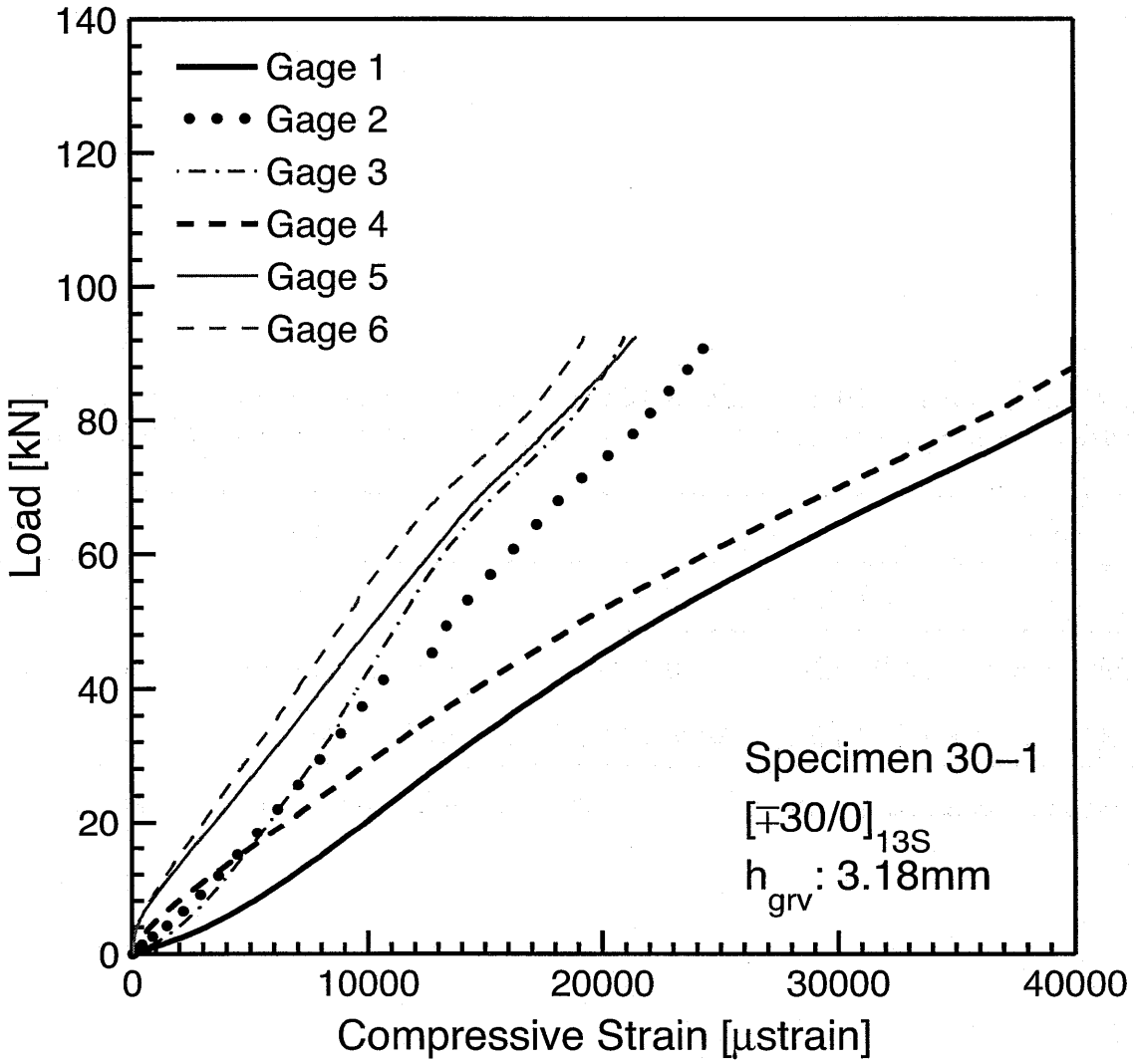

Figure 8.31 Load vs. compressive strain plot for Specimen 30-1: layup $[\mp 30/0]_{13S}$ with $h_{\text{grv}} = 3.18$ mm.

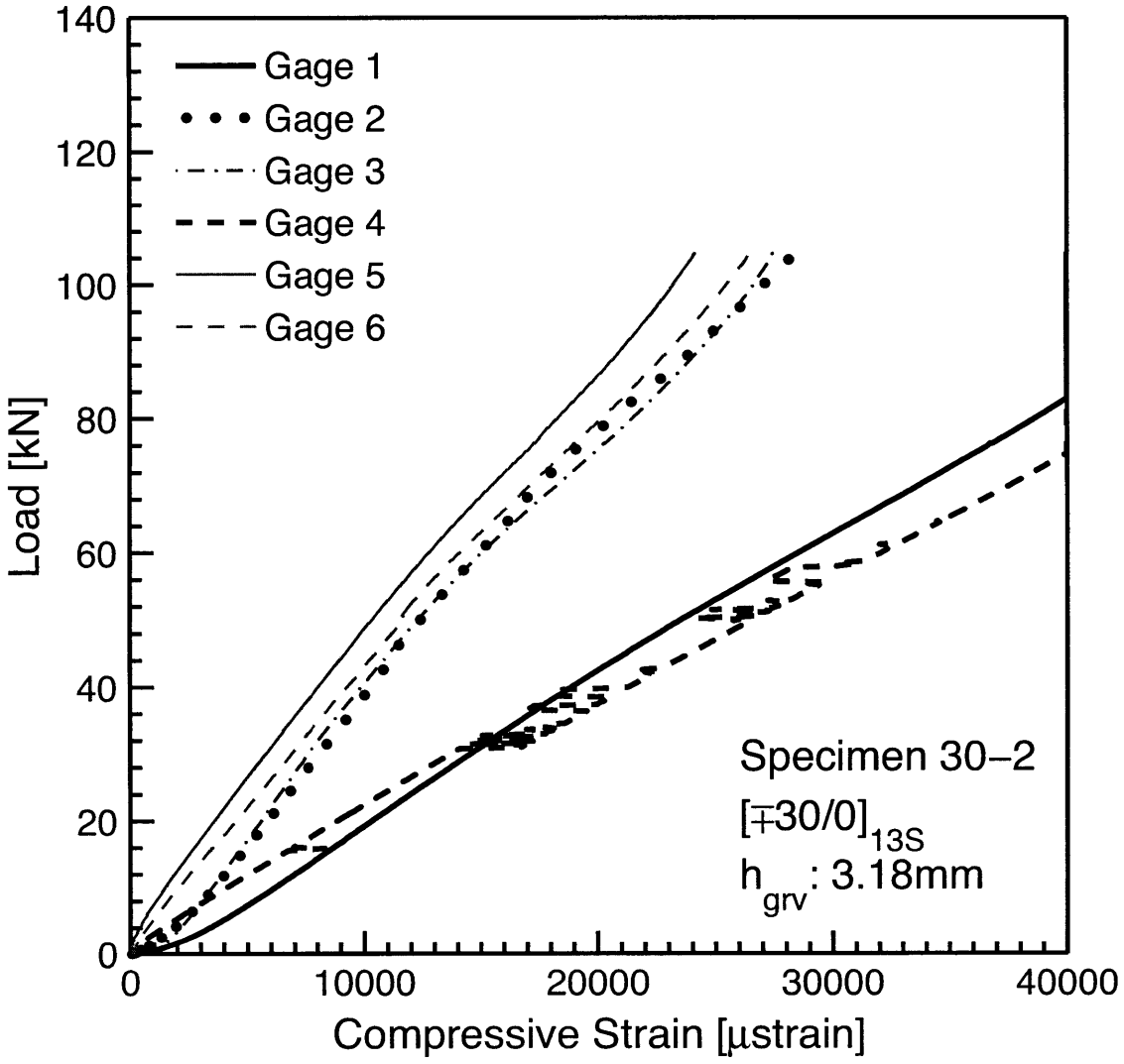

Figure 8.32 Load vs. compressive strain plot for Specimen 30-2: layup $[\mp 30/0]_{13S}$ with $h_{\text{grv}} = 3.18$ mm.

Table 8.7 Comparison of strain data of Specimens 30-1 and 30-2 at load of 40 kN (Average value in [μstrain] and variation in %)

	Gages				
Specimen	1 & 4	2 & 5	3 & 6	2 & 3	5 & 6
30-1	$16200 \pm 10\%$	$9200 \pm 12\%$	$8300 \pm 15\%$	$10000 \pm 4\%$	$7600 \pm 7\%$
30-2	$(20200 \pm 6\%)^*$	$9200 \pm 12\%$	$9600 \pm 3\%$	$10100 \pm 3\%$	$8700 \pm 7\%$

*parentheses indicate validity of data is questioned as noted in text.

Table 8.8 Results of the specimens with alternate layup $[\mp 30/0]_{13S}$

Specimen	Max. Load [kN]	Load/Stroke [kN/mm]
30-1	92.6	118.1
30-2	104.8	110.4
30-3	96.4	118.3
30-4	100.5	121.8
30-5	118.6	113.5
30-6	103.1	118.1

Table 8.9 Locations of delamination of the specimens with alternate layup $[\mp 30/0]_{13S}$

	Delamination Location	
Specimen	Left	Right
30-1	N/A*	$+30°(7)/0°(7)$
30-2	N/A	$+30°(7)/0°(7)$
30-3	$+30°(7)/0°(7)$	N/A
30-4	N/A	$+30°(7)/0°(7)$
30-5	N/A	$-30°(7)//0°(8)$
30-6	N/A	$+30°(7)//-30°(8)$

*N/A = none observed

Photographs after failure and illustrations of the damage are given in Figures 8.35 through 8.38. Although the delamination of Specimen 30-5 involved more plies than the other specimens, all specimens had a delamination above the bottom of the groove, and at the interface of plies $+30°(7)$ and $0°(7)$. A failure mode that is similar to Mode B in the standard layup specimens, including the crack under the groove, was not observed for this layup.

8.5 Discussion

It was presented in Section 8.3 that the acquired strain data verified that the established specimen and test method were valid for generating a "two-dimensional" stress-strain state (one that did not vary in the x_2-direction) in the specimen. Although the failure modes were not exactly the same for every specimen, it is clear that the failure occurred around the groove for all cases. No damage or obvious deformation was seen near the rigid backface boundary condition. This was also true for the specimens with the alternate layup. With all these facts taken into account, it can be concluded that the final specimen configuration and test method is valid for the objective of the current work – to observe the local response of a grooved composite affected by the groove, separated from any other effects. As noted previously, the strain measurements that are performed in this work do not have a high accuracy. Thus the data can be used only for a basic comparison of strain on two faces. In order to profile the strain field on a surface, other strain measurement methods, such as strain mapping, would be necessary.

It was demonstrated in Section 8.3 that specimens of the standard layup, $[\mp 45/0/90]_{10S}$, with the groove at $-45°$ ply of the 6th set failed in two different modes. These two modes were observed in specimens from both Plates C and D, and thus the difference in the failure mode is not a result of the manufacturing process. From the observation of Specimen 30, which was unloaded before failing in Mode B, that failure process can be explained as follows. First, due to the large contact load at the bottom of the groove, the specimen is subjected to large stress

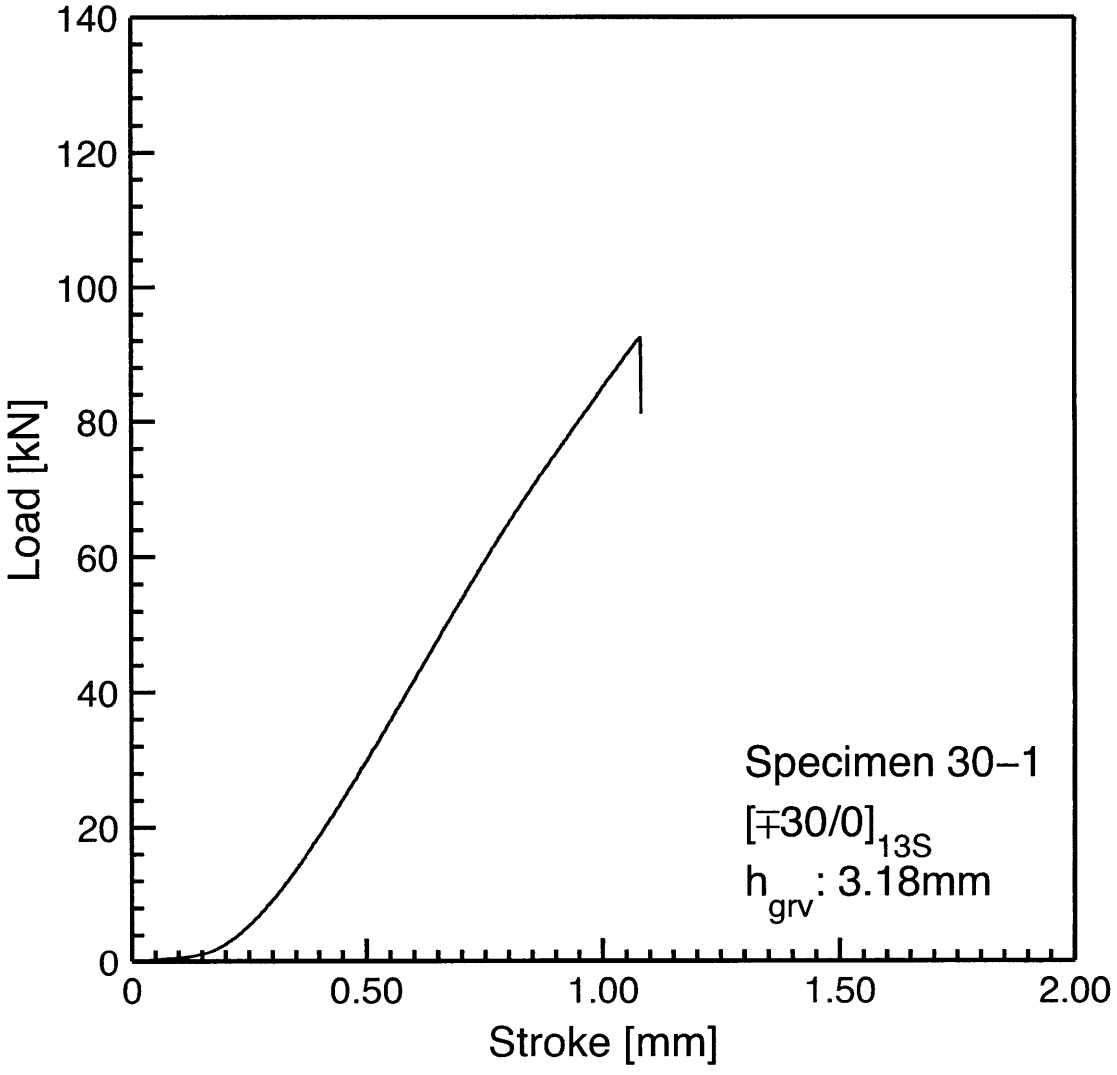

Figure 8.33 Load vs. stroke plot for Specimen 30-1: layup $[\mp 30/0]_{13S}$ with $h_{\text{grv}} = 3.18$ mm.

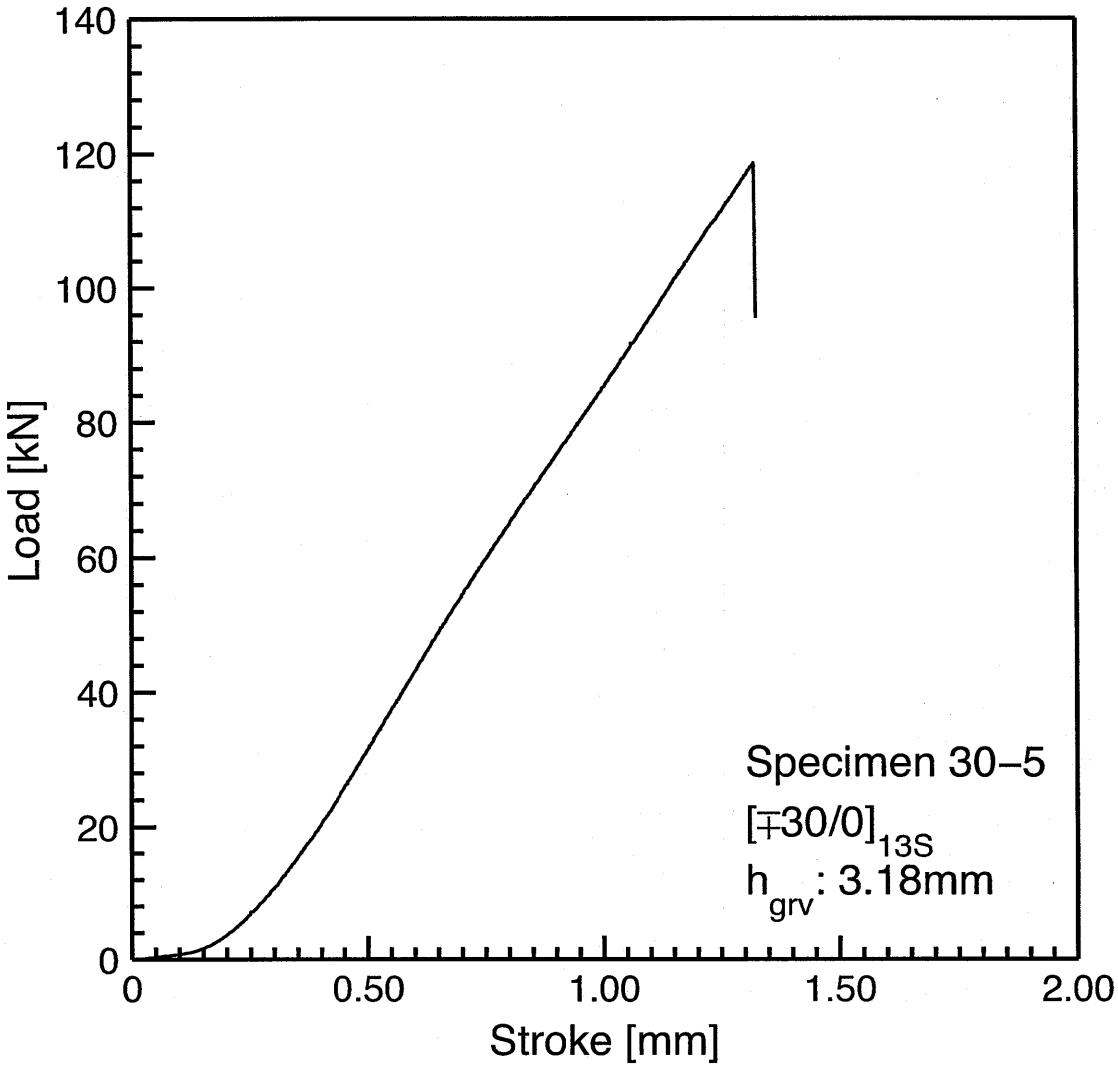

Figure 8.34 Load vs. stroke plot for Specimen 30-5: layup $[\mp 30/0]_{13S}$ with $h_{\text{grv}} = 3.18$ mm.

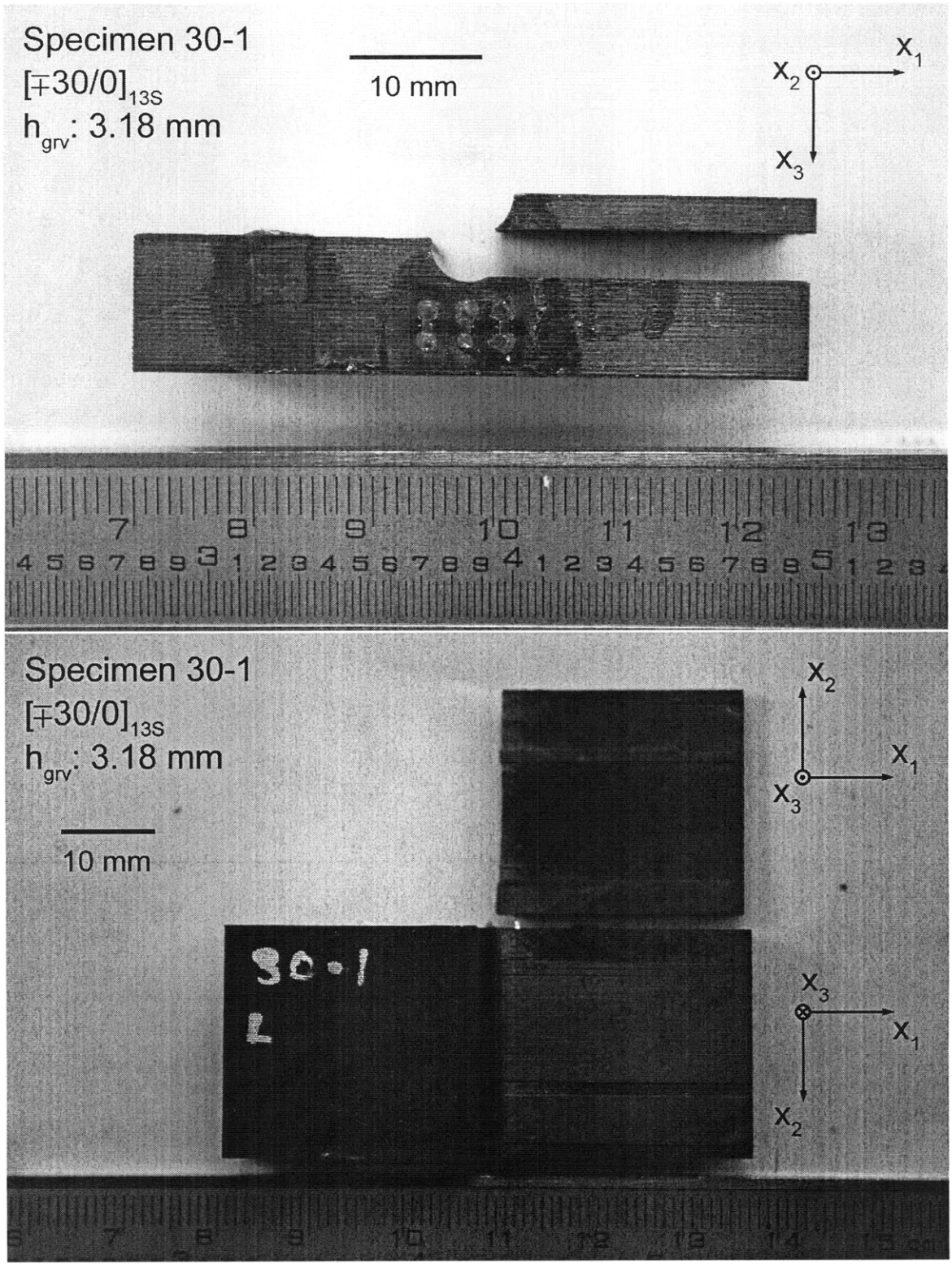

Figure 8.35 Photographs after failure of Specimen 30-1 (layup $[\mp 30/0]_{13S}$ with $h_{\text{grv}} = 3.18$ mm) with *(upper)* side view, and *(lower)* failure surface view.

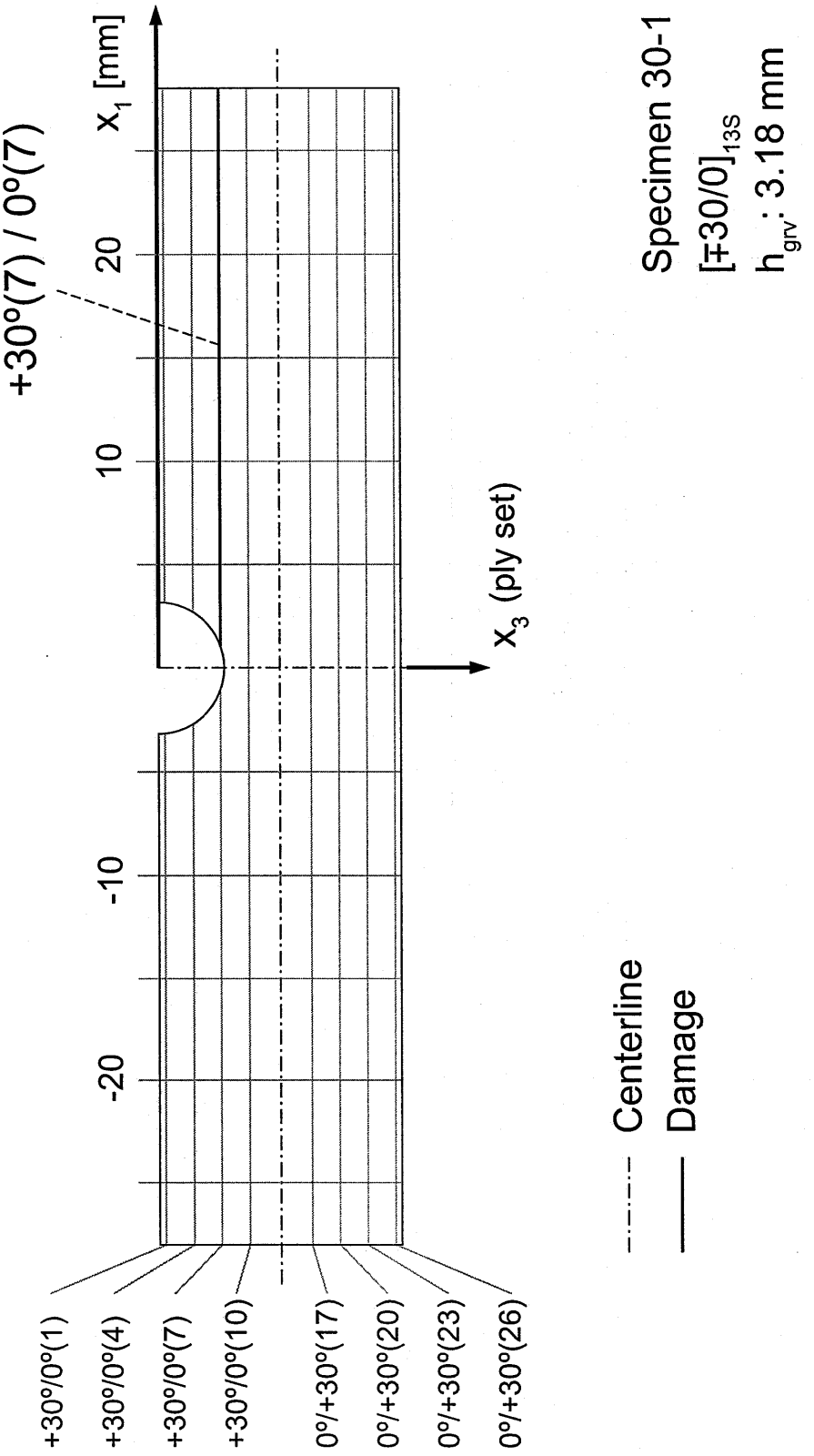

Figure 8.36 Illustration of failure for Specimen 30-1: layup $[\mp 30/0]_{13S}$ with $h_{\text{grv}} = 3.18$ mm.

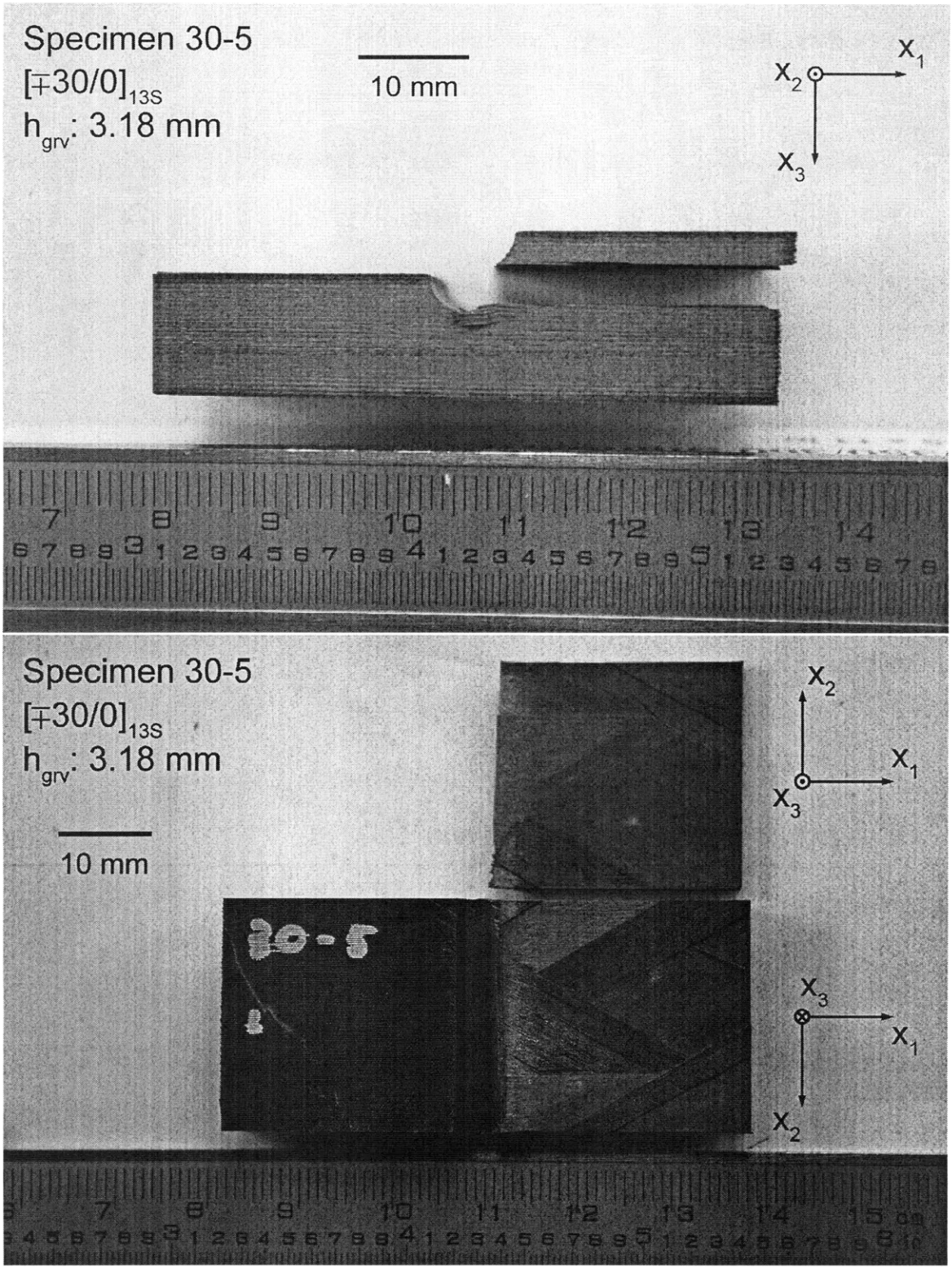

Figure 8.37 Photographs after failure of Specimen 30-5 (layup $[\mp 30/0]_{13S}$ with $h_{\text{grv}} = 3.18$ mm) with *(upper)* side view, and *(lower)* failure surface view.

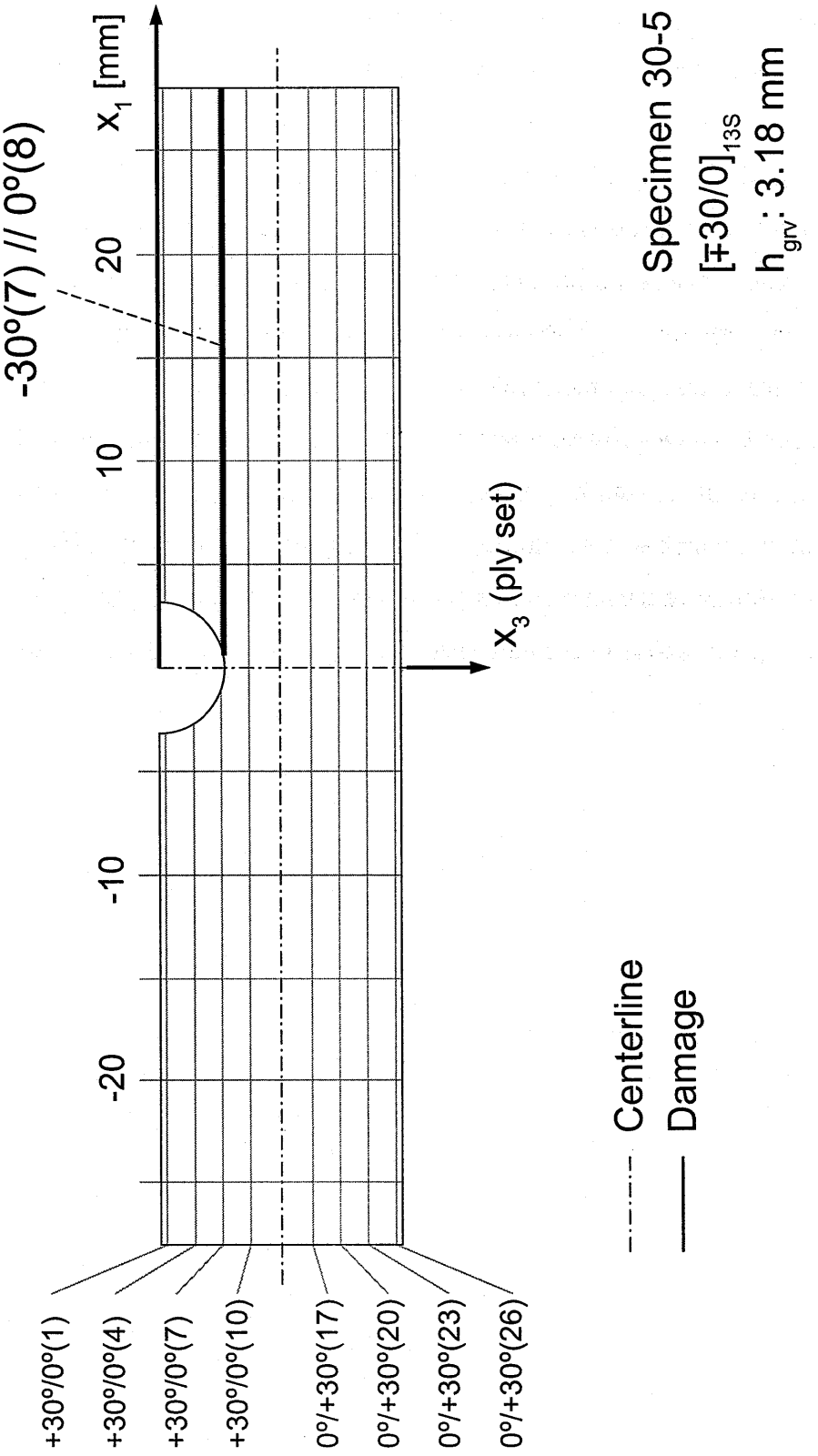

Figure 8.38 Illustration of failure for Specimen 30-5: layup $[\mp 30/0]_{13S}$ with $h_{\text{grv}} = 3.18$ mm.

there. Thus, the specimen deforms substantially at that point, resulting in a small delamination and/or matrix cracking. Second, when this small damage propagates in the x_1-direction as a delamination, the specimen fails in Mode A, or when this small damage propagates in the x_3-direction as a combination of matrix cracks and small delamination, Mode B is generated. Further loading tests on specimens with the same groove ply parameter, $-45°(6)$, should be conducted in order to observe the repetition of each failure mode. In addition to these, attempts should be taken to stop the test during the load region where a decrease in the load increase rate is seen, in order to observe the behavior of the damage propagation.

It is difficult to make conclusions with regard to the effect of the groove parameter on the failure of the specimen, since only a single test was done for each different groove depth. The variation of the results of those specimens, however, does not exceed the variation that is seen in the specimens where the groove ply parameter was maintained, $-45°(6)$. Thus, it appears that the orientation of the segmented ply at the bottom of the groove has relatively little effect on the behavior of the specimen, as long as the groove depth does not change over 0.5 mm. Multiple tests with different groove ply parameters that are close to the base parameter, i.e. $90°(5)$, $+45°(6)$, and $0°(6)$, are recommended to better observe the effect of the groove parameter on the behavior of failure and the failure load.

Comparing results from the specimens with the alternate layup, $[\mp 30/0]_{13S}$, show that the layup has a large effect on the behavior. As described in Section 8.4, the "knee load" is not observed in the alternate layup, while it is obvious in the standard layup specimens. For the alternate layup, the delamination location was observed as consistent in 5 of the 6 specimens with the other case being somewhat different, but not to the degree of categorizing that as another failure mode. In no cases was Mode B observed, contrary to the specimens with the standard layup. One possible cause of these differences between the two layups is the presence of the 90° plies in the standard layup of $[\mp 45/0/90]_{10S}$ and not in the alternate layup of $[\mp 30/0]_{13S}$. Because the fibers are aligned parallel to the indenter in the 90° plies, through-ply matrix cracks are generated more easily there than in the other plies. Matrix cracks

can propagate in the x_3-direction, which can be a trigger to a failure in Mode B. The cause of the "knee" in the load-versus-stroke plots cannot be explained from the results of the current work.

For specimens with either the standard layup or the alternate layup, the "two-dimensional" strain state was verified and the failure was clearly observed to occur around the groove. However, differences in the behavior of the specimens, both in the load-stroke response and the failure mode, were observed. This fact supports the statement that the specimen and the test method established in this work is applicable to specimens with various layups and, moreover, valid to observe the effect of altering the layup parameter. Thus, it can be concluded that the specimen and the test method established here can be utilized in future work with different layup parameters to observe the effect of this parameter on the load-stroke response and the failure. Other parameters, as earlier discussed and established, can be examined as well.

Chapter 9

CONCLUSIONS AND RECOMMENDATIONS

In this work, a specimen with an experimental method to observe the response of a grooved composite subjected to out-of-plane contact loading is established. The machining procedures and test procedures are established in detail in order to transfer the load from the indenter to the specimen with negligible variability across the width of the specimen. A number of tests are performed to verify the validity of the test method.

The conclusions drawn from this investigation are:

1. The simply-supported boundary conditions are not appropriate for the objectives of the test. The failure of the specimens tested in such configurations are in transverse shear mode, which is a result of the global response of the specimen and not the local response around the groove.

2. The surface of the bottom of the groove must be parallel to the bottom face of the specimen in order to achieve the needed uniform contact and loading between the indenter and the specimen. In order to realize this, the manufacturing and machining procedures need to be performed with appropriate care. In particular, milling the faces of the specimen to be parallel / perpendicular to each other is necessary before the grooving procedure.

3. Due to the maximum loads during the test, the material of the indenter must be sufficiently hard to avoid deformation during the test. An M2/M7 steel alloy is chosen for the current work, and verified to have no obvious deformation during the test.

4. Alignment of the testing setup needs to be done to the accuracy of 0.5 mm in order to avoid undesired rotations of the self-leveling top head of the testing machine.

5. The final specimen has a thickness of approximately 12.5 mm (equivalent to 80 plies), width of 25.00 mm, length of 56.00 mm, and a maximum groove depth of 3.48 mm. The boundary conditions are set to be of rigid backface. These values and conditions are verified to be appropriate for the objectives of the test.

6. Strain measurements from the gages on the $\pm x_2$-faces demonstrated that the strains on the two faces had small differences, and that the strain state of the specimen had small variability along the x_2-axis as needed.

7. For the standard layup of $[\mp 45/0/90]_{10S}$, two modes of failure are observed, indicating the basic behavior variability within specimens with the same "groove ply parameter": a failure with a delamination near the bottom of the groove (Mode A), and a failure with a crack under the bottom of the groove, propagating to a delamination near the midplane of the specimen (Mode B).

8. Before the final failure of Mode B, damage under the groove emerges. This damage is a combination of delamination and "through-ply" matrix cracks.

9. Large differences in the values of the load-per-stroke slope and the "knee load" are observed between specimens that are cut from different plates. This is attributable to the difference in the fiber volume fraction, which is indicated by the difference in the plate thicknesses.

10. An effect was not clearly observed for the small variation in the "groove ply parameter" tested, as differences observed in the behavior did not exceed the

variation observed in the specimens with the same "groove ply parameter".

11. For the alternate layup of $[\mp 30/0]_{13S}$, the specimens had a generally consistent failure that can be categorized as similar to the Mode A of the standard $[\mp 45/0/90]_{10S}$ layup, while damage similar to Mode B failure was not observed. The definition of "knee load" is not applicable to the alternate layup specimens.

12. The differences between the standard and alternate layup specimens are attributable to the presence of the 90° plies that are more likely to result in matrix cracks than other angled plies.

13. The test results clearly show that a proper experimental specimen is established and verified for the objectives of the current work. It is also clarified that this specimen and experimental method can be used for tests with different test parameters.

Based on the results of this investigation, recommendations for further research are:

1. Further tests should be performed with the standard layup of $[\mp 45/0/90]_{10S}$ with the base groove ply parameter of $-45°(6)$ to observe and gather data of repetition of the failure modes and loads.

2. Further tests should be run with attempts to stop the test during the load region where a decrease in the load increase rate is seen, in order to observe the behavior of the pre-failure damage propagation.

3. Multiple tests should be performed with the standard layup with different groove ply parameters to better observe the effects of this parameter and the associated repeatability of the data.

4. Specimens with different layups should be tested in order to observe the effect of this test parameter. In particular, the effect of the 90° plies should be closely investigated.

5. Tests with a spherical indenter should be done in order to observe the response of a specimen with variability in the x_2-axis, in order to study the difference in behavior when the applied stress state has variability in the x_2-direction.

REFERENCES

[1] M. Hinton, A. Kaddour, and P. Soden, "A Comparison of the Predictive Capabilities of Current Failure Theories for Composite Laminates, Judged against Experimental Evidence," *Composites Science and Technology*, vol. 62, pp. 1725–1797, 2002.

[2] CompositesWorld.com, *Boeing Sets Pace for Composite Usage in Large Civil Aircraft.* World Wide Web, http://www.compositesworld.com/hpc/issues/2005/May/865, 2005.

[3] P. Lagace, J. Williamson, P. Tsang, E. Wolf, and S. Thomas, "A Preliminary Proposition for a Test Method to Measure (Impact) Damage Resistance," *Journal of Reinforced Plastics and Composites*, vol. 12, pp. 584–601, 1993.

[4] W. Jackson and C. Poe, Jr., "The Use of Impact Force as a Scale Parameter for the Impact Response of Composite Laminates," *Journal of Composites Technology and Research*, vol. 15, no. 4, pp. 282–289, 1993.

[5] Y. Kwon and B. Sankar, "Indentation-Flexure and Low-Velocity Impact Damage in Graphite Epoxy Laminates," *Journal of Composites Technology and Research*, vol. 15, no. 2, pp. 101–111, 1993.

[6] M. Czajkowski, G. Clausen, and B. Sarh, "Telescopic Wing of an Advanced Flying Automobile," AIAA Paper 1997-5602, World Aviation Congress, Anaheim, CA, Oct. 13-16 1997.

[7] B. Sarh, *Advanced Flying Automobile.* http://www.afaco.com, 2008.

[8] F. Longobardi, *Combination Vehicle.* Patent #1,286,679, United States Patent Office, December 1918.

[9] G. Montay, O. Sicot, X. Gong, A. Cherouat, and J. Lu, "Determination of the Residual Stresses in Composite Laminate Using the Compliance Method," in *Proceedings of the 7th International Conference on Residual Stresses (ICRS-7)*, vol. 490-491, pp. 533–538, Materials Science Forum, 2005.

[10] C. Hoppel, T. Bogetti, and J. J.W. Gillespie, "Devices for Transmitting High Shear Loads in Composite Structures," in *Proceedings of the American Society for Composites Eleventh Technical Conference*, pp. 437–446, American Society for Composites, 1996.

[11] C. Liu, A. Nijhof, and L. Ernst, "Modeling Failure Interaction in Notched Cross-Ply Laminates," *Journal of Composite Materials*, vol. 42, no. 20, pp. 2175–2193, 2008.

[12] C. Bastien, "Response of a Grooved Plate Subjected to Out-of -Plane Contact Loading," S.M. thesis, Massachusetts Institute of Technology, 2008.

[13] S. Abrate, "Impact on Laminated Composite Materials," *Applied Mechanics Review*, vol. 44, no. 4, pp. 155–190, 1991.

[14] S. Abrate, "Impact on Laminated Composites: Recent Advances," *Applied Mechanics Review*, vol. 47, no. 11, pp. 517–544, 1994.

[15] ASTM D 7136/D 7136M - 07, *Standard Test Method for Measuring the Damage Resistance of a Fiber-Reinforced Polymer-Matrix Composite to a Drop-Weight Impact Event.* American Society for Testing and Materials, October 2007.

[16] ASTM D 6264/D 6264M - 07, *Standard Test Method for Measuring the Damage Resistance of a Fiber-Reinforced Polymer-Matrix Composite to a Concentrated Quasi-Static Indentation Force.* American Society for Testing and Materials, December 2007.

[17] H. Hertz, "Uber die Beruhrung fester Elastischer Korper," *Journal Reine Angle Math*, vol. 92, p. 155, 1881.

[18] S. Yang and C. Sun, "Indentation Law for Composite Laminates," in *Composite Materials: Testing and Design*, pp. 425–449, American Society for Testing and Materials, 1982.

[19] T. Tan and C. Sun, "Use of Statical Indentation Laws in the Impact Analysis of Laminated Composite Plates," *Journal of Applied Mechanics*, vol. 52, pp. 6–12, 1985.

[20] D. Cairns and P. Lagace, "Thick Composite Plates Subjected to Lateral Loading," *Journal of Applied Mechanics*, vol. 54, pp. 611–616, 1987.

[21] P. Mahajan, "Contact Behavior of an Orthotropic Laminated Beam Indented by a Rigid Cylinder," *Composites Science and Technology*, vol. 58, pp. 505–513, 1998.

[22] K. Váradi, Z. Néder, J. Flock, and K. Friedrich, "Numerical and Experimental Contact Analysis of a Steel Ball Indented into a Fibre Reinforced Polymer Composite Material," *Journal of Materials Science*, vol. 33, pp. 841–851, 1998.

[23] Y. Aoki, H. Suemasu, and T. Ishikawa, "Damage Propagation in CFRP Laminates Subjected to Low Velocity Impact and Static Indentation," *Advanced Composite Materials*, vol. 16, no. 1, pp. 45–61, 2007.

[24] K. Kedward, "On The Short Beam Test Method," *Fiber Science and Technology*, vol. 5, pp. 85–95, 1972.

[25] J. Whitney and C. Browning, "On Short-Beam Shear Tests for Composite Materials," *Experimental Mechanics*, vol. 25, pp. 294–300, 1985.

[26] D. Adams and E. Lewis, "Current Status of Composite Material Shear Test Methods," *SAMPE*, vol. 31, pp. 32–41, 1994.

[27] B. Sankar, "Smooth Indentation of Orthotropic Beams," *Composites Science and Technology*, vol. 34, pp. 95–111, 1989.

[28] E. Wu and K. Shyu, "Response of Composite Laminates to Contact Loads and Relationship to Low Velocity Impact," *Journal of Composite Materials*, vol. 27, pp. 1443–1464, 1993.

[29] P. Chen, J. Xiong, and Z. Shen, "Thickness Effect on the Contact Behavior of a Composite Laminate Indented by a Rigid Sphere," *Mechanics of Materials*, vol. 40, pp. 183–194, 2008.

[30] T. Harris and M. Kotzalas, *Essential Concepts of Bearing Technology.* Rolling Bearing Analysis, CRC Press, 5^{th} ed., 2007.

[31] ASTM D 2344/D 2344M - 00, *Standard Test Method for Short-Beam Strength of Polymer Matrix Composite Materials and Their Laminates.* American Society for Testing and Materials, March 2000.

[32] P. Lagace, M. Beaumont, J. Brewer, and C. Varnerin, *TELAC Manufacturing Course Class Notes.* Massachusetts Institute of Technology, TELAC Report No. 88-4b ed., September 1991.

Appendix A

Load-Stroke Response Data for Final Specimens

Load-stroke response plots for all the "final specimens" (as addressed in Chapter 8) are presented in this appendix. Specimens 13 through 30 have the standard layup, $[\mp 45/0/90]_{10S}$. Specimens 30-1 through 30-6 have the alternate layup, $[\mp 30/0]_{13S}$. The general testing procedures are described in Chapter 5, with further details in Section 8.1 of Chapter 8. The groove ply parameter or the groove depth is noted in the plots and the figure titles. All the tests were loaded until failure except for Specimen 30 (details are described in Chapter 8).

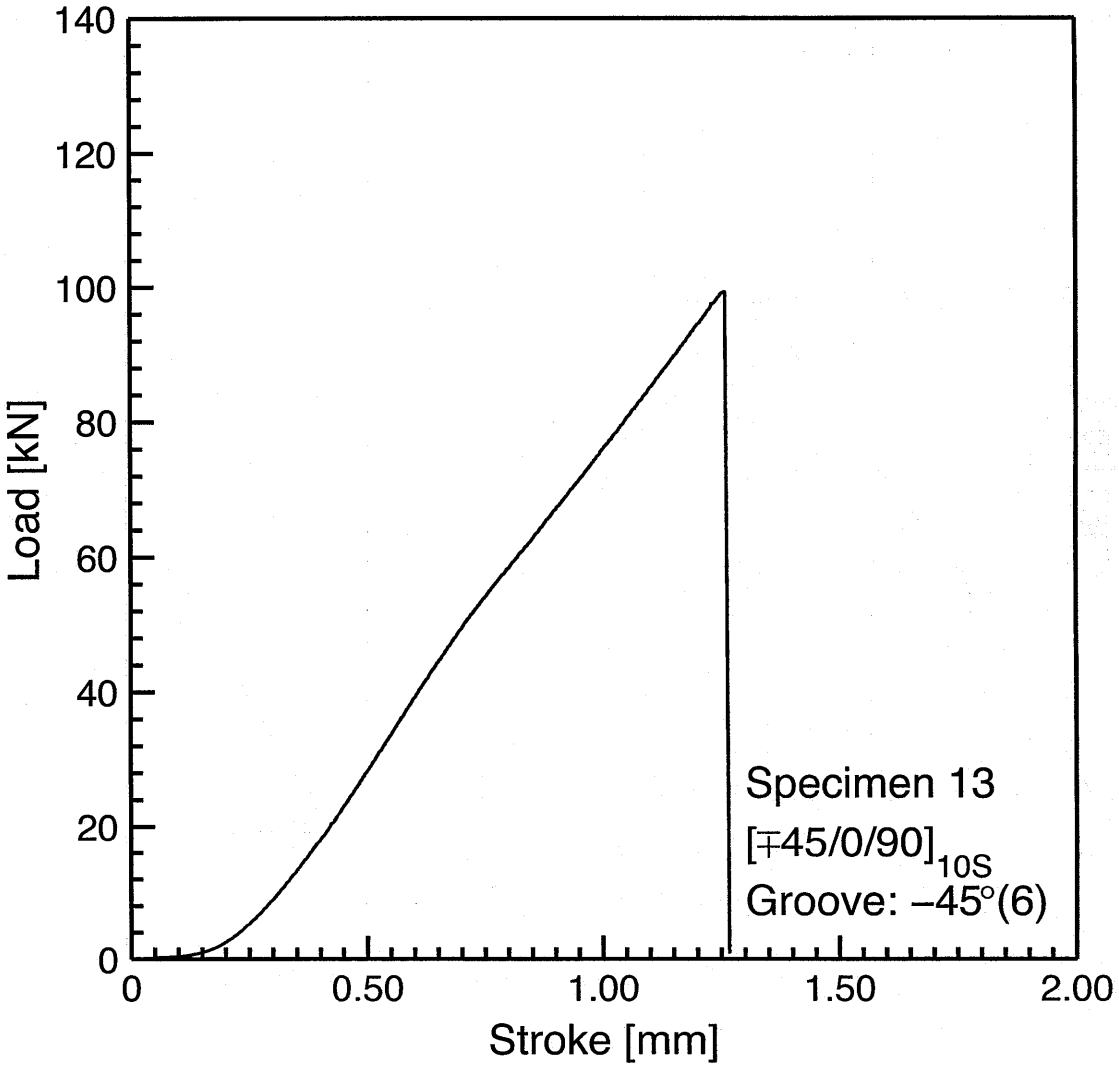

Figure A.1 Load vs. stroke plot for Specimen 13: layup $[\mp 45/0/90]_{10S}$ with groove at $-45°$ ply in 6th set.

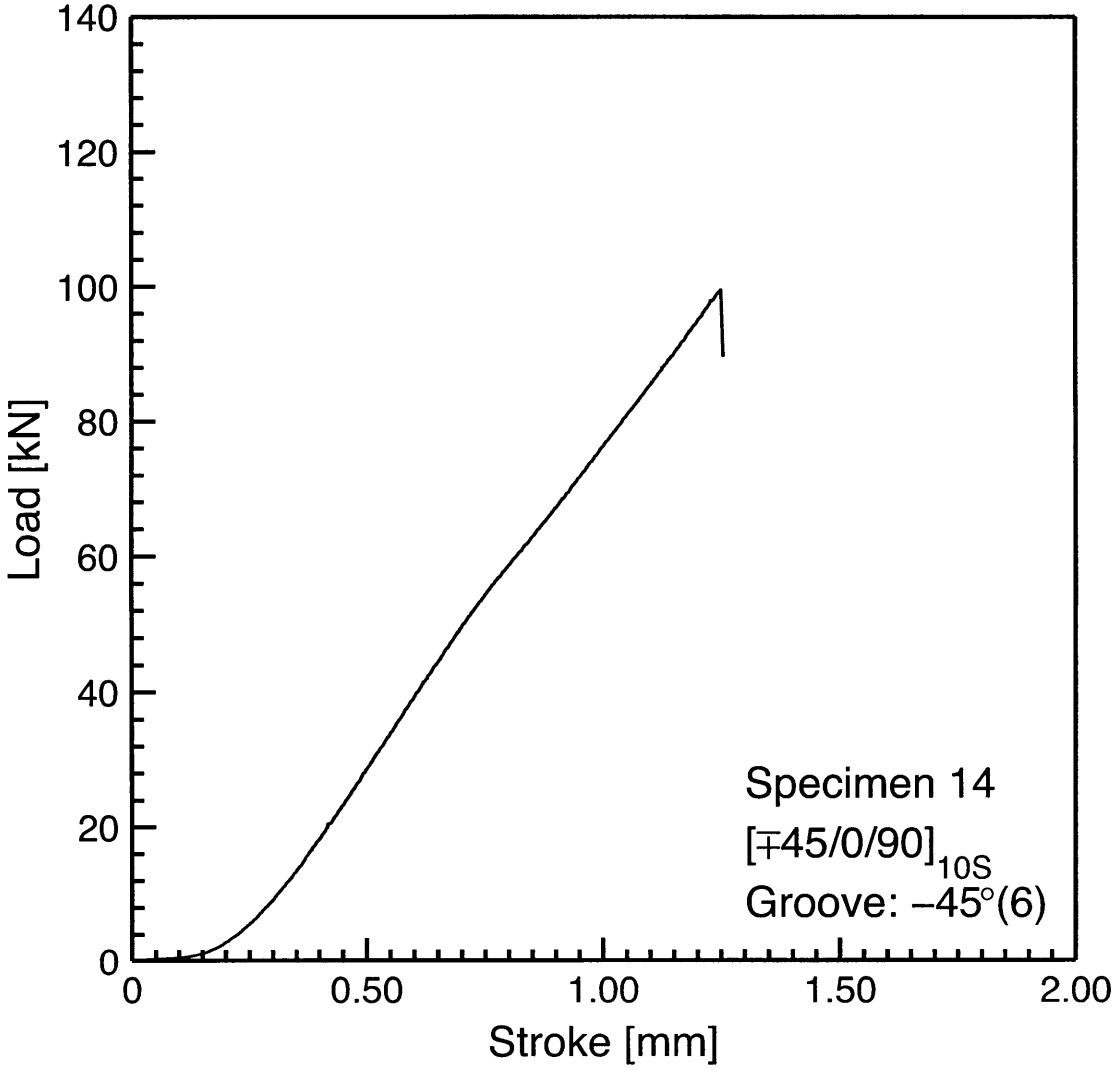

Figure A.2 Load vs. stroke plot for Specimen 14: layup $[\mp 45/0/90]_{10S}$ with groove at $-45°$ ply in 6th set.

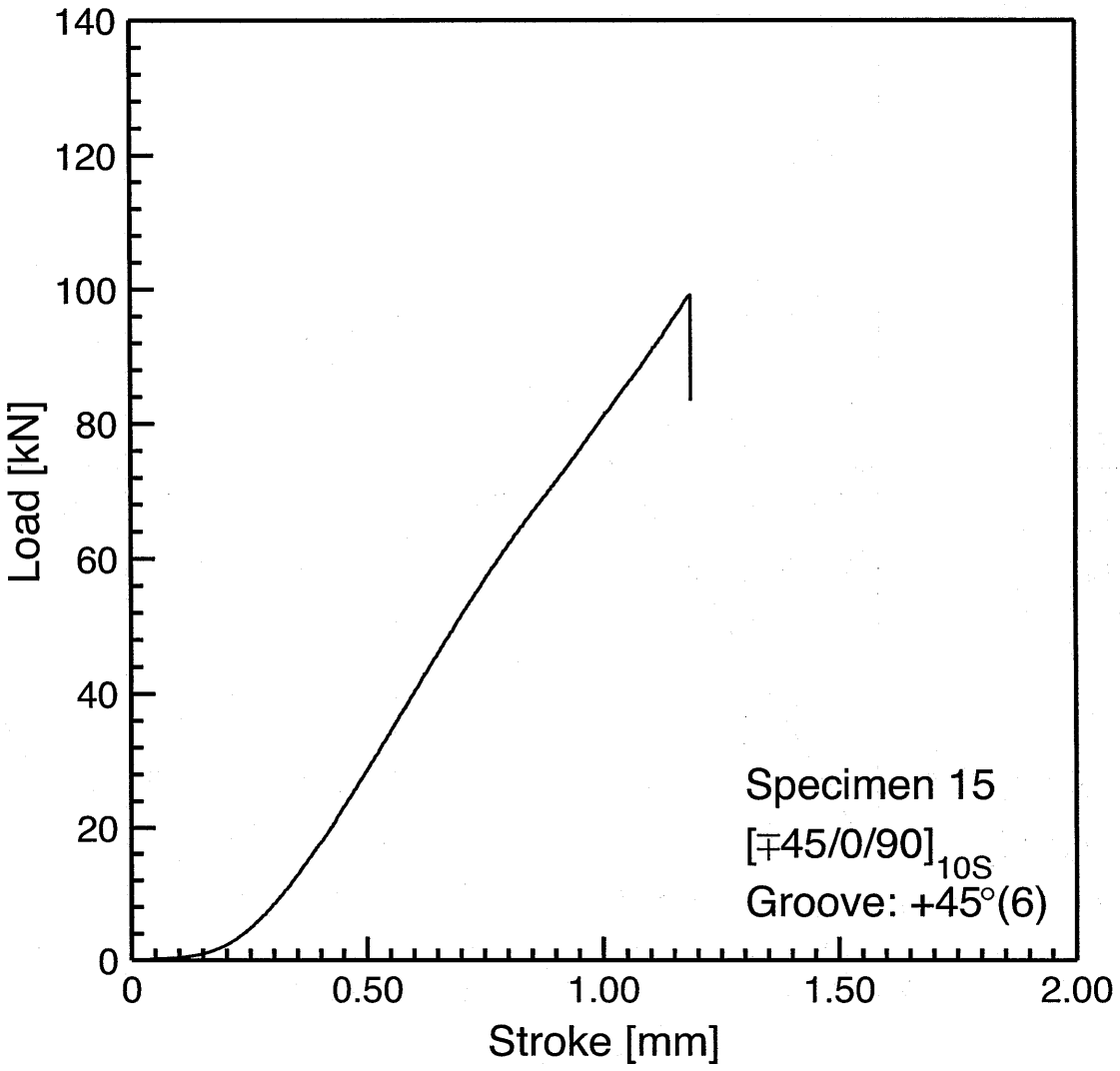

Figure A.3 Load vs. stroke plot for Specimen 15: layup $[\mp 45/0/90]_{10S}$ with groove at $+45°$ ply in 6th set.

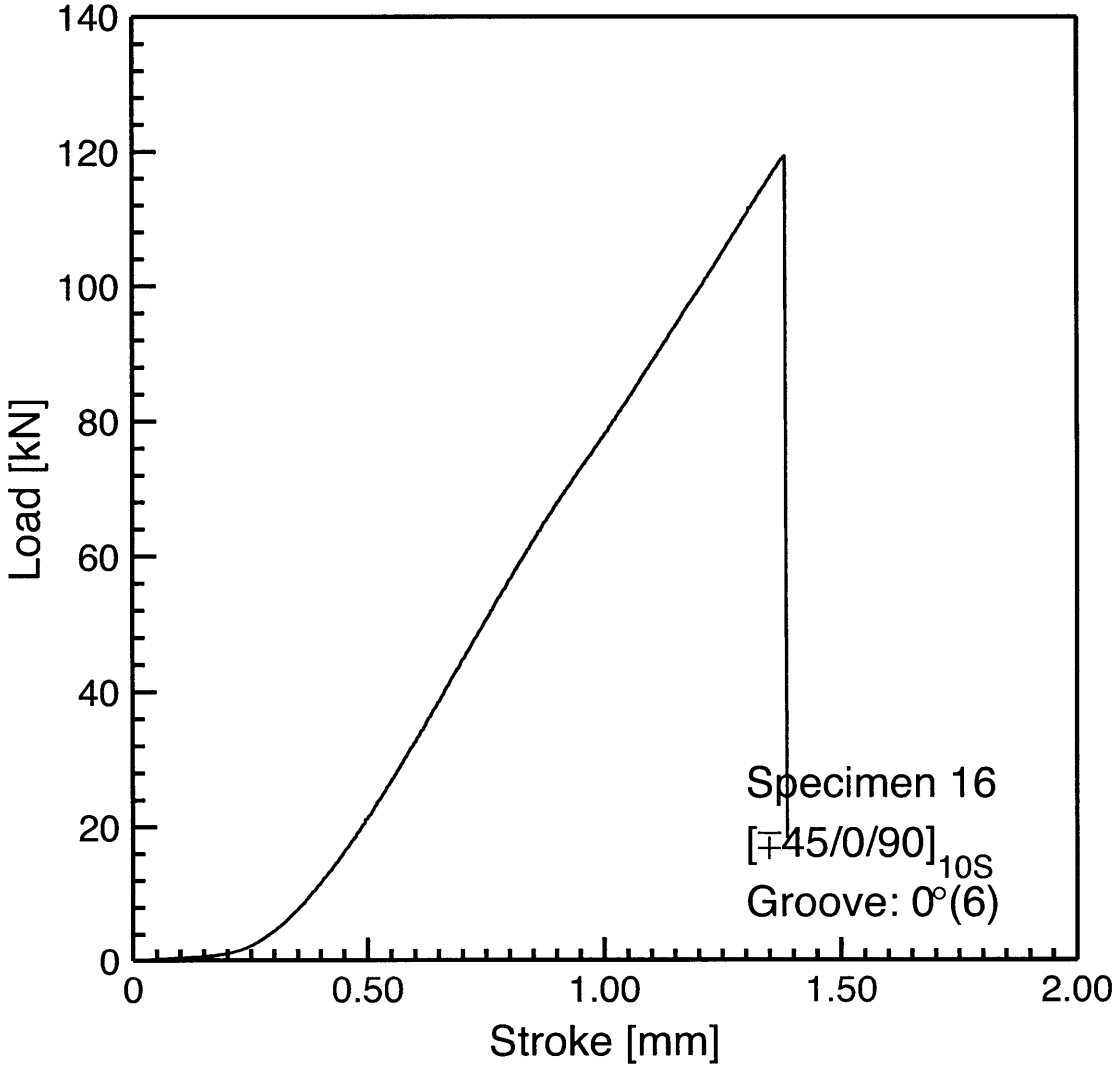

Figure A.4 Load vs. stroke plot for Specimen 16: layup $[\mp 45/0/90]_{10S}$ with groove at 0° ply in 6th set.

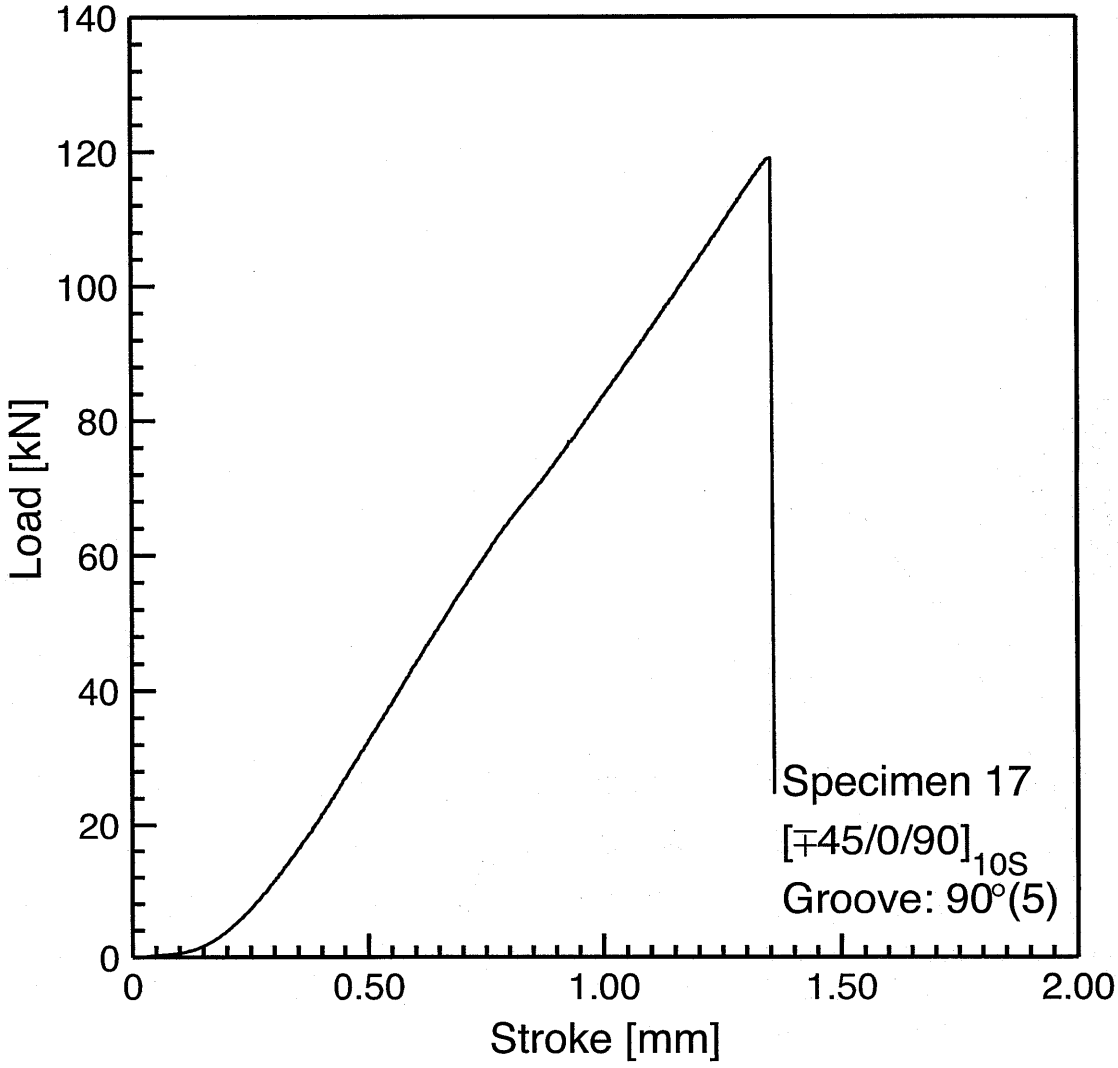

Figure A.5 Load vs. stroke plot for Specimen 17: layup $[\mp 45/0/90]_{10S}$ with groove at 90° ply in 5th set.

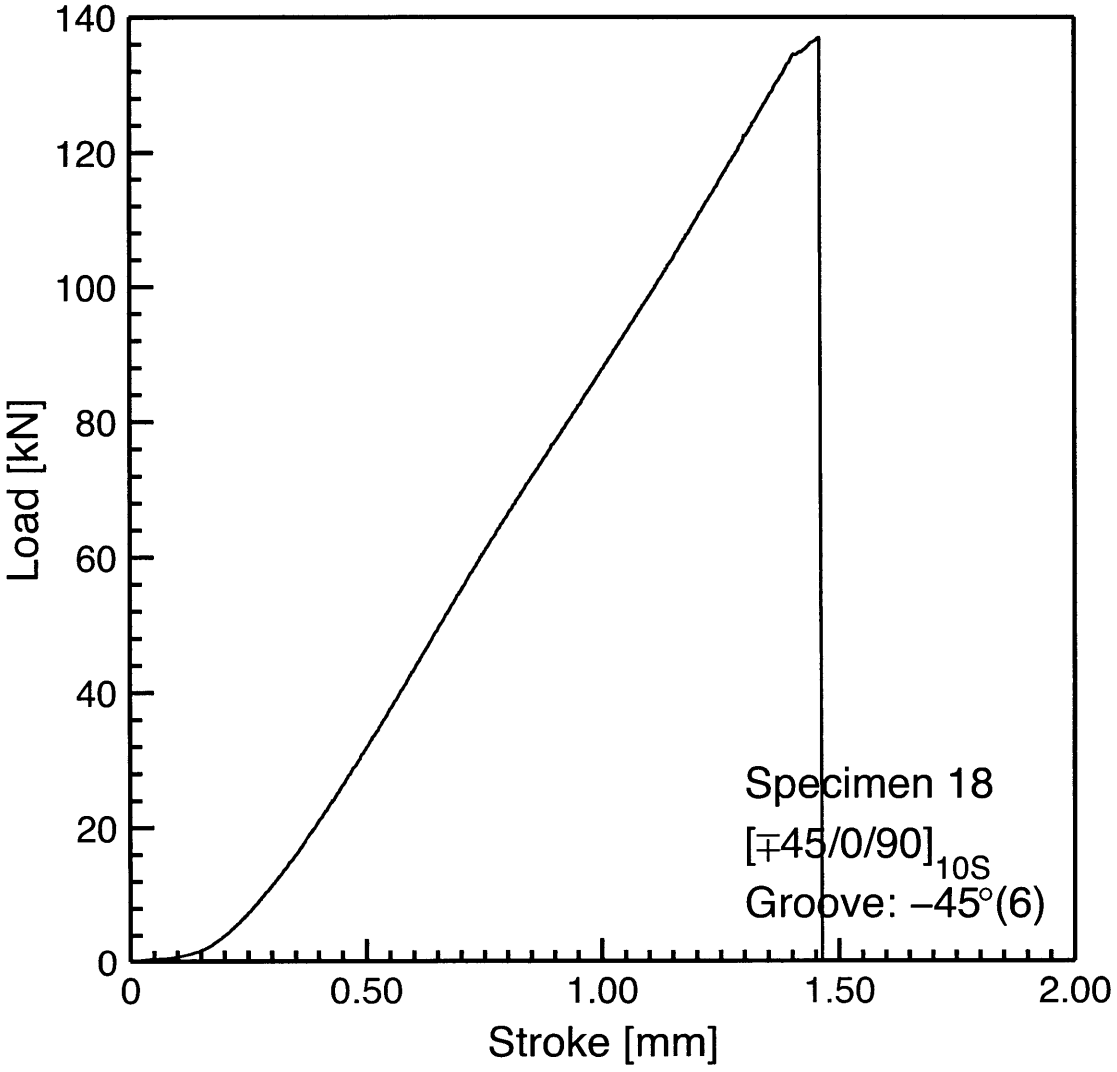

Figure A.6 Load vs. stroke plot for Specimen 18: layup $[\mp 45/0/90]_{10S}$ with groove at $-45°$ ply in 6th set.

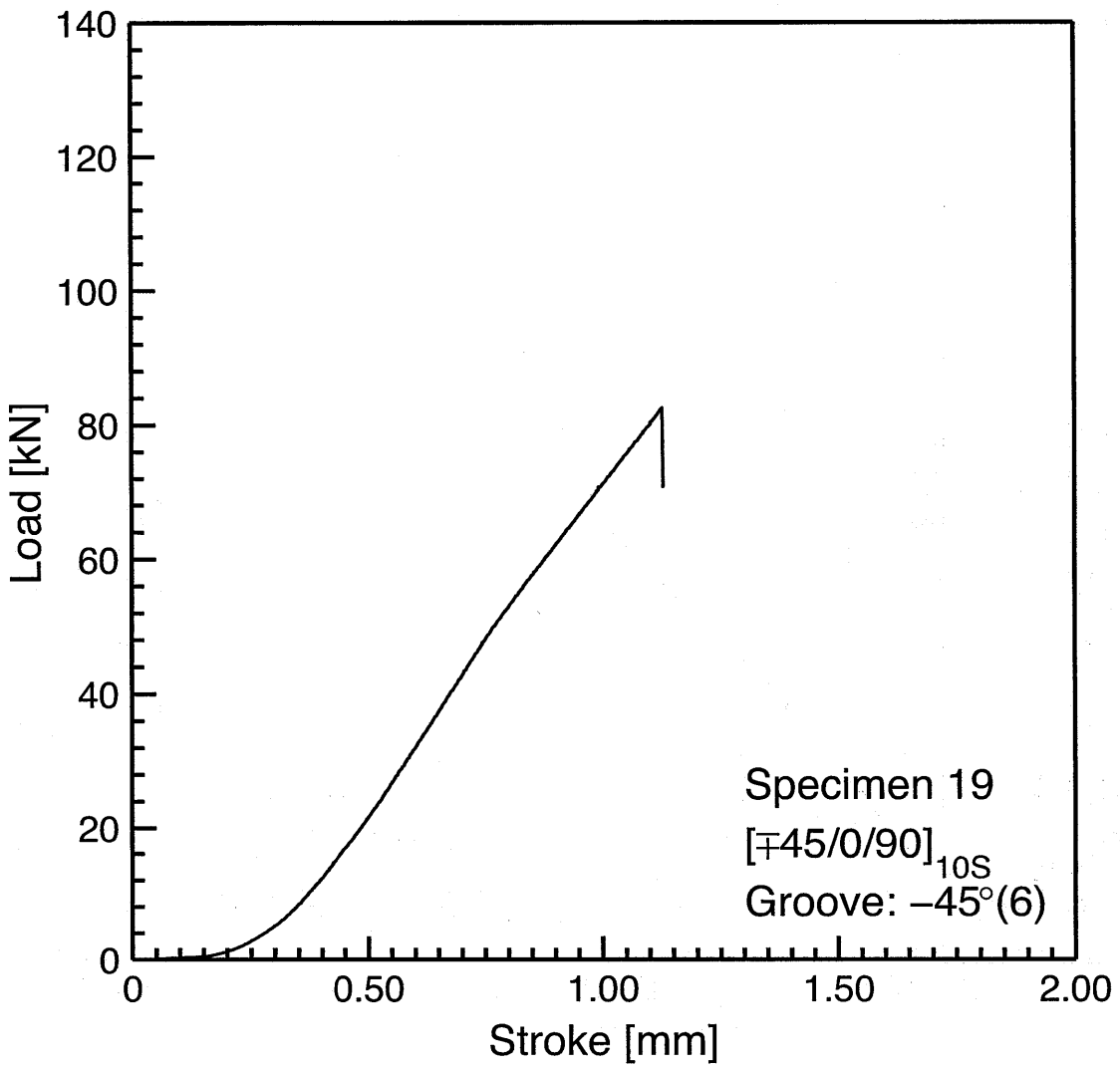

Figure A.7 Load vs. stroke plot for Specimen 19: layup $[\mp 45/0/90]_{10S}$ with groove at $-45°$ ply in 6th set.

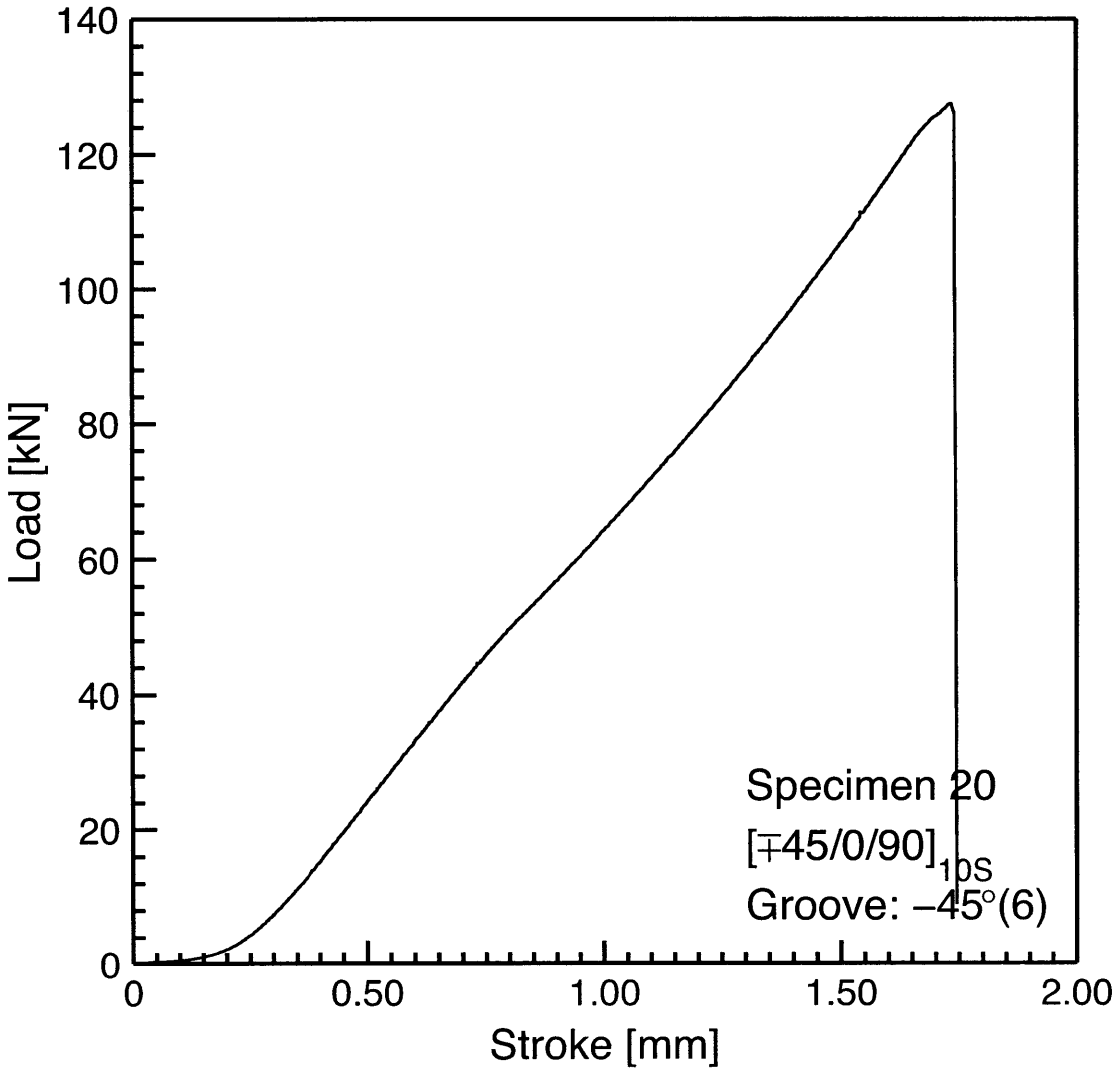

Figure A.8 Load vs. stroke plot for Specimen 20: layup $[\mp 45/0/90]_{10S}$ with groove at $-45°$ ply in 6th set.

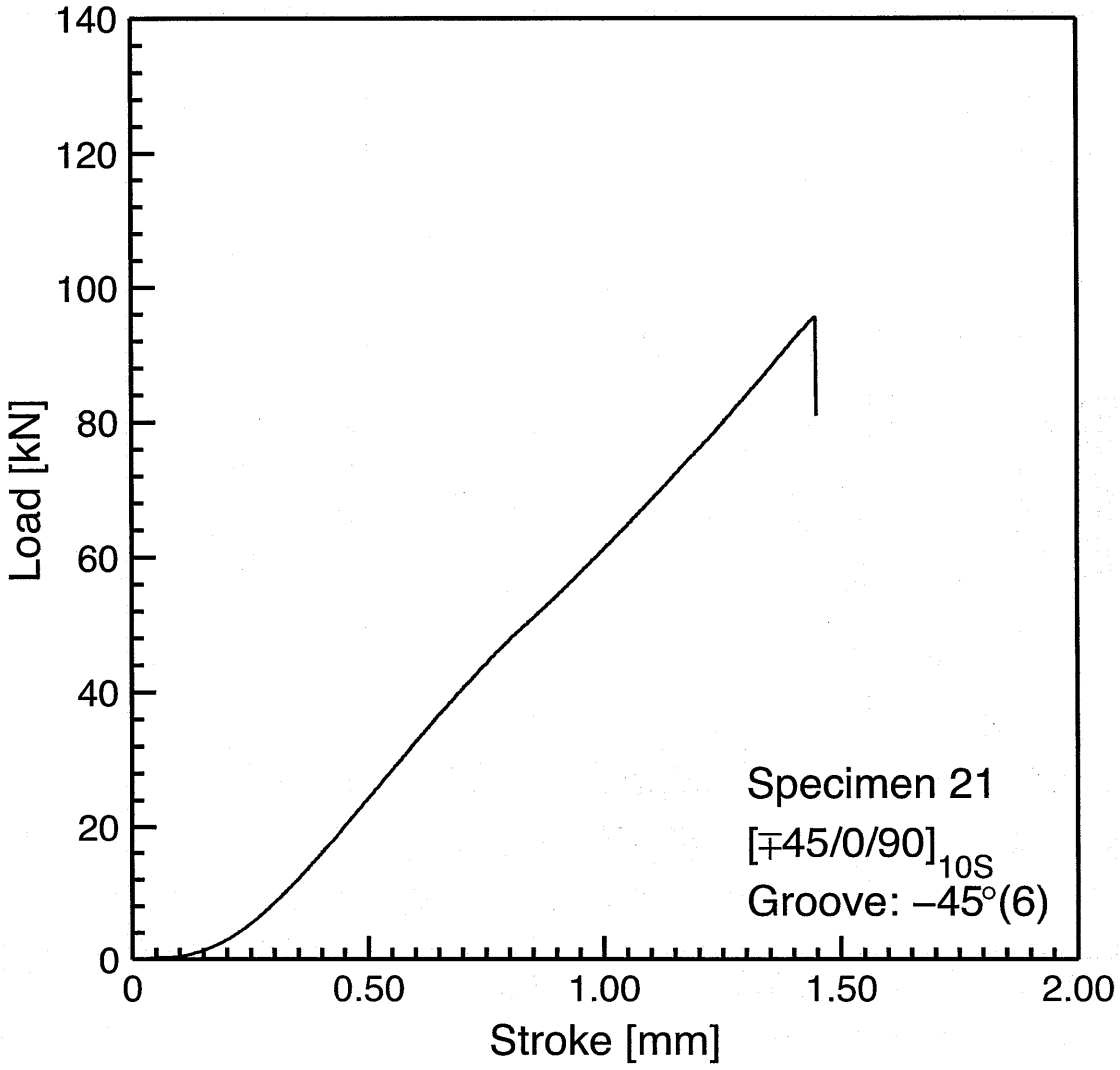

Figure A.9 Load vs. stroke plot for Specimen 21: layup $[\mp 45/0/90]_{10S}$ with groove at $-45°$ ply in 6th set.

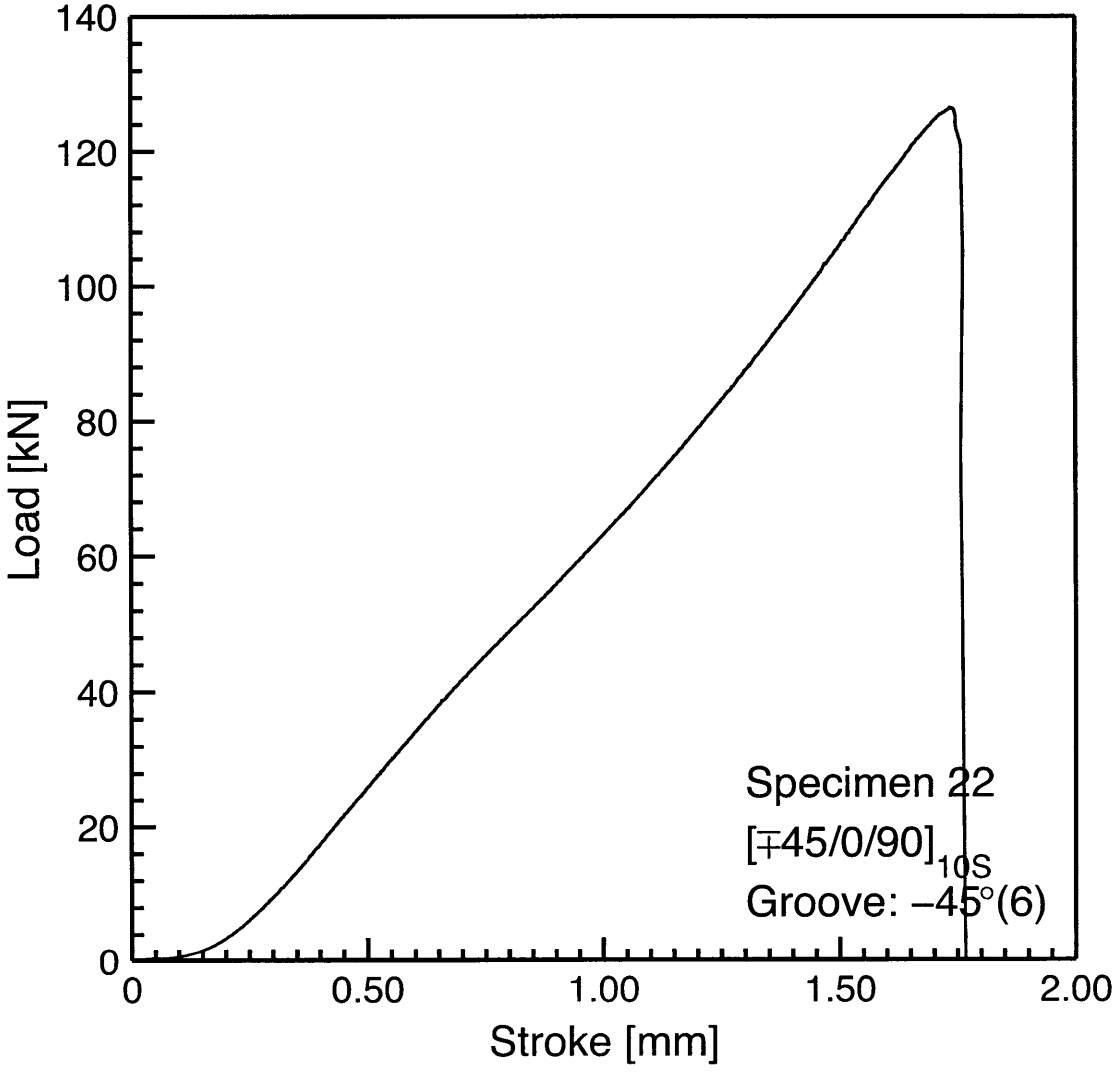

Figure A.10 Load vs. stroke plot for Specimen 22: layup $[\mp 45/0/90]_{10S}$ with groove at $-45°$ ply in 6th set.

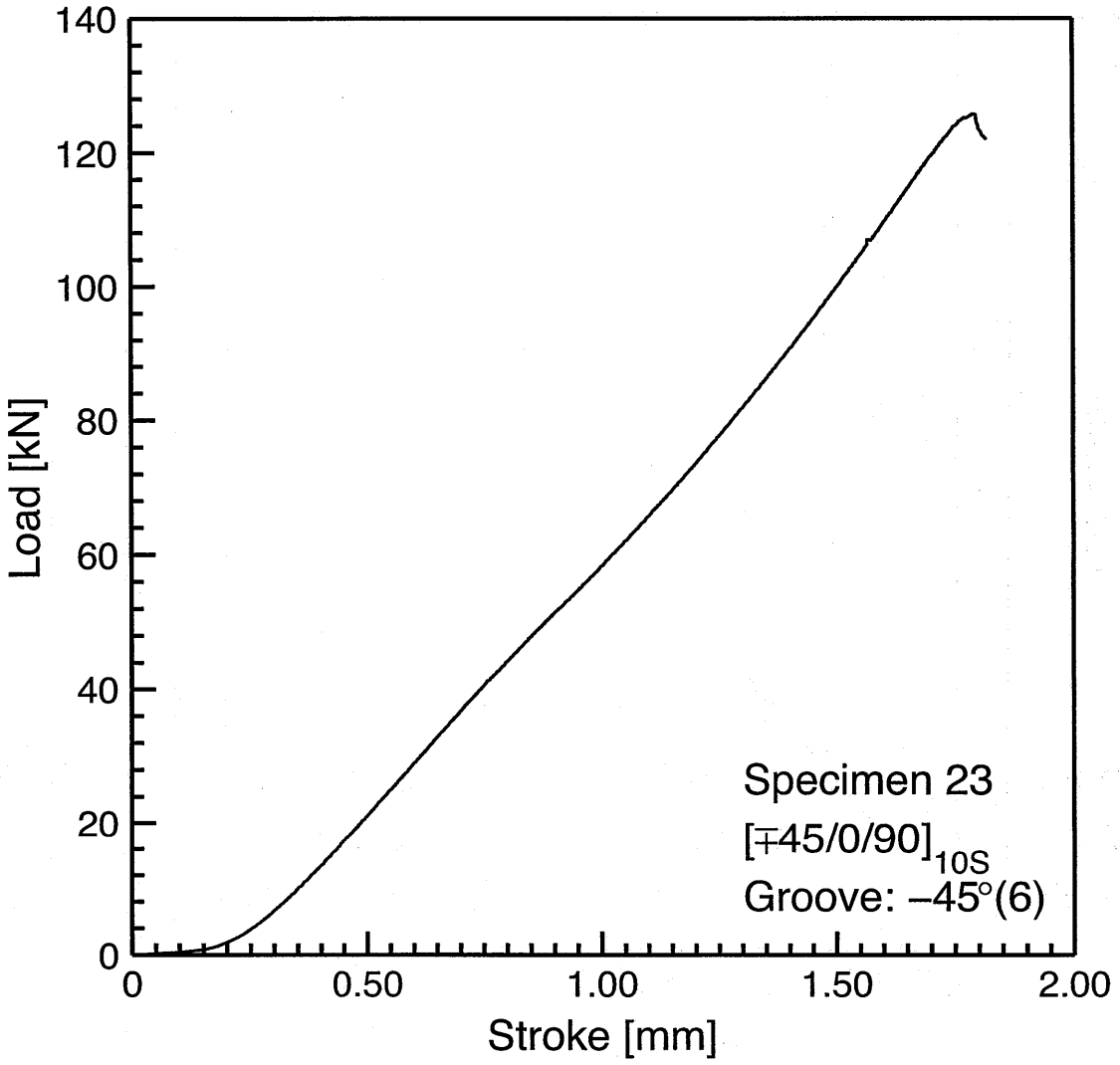

Figure A.11 Load vs. stroke plot for Specimen 23: layup $[\mp 45/0/90]_{10S}$ with groove at $-45°$ ply in 6th set.

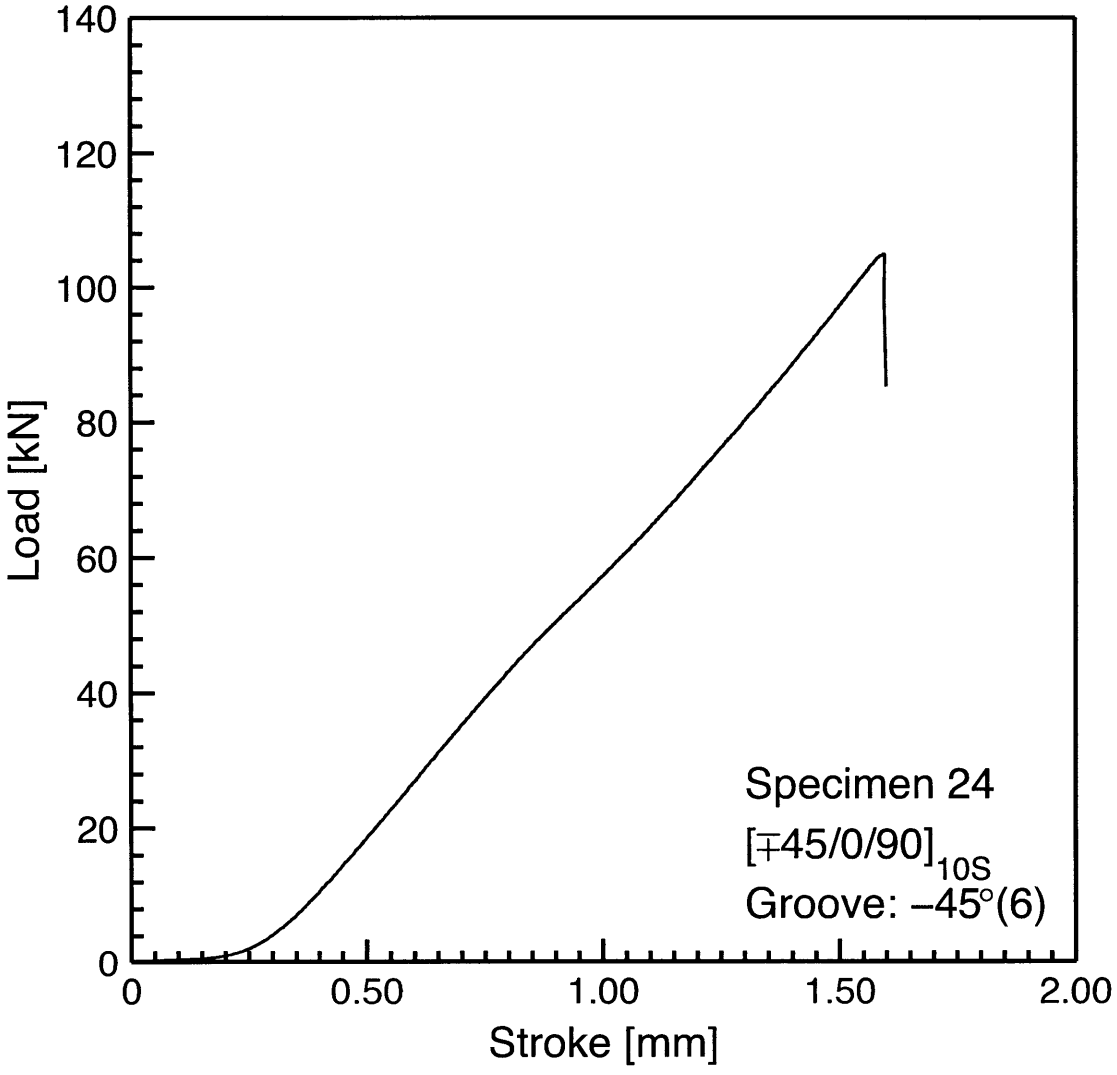

Figure A.12 Load vs. stroke plot for Specimen 24: layup $[\mp 45/0/90]_{10S}$ with groove at $-45°$ ply in 6th set.

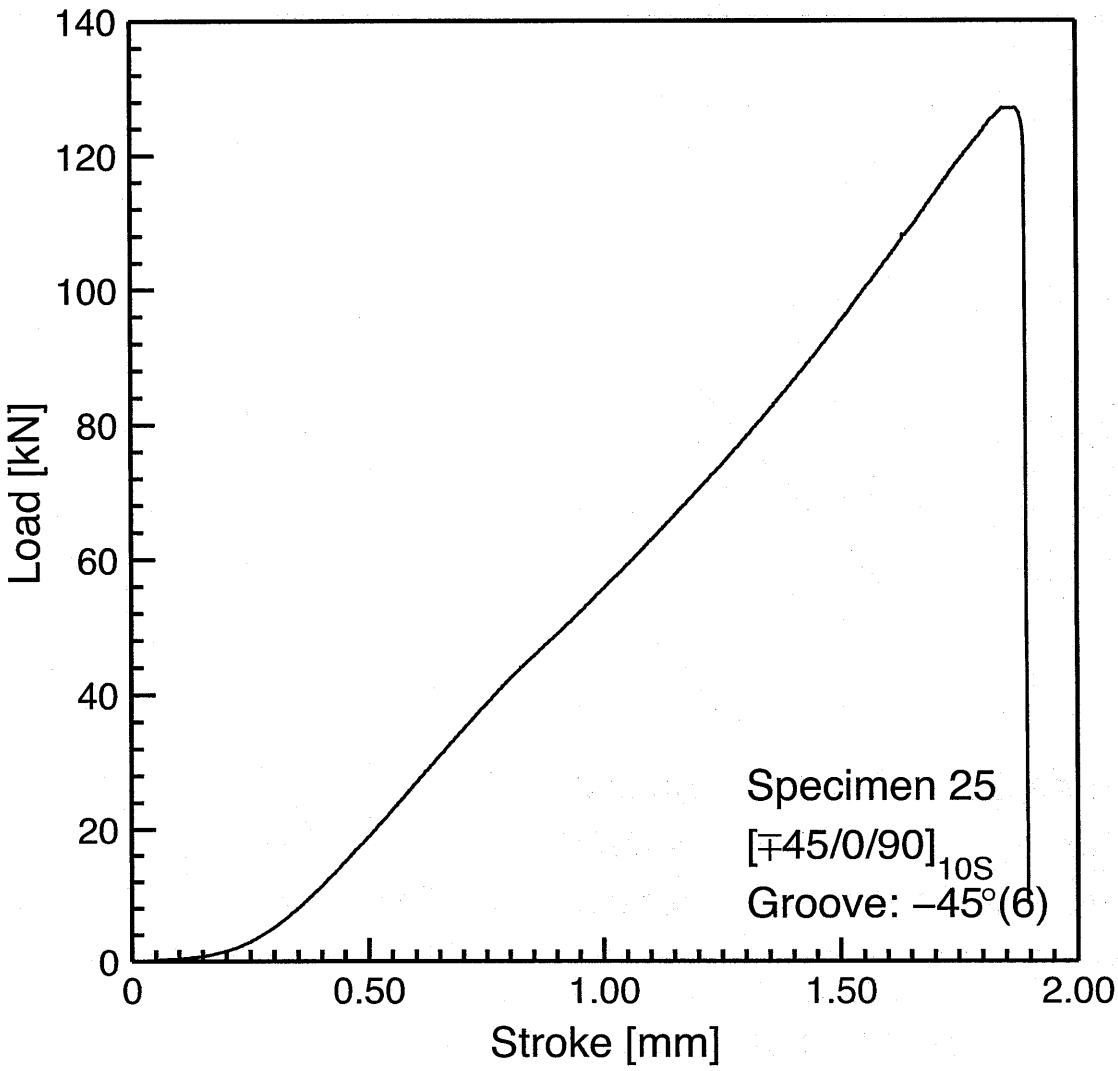

Figure A.13 Load vs. stroke plot for Specimen 25: layup $[\mp 45/0/90]_{10S}$ with groove at $-45°$ ply in 6th set.

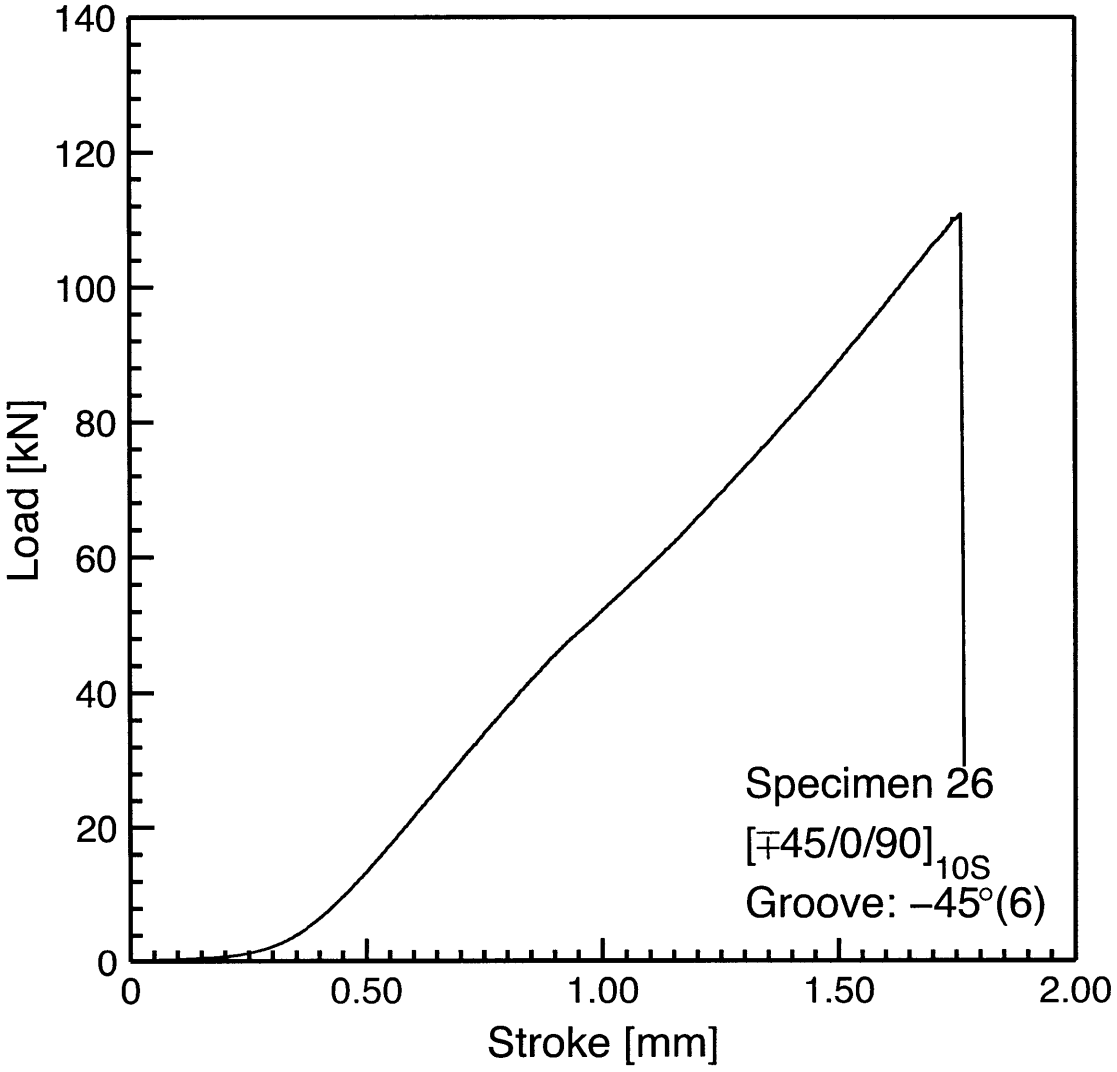

Figure A.14 Load vs. stroke plot for Specimen 26: layup $[\mp 45/0/90]_{10S}$ with groove at $-45°$ ply in 6th set.

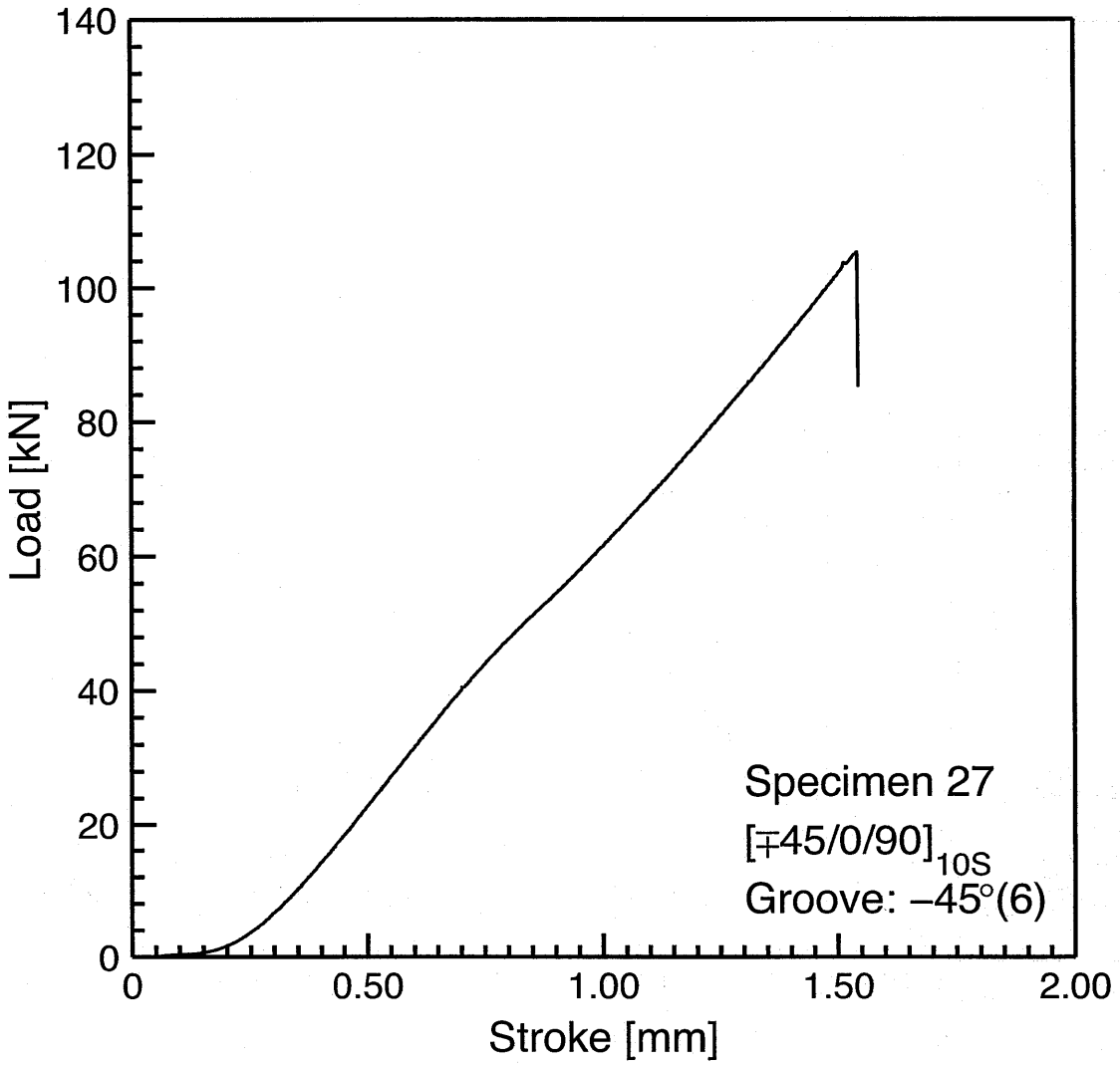

Figure A.15 Load vs. stroke plot for Specimen 27: layup $[\mp 45/0/90]_{10S}$ with groove at $-45°$ ply in 6th set.

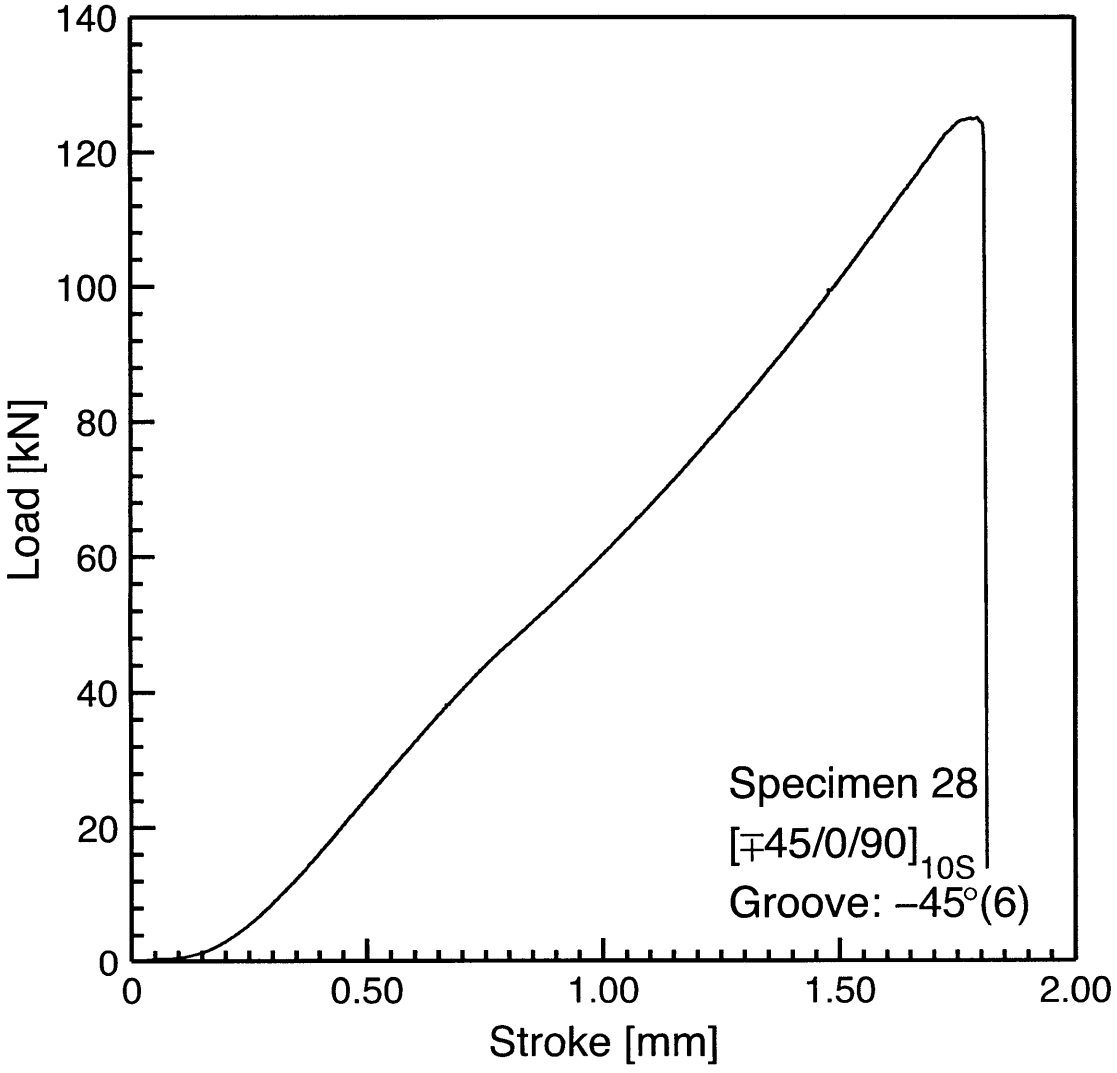

Figure A.16 Load vs. stroke plot for Specimen 28: layup $[\mp 45/0/90]_{10S}$ with groove at $-45°$ ply in 6th set.

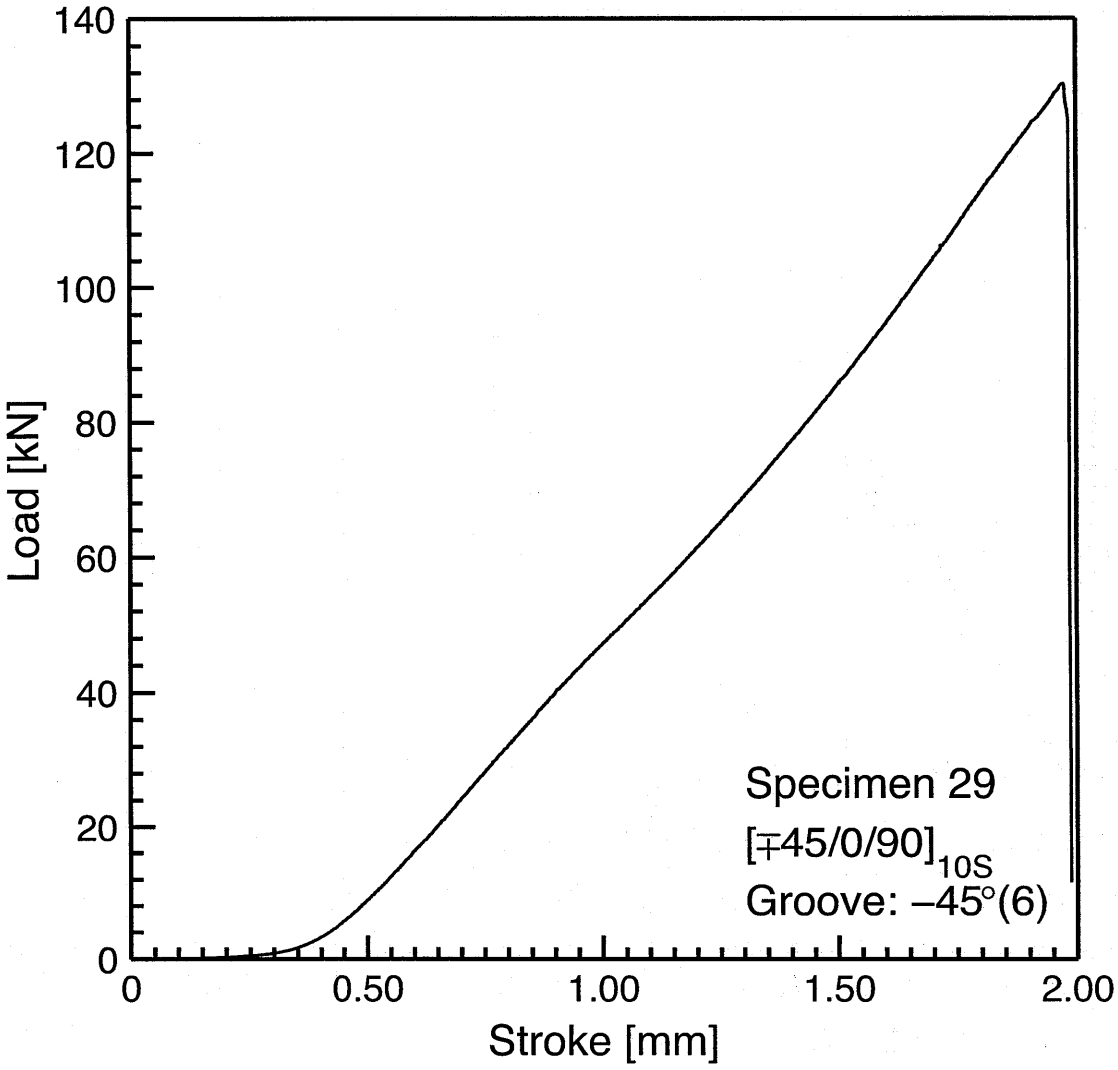

Figure A.17 Load vs. stroke plot for Specimen 29: layup $[\mp 45/0/90]_{10S}$ with groove at $-45°$ ply in 6th set.

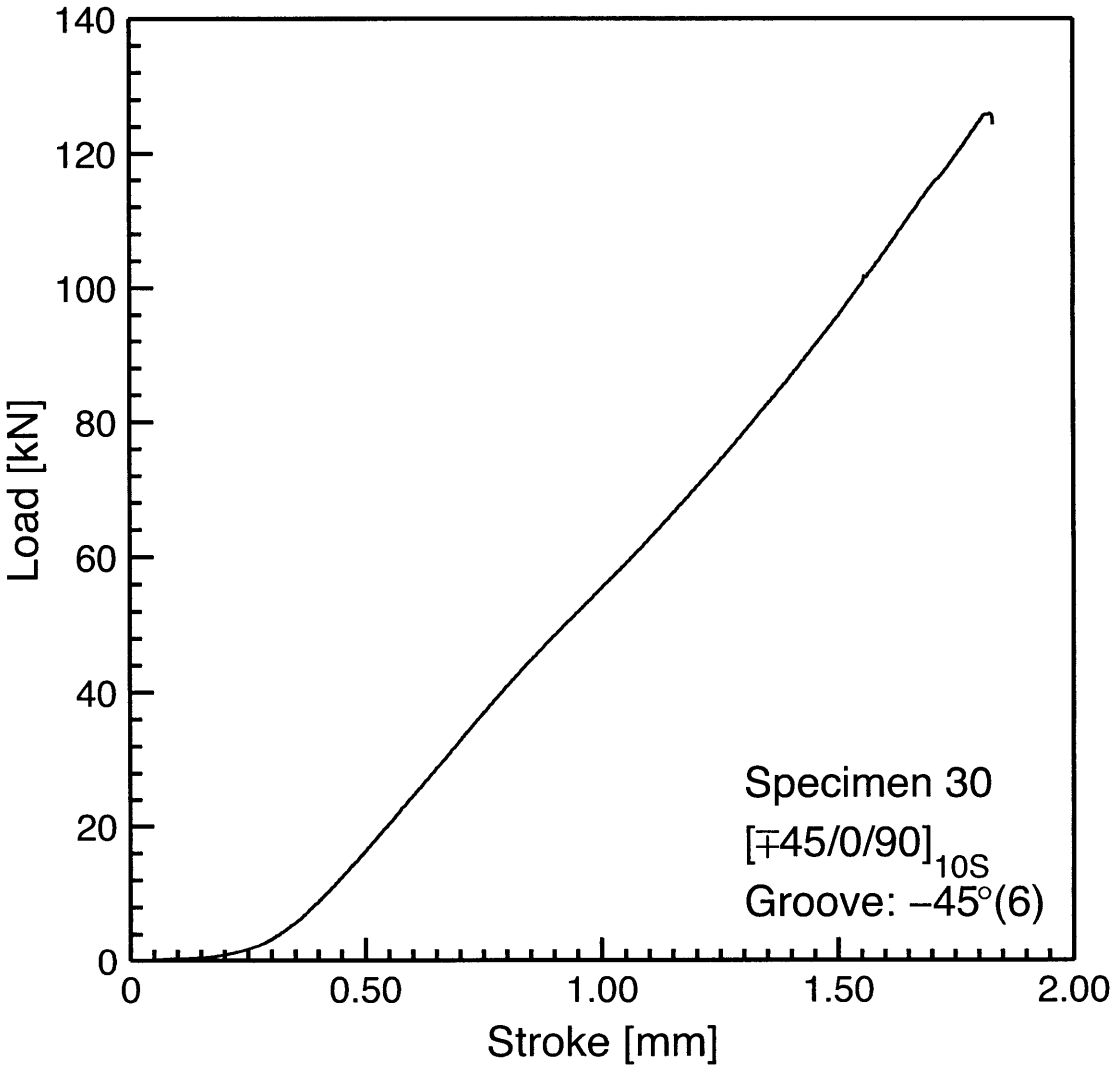

Figure A.18 Load vs. stroke plot (stopped before failure) for Specimen 30: layup $[\mp 45/0/90]_{10S}$ with groove at $-45°$ ply in 6th set.

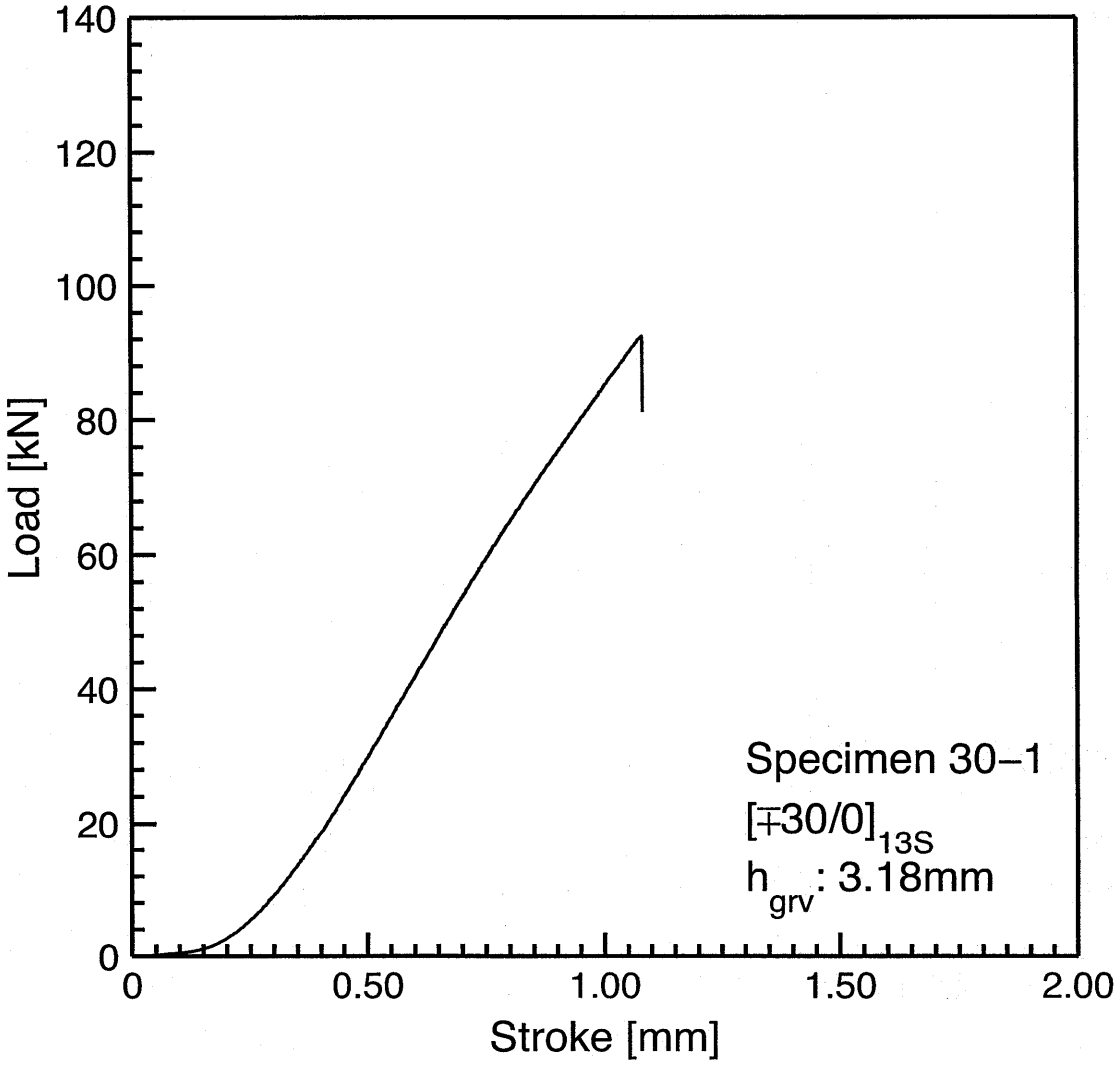

Figure A.19 Load vs. stroke plot for Specimen 30-1: layup $[\mp 30/0]_{13S}$ with $h_{\text{grv}} = 3.18$ mm.

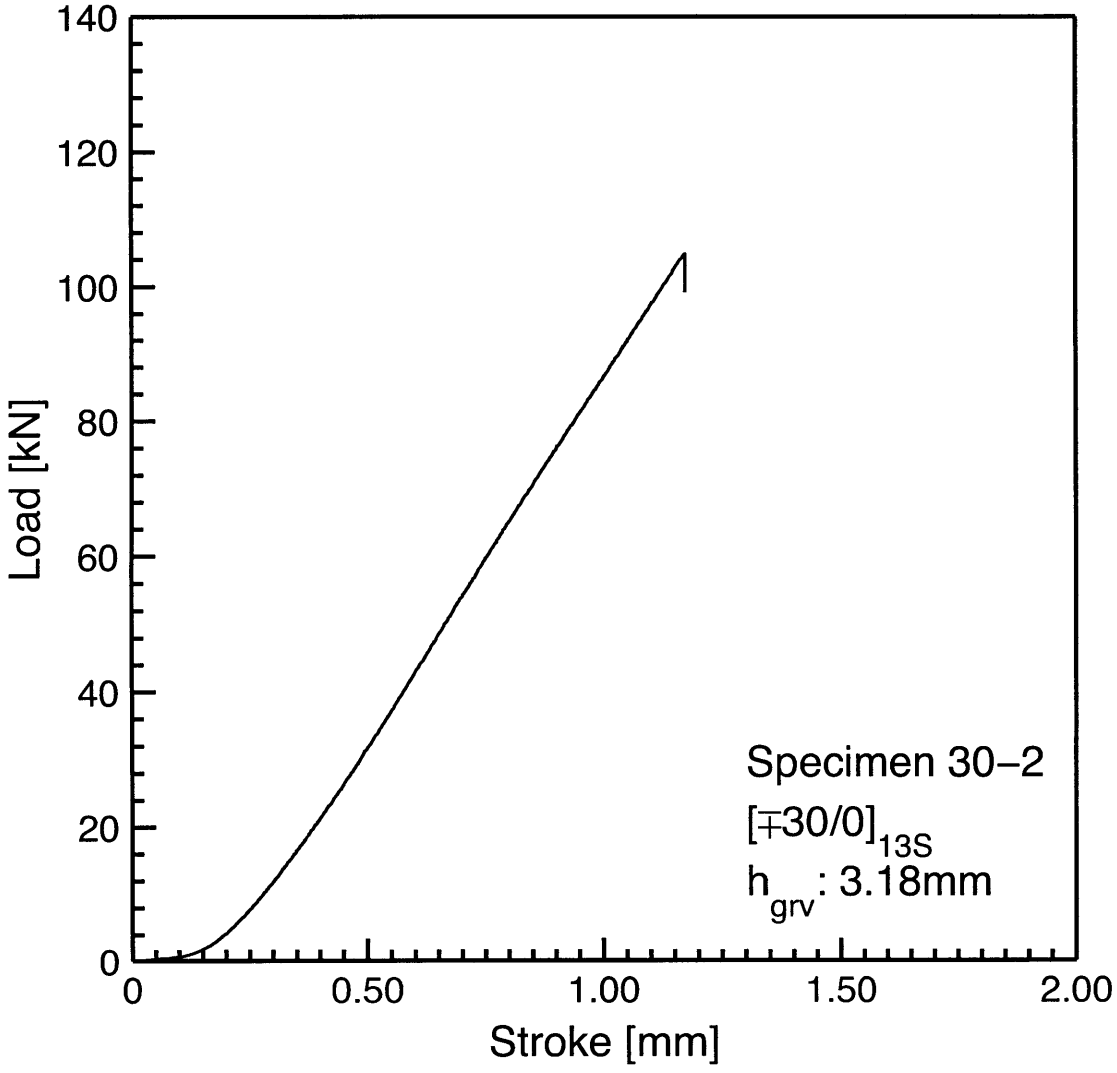

Figure A.20 Load vs. stroke plot for Specimen 30-2: layup $[\mp 30/0]_{13S}$ with $h_{\text{grv}} = 3.18$ mm.

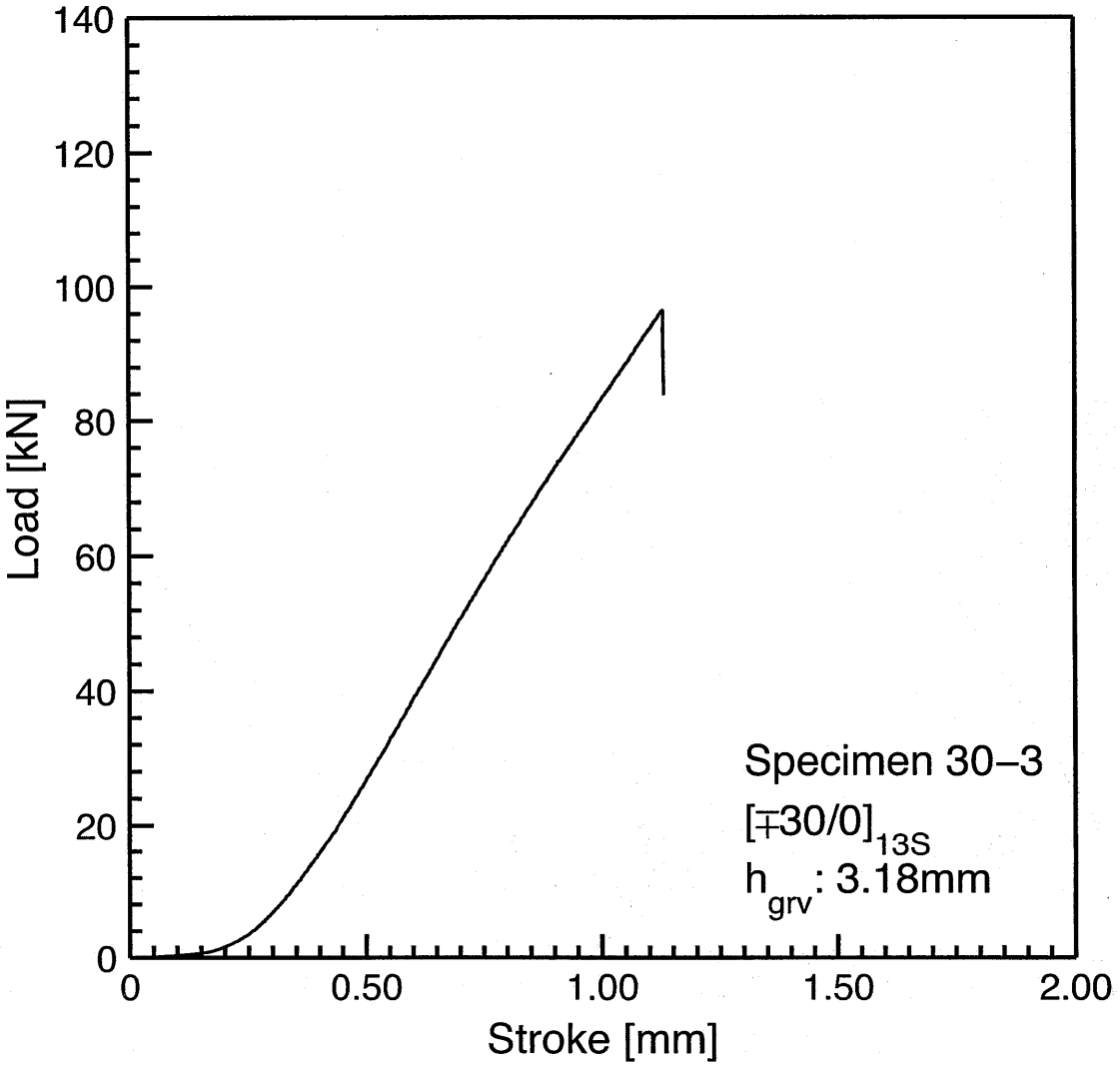

Figure A.21 Load vs. stroke plot for Specimen 30-3: layup $[\mp 30/0]_{13S}$ with $h_{\text{grv}} = 3.18$ mm.

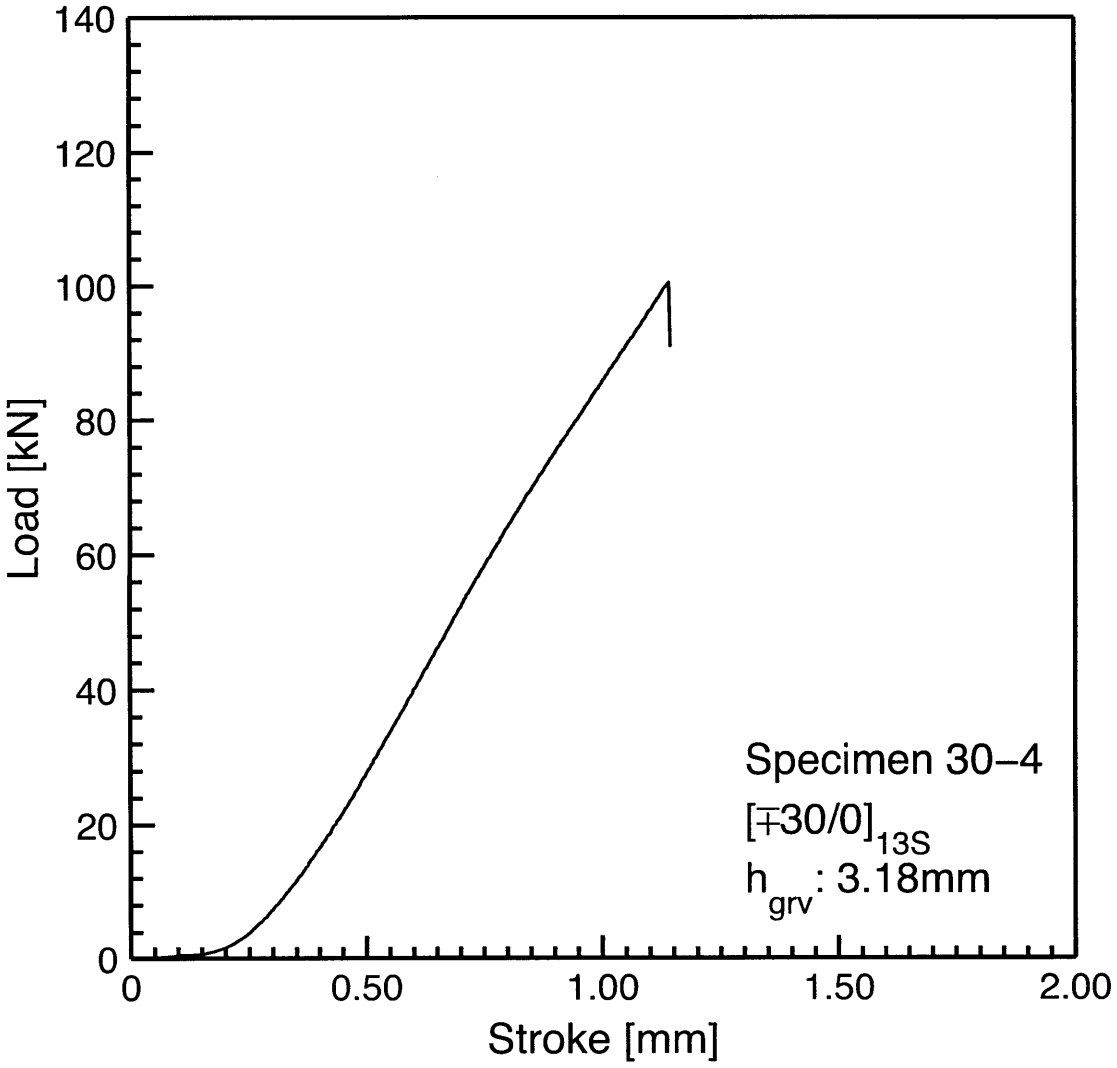

Figure A.22 Load vs. stroke plot for Specimen 30-4: layup $[\mp 30/0]_{13S}$ with $h_{\text{grv}} = 3.18$ mm.

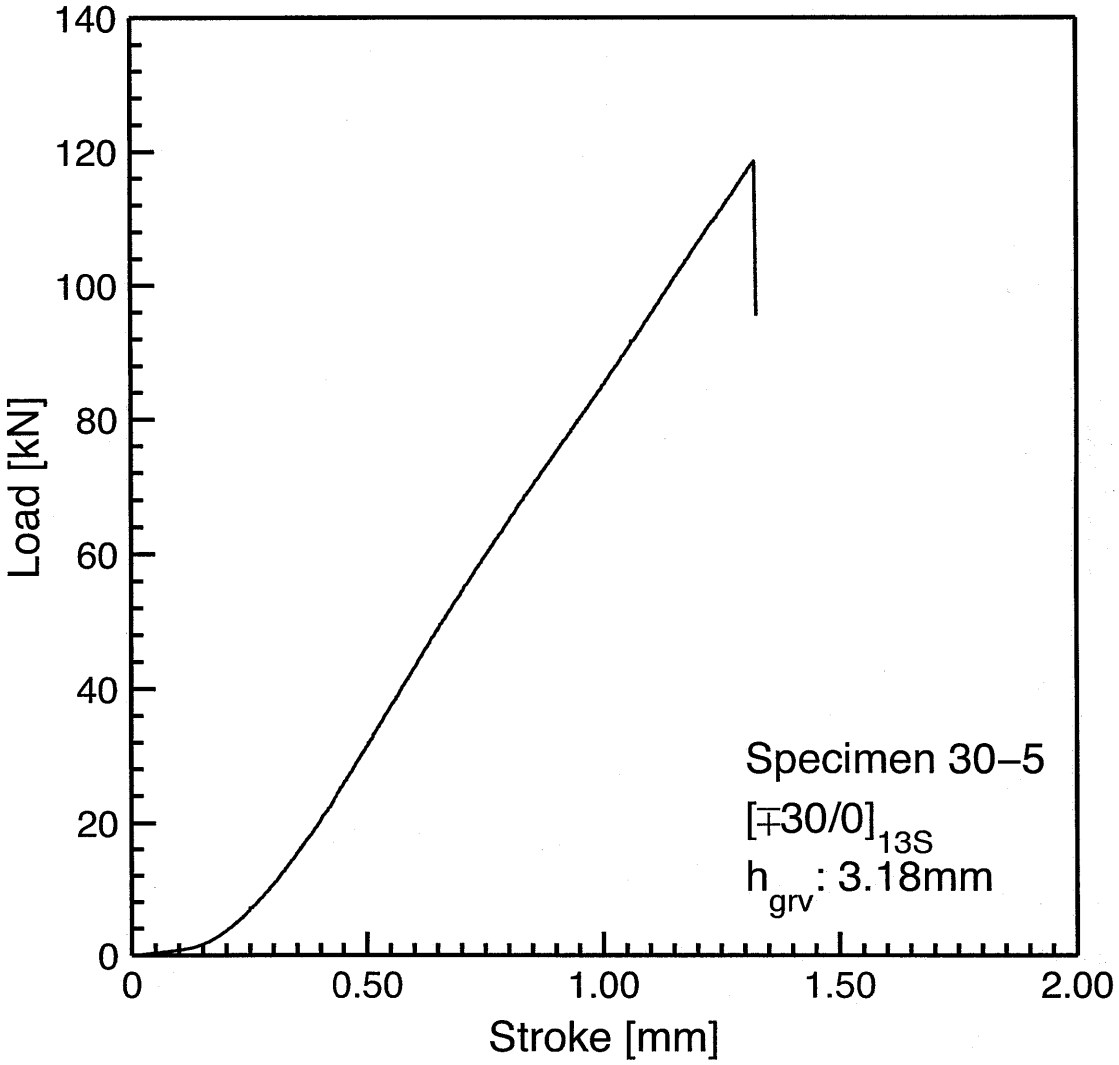

Figure A.23 Load vs. stroke plot for Specimen 30-5: layup $[\mp 30/0]_{13S}$ with $h_{\text{grv}} = 3.18$ mm.

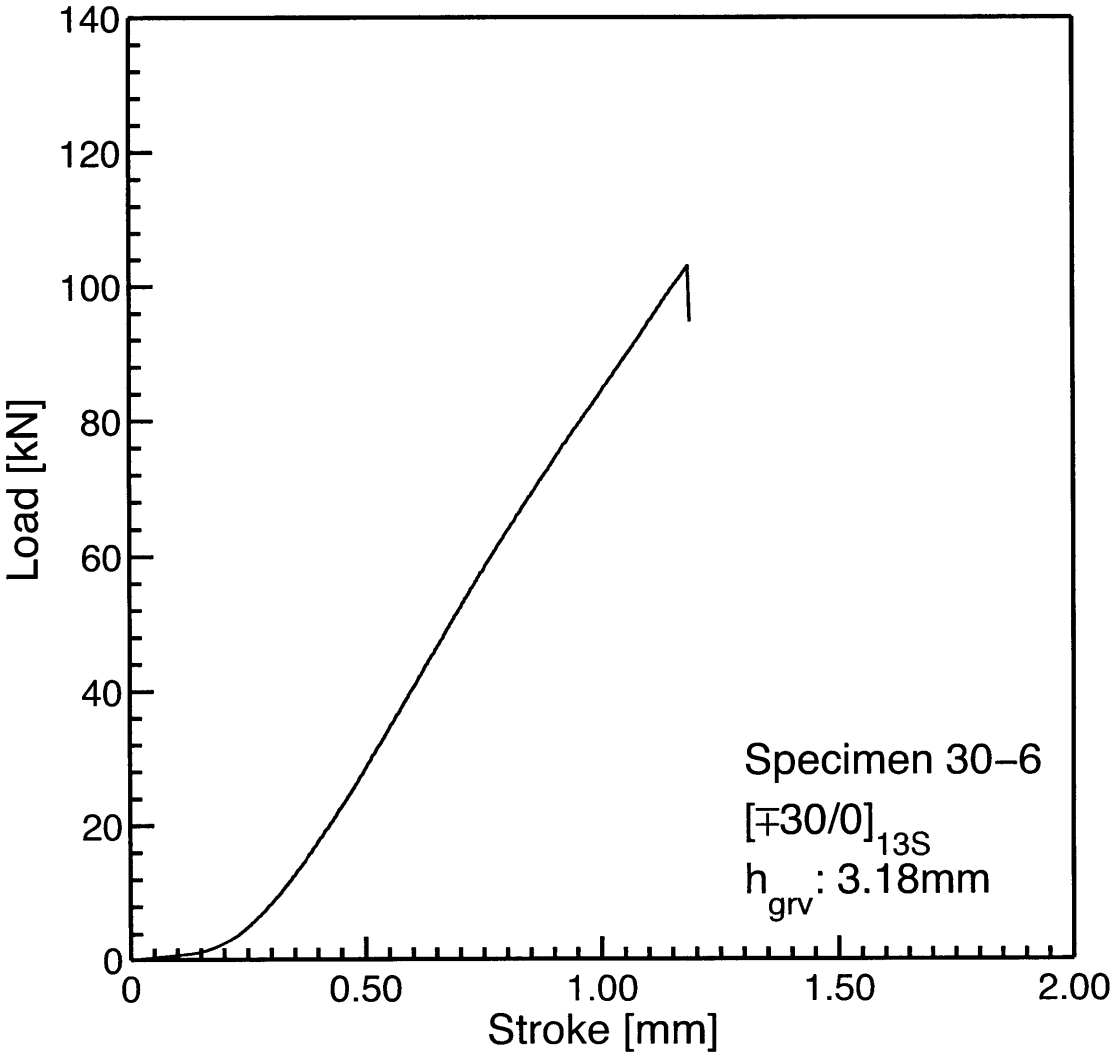

Figure A.24 Load vs. stroke plot for Specimen 30-6: layup $[\mp 30/0]_{13S}$ with $h_{\text{grv}} = 3.18$ mm.

Appendix B

Damage Data for Final Specimens

Photographs taken after the test and an illustration of damage for all the "final specimens" (as addressed in Chapter 8) are presented in this appendix. Specimens 13 through 30 have the standard layup, $[\mp 45/0/90]_{10S}$. Specimens 30-1 through 30-6 have the alternate layup, $[\mp 30/0]_{13S}$. The general testing procedures are described in Chapter 5, with further details in Section 8.1 of Chapter 8. The groove ply parameter or the groove depth is noted in the plots and the figure titles. All the tests were loaded until failure except for Specimen 30 (details are described in Chapter 8).

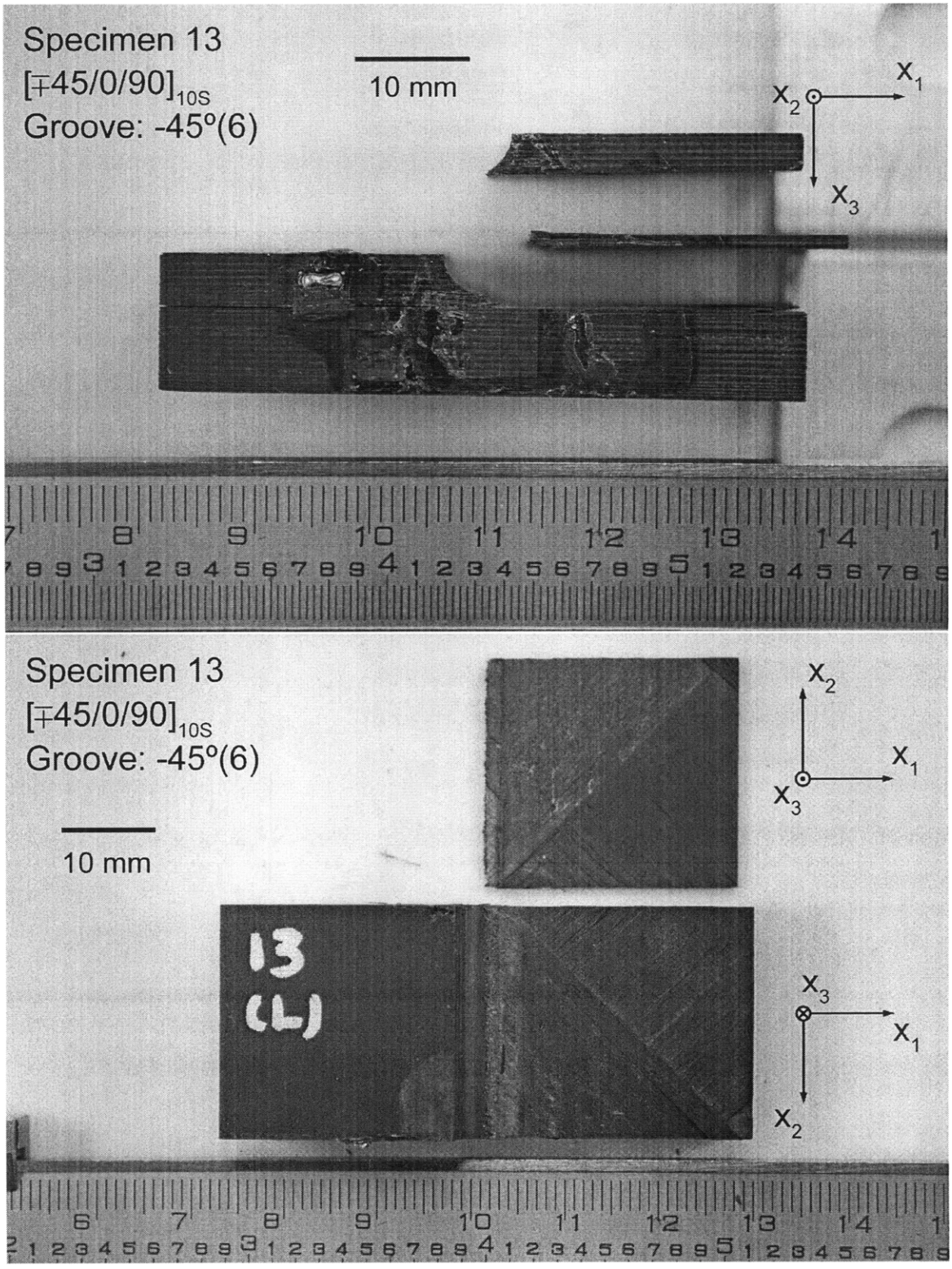

Figure B.1 Photographs after failure of Specimen 13 (layup $[\mp 45/0/90]_{10S}$ with groove at $-45°$ ply in 6th set) with *(upper)* side view, and *(lower)* failure surface view of the bottom two pieces.

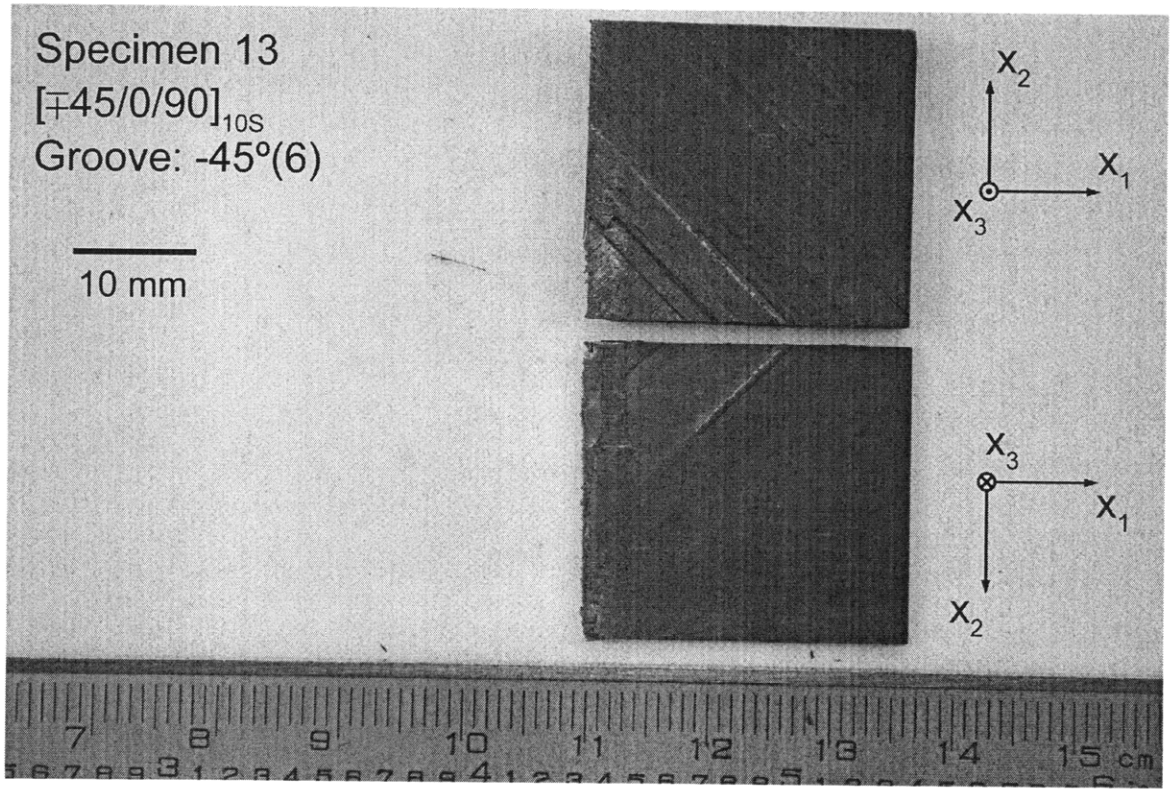

Figure B.2 Failure surface view photographs of the top two pieces after failure of Specimen 13 (layup $[\mp 45/0/90]_{10S}$ with groove at $-45°$ ply in 6th set).

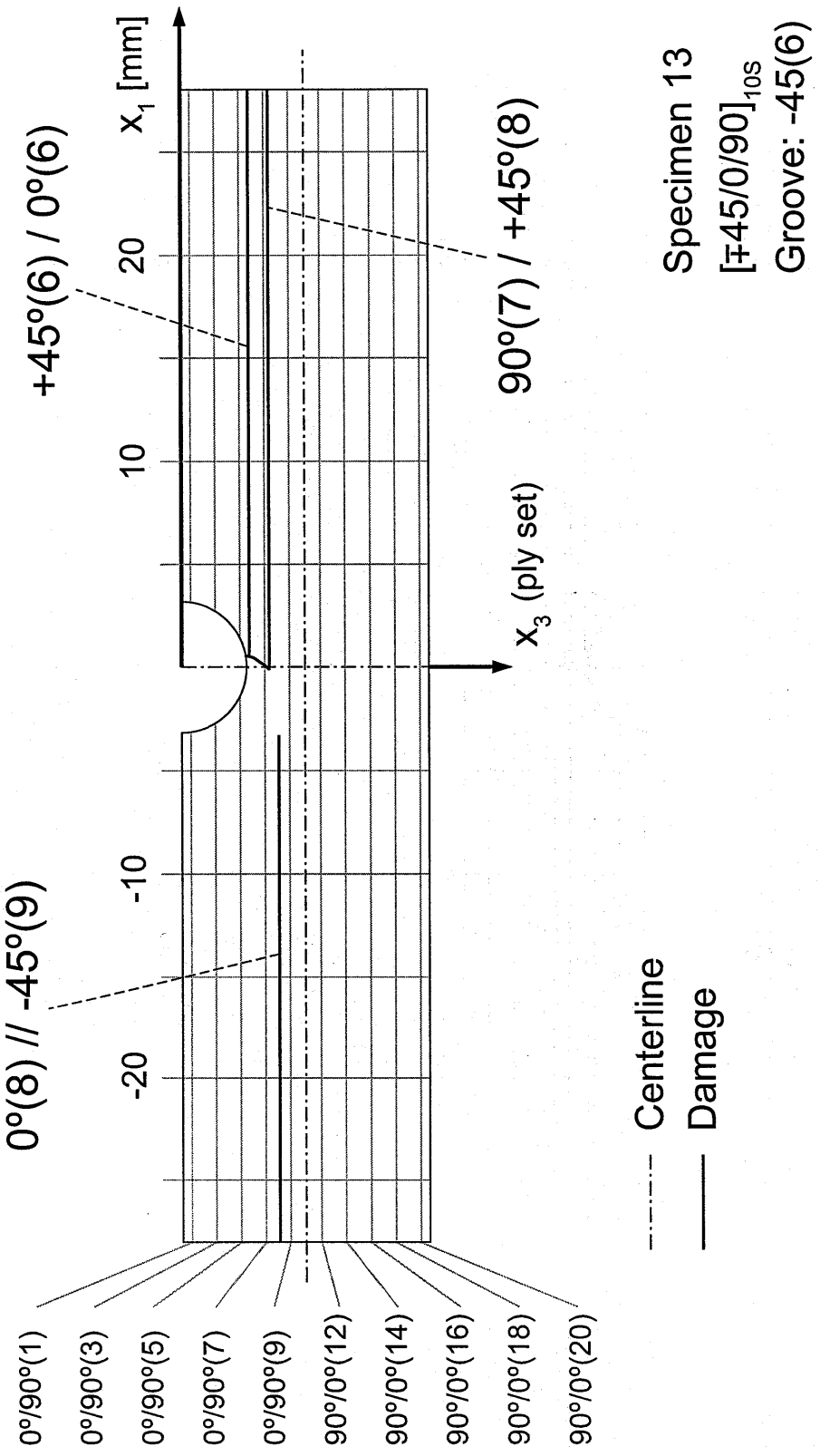

Figure B.3 Illustration of failure for Specimen 13: layup $[\mp 45/0/90]_{10S}$ with groove at $-45°$ ply in 6th set.

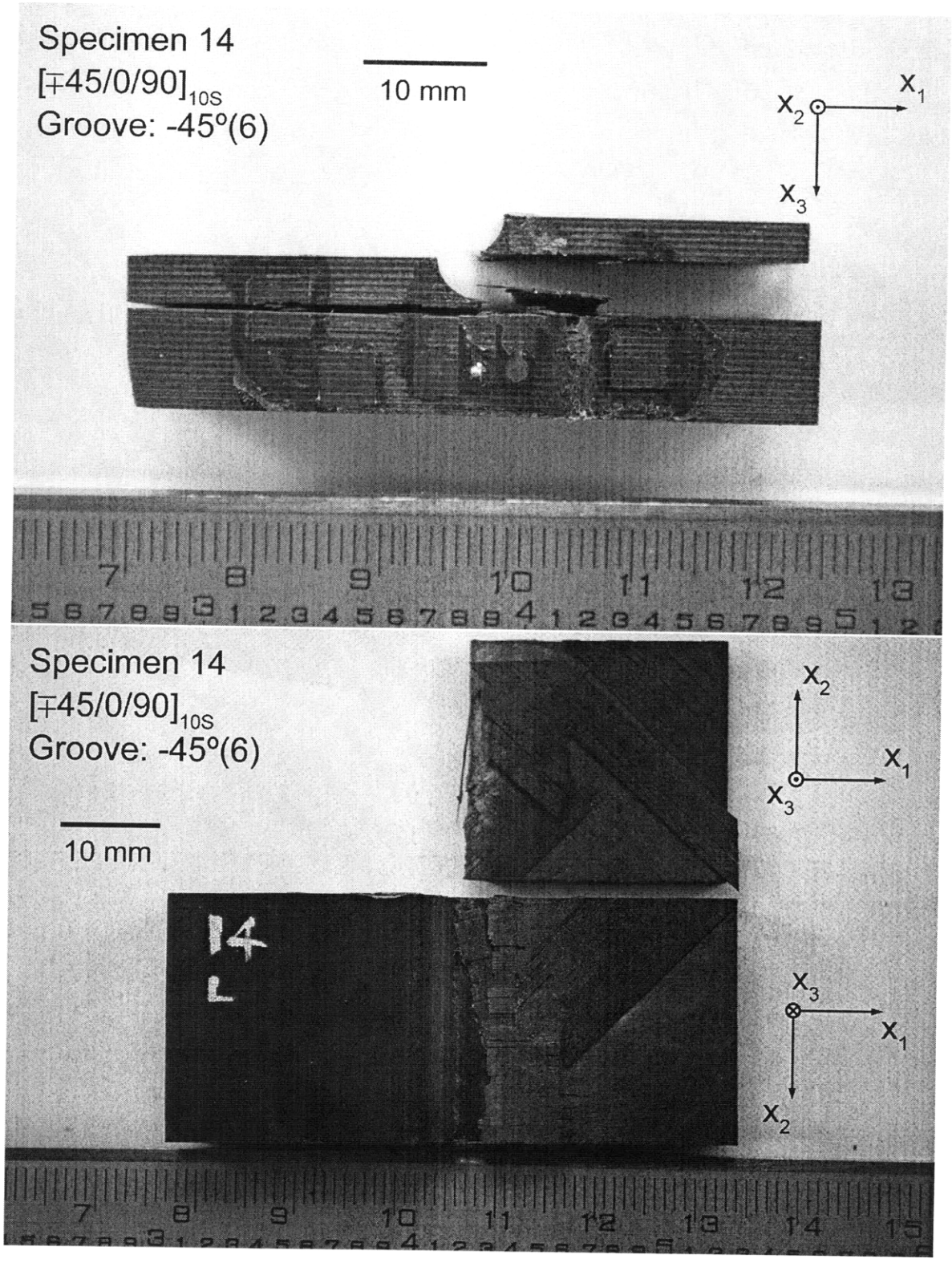

Figure B.4 Photographs after failure of Specimen 14 (layup $[\mp 45/0/90]_{10S}$ with groove at $-45°$ ply in 6th set) with *(upper)* side view, and *(lower)* failure surface view.

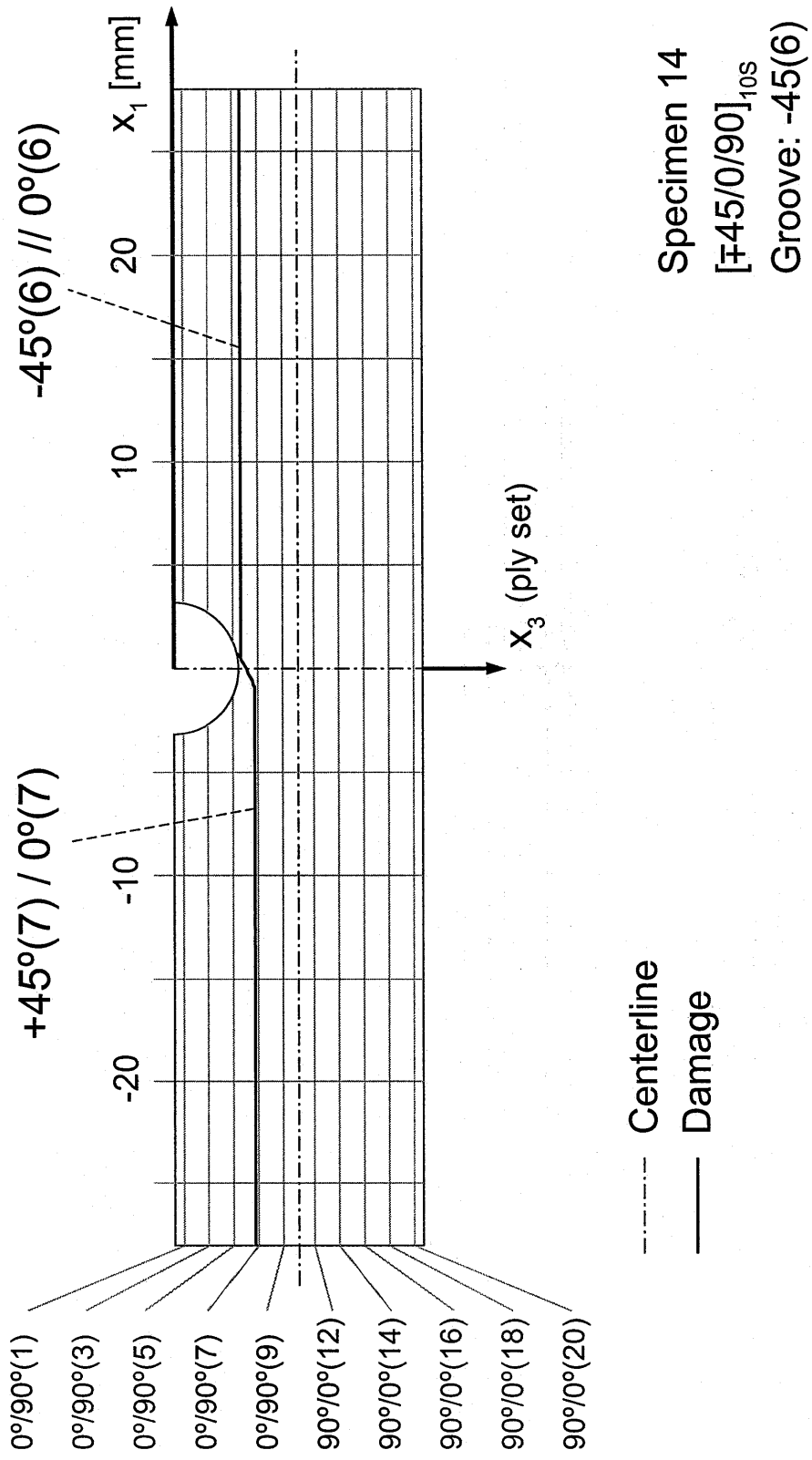

Figure B.5 Illustration of failure for Specimen 14: layup $[\mp 45/0/90]_{10S}$ with groove at $-45°$ ply in 6th set.

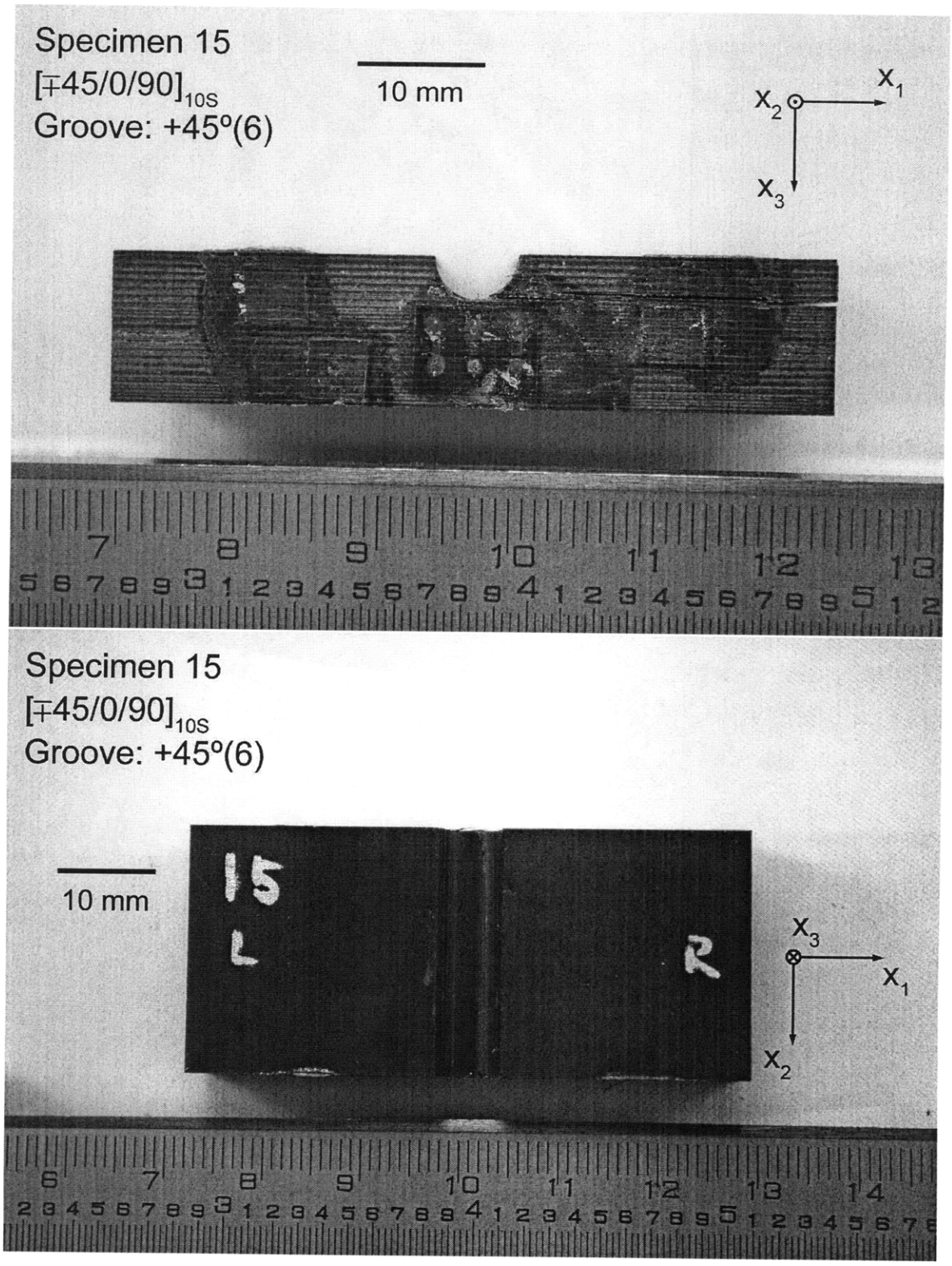

Figure B.6 Photographs after failure of Specimen 15 (layup $[\mp 45/0/90]_{10S}$ with groove at +45° ply in 6th set) with *(upper)* side view, and *(lower)* failure surface view.

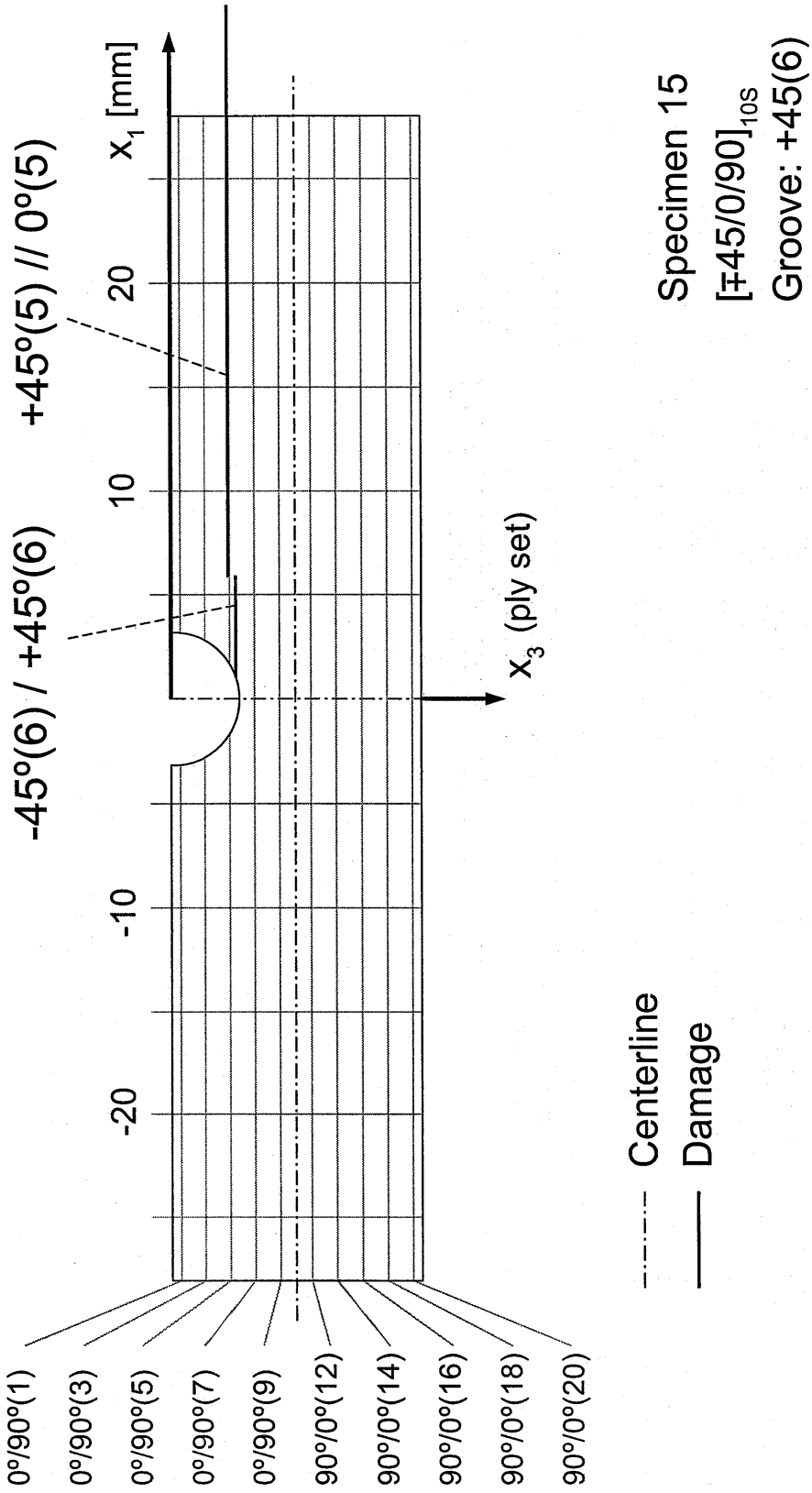

Figure B.7 Illustration of failure for Specimen 15: layup $[\mp 45/0/90]_{10S}$ with groove at +45° ply in 6th set.

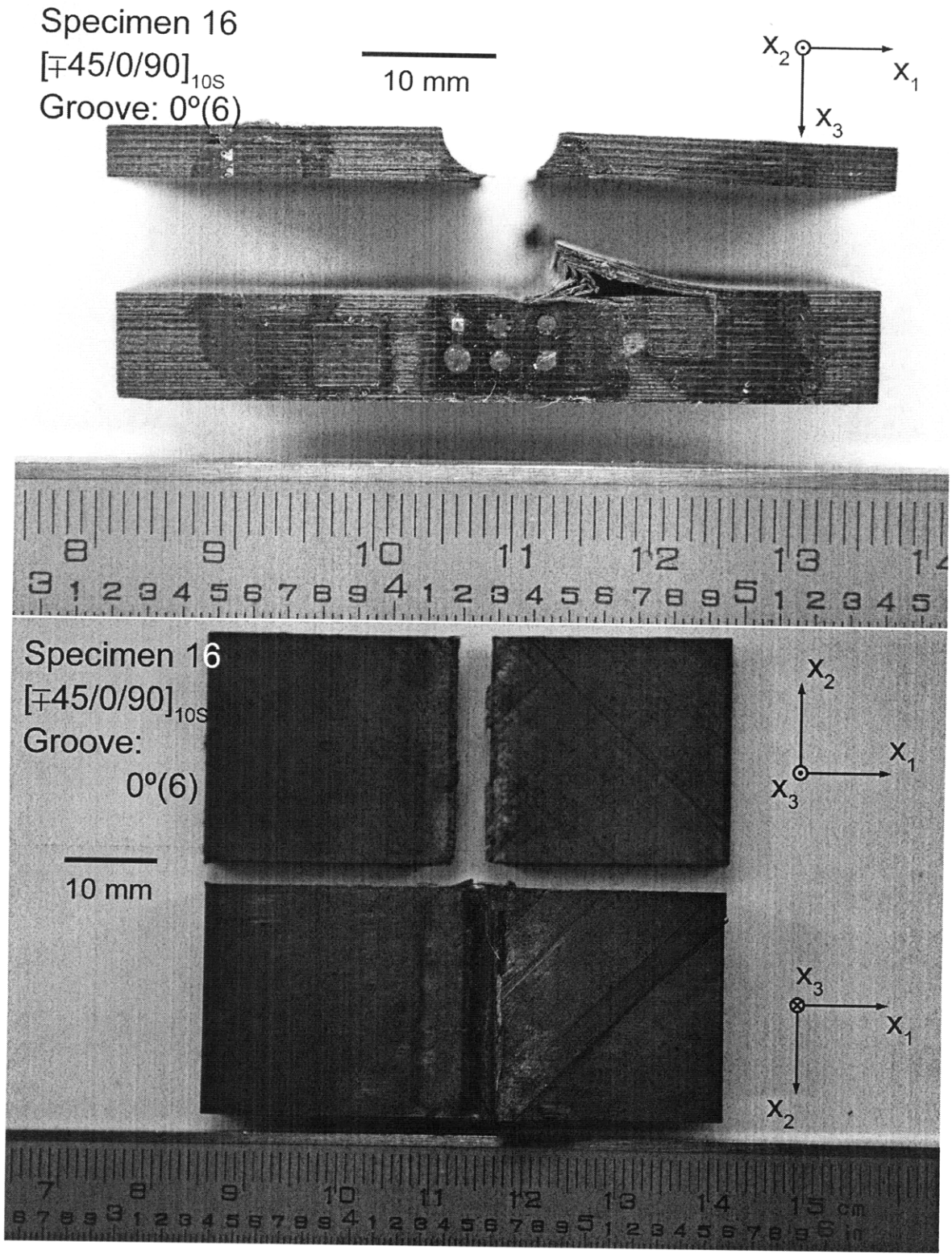

Figure B.8 Photographs after failure of Specimen 16 (layup $[\mp 45/0/90]_{10S}$ with groove at 0° ply in 6th set) with *(upper)* side view, and *(lower)* failure surface view.

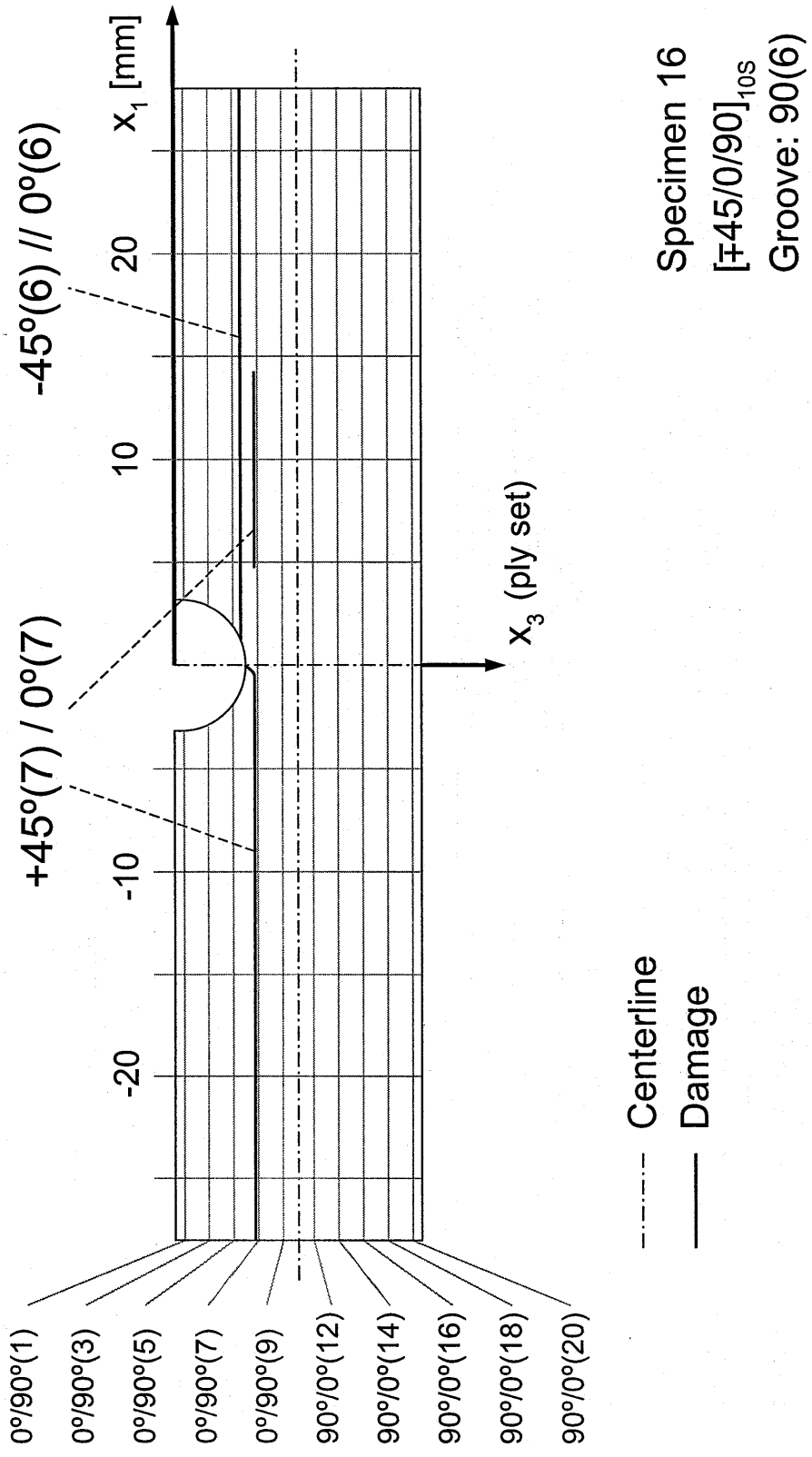

Figure B.9 Illustration of failure for Specimen 16: layup $[\mp 45/0/90]_{10S}$ with groove at 0° ply in 6th set.

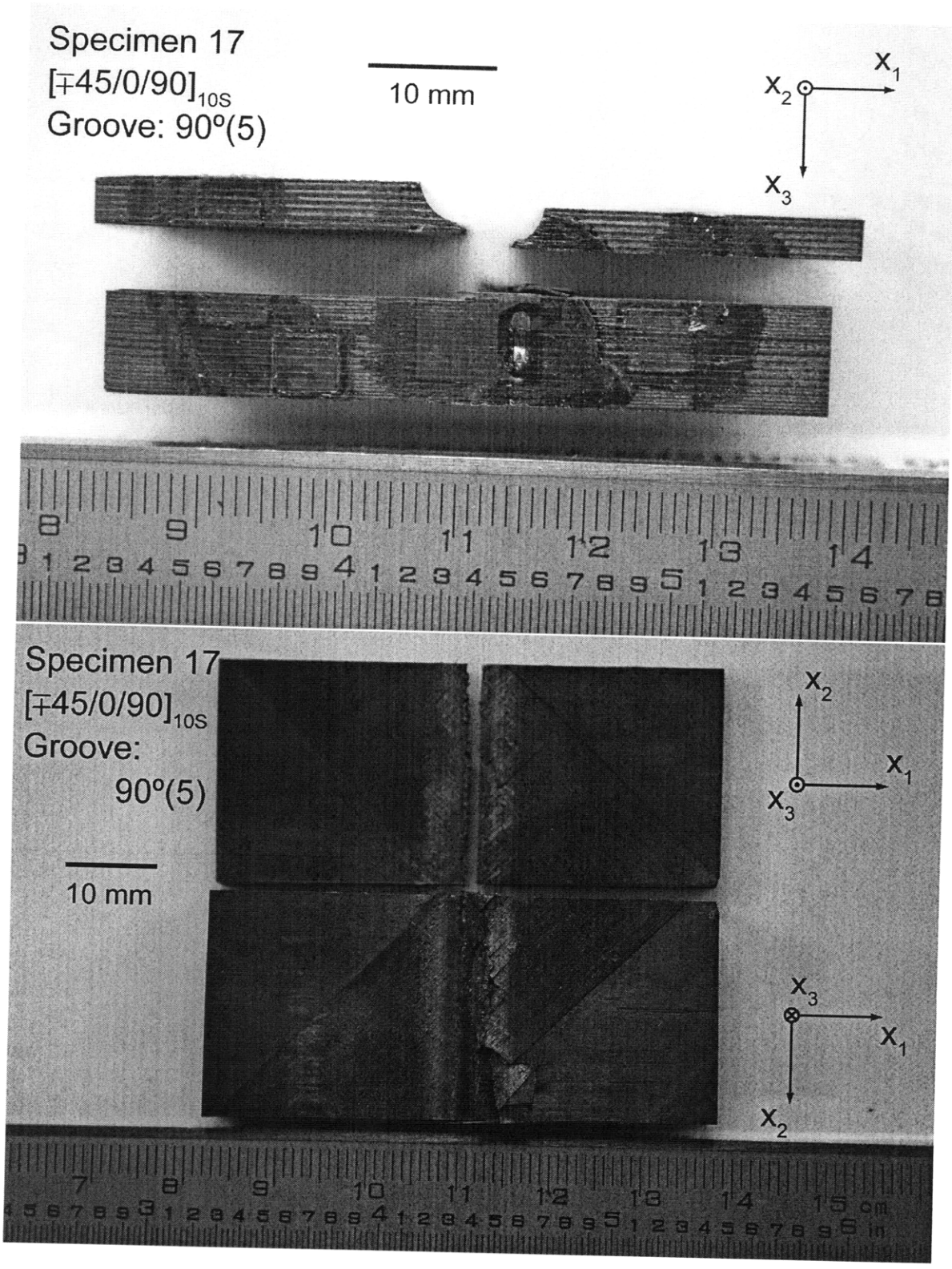

Figure B.10 Photographs after failure of Specimen 17 (layup $[\mp 45/0/90]_{10S}$ with groove at 0° ply in 5th set) with *(upper)* side view, and *(lower)* failure surface view.

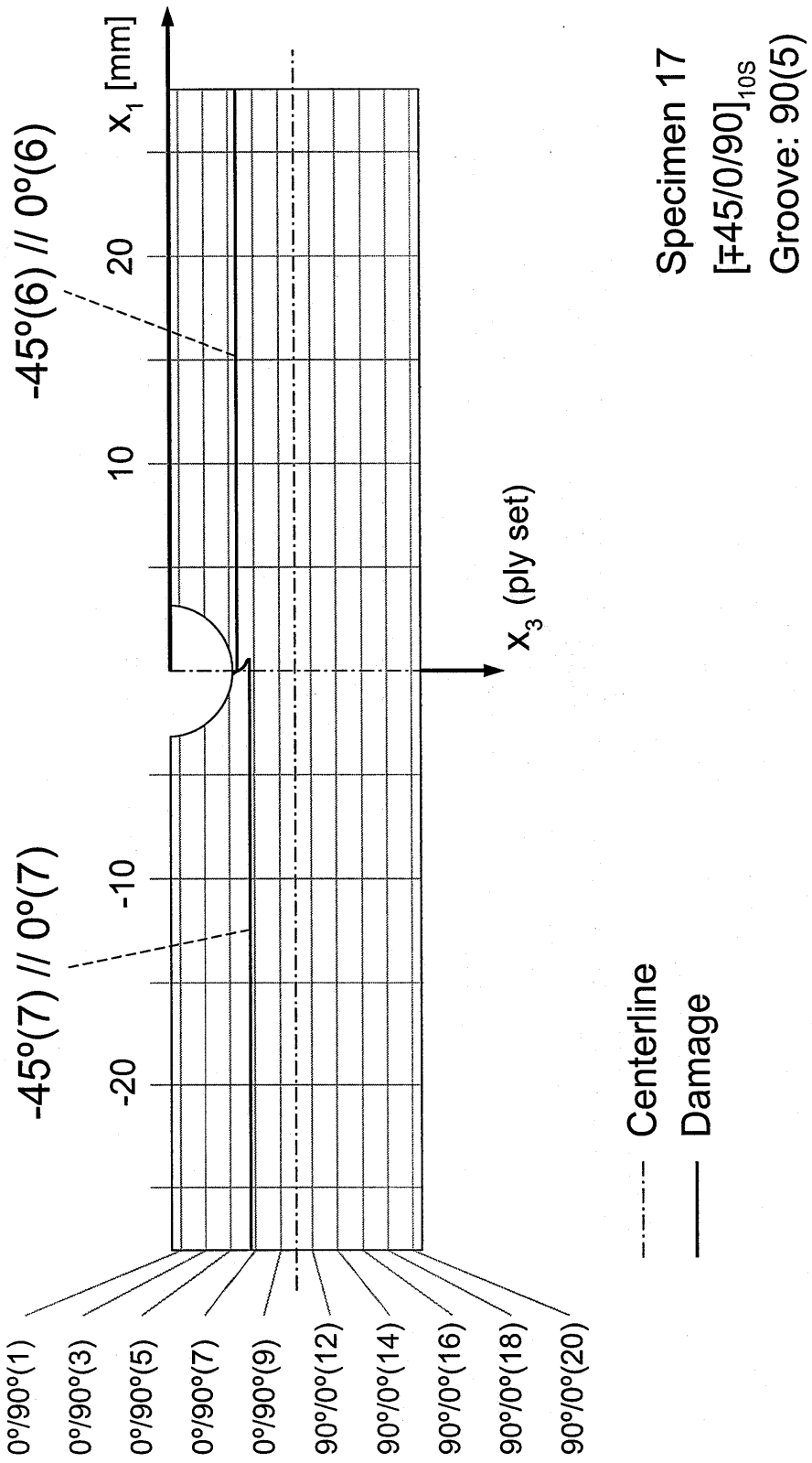

Figure B.11 Illustration of failure for Specimen 17: layup $[\mp 45/0/90]_{10S}$ with groove at 90° ply in 5th set.

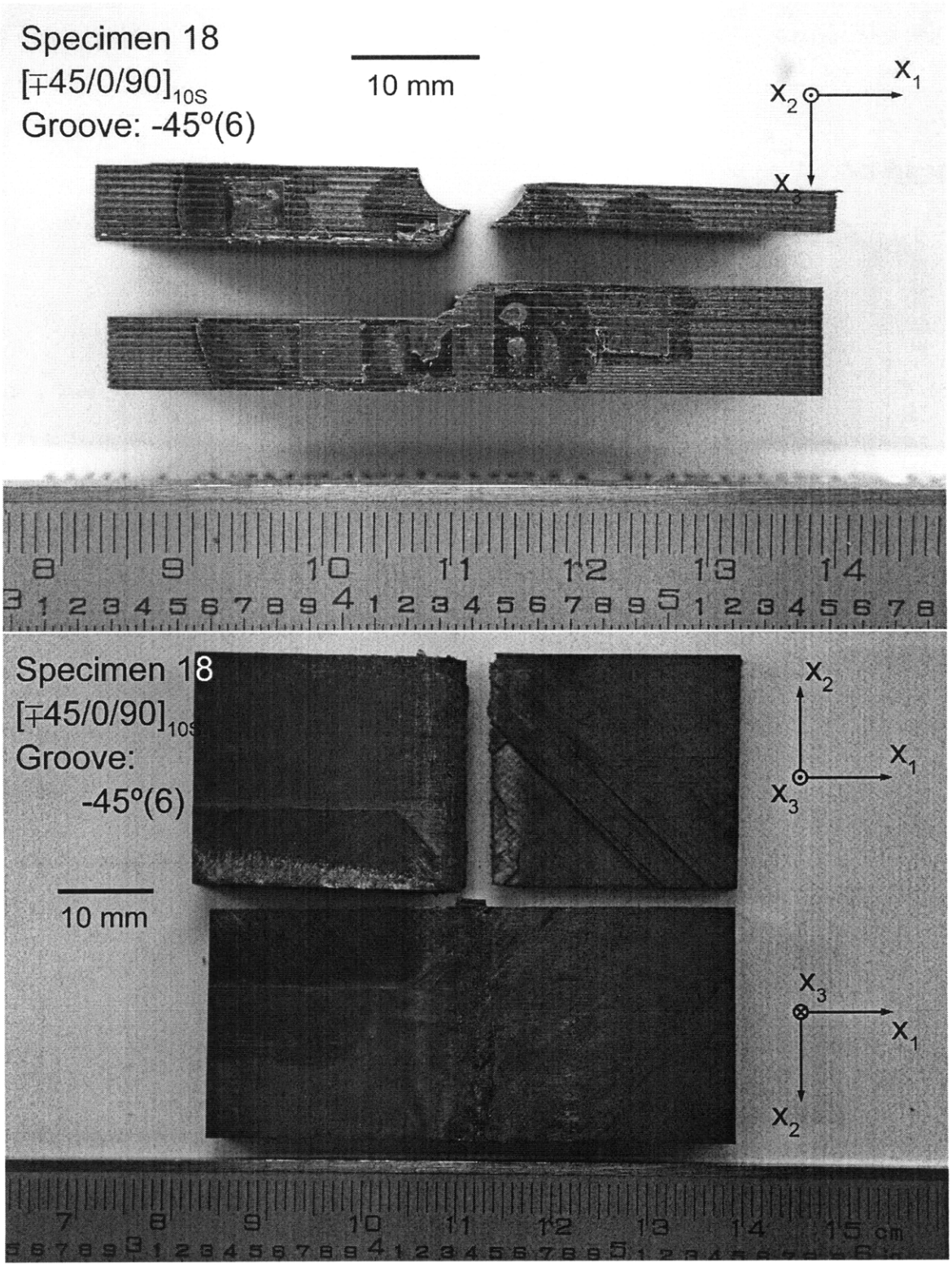

Figure B.12 Photographs after failure of Specimen 18 (layup $[\mp 45/0/90]_{10S}$ with groove at $-45°$ ply in 6th set) with *(upper)* side view, and *(lower)* failure surface view.

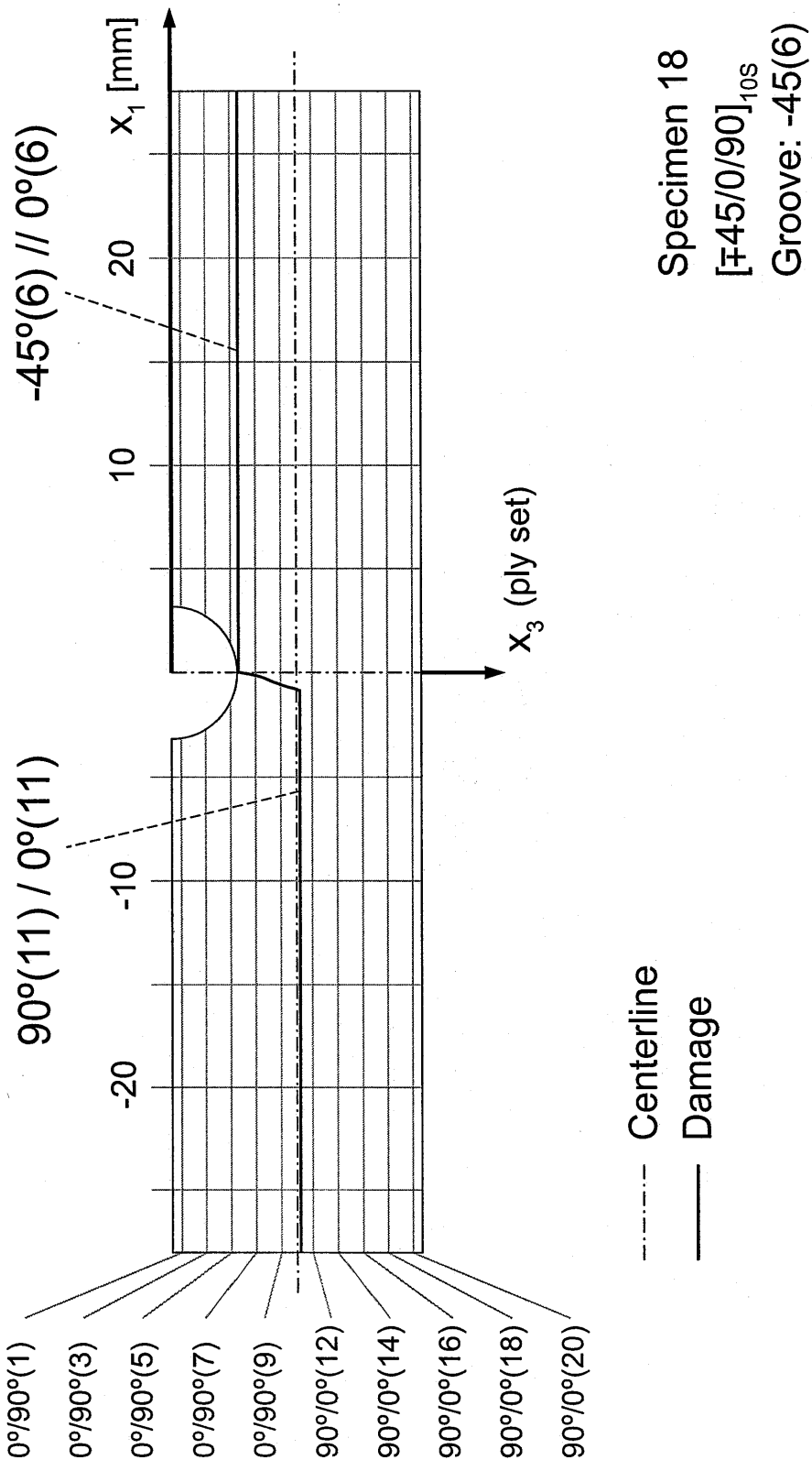

Figure B.13 Illustration of failure for Specimen 18: layup $[\mp 45/0/90]_{10S}$ with groove at $-45°$ ply in 6th set.

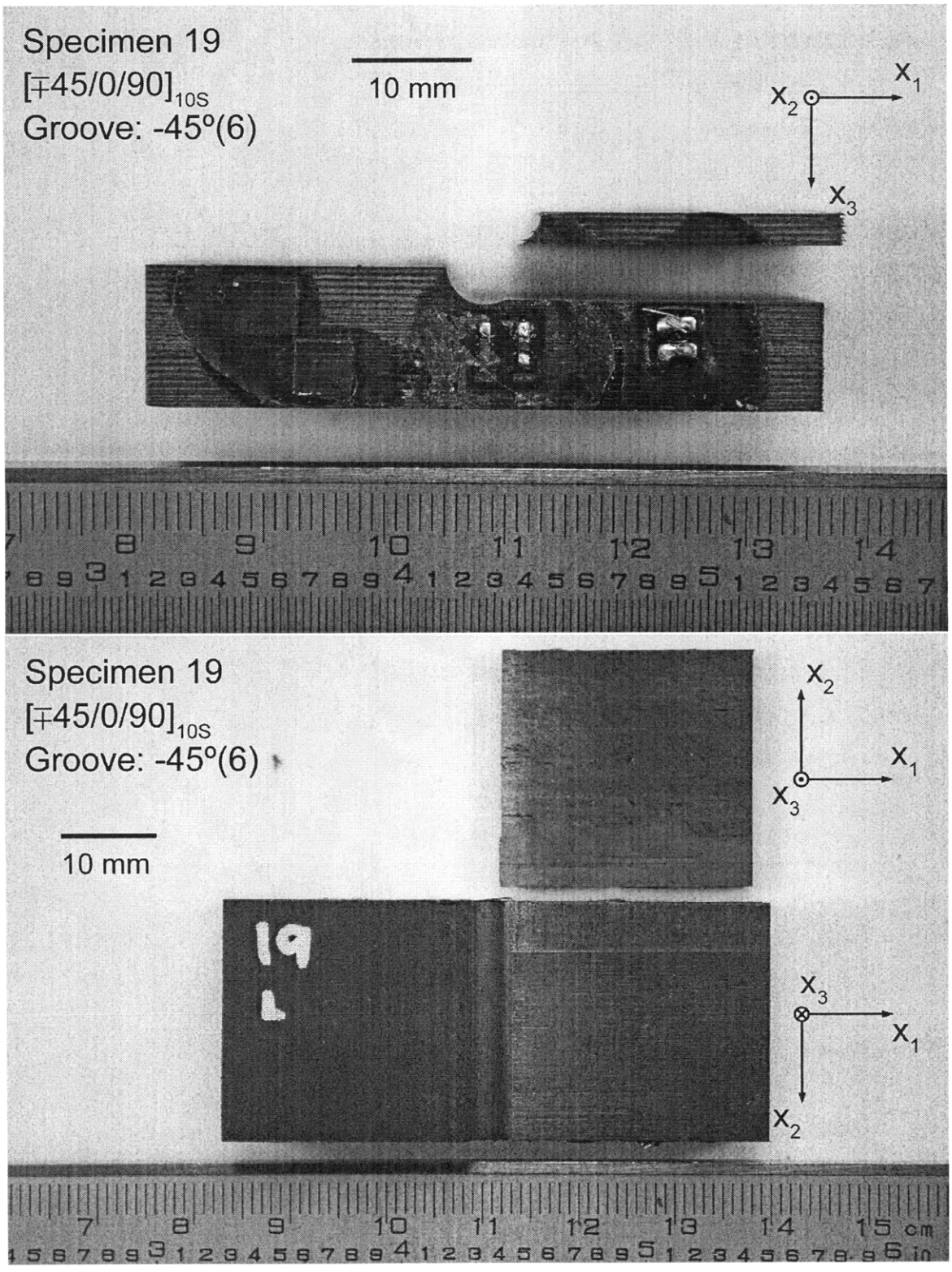

Figure B.14 Photographs after failure of Specimen 19 (layup $[\mp 45/0/90]_{10S}$ with groove at $-45°$ ply in 6th set) with *(upper)* side view, and *(lower)* failure surface view.

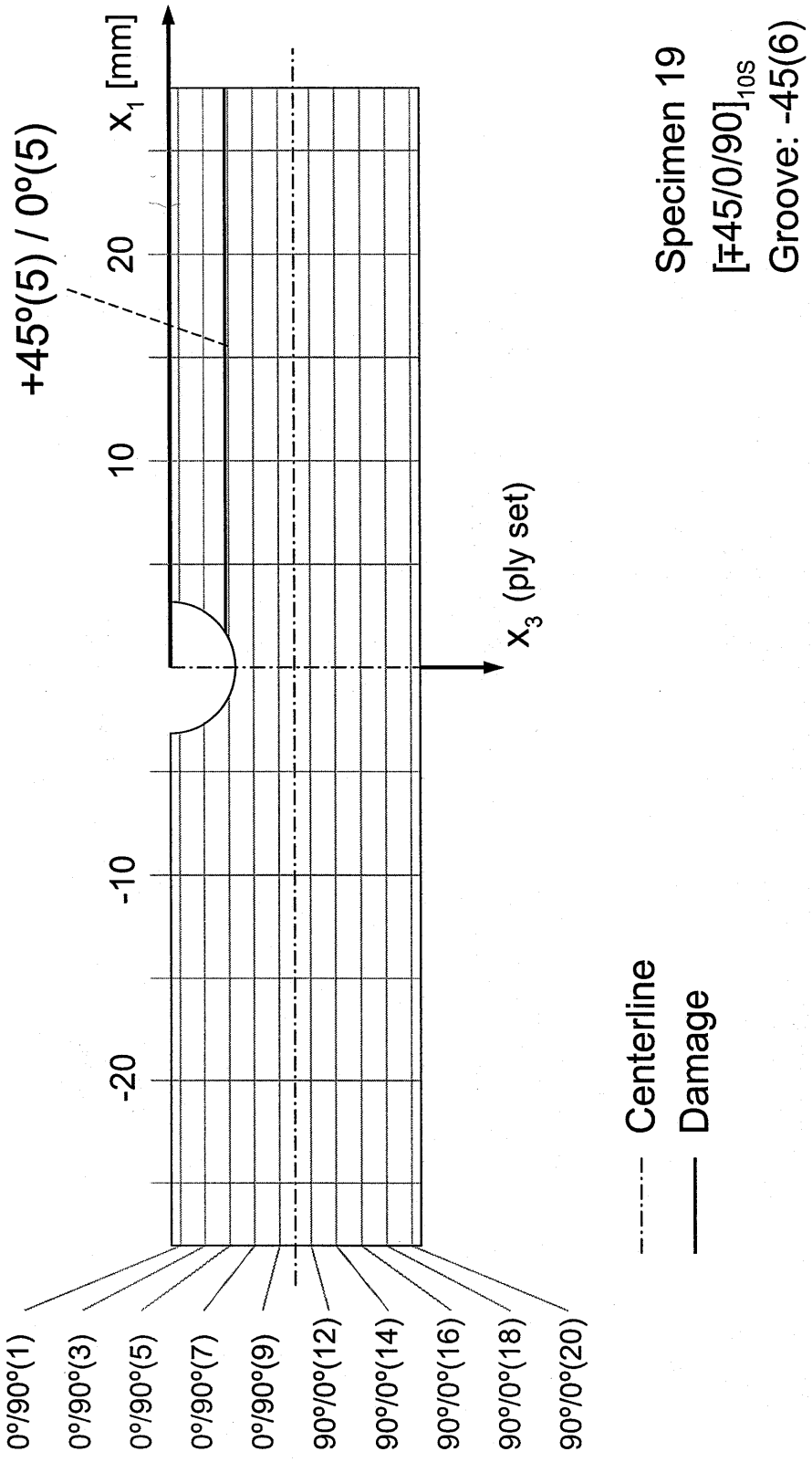

Figure B.15 Illustration of failure for Specimen 19: layup $[\mp 45/0/90]_{10S}$ with groove at $-45°$ ply in 6th set.

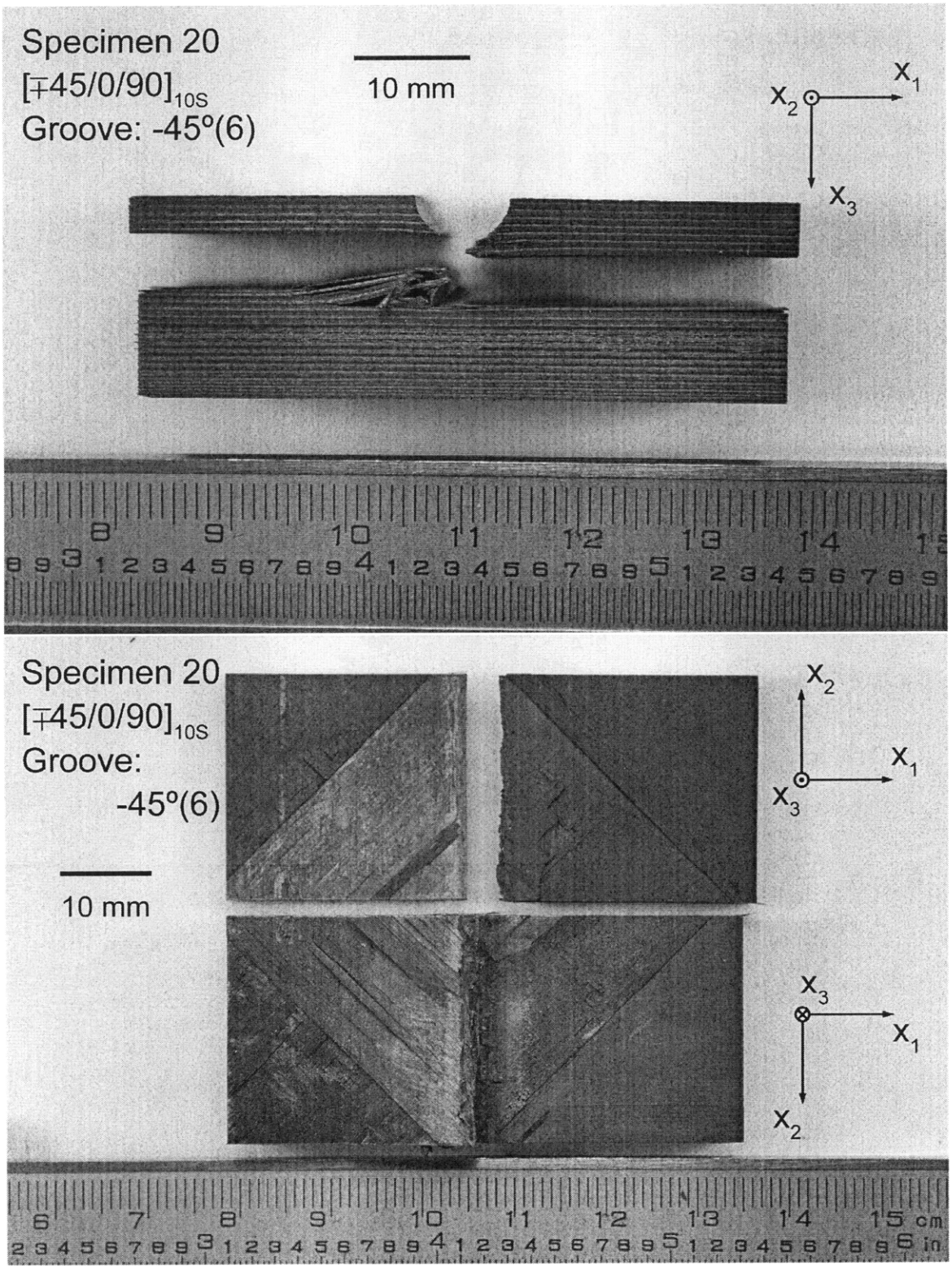

Figure B.16 Photographs after failure of Specimen 20 (layup $[\mp 45/0/90]_{10S}$ with groove at $-45°$ ply in 6th set) with *(upper)* side view, and *(lower)* failure surface view.

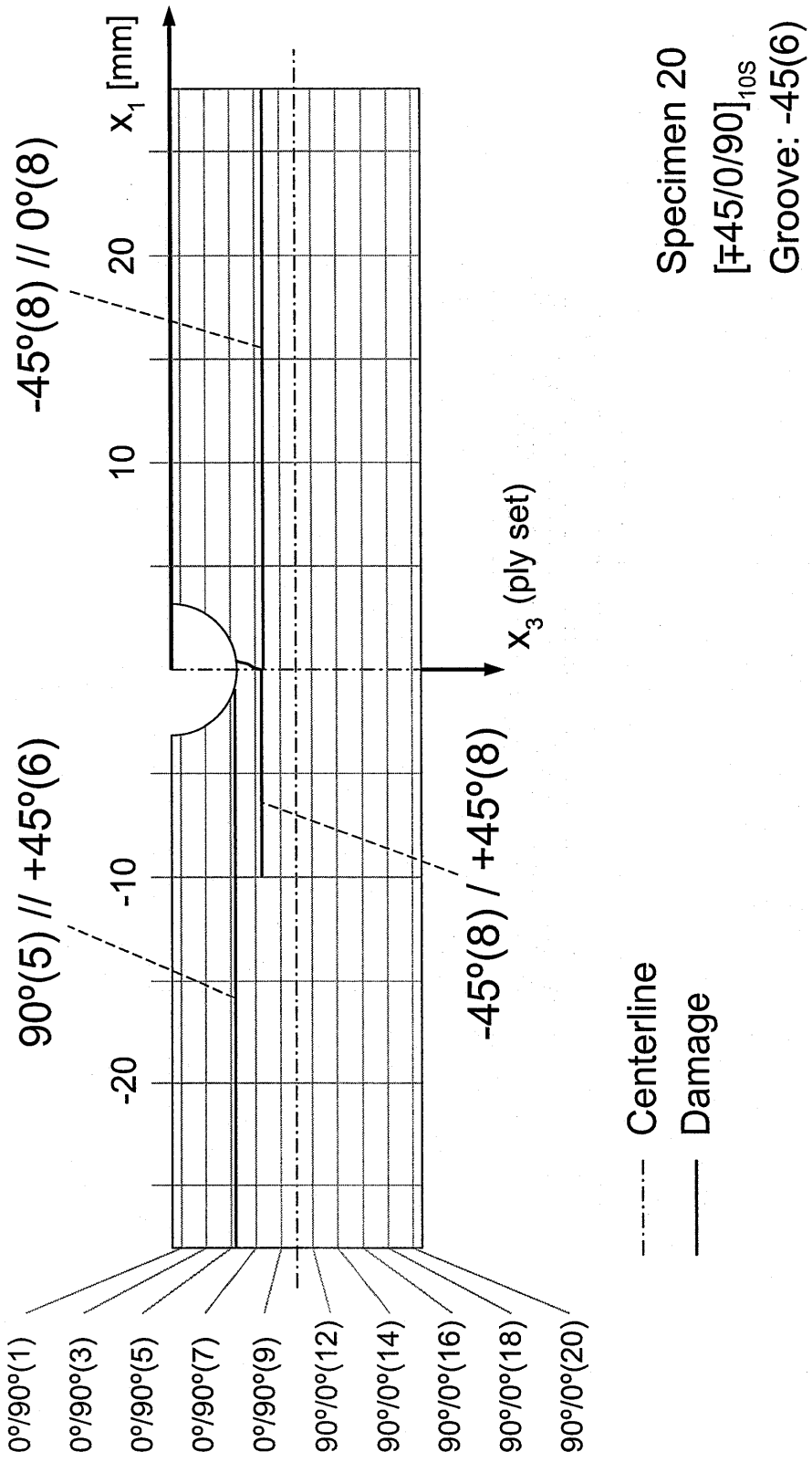

Figure B.17 Illustration of failure for Specimen 20: layup $[\mp 45/0/90]_{10S}$ with groove at $-45°$ ply in 6th set.

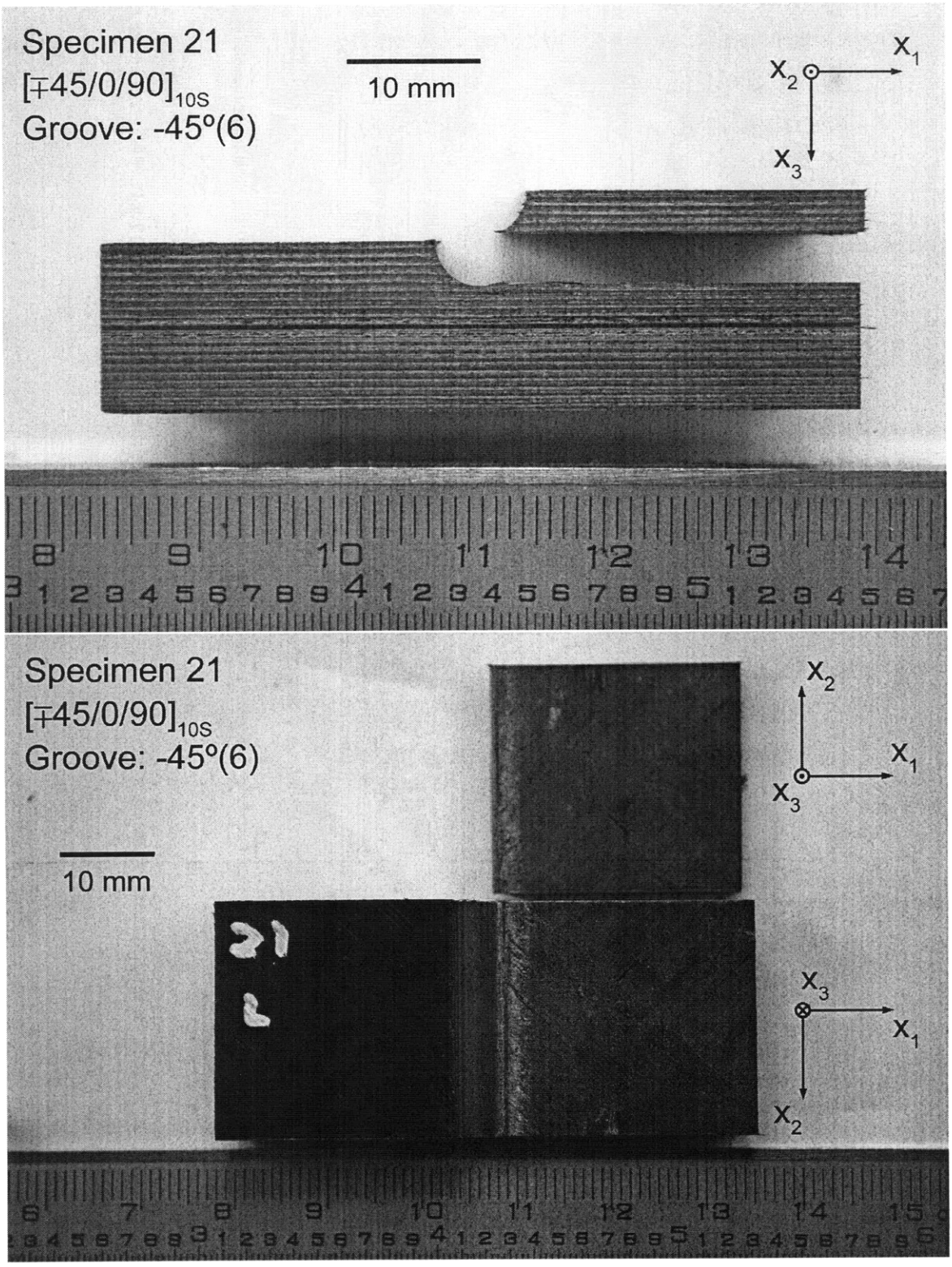

Figure B.18 Photographs after failure of Specimen 21 (layup $[\mp 45/0/90]_{10S}$ with groove at $-45°$ ply in 6th set) with *(upper)* side view, and *(lower)* failure surface view.

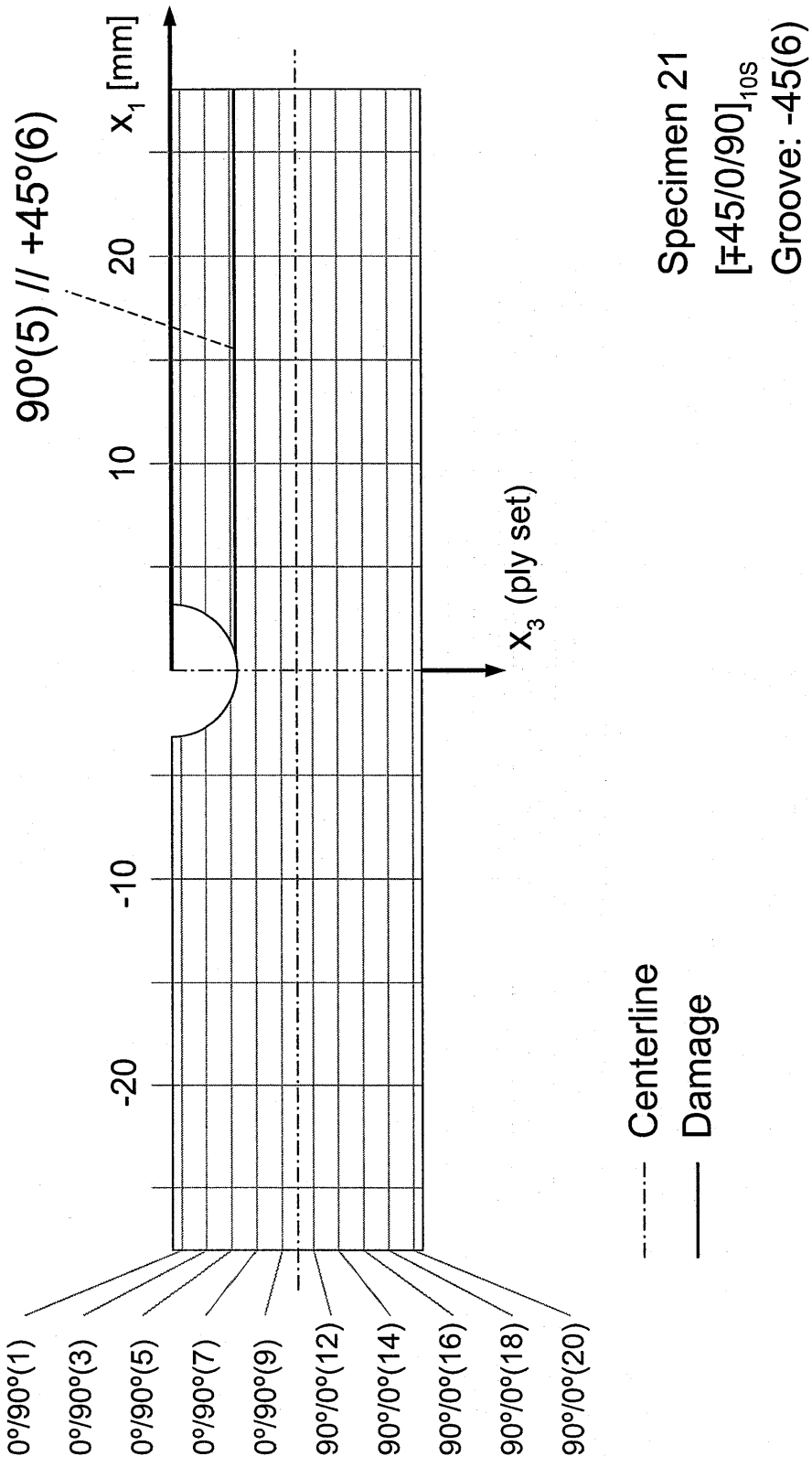

Figure B.19 Illustration of failure for Specimen 21: layup $[\mp 45/0/90]_{10S}$ with groove at $-45°$ ply in 6th set.

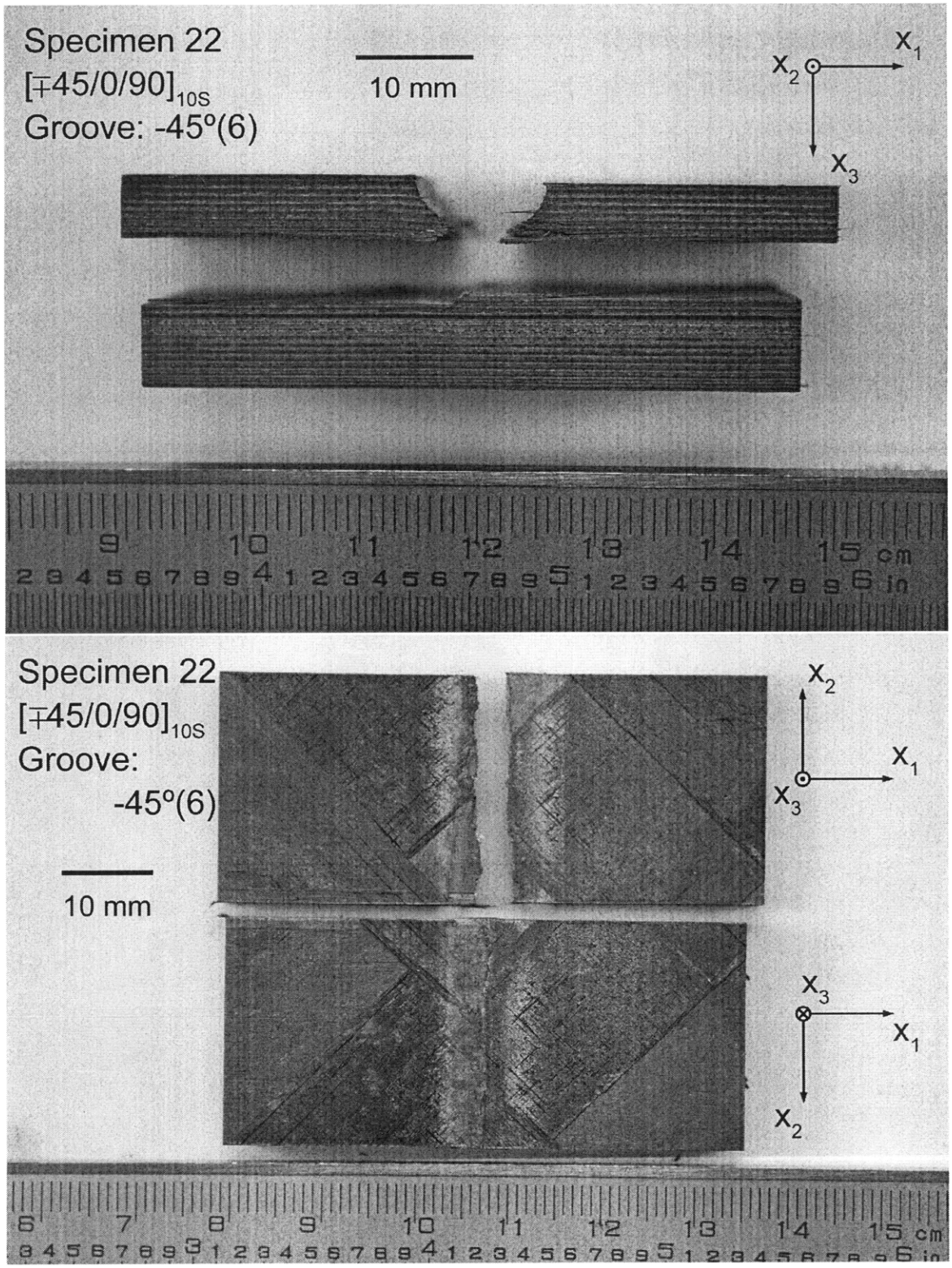

Figure B.20 Photographs after failure of Specimen 22 (layup $[\mp 45/0/90]_{10S}$ with groove at $-45°$ ply in 6th set) with *(upper)* side view, and *(lower)* failure surface view.

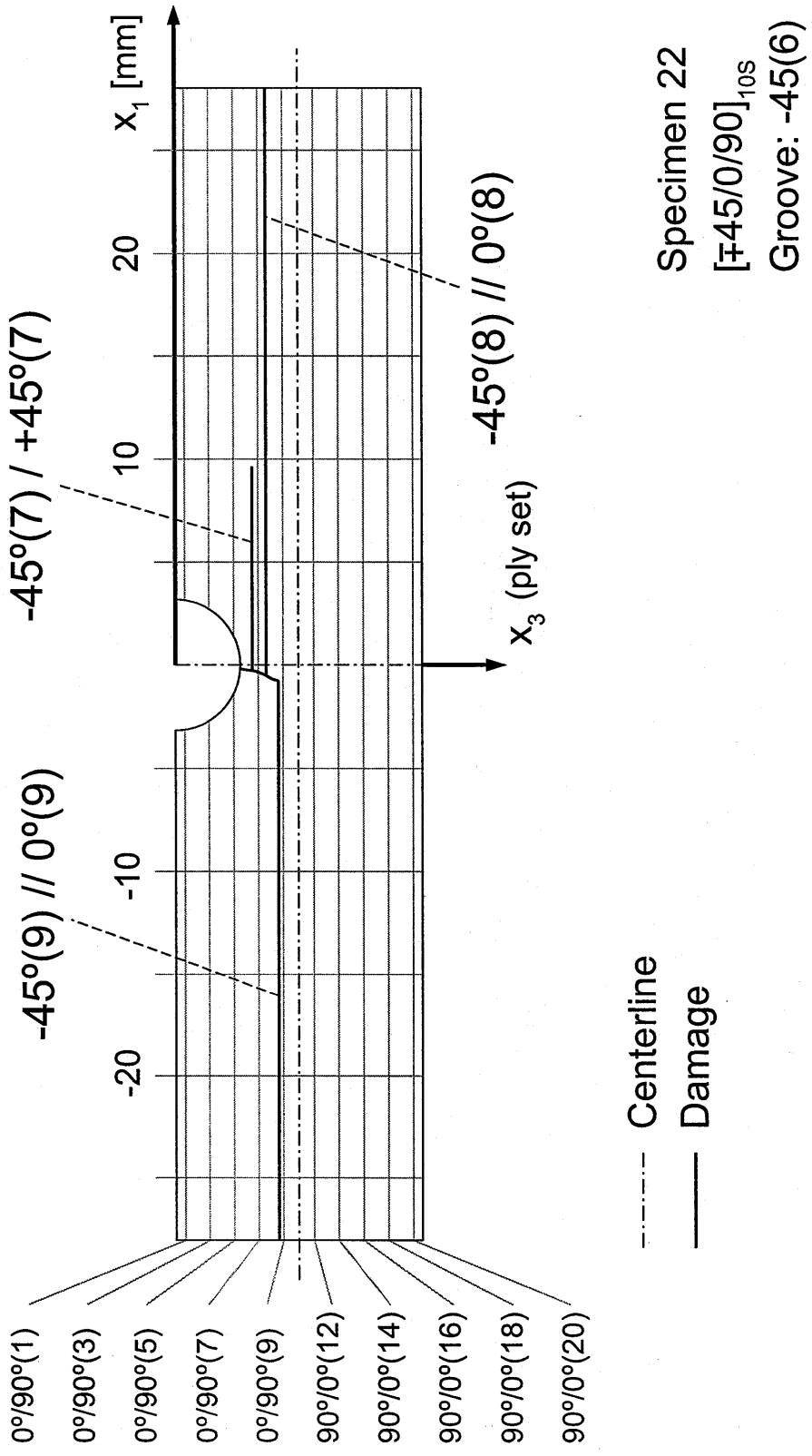

Figure B.21 Illustration of failure for Specimen 22: layup $[\mp 45/0/90]_{10S}$ with groove at $-45°$ ply in 6th set.

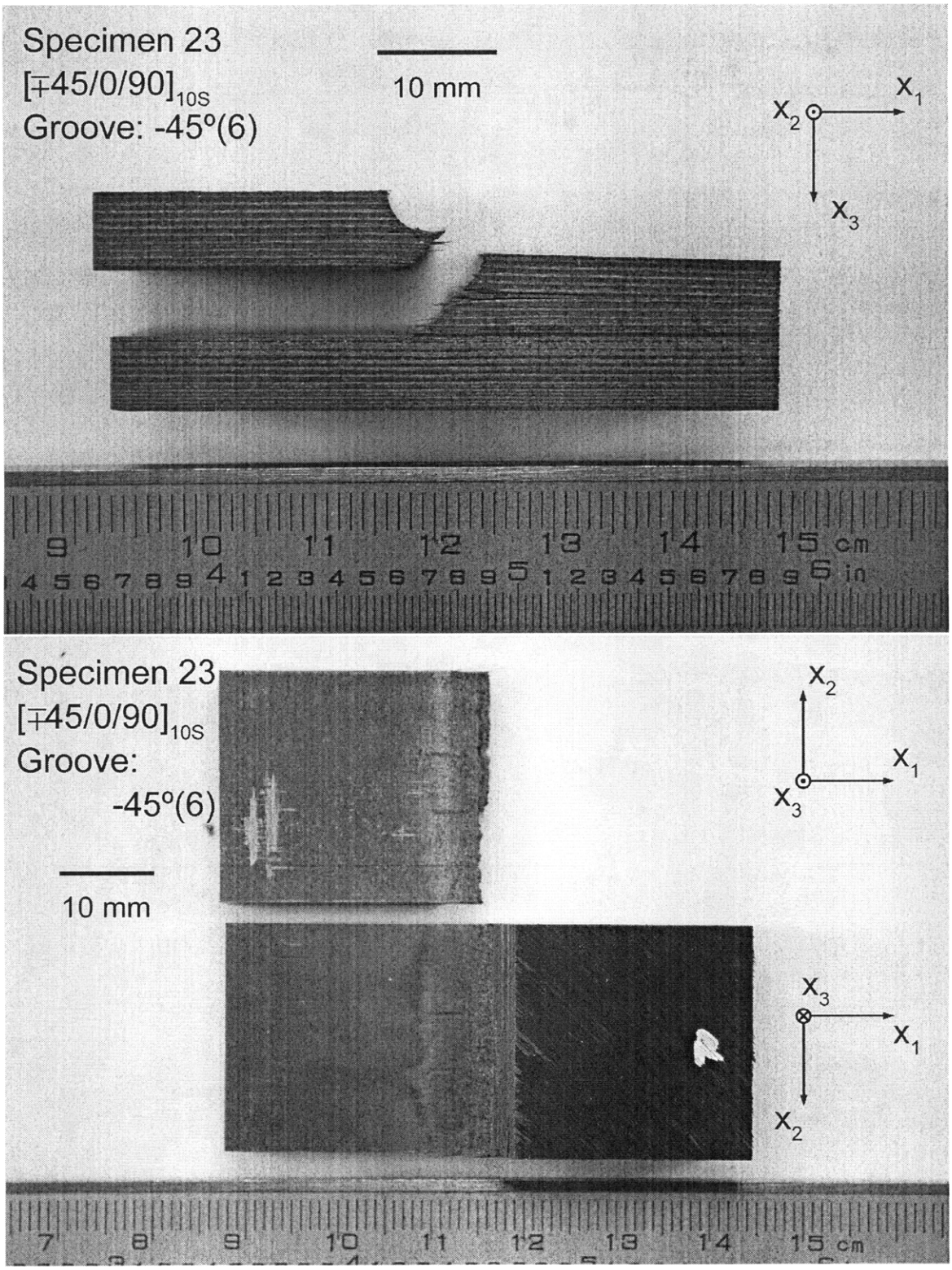

Figure B.22 Photographs after failure of Specimen 23 (layup $[\mp 45/0/90]_{10S}$ with groove at $-45°$ ply in 6th set) with *(upper)* side view, and *(lower)* failure surface view.

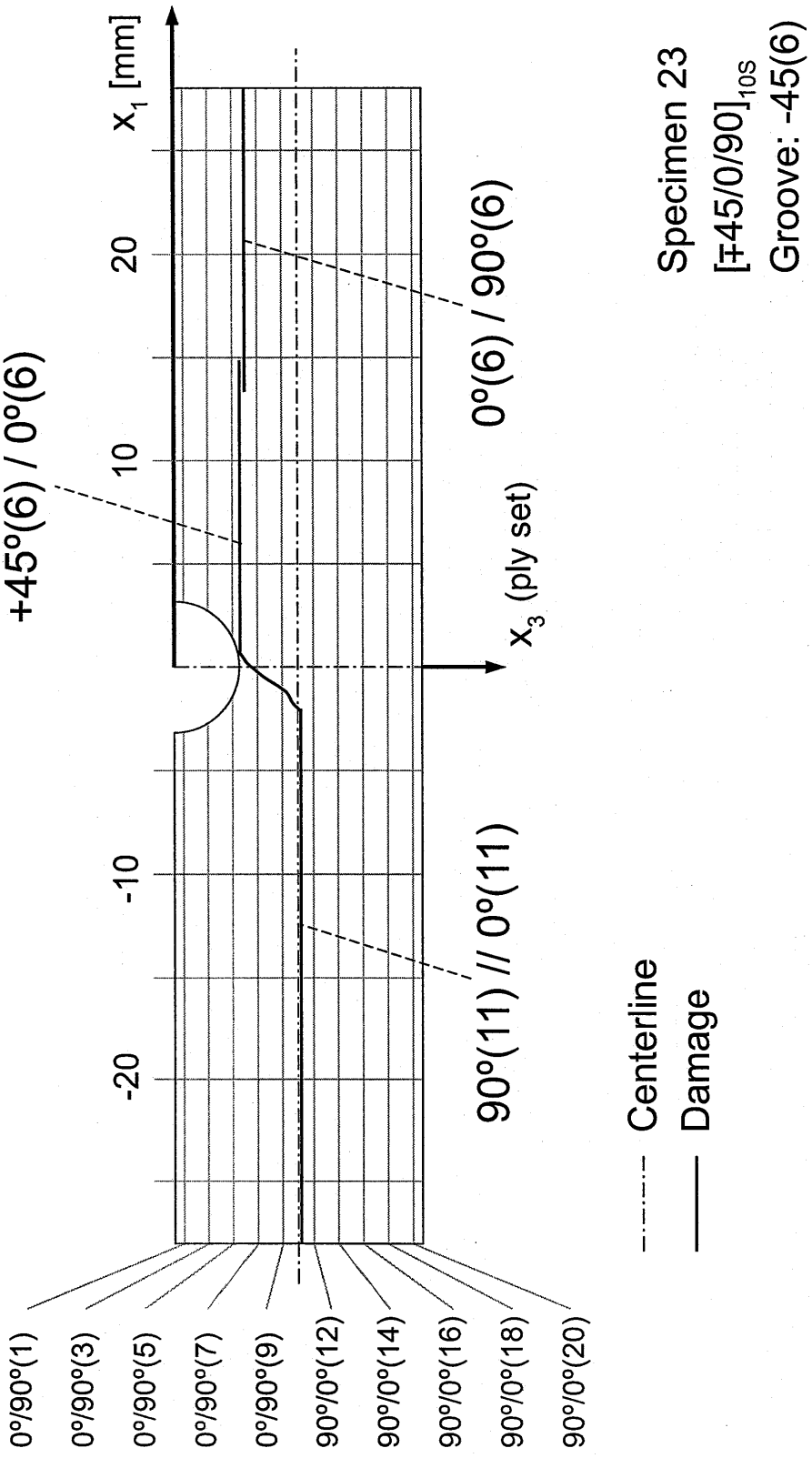

Figure B.23 Illustration of failure for Specimen 23: layup $[\mp 45/0/90]_{10S}$ with groove at $-45°$ ply in 6th set.

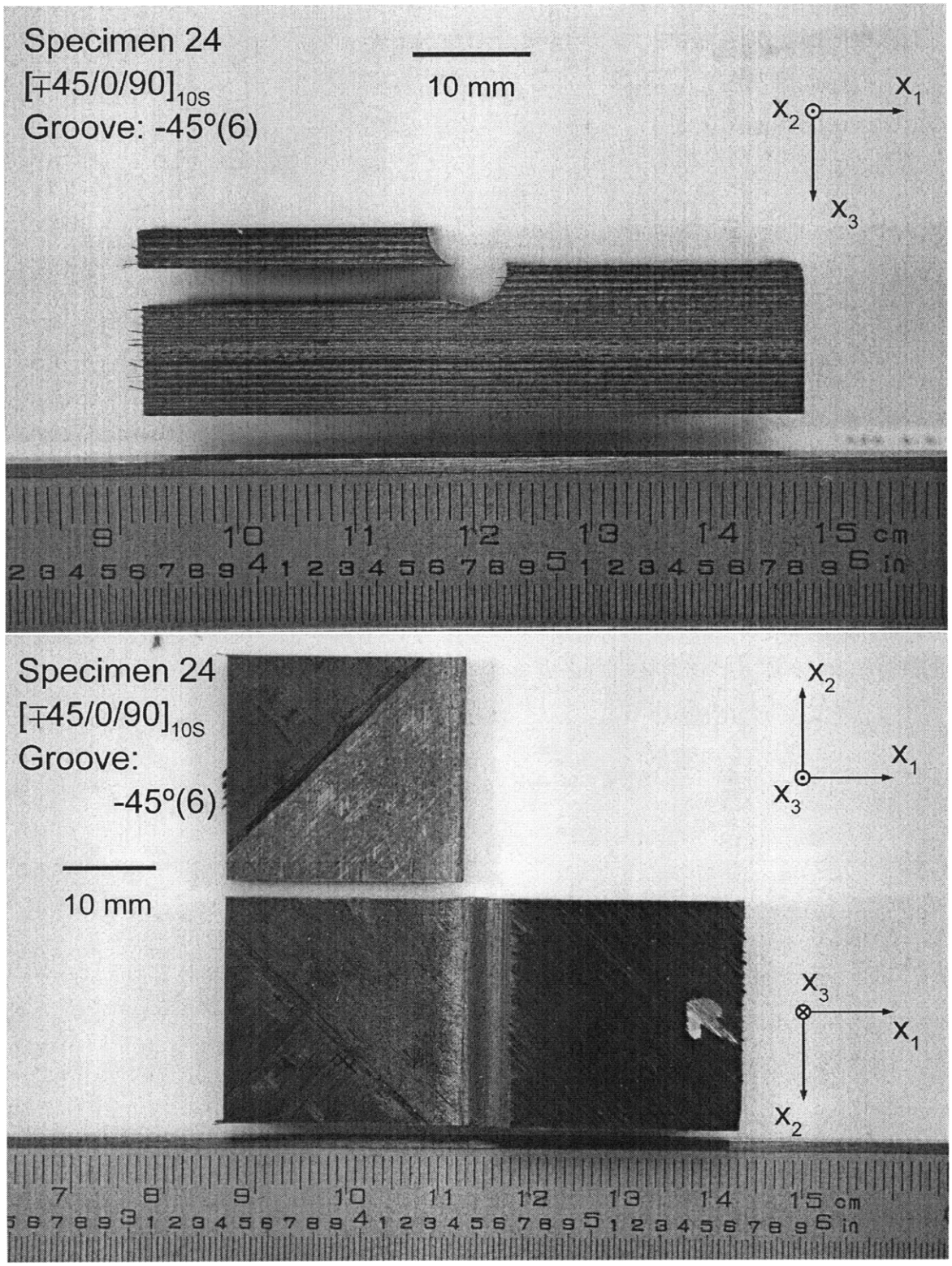

Figure B.24 Photographs after failure of Specimen 24 (layup $[\mp 45/0/90]_{10S}$ with groove at $-45°$ ply in 6th set) with *(upper)* side view, and *(lower)* failure surface view.

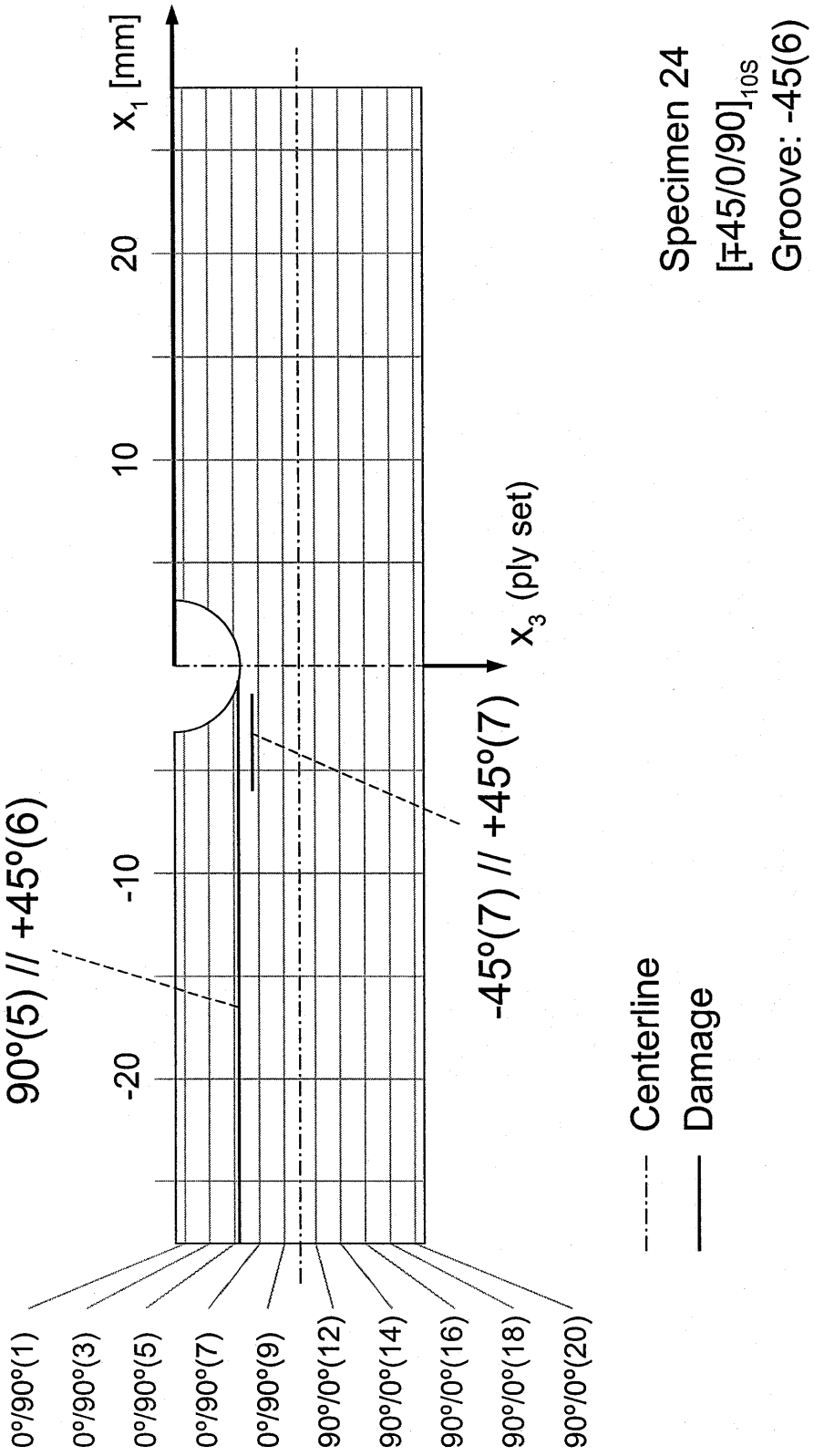

Figure B.25 Illustration of failure for Specimen 24: layup $[\mp 45/0/90]_{10S}$ with groove at $-45°$ ply in 6th set.

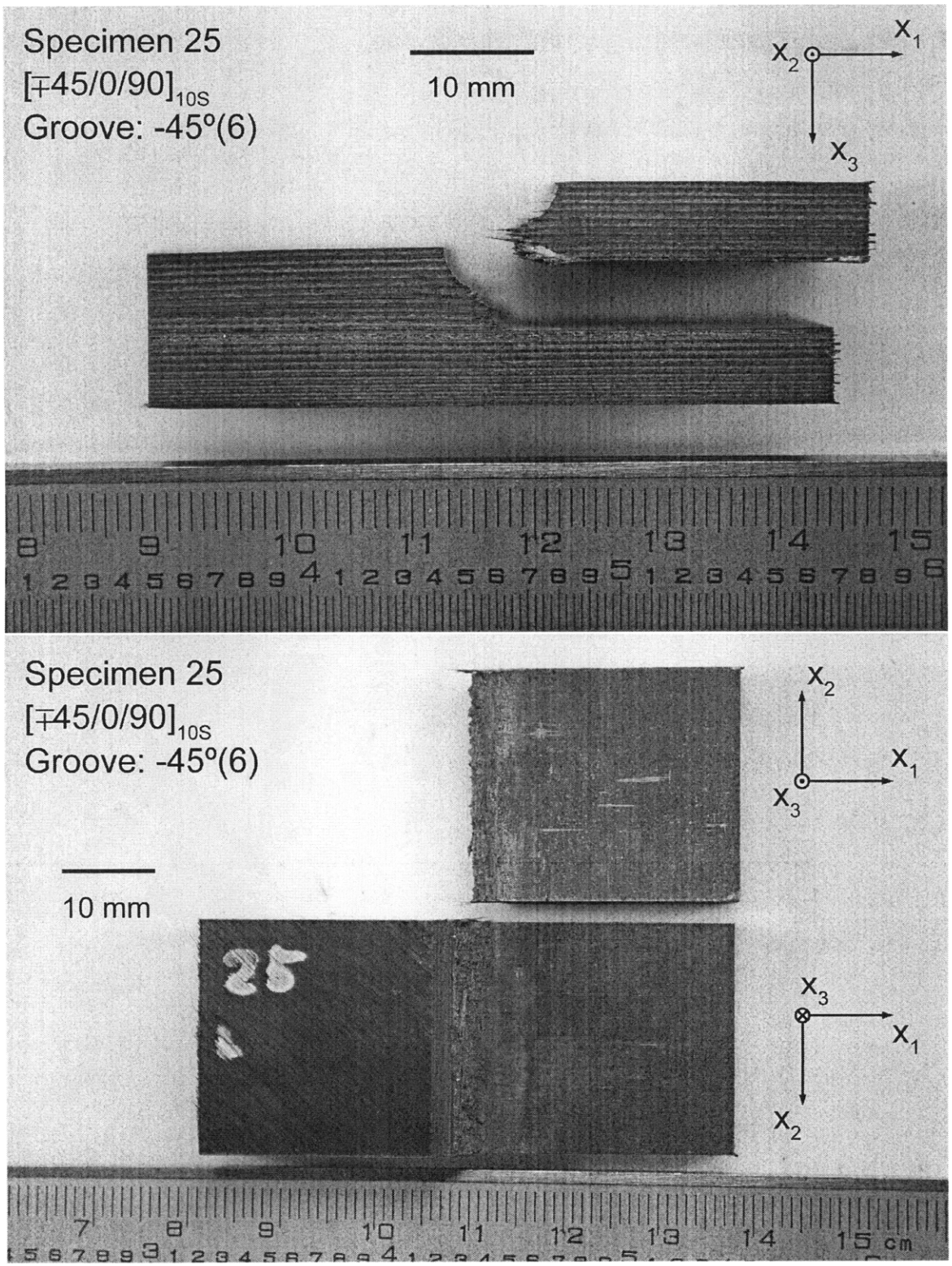

Figure B.26 Photographs after failure of Specimen 25 (layup $[\mp 45/0/90]_{10S}$ with groove at $-45°$ ply in 6th set) with *(upper)* side view, and *(lower)* failure surface view.

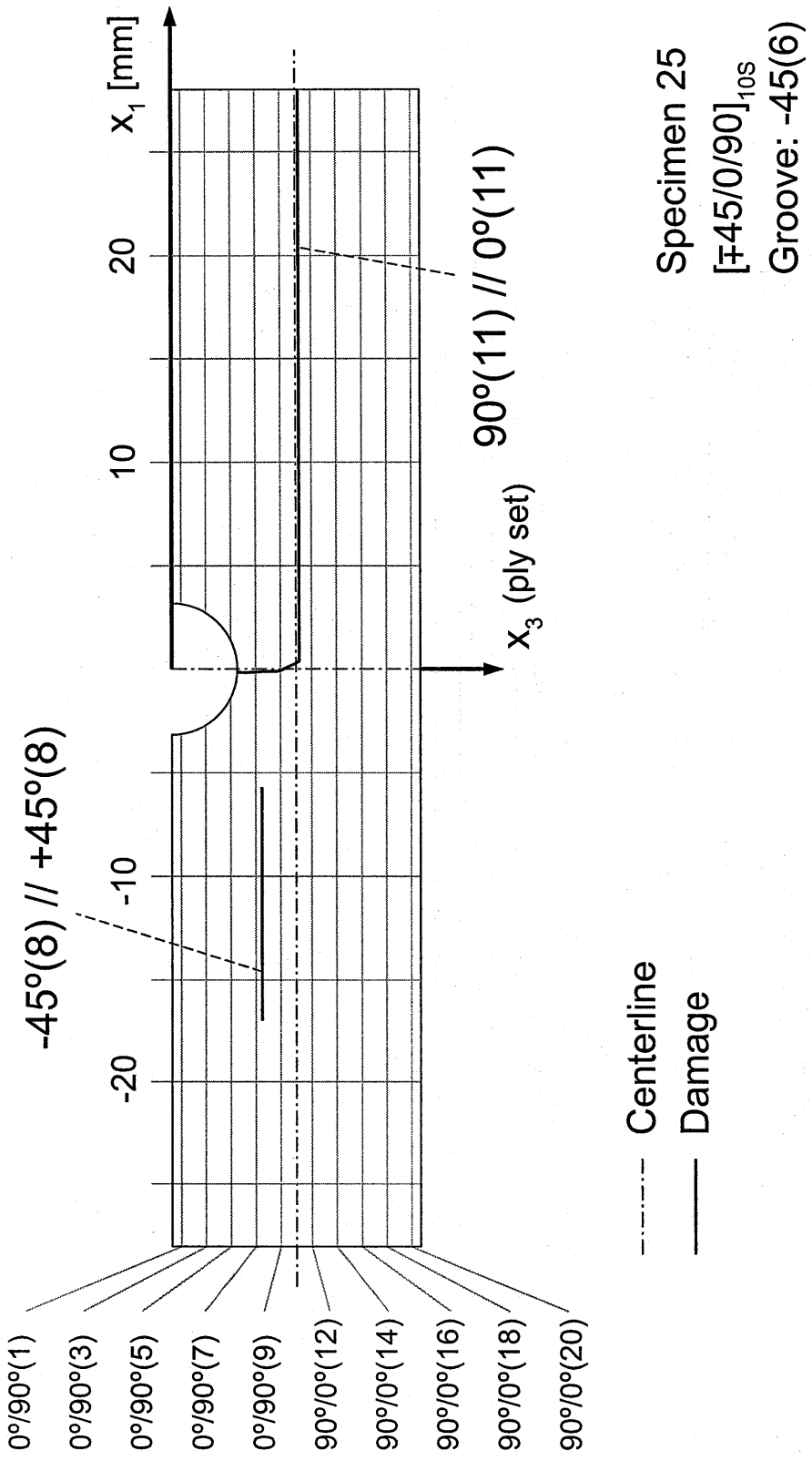

Figure B.27 Illustration of failure for Specimen 25: layup $[\mp 45/0/90]_{10S}$ with groove at $-45°$ ply in 6th set.

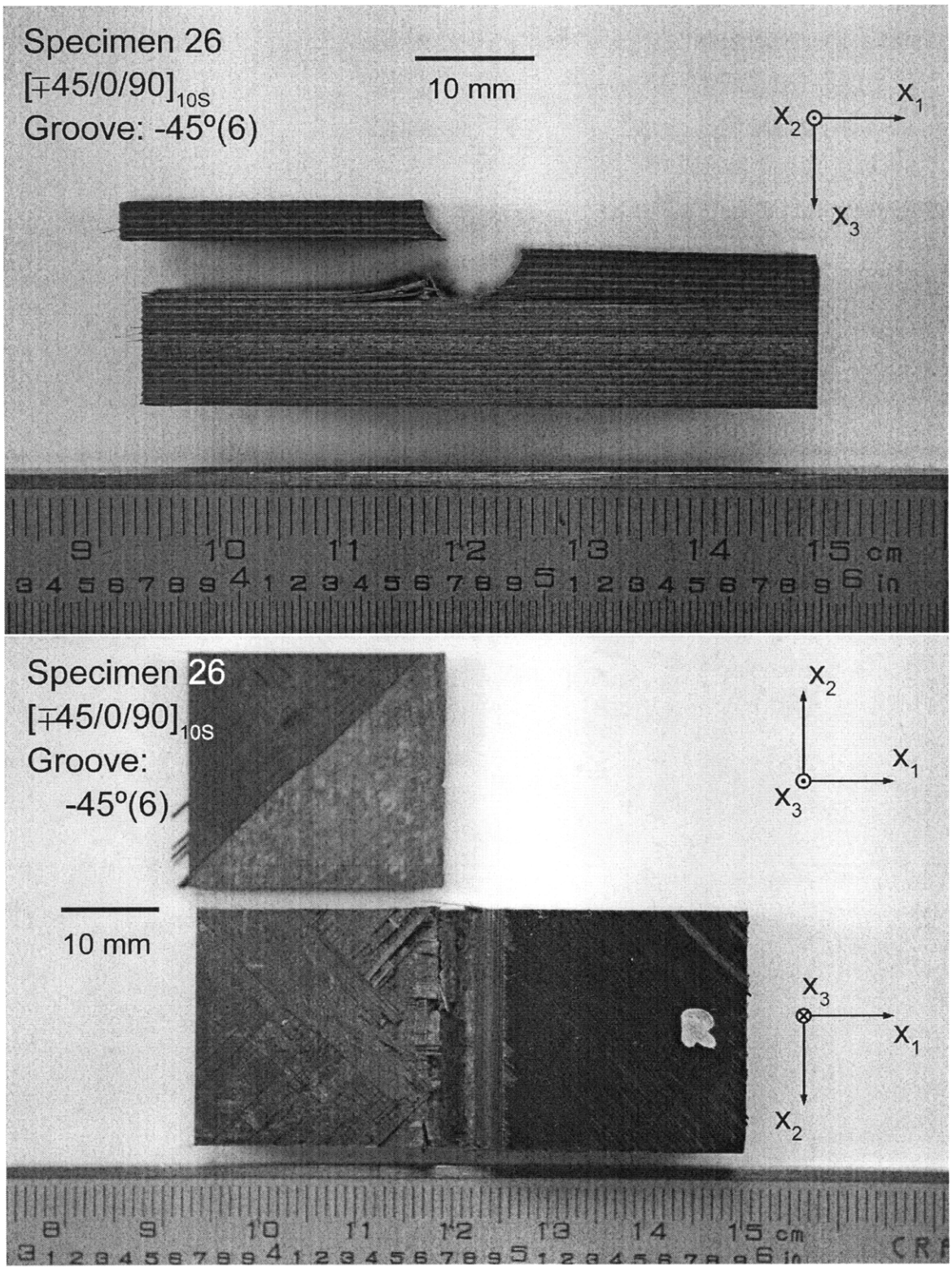

Figure B.28 Photographs after failure of Specimen 26 (layup $[\mp 45/0/90]_{10S}$ with groove at $-45°$ ply in 6th set) with *(upper)* side view, and *(lower)* failure surface view.

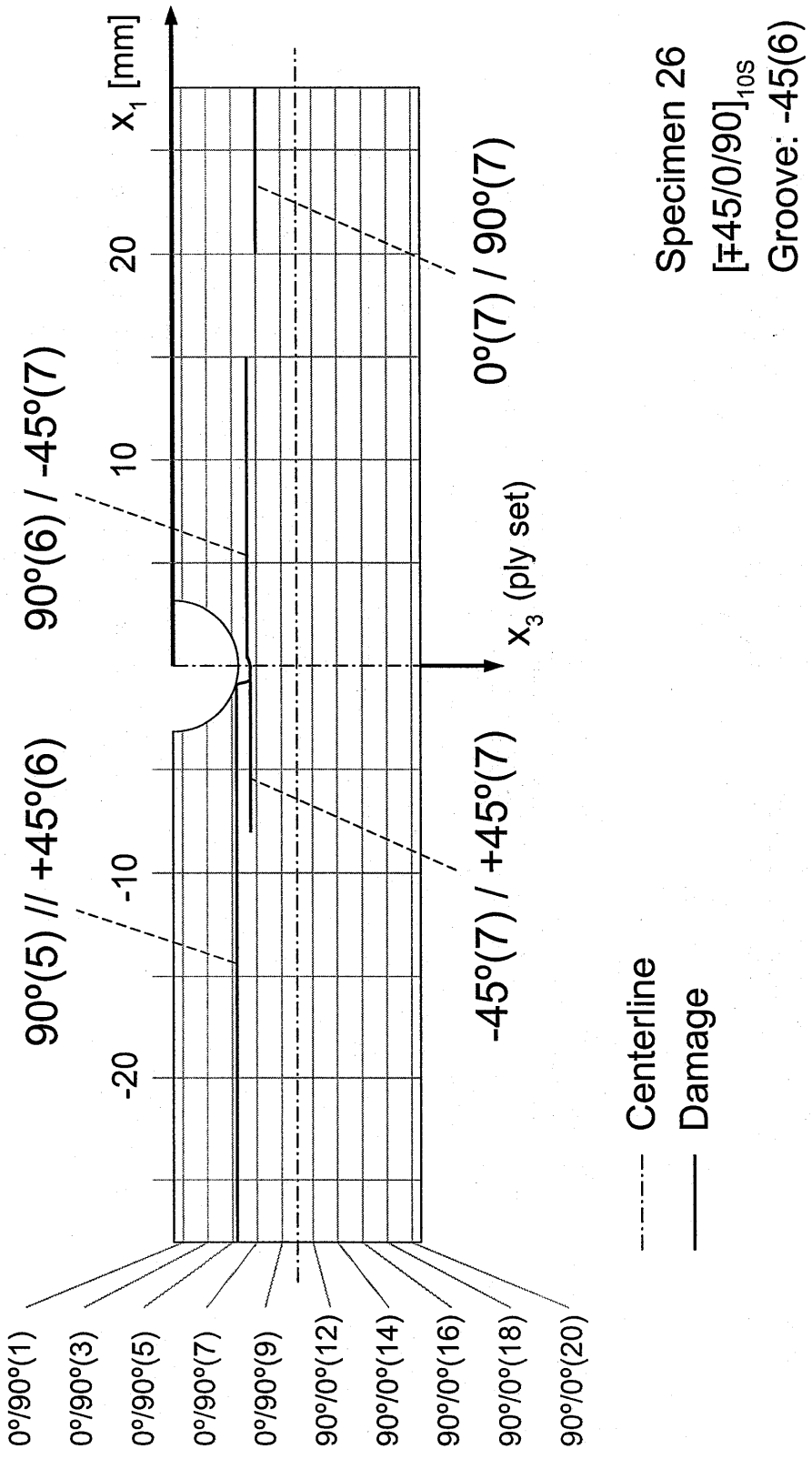

Figure B.29 Illustration of failure for Specimen 26: layup $[\mp 45/0/90]_{10S}$ with groove at $-45°$ ply in 6th set.

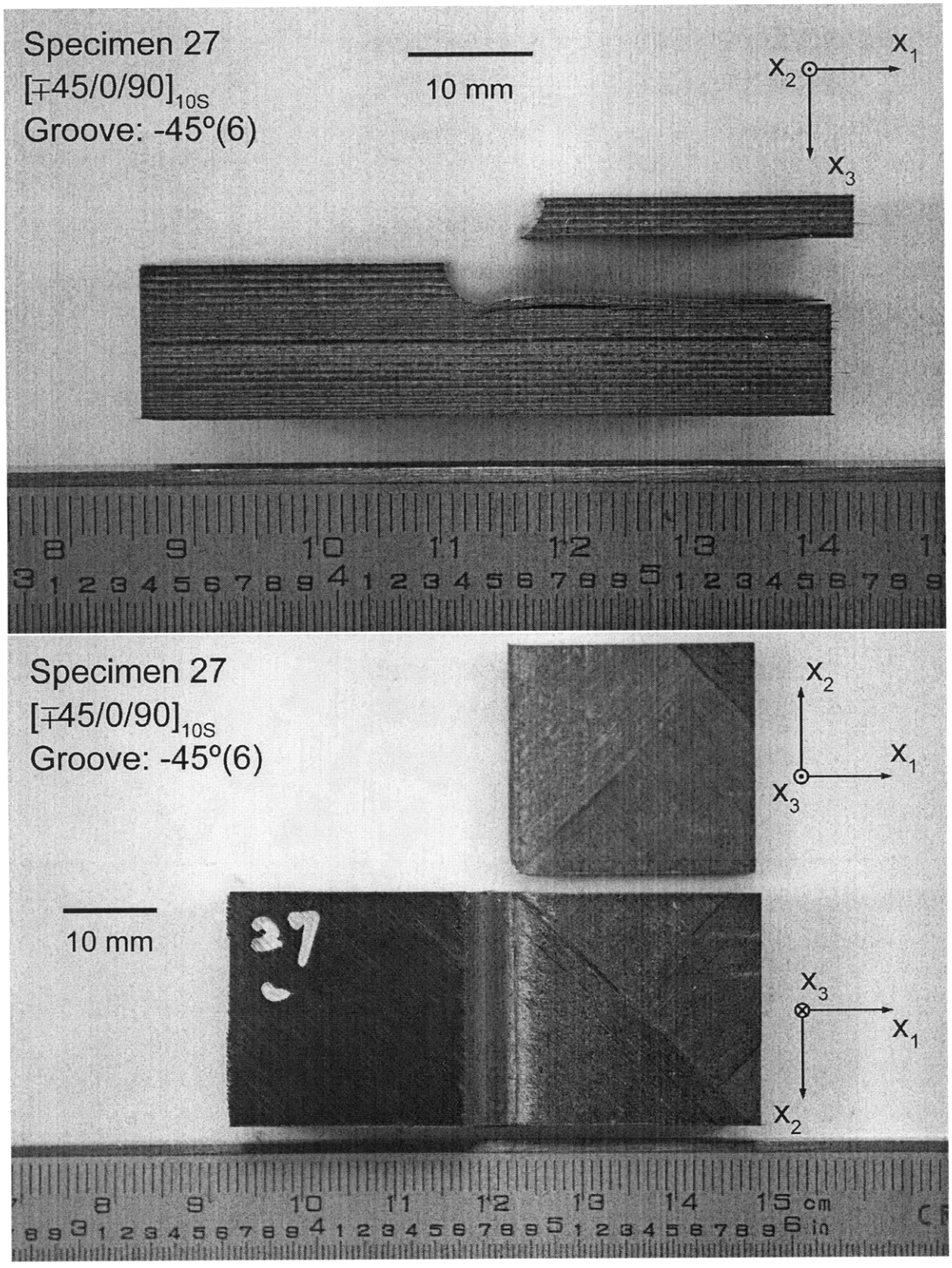

Figure B.30 Photographs after failure of Specimen 27 (layup $[\mp 45/0/90]_{10S}$ with groove at $-45°$ ply in 6th set) with *(upper)* side view, and *(lower)* failure surface view.

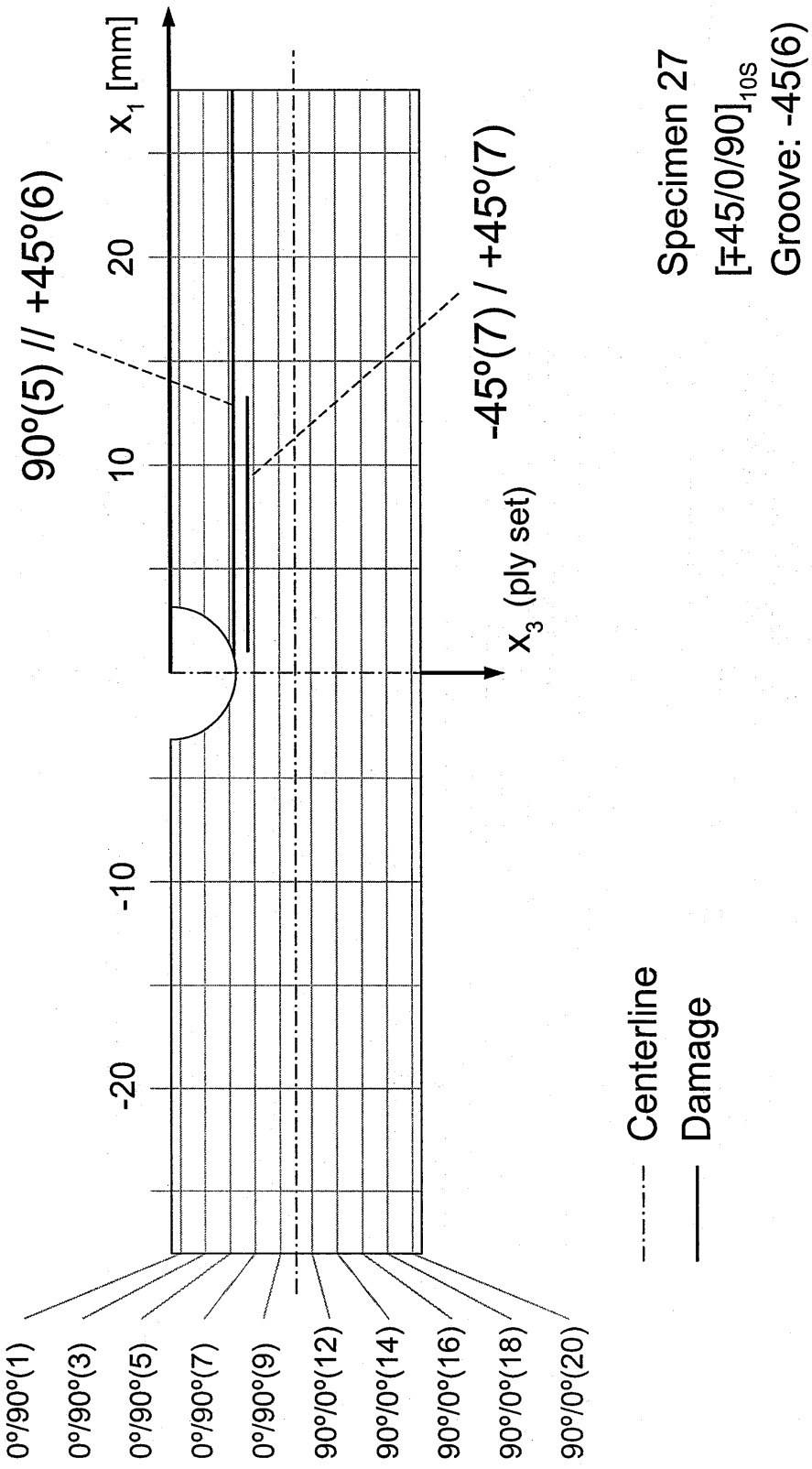

Figure B.31 Illustration of failure for Specimen 27: layup $[\mp 45/0/90]_{10S}$ with groove at $-45°$ ply in 6th set.

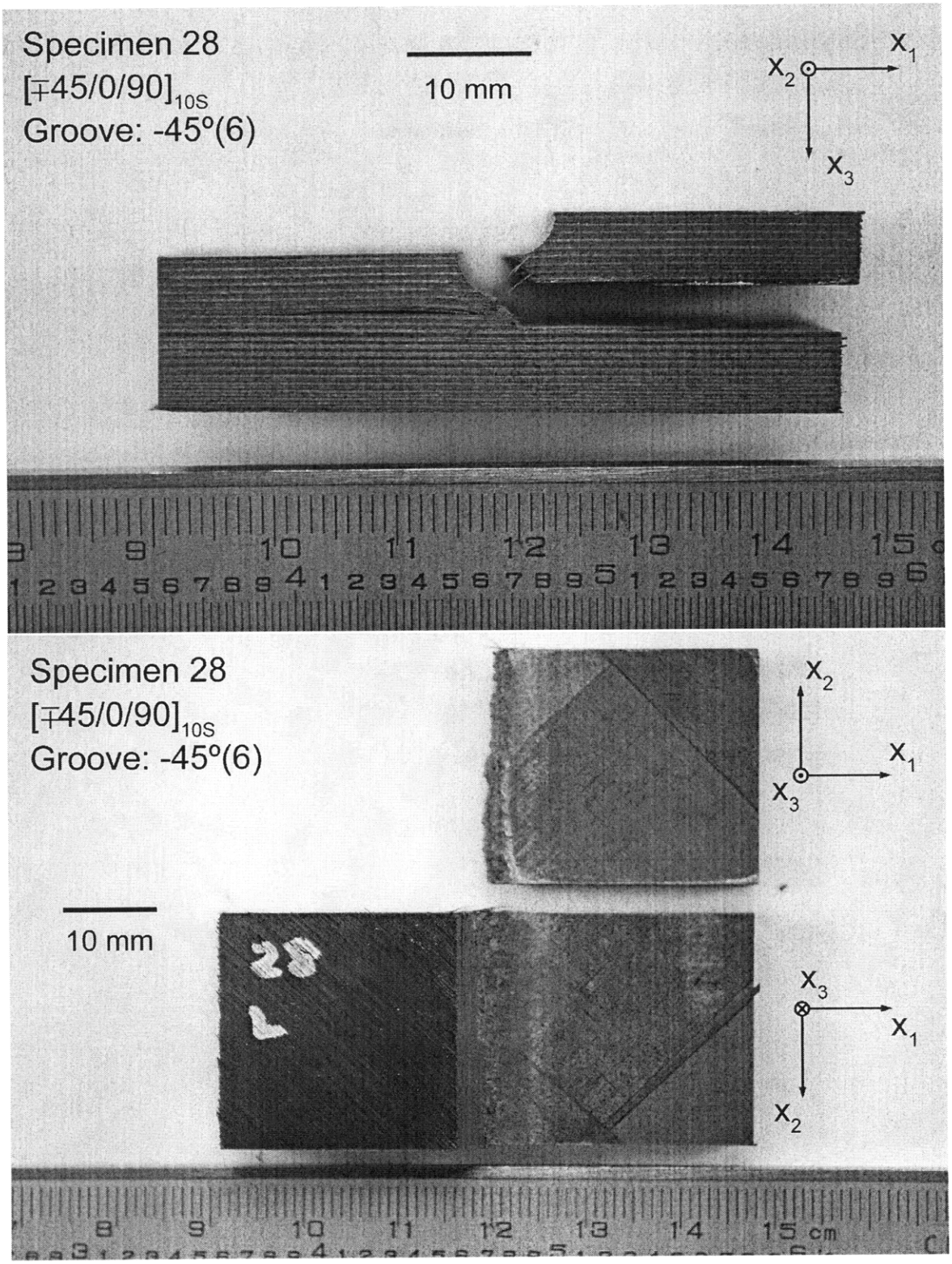

Figure B.32 Photographs after failure of Specimen 28 (layup $[\mp 45/0/90]_{10S}$ with groove at $-45°$ ply in 6th set) with *(upper)* side view, and *(lower)* failure surface view.

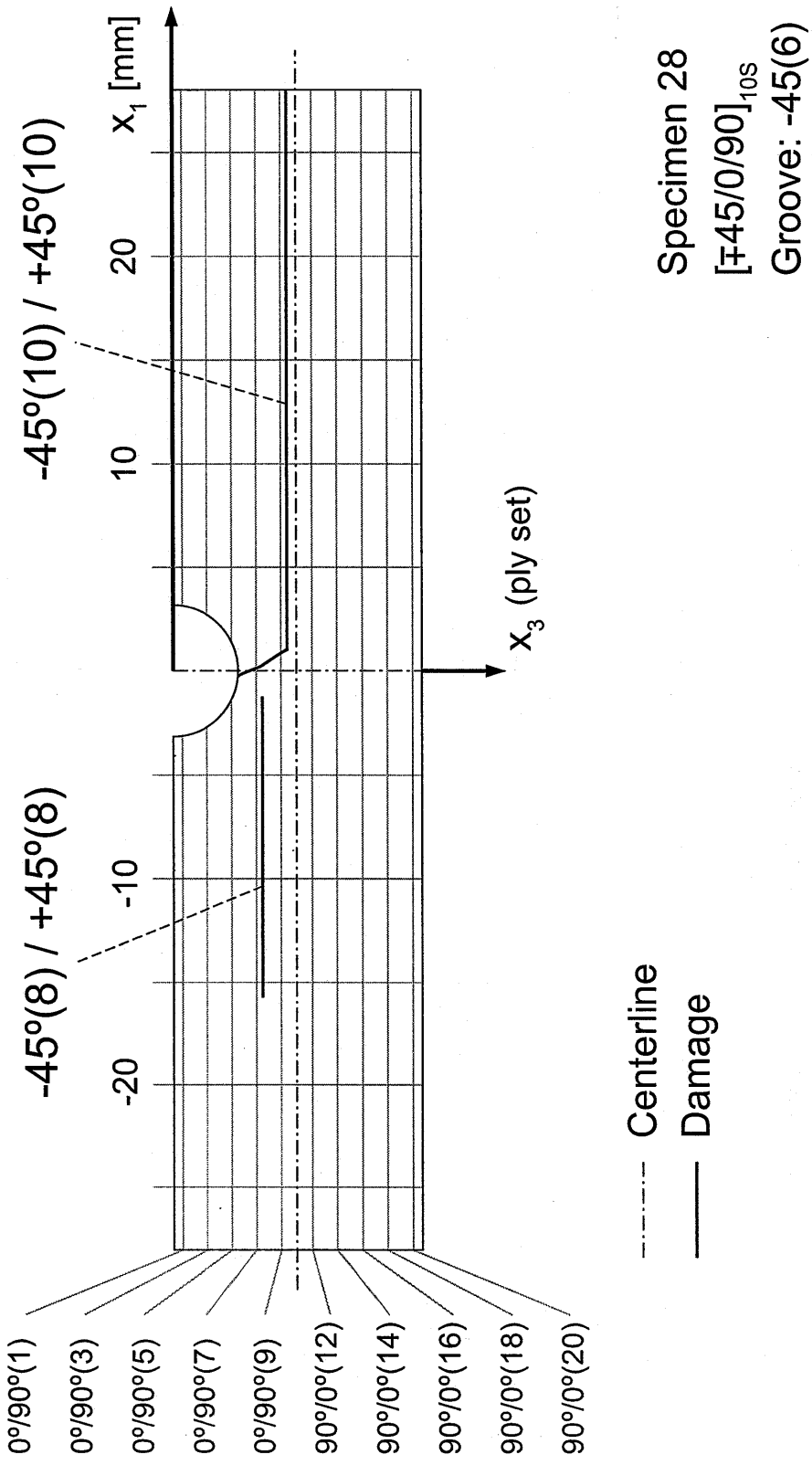

Figure B.33 Illustration of failure for Specimen 28: layup $[\mp 45/0/90]_{10S}$ with groove at $-45°$ ply in 6th set.

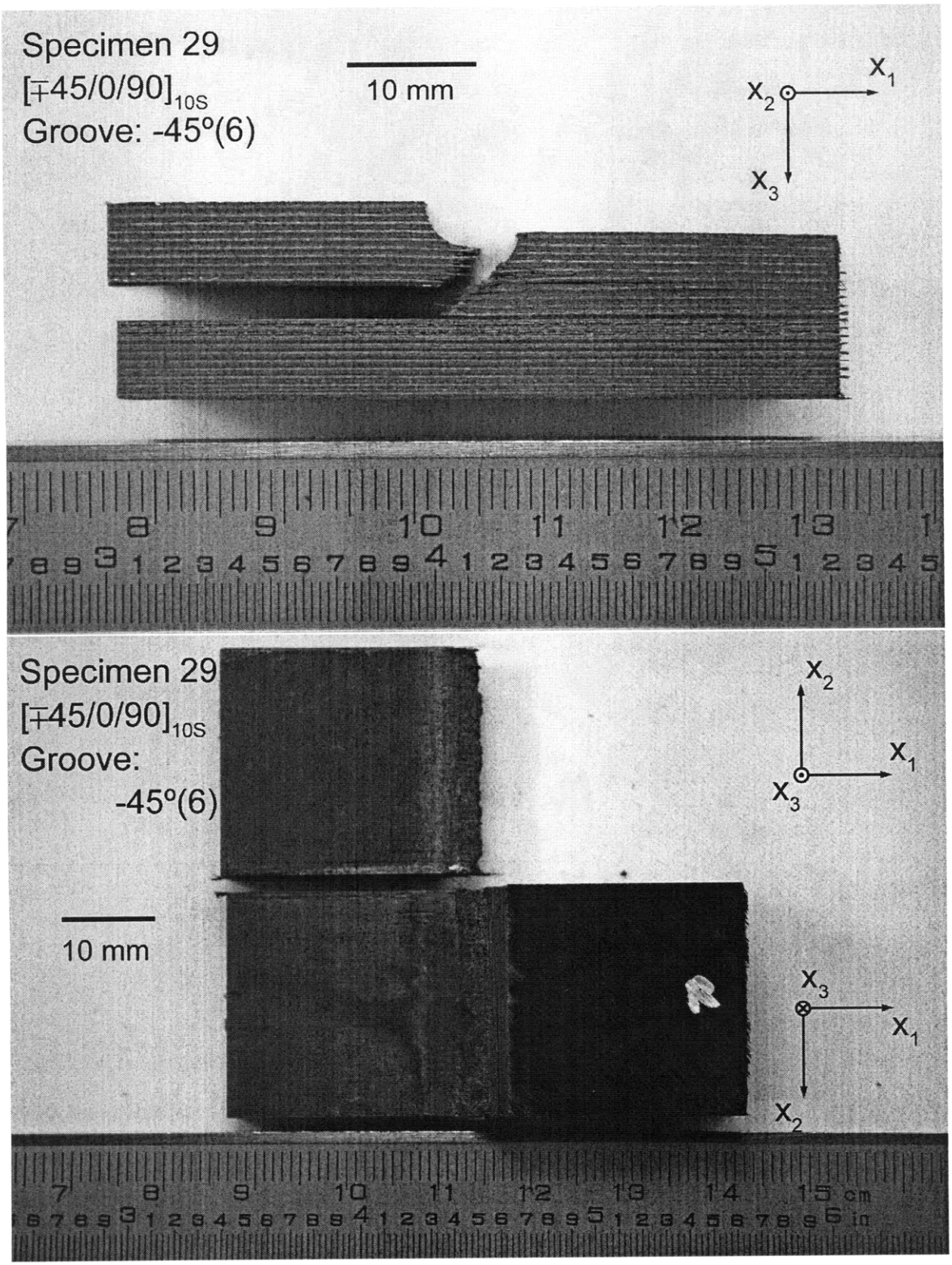

Figure B.34 Photographs after failure of Specimen 29 (layup $[\mp 45/0/90]_{10S}$ with groove at $-45°$ ply in 6th set) with *(upper)* side view, and *(lower)* failure surface view.

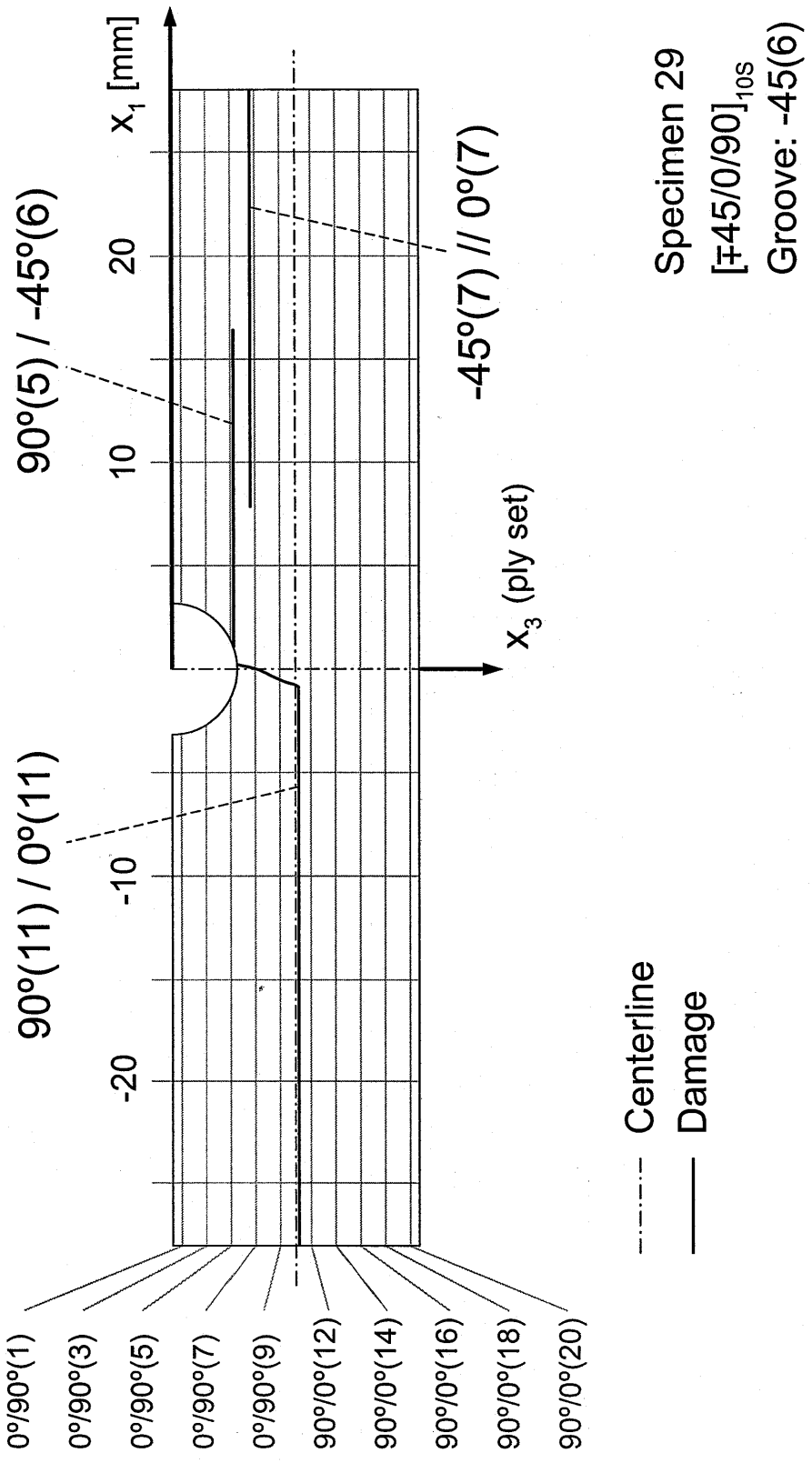

Figure B.35 Illustration of failure for Specimen 29: layup $[\mp 45/0/90]_{10S}$ with groove at $-45°$ ply in 6th set.

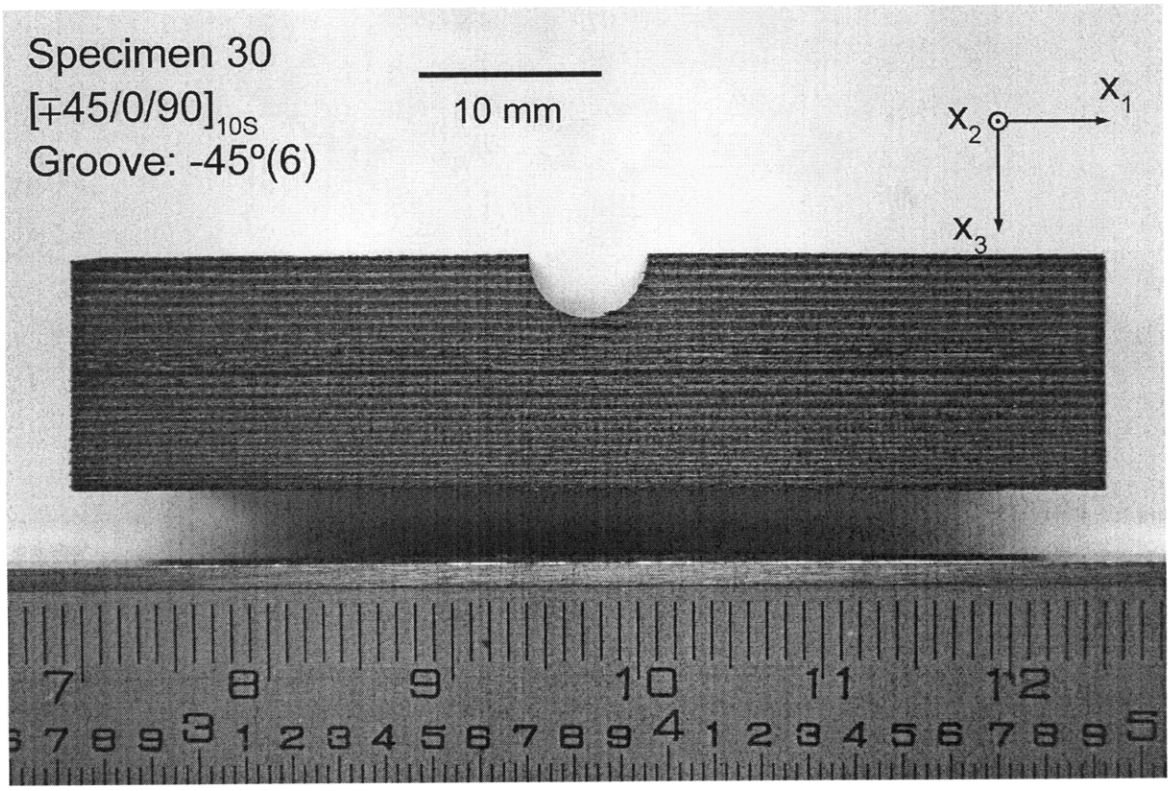

Figure B.36 Side view photograph after test of Specimen 30 (layup $[\mp 45/0/90]_{10S}$ with groove at $-45°$ ply in 6th set).

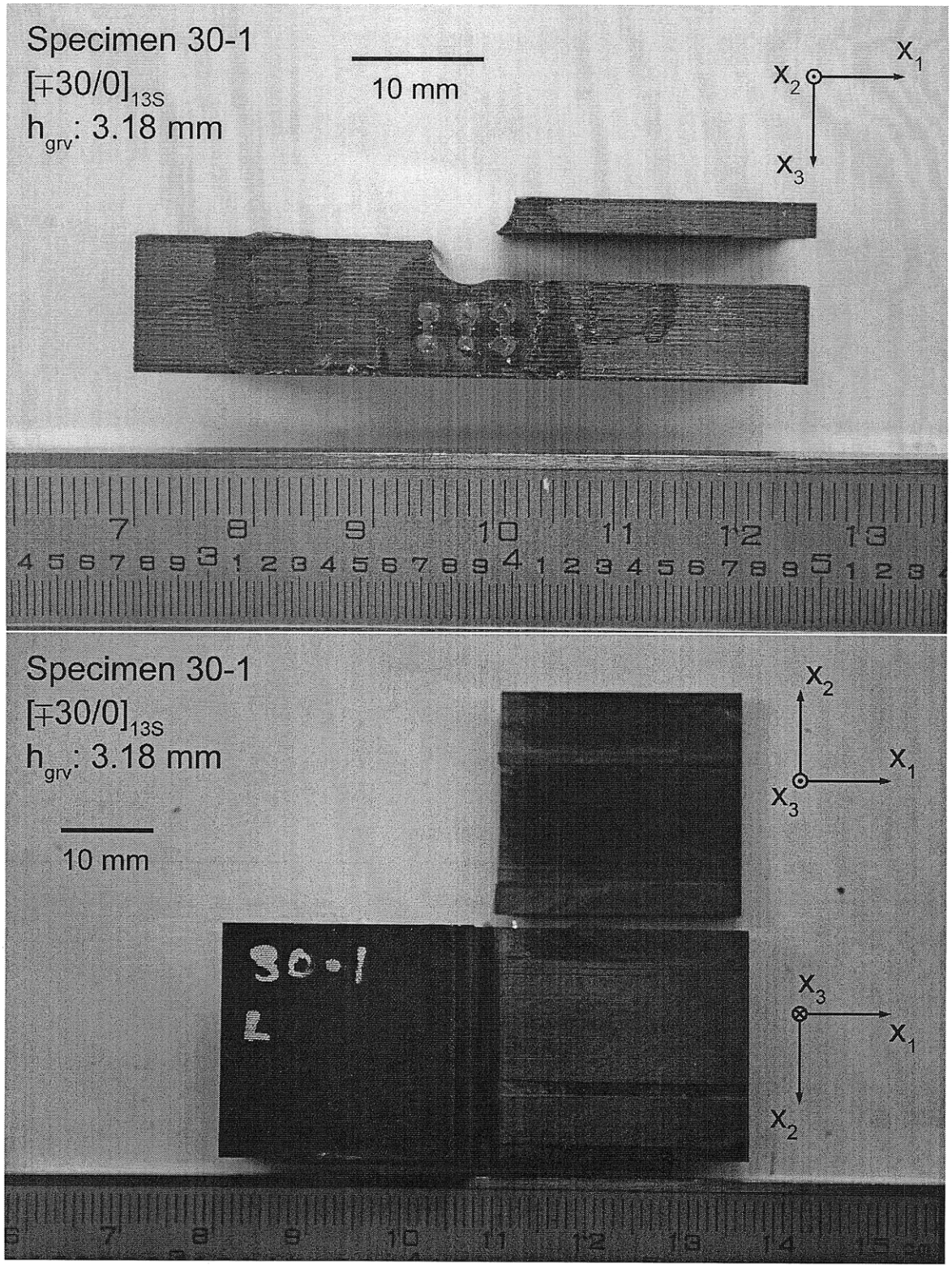

Figure B.37 Photographs after failure of Specimen 30-1 (layup $[\mp 30/0]_{13S}$ with $h_{\text{grv}} = 3.18$ mm) with *(upper)* side view, and *(lower)* failure surface view.

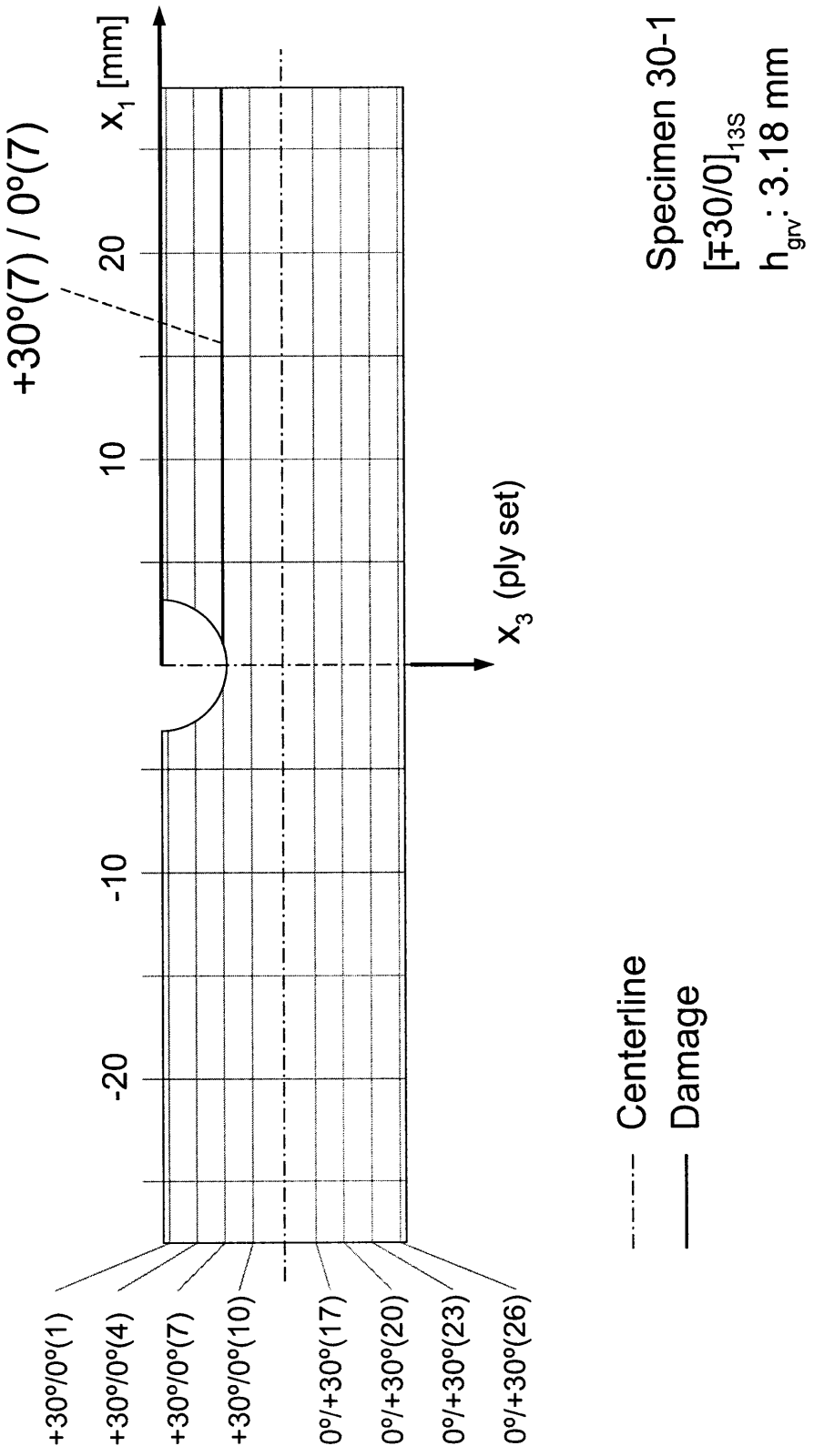

Figure B.38 Illustration of failure for Specimen 30-1: layup $[\mp 30/0]_{13S}$ with $h_{\text{grv}} = 3.18$ mm.

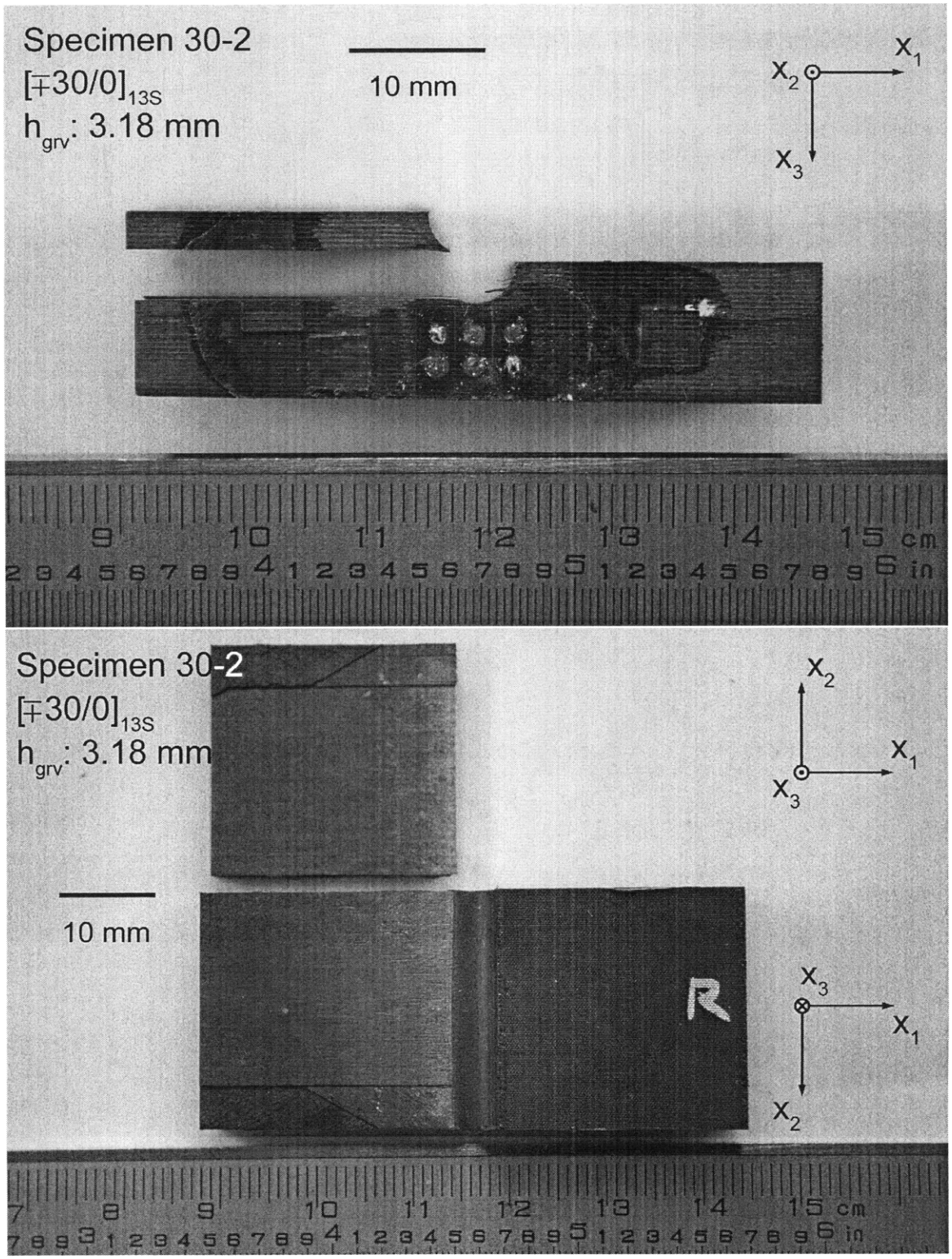

Figure B.39 Photographs after failure of Specimen 30-2 (layup $[\mp 30/0]_{13S}$ with $h_{\text{grv}} = 3.18$ mm) with *(upper)* side view, and *(lower)* failure surface view.

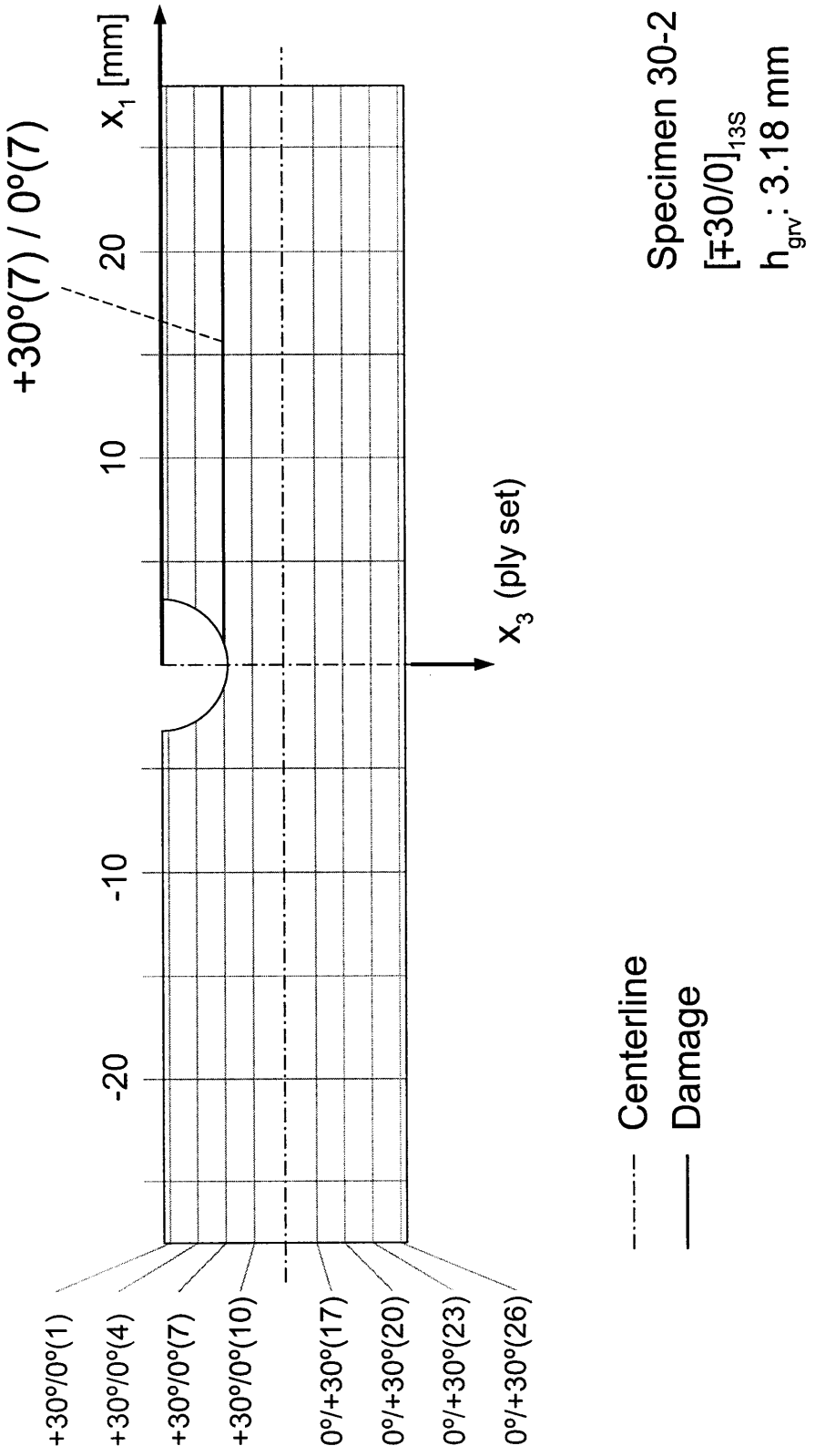

Figure B.40 Illustration of failure for Specimen 30-2: layup $[\mp 30/0]_{13S}$ with $h_{\text{grv}} = 3.18$ mm.

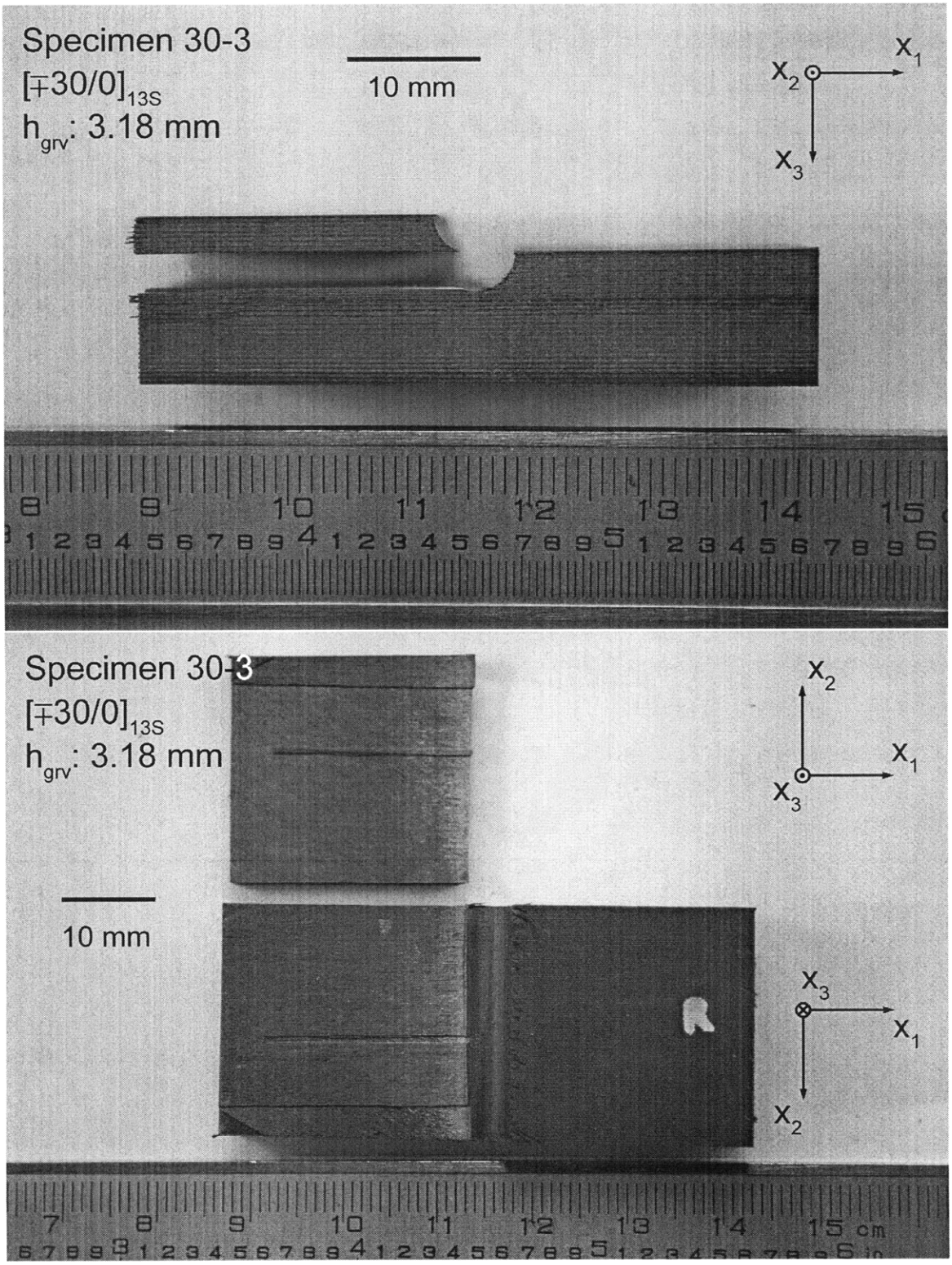

Figure B.41 Photographs after failure of Specimen 30-3 (layup $[\mp 30/0]_{13S}$ with $h_{\text{grv}} = 3.18$ mm) with *(upper)* side view, and *(lower)* failure surface view.

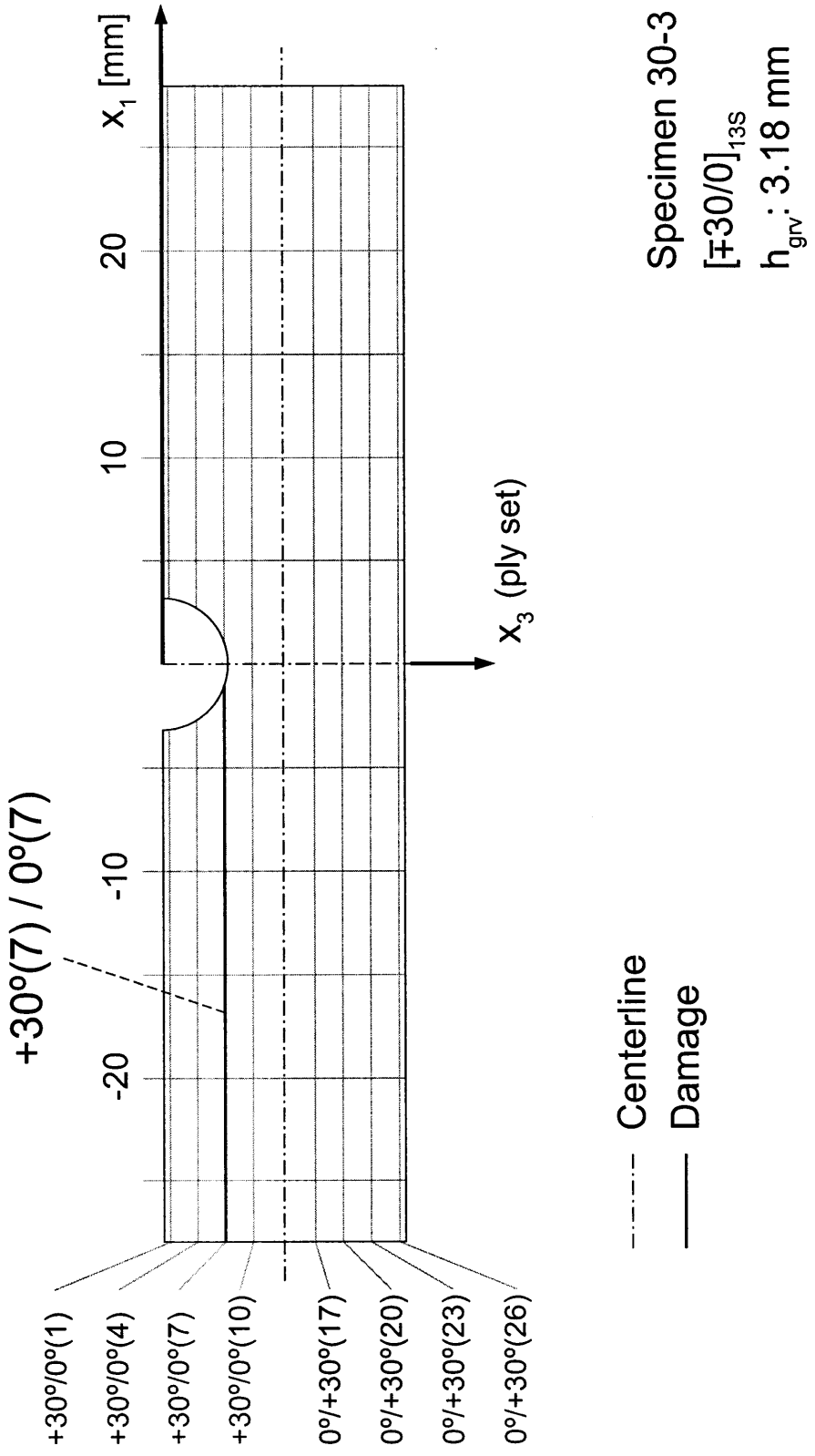

Figure B.42 Illustration of failure for Specimen 30-3: layup $[\mp 30/0]_{13S}$ with $h_{\text{grv}} = 3.18$ mm.

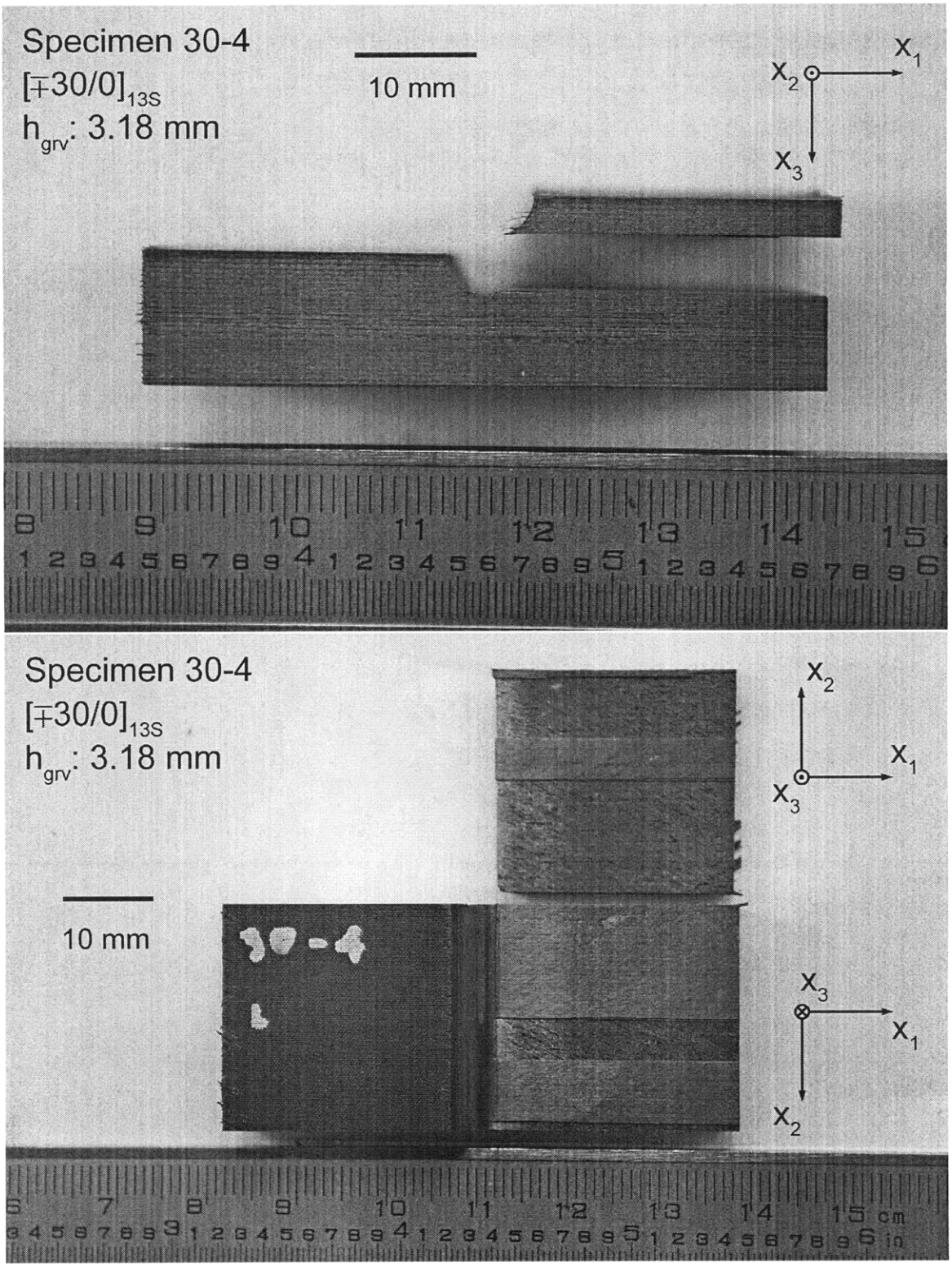

Figure B.43 Photographs after failure of Specimen 30-4 (layup $[\mp 30/0]_{13S}$ with $h_{\text{grv}} = 3.18$ mm) with *(upper)* side view, and *(lower)* failure surface view.

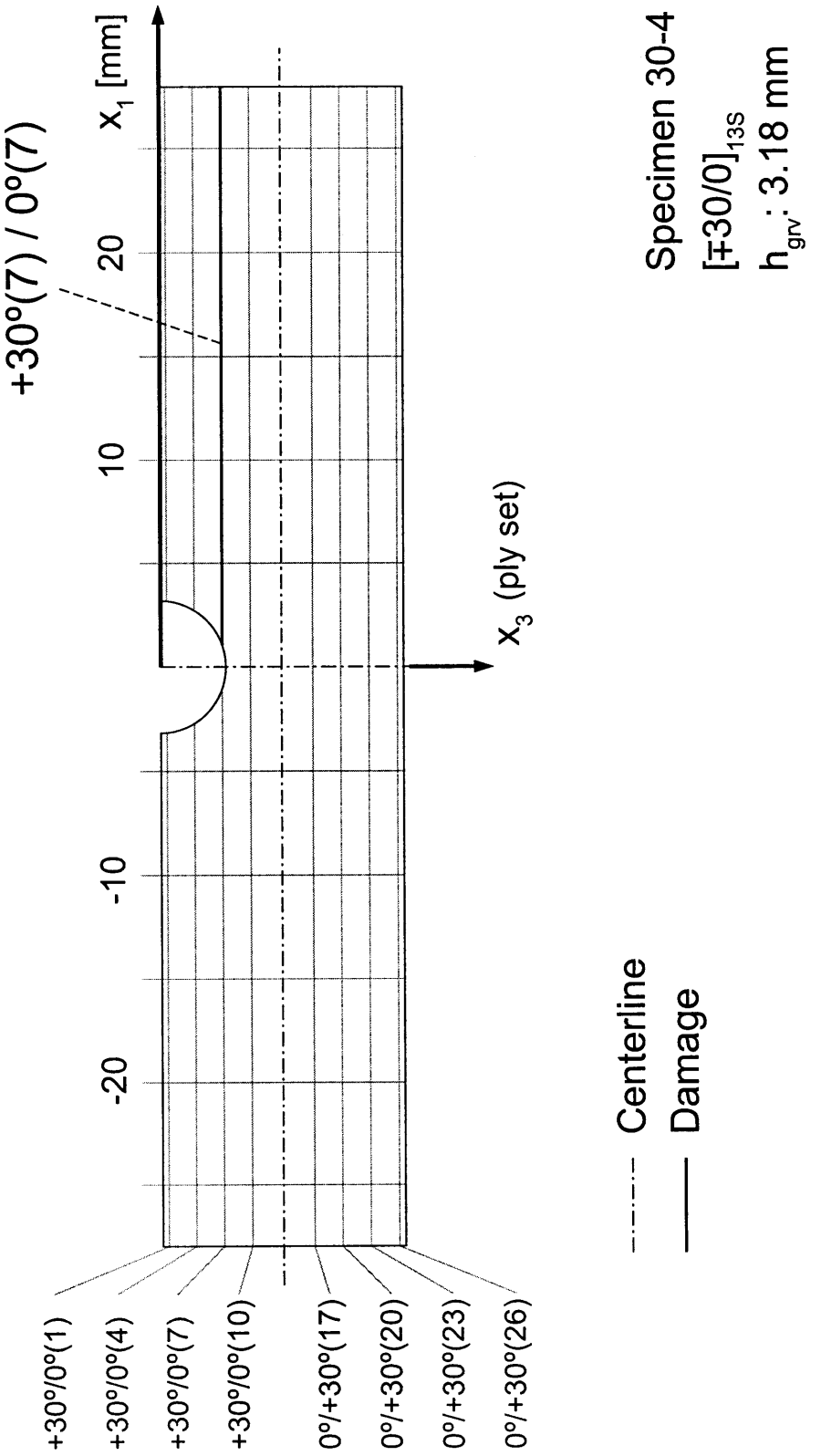

Figure B.44 Illustration of failure for Specimen 30-4: layup $[\mp 30/0]_{13S}$ with $h_{\text{grv}} = 3.18$ mm.

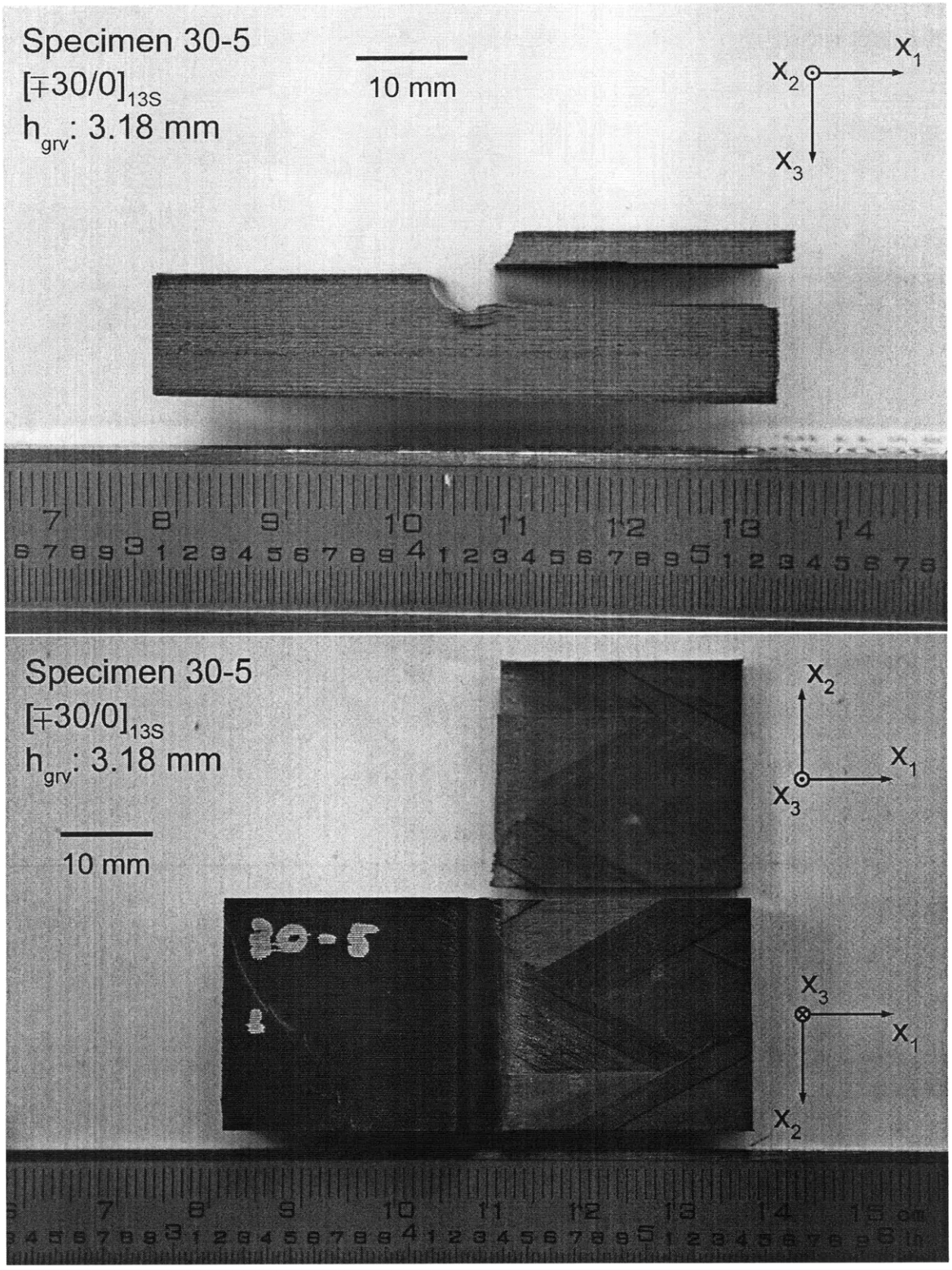

Figure B.45 Photographs after failure of Specimen 30-5 (layup $[\mp 30/0]_{13S}$ with $h_{\text{grv}} = 3.18$ mm) with *(upper)* side view, and *(lower)* failure surface view.

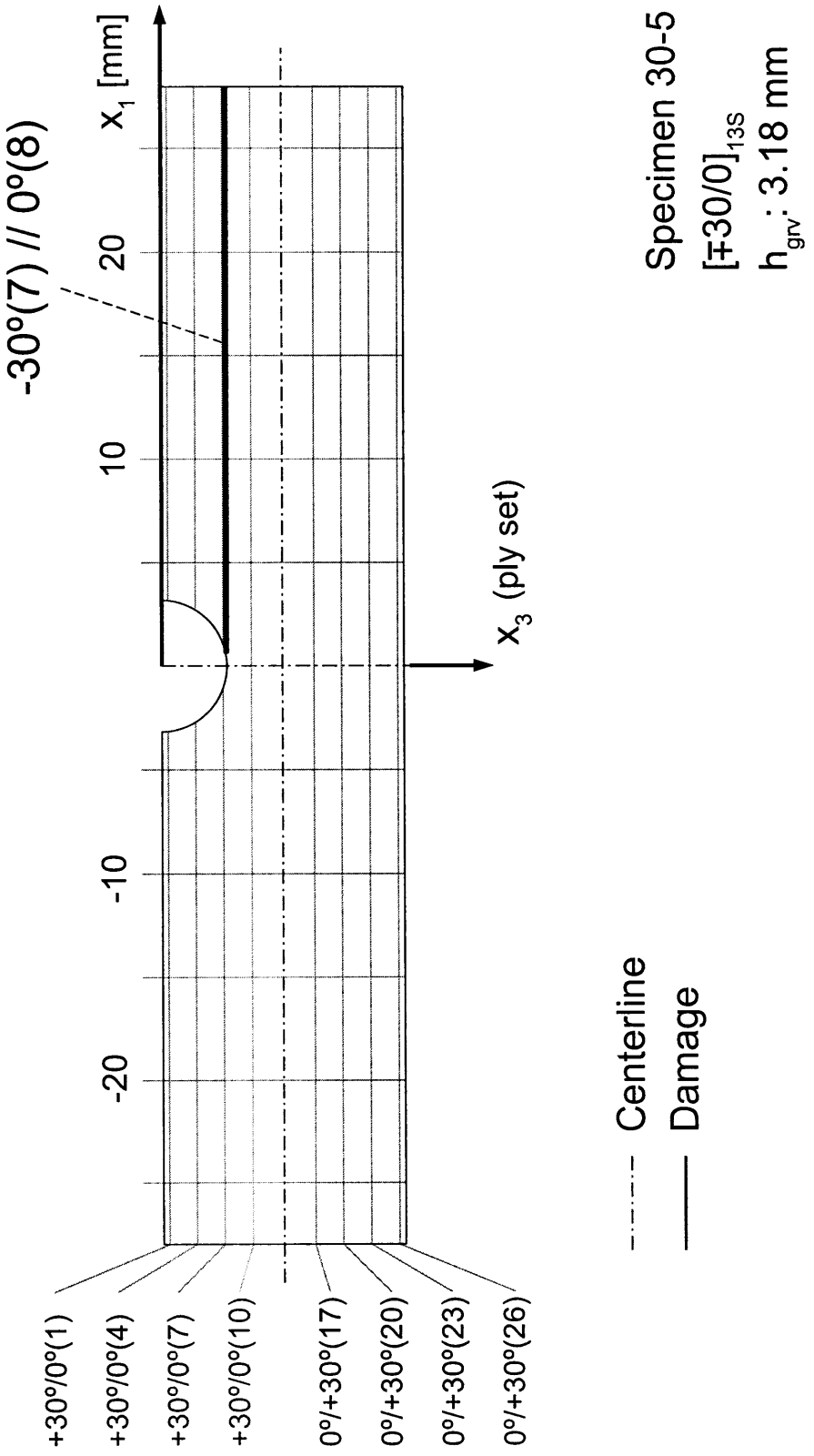

Figure B.46 Illustration of failure for Specimen 30-5: layup $[\mp 30/0]_{13S}$ with $h_{\text{grv}} = 3.18$ mm.

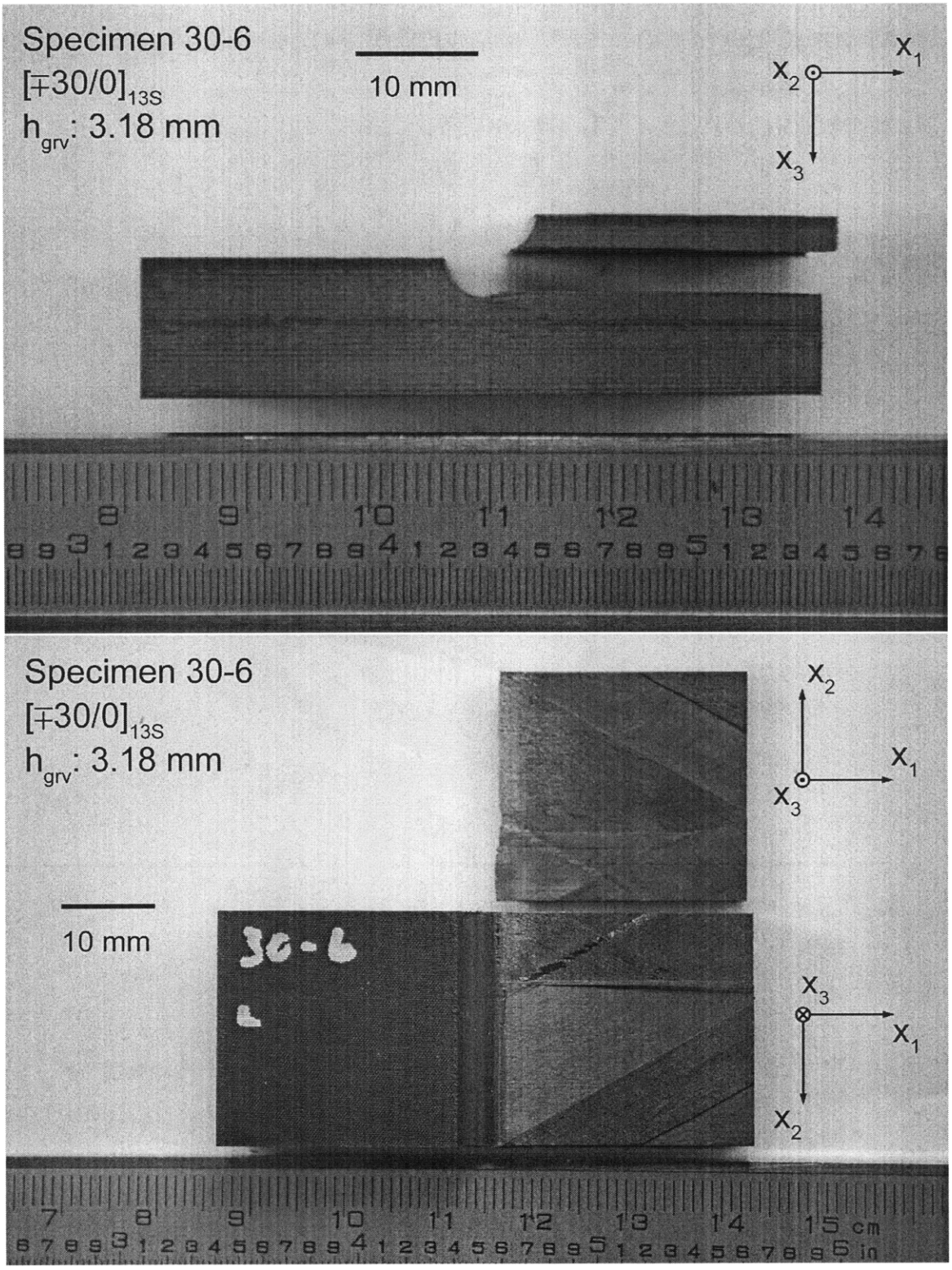

Figure B.47 Photographs after failure of Specimen 30-6 (layup $[\mp 30/0]_{13S}$ with $h_{\text{grv}} = 3.18$ mm) with *(upper)* side view, and *(lower)* failure surface view.

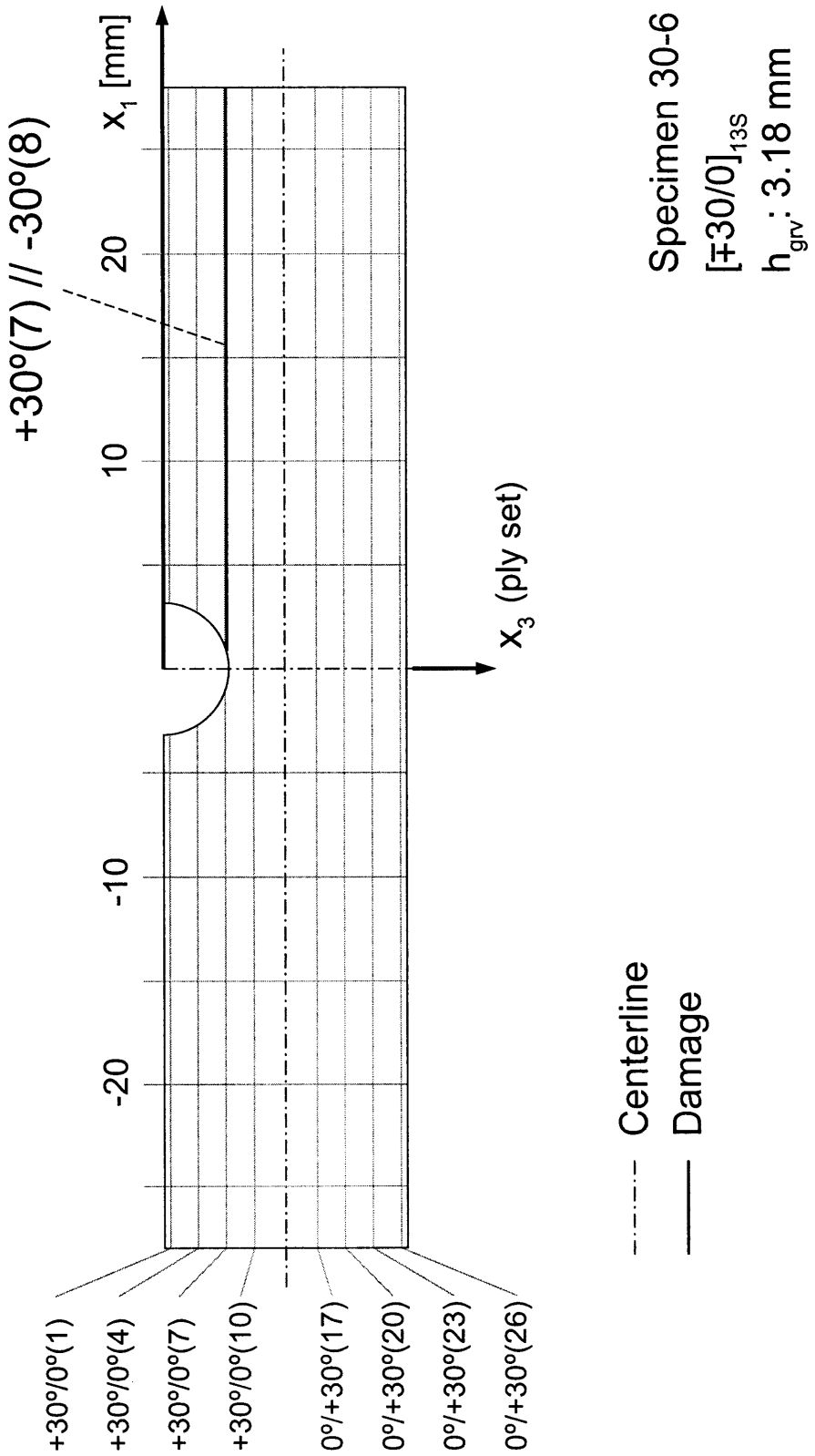

Figure B.48 Illustration of failure for Specimen 30-6: layup $[\mp 30/0]_{13S}$ with $h_{\text{grv}} = 3.18$ mm.